AD

USAAMRDL TECHNICAL REPORT 71-30

A THREE-AXIS FLUIDIC STABILITY AUGMENTATION SYSTEM

By

Harvey D. Ogren

October 1971

EUSTIS DIRECTORATE
U. S. ARMY AIR MOBILITY RESEARCH AND DEVELOPMENT LABORATORY
FORT EUSTIS, VIRGINIA

CONTRACTS DAAJ02-68-C-0039 AND DAAJ02-69-C-0036
HONEYWELL, INC.
MINNEAPOLIS, MINNESOTA

Approved for public release;
distribution unlimited.

312

DISCLAIMERS

The findings in this report are not to be construed as an official Department of the Army position unless so designated by other authorized documents.

When Government drawings, specifications, or other data are used for any purpose other than in connection with a definitely related Government procurement operation, the United States Government thereby incurs no responsibility nor any obligation whatsoever; and the fact that the Government may have formulated, furnished, or in any way supplied the said drawings, specifications, or other data is not to be regarded by implication or otherwise as in any manner licensing the holder or any other person or corporation, or conveying any rights or permission, to manufacture, use, or sell any patented invention that may in any way be related thereto.

Trade names cited in this report do not constitute an official endorsement or approval of the use of such commercial hardware or software.

DISPOSITION INSTRUCTIONS

Destroy this report when no longer needed. Do not return it to the originator.

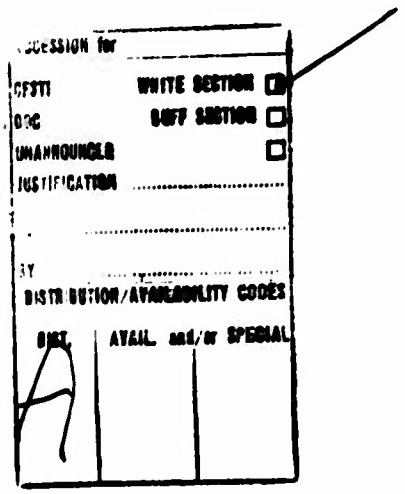

DEPARTMENT OF THE ARMY
U. S. ARMY AIR MOBILITY RESEARCH & DEVELOPMENT LABORATORY
EUSTIS DIRECTORATE
FORT EUSTIS, VIRGINIA 23604

This report has been reviewed by the Eustis Directorate, U. S. Army Air Mobility Research and Development Laboratory and is considered to be technically sound. The purpose of the program was to develop and operationally demonstrate in the laboratory, under a simulated helicopter operating environment, a three-axis hydrofluidic stability augmentation system. The report is published for the exchange of information and appropriate application. The technical monitor for this contract was Mr. George W. Fosdick, Aeromechanics Division.

Task 1F162203A14186
Contracts DAAJ02-68-C-0039
and DAAJ02-69-C-0036
USAAMRDL Technical Report 71-30
October 1971

A THREE-AXIS FLUIDIC STABILITY AUGMENTATION SYSTEM

Final Report

Honeywell Document 21192-FR

By

Harvey Ogren

Prepared by

Honeywell Inc.
Government and Aeronautical Products Division
Minneapolis, Minnesota

for

EUSTIS DIRECTORATE
U.S. ARMY AIR MOBILITY
RESEARCH AND DEVELOPMENT LABORATORY
FORT EUSTIS, VIRGINIA

Unclassified

Security Classification

DOCUMENT CONTROL DATA - R & D

(Security classification of title, body of abstract and indexing annotation must be entered when the overall report is classified)

1. ORIGINATING ACTIVITY (Corporate author) Honeywell Inc. 2600 Ridgway Parkway N. E. Minneapolis, Minnesota	2a. REPORT SECURITY CLASSIFICATION Unclassified 2b. GROUP

3. REPORT TITLE

A THREE-AXIS FLUIDIC STABILITY AUGMENTATION SYSTEM

4. DESCRIPTIVE NOTES (Type of report and inclusive dates)

Final Technical Report

5. AUTHOR(S) (First name, middle initial, last name)

Harvey D. Ogren

6. REPORT DATE	7a. TOTAL NO. OF PAGES	7b. NO. OF REFS
October 1971	310	0

8a. CONTRACT OR GRANT NO.	9a. ORIGINATOR'S REPORT NUMBER(S)
DAAJ02-68-C-0039 and b. PROJECT NO. DAAJ02-69-C-0036	USAAMRDL Technical Report 71-30
c. Task 1F162203A14186 d.	9b. OTHER REPORT NO(S) (Any other numbers that may be assigned this report) Honeywell GAPD 21192-FR

10. DISTRIBUTION STATEMENT

Approved for public release; distribution unlimited.

11. SUPPLEMENTARY NOTES	12. SPONSORING MILITARY ACTIVITY
	U.S. Army Air Mobility Research and Development Laboratory, Eustic Directorate, Fort Eustis, Virginia

13. ABSTRACT

This report covers the analysis, design, fabrication and laboratory tests of a three-axis hydrofluidic stability augmentation system for a UH-1-type helicopter. The design goal was to improve the handling qualities of the aircraft, without stabilizer bar, in the speed range of 60 to 120 knots.

The control problem was analyzed and a system defined through the use of analog computer simulation techniques. The defined system was mechanized into three separate controller packages, one for each axis. These were fabricated, calibrated, and open-loop tested. The system was subjected to temperature and vibration flightworthiness tests. The final tests conducted were closed-loop performance checks using an analog computer to simulate the aircraft dynamics.

The system demonstrated improved handling performance of the aircraft when compared with the unaugmented case.

DD FORM 1 NOV 68 1473 REPLACES DD FORM 1473, 1 JAN 64, WHICH IS OBSOLETE FOR ARMY USE.

Unclassified

Security Classification

14. KEY WORDS	LINK A		LINK B		LINK C	
	ROLE	WT	ROLE	WT	ROLE	WT
Aircraft handling qualities						
Analysis						
Design						
Fabrication						
Laboratory test						
Three-axis hydrofluidic stability augmentation system (FSAS)						
UH-1-type helicopter with and without stabilizer bar						
Speed range 60 to 120 knots						
Pitch-axis controller						
Roll-axis controller						
Yaw-axis controller						
Analog computer simulation						
Temperature and vibration flightworthiness tests						

ABSTRACT

This report covers the analysis, design, fabrication and laboratory tests of a three-axis hydrofluidic stability augmentation system for a UH-1-type helicopter. The design goal was to improve the handling qualities of the aircraft, without stabilizer bar, in the speed range of 60 to 120 knots.

The control problem was analyzed and a system defined through the use of analog computer simulation techniques. The defined system was mechanized into three separate controller packages, one for each axis. These were fabricated, calibrated, and open-loop tested. The system was subjected to temperature and vibration flightworthiness tests. The final tests conducted were closed-loop performance checks using an analog computer to simulate the aircraft dynamics.

The system demonstrated improved handling performance of the aircraft when compared with the unaugmented case.

FOREWORD

This document is the final report on a program conducted for the Eustis Directorate, U. S. Army Air Mobility Research and Development Laboratory under Contracts DAAJ02-68-C-0039 and DAAJ02-69-C-0036, DA Task 1F162203A14186. This program is part of the Army's effort to develop stability augmentation systems for helicopters. The objective was to analyze design, build, and test a hydrofluidic damper system for demonstration on the UH-1-type aircraft. The work presented here started 15 November 1968 and was completed 28 October 1970.

The technical monitor of this program was G. W. Fosdick. Appendix I was written by M. E. Ebsen and W. M. Posingies; Appendix II, by G. E. Trull; and Appendix III, by G. E. Trull and R. R. Gascon.

TABLE OF CONTENTS

TABLE OF CONTENTS (CONCLUDED)

LIST OF ILLUSTRATIONS

LIST OF ILLUSTRATIONS (CONTINUED)

LIST OF ILLUSTRATIONS (CONTINUED)

LIST OF ILLUSTRATIONS (CONTINUED)

LIST OF ILLUSTRATIONS (CONTINUED)

LIST OF ILLUSTRATIONS (CONTINUED)

LIST OF ILLUSTRATIONS (CONTINUED)

LIST OF ILLUSTRATIONS (CONTINUED)

LIST OF ILLUSTRATIONS (CONTINUED)

LIST OF ILLUSTRATIONS (CONCLUDED)

LIST OF TABLES

LIST OF TABLES (CONTINUED)

LIST OF TABLES (CONCLUDED)

LIST OF SYMBOLS

C	bellows capacitance, $in.^5/lb$
e	2.7314
g	acceleration due to gravity, ft/sec^2
gpm	gallons per minute
I_{xx}	moment of inertia around roll axis, $slug\text{-}ft^2$
I_{yy}	moment of inertia around pitch axis, $slug\text{-}ft^2$
I_{zz}	moment of inertia around vertical axis, $slug\text{-}ft^2$
K	pitch inclination of stabilizer bar, rad
L	roll moment, ft-lb
M	pitch moment, ft-lb
MR	mass ratio, control flow/power flow
N	yaw moment, ft-lb
N_R	Reynolds number
o	used as subscript means initial steady-state conditions
O/SH	overshoot, percent
psi	pounds per square inch
P_b	backpressure, psi
P_s	power supply pressure, psi
P_o	recovered pressure, psi
P_c	control pressure, psi
P_i	internal pressure, psi
P_e	external pressure, psi
ΔP_c	differential pressure on control ports of amplifier, psi

LIST OF SYMBOLS (CONTINUED)

ΔP_o	differential pressure at output ports of amplifier, psi
R_i	input impedance, lb-sec/in.^{5}
R_o	output impedance, lb-sec/in.^{5}
R_i'	effective input impedance, lb-sec/in.^{5}
R_o'	effective output impedance, lb-sec/in.^{5}
S	Laplace operator
$t_{90\%}$	time to reach 90 percent of final value, sec
T	time constant, sec
T_{lag}	time constant lag, sec
T_{HP}	time constant high-pass, sec
T_{lead}	time constant lead, sec
u	X-body-axis perturbation velocity, ft/sec
u_c	airspeed change, ft/sec
u_g	longitudinal gust, ft/sec
U	forward velocity, ft/sec
$\dot{u}$	forward acceleration, ft/sec^2
v	Y-body-axis perturbation velocity, ft/sec
v_g	lateral gust, ft/sec
V	side velocity, ft/sec
V_{NE}	helicopter velocity never to exceed, kn
w	Z-body-axis perturbation velocity, ft/sec
w_g	vertical gust, ft/sec
$\dot{w}$	differential of w, ft/sec^2
W	Z-body-axis velocity, ft/sec

LIST OF SYMBOLS (CONTINUED)

W_M	maximum overload gross weight of helicopter, lb
$\dot{W}$	Z-body-axis acceleration, ft/sec^2
X	forward force, lb
X_u, X_w, etc.	dimensionless aerodynamics, $\partial X/\partial u$, $\partial u/\partial w$, etc.
Y	side force, lb
Z	vertical force, lb
ψ*	yaw-angle, deg
$\dot{\psi}$	yaw-axis angular rate, deg/sec
$\ddot{\psi}$	yaw angular acceleration, rad/sec^2
δ_{ψ_m}*	yaw-axis mechanical pedal displacement, deg
$\delta_{\psi_{aug}}$	yaw-axis augmented servoactuator command from pilot's pedals, deg
δ_{ψ_s}	yaw-axis servoactuator displacement, deg
$\delta\psi_a$	yaw boost actuator deflection, deg
δ_ψ	tail rotor control, deg
K_{δ_ψ}	augmented servoactuator command deg/mechanical tail rotor command, deg
K_ψ	tail rotor angle, deg/aircraft turning rate, deg/sec
ϕ*	roll angle, deg
$\dot{\phi}$	roll angular rate, deg/sec
$\ddot{\phi}$	roll angular acceleration, rad/sec^2
δ_{ϕ_m}	roll-axis mechanical cyclic displacement, deg

*Note: In Appendix I, Section III these symbols are in rad.

LIST OF SYMBOLS (CONCLUDED)

δ_{ϕ_s}	roll-axis servoactuator displacement, deg
δ_{ϕ_a}	roll boost actuator deflection, deg
$\delta_\phi{}^*$	cyclic roll control, deg
K_ϕ	lateral blade angle, deg/aircraft turning rate, deg/sec
θ^*	pitch angle, deg
$\dot{\theta}$	pitch angular rate, deg/sec
$\ddot{\theta}$	pitch angular acceleration, rad/sec^2
δ_{θ_m}	pitch-axis mechanical cyclic displacement, deg
δ_{θ_s}	pitch-axis servoactuator displacement, deg
δ_{θ_a}	pitch boost actuator deflection, deg
$\delta_\theta{}^*$	cyclic pitch control, deg
K_θ	longitudinal blade angle, deg/aircraft turning rate, deg/sec
δ_L	collective mechanical displacement, rad
β^*	pitch blade flapping angle, deg
ξ	damping ratio
λ	roll inclination of stabilizer bar, rad
γ	pitch blade flapping angle, rad
τ	vortex rate sensor transport delay, sec
ω_n	servoactuator natural frequency, rad/sec

SECTION I
SUMMARY

SYSTEM DESIGN

This phase of the program was conducted under Contract DAAJ02-68-C-0039. It consisted of a closed-loop computer study using the equations of motion of the UH-1B helicopter to determine the proper shaping networks and system gains for a three-axis hydrofluidic stability augmentation system. The system was designed to improve aircraft handling qualities over the 60- to 120-knot speed range. Gain, time constants, and servoactuator performance were varied to determine the allowable limits and still obtain adequate aircraft handling qualities. The report covering this effort is included as Appendix I.

From this study, a detailed specification was written to which the three-axis hydrofluidic stability augmentation system was designed.

HARDWARE DESIGN AND FABRICATION

The three-axis hydrofluidic stability augmentation system was designed in accordance with the detailed specification written during the system design phase. The final controller packages are shown in Figure 1. Each controller was designed to be as small as practical, to have commonality of parts, to include null adjust in the vortex rate sensor, to have built-in-test (BIT) capability, and to be able to connect the pitch-axis and roll-axis controllers without tubings and fittings.

The pitch-axis controller contained a vortex rate sensor, four amplifiers, and four bellows that made up the high-pass and lead-lag networks.

The roll-axis controller contained a vortex rate sensor that was interchangeable with the pitch sensor, two amplifiers, and two bellows that made up the high-pass network.

The yaw-axis controller contained a vortex rate sensor, four amplifiers, a pilot-input device, and three bellows that made up the high-pass and lag networks.

Each controller had BIT capability and a null adjust with interchangeable parts. All amplifiers had the same performance and were interchangeable. Internal parts of the vortex rate sensors were also interchangeable.

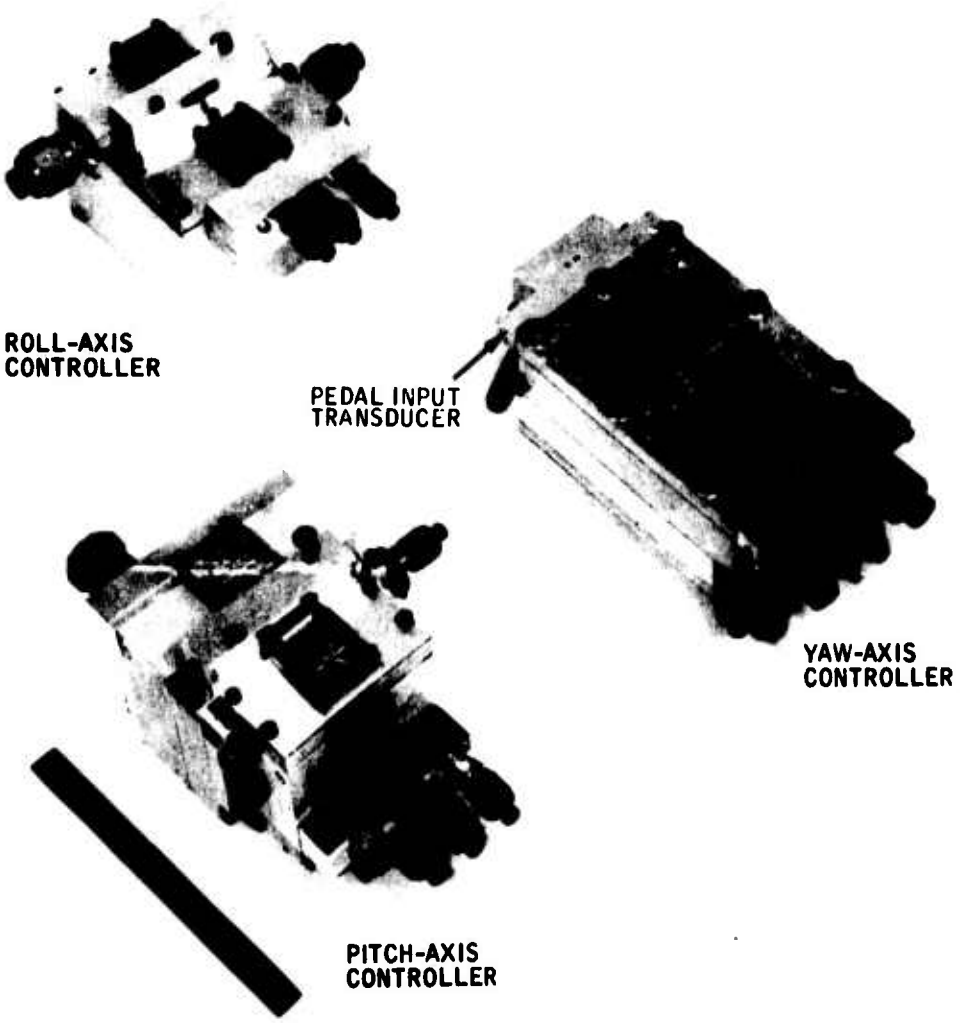

Figure 1. Final Controller Packages.

DEVELOPMENT TESTS

Each controller was calibrated for proper gain, noise level, nulls, and time constants. In doing this work, a number of problems were encountered. The more significant events are summarized as follows:

- Some original amplifiers exhibited nonlinearities; therefore, new amplifiers that did not exhibit nonlinearities were fabricated and tested. Development effort had been accomplished under Contract DAAJ02-68-C-0039.

- The original design of the vortex rate sensor would not perform properly with the desired large flow split between the primary and secondary sinks. The large flow through the sensor was desired to maximize response. An annulus-type outlet was incorporated in the vortex rate sensor sink region to obtain the desired sensor flow and response.

- The original bellows purchased were found to be nonlinear. This was found to be characteristic of the normal off-the-shelf bellows. New bellows were purchased that were specifically heat-treated to obtain linearity.

- Two types of servoactuators were obtained. One was a spool valve type, and the other was a fluidic vortex valve type furnished as GFE. Because of the servoactuator input configuration, both exhibited an underdamped condition when driven with a fluid amplifier. In addition, weak input force capsules made it necessary to use extreme care to prevent sudden surges of pressure from occurring across the bellows, causing damage.

- Back pressure on the controllers was found to affect output noise level. By using a back pressure of at least 160 psi, the noise level was kept consistently low.

- The controllers were temperature-compensated by controlling the flow split in the vortex rate sensor with a viscous restrictor in the secondary outlet.

- The controllers were strengthened to make them compatible with the power system required by the use of the vortex valve servoactuators.

The final performance obtained from the three controller-servoactuators incorporating the modifications listed above is given in Table I.

TABLE I. SUMMARY OF FSAS PERFORMANCE

Axis	Temperature (°F)	Gain (in./deg/sec)	Noise* (in.)	Threshold (deg/sec)	Null (in.)
Pitch	120	0.0420	0.028	<0.5	0.005
	60	0.0096	0.010	<0.5	0.005
	185	0.0240	0.140	<0.5	0.020
Roll	120	0.0064	0.005	<0.5	0.020
	60	0.0016	0.020	1.7	0.020
	185	0.0044	0.010	<0.5	0.010
Yaw	120	0.0216	0.028	<0.5	0.040
	60	0.0100	0.022	<0.5	0.022
	185	0.0120	0.024	<0.5	0.030

*Peak-to-Peak

ACCEPTANCE TESTS

Flightworthiness tests were conducted on the controllers, spool valve servoactuators, and vortex valve servoactuators. The tests consisted of performance checks at oil temperatures of 60°F, 120°F, and 180°F, and 15-minute vibration scans in each orthogonal axis.

The controllers and spool valve servoactuators were connected with an analog computer to simulate the helicopter characteristics, and closed-loop performance data were taken and compared with the study phase analysis predictions.

CONCLUSIONS AND RECOMMENDATIONS

This program demonstrated that a fluidic three-axis stability augmentation system could: (1) be designed, fabricated, and tested to meet a given set of requirements; (2) be made small and compact; and (3) be competitive with conventional electromechanical systems. A built-in-test capability was also demonstrated.

It is recommended that the system be flight tested in a UH-1-type helicopter. Also, further development effort should be applied to improve temperature compensation, to eliminate servoactuator deficiencies, and to extend the electroform conductive wax process to fabricate manifolds.

SECTION II
SYSTEM DESIGN

PREVIOUS STUDY EFFORT

The objective of the analysis program was to define mathematically the system block diagrams for a simple hydrofluidic stability augmentation system to augment the roll, pitch, and yaw axes of the UH-1B helicopter. No performance requirements were specified other than that the fluidic stability augmentation systems (FSAS) must improve vehicle damping and improve the handling qualities of the UH-1B helicopter during the high-speed gunfiring mission. With these general requirements in mind, a set of detailed design goals was generated that permitted FSAS performance evaluation in light of these self-imposed system requirements.

Nominal FSAS performance was evaluated in light of the design goals and the time histories, and data showed that the requirements of the design were satisfied. FSAS performance is summarized briefly as follows:

- Yaw-axis damping ratio was increased from 0.3 to approximately 0.6, or greater.
- The pedal position input loop eliminated the hover and low-speed problem of the yaw-axis damper fighting pilot input commands.
- Pitch-axis damping ratio was increased from 0.3 to 0.5, or greater.
- Roll-axis control effectivenss was adjusted to provide a more controllable vehicle.
- Roll and pitch responses were designed for a rate response proportional to control stick deflection.

The parameter variation study results showed that nominal FSAS performance may be achieved for ±20-percent tolerance variations. In some cases, parameters such as high-pass time constants and pedal position feedback gain are considered to be noncritical from the stability standpoint, and larger tolerance variations from nominal may be allowed so long as their effects on system transient response are considered.

The primary goal of the analysis was to show hydrofluidic three-axis SAS feasibility using simplified control techniques. The use of flight path sensors is considered to be beyond the scope of this FSAS control system program.

The use of collective pitch and roll crossfeeds was considered during the "Fluid State Hydraulic Damper" program, under Contract DA 44-177-AMC-294(T), and was rejected for the following reasons:

- Airframe data to permit evaluation of a collective crossfeed were not available.
- Complexity of the system would be increased far beyond that necessary to demonstrate fluid system feasibility.

These control concepts were also considered during this analysis and were not pursued for reasons similar to those mentioned above.

The analysis results presented in Appendix I show that a fixed-gain rate feedback system is suitable to demonstrate the feasibility of using a hydrofluidic SAS to increase vehicle damping and produce a short-term rate response proportional to control stick deflection.

A detailed specification for the three-axis stability augmentation system was written. It called out the specific requirements such as gains, frequency response, noise, nulls, temperature, and vibration for each controller and servoactuator. Figures 2, 3, and 4 show the analytical block diagram, gain and frequency response requirements, and component gains for each controller. The complete detail specification is contained in Appendix I.

DEVELOPMENT EFFORT

The present contract involved the design, fabrication, and testing of the three-axis stability augmentation system per the established requirements. One deviation made from the study contract requirements was the use of a different technique for producing a pedal input signal for the yaw-axis controller. The original concept was to be a spring-bellows-type device that was essentially a long-time-constant high-pass network. Reevaluation indicated that, because of the size of the bellows and the questionable performance of a high-pass network combined with a lag, this technique was not desirable. A simple flapper nozzle concept was finally selected. This concept was successfully developed and provides a constant output for a constant pedal position rather than a slowly decaying output for a constant pedal position .

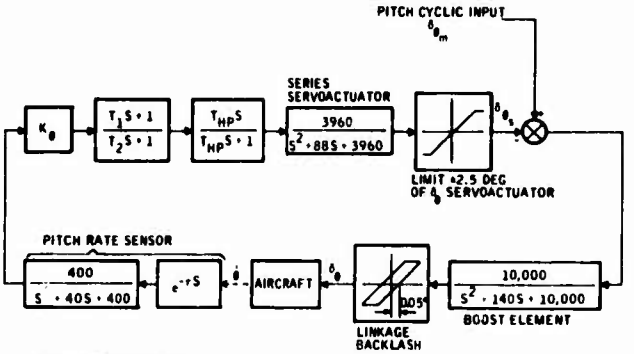

A. ANALYTIC BLOCK DIAGRAM

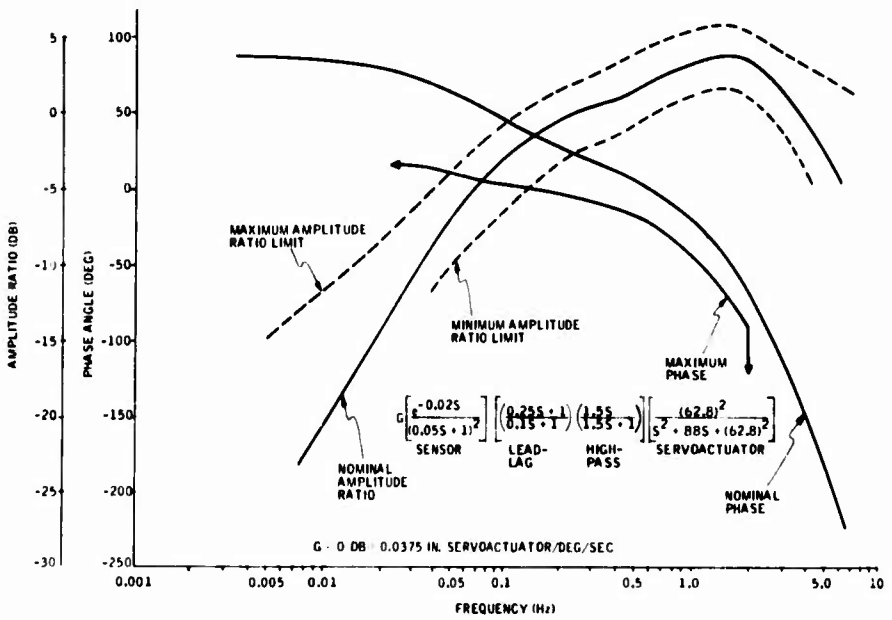

B. RESPONSE REQUIREMENTS

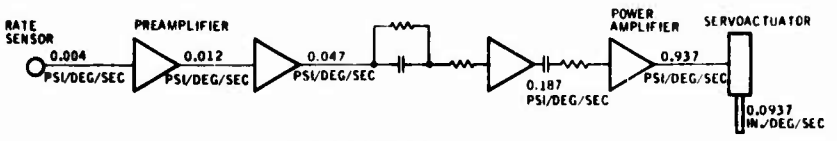

C. COMPONENT GAINS

Figure 2. Pitch-Axis Design Data.

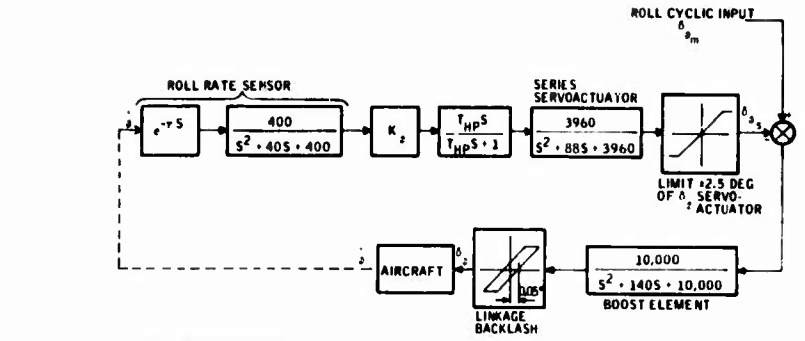

τ = 20-ms TRANSPORT DELAY
K_δ = 0.055 DEG LATERAL BLADE ANGLE/DEG/SEC
T_{HP} = 10.0 SEC
LATERAL CYCLIC STICK SENSITIVITY 1.54 DEG LATERAL BLADE ANGLE/IN. STICK

A. ANALYTIC BLOCK DIAGRAM

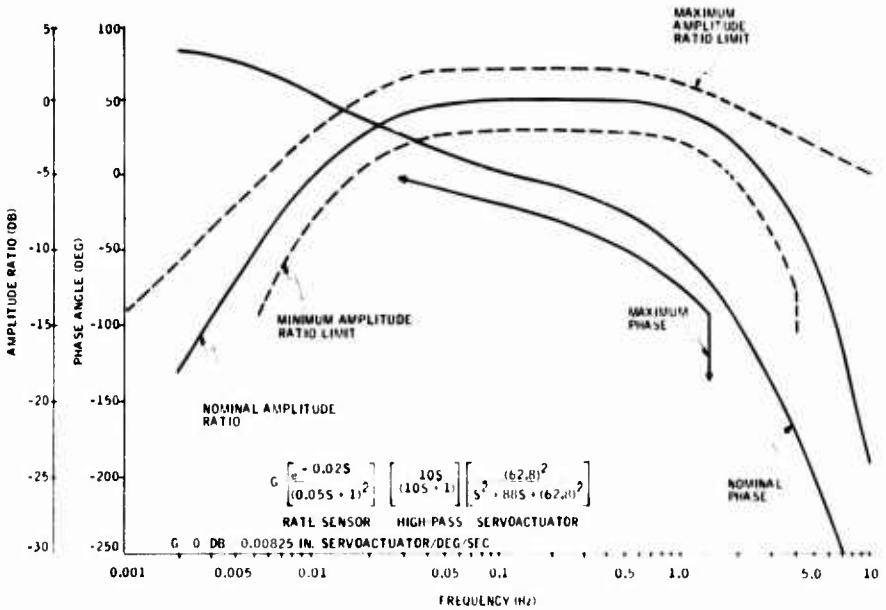

B. RESPONSE REQUIREMENTS

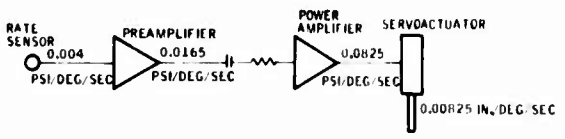

C. COMPONENT GAINS

Figure 3. Roll-Axis Design Data.

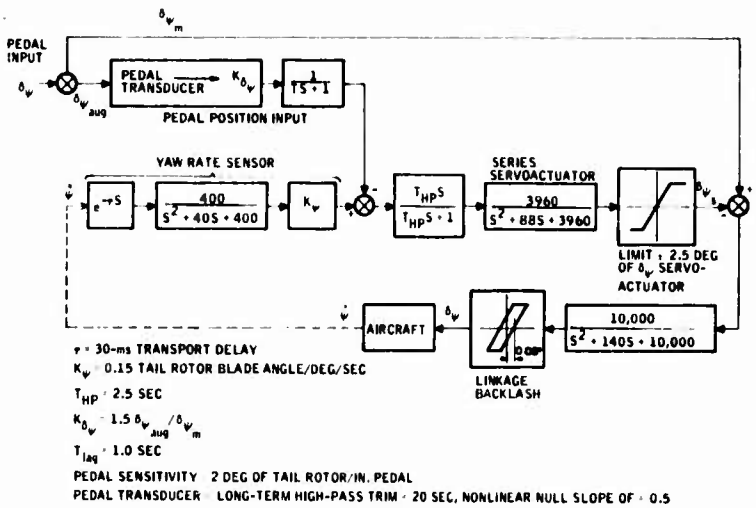

A. ANALYTIC BLOCK DIAGRAM

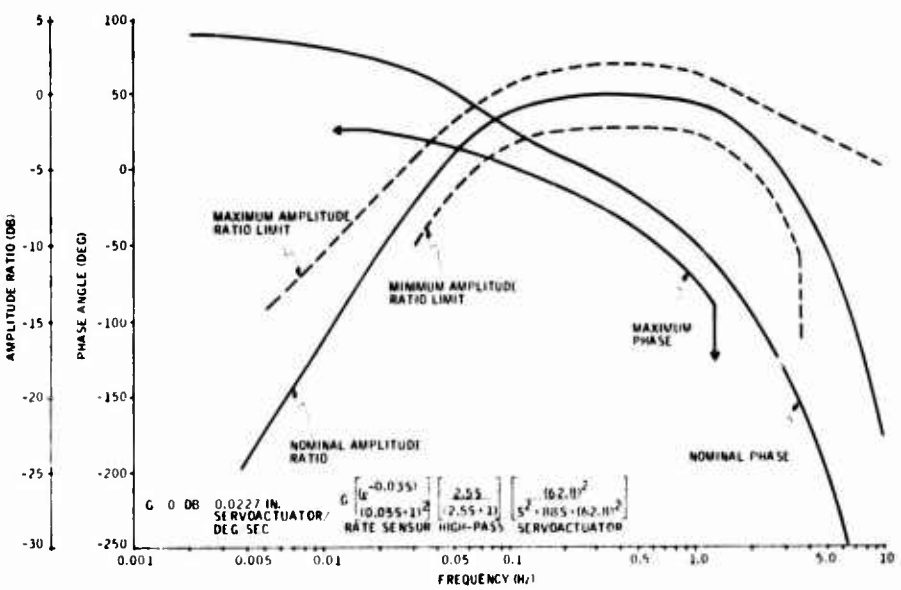

B. RESPONSE REQUIREMENTS

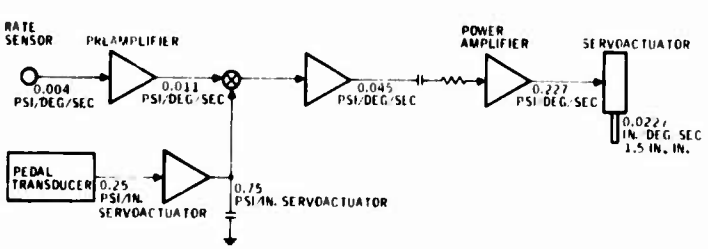

C. COMPONENT GAINS

Figure 4. Yaw-Axis Design Data.

SECTION III
HARDWARE DESIGN AND FABRICATION

HARDWARE DESIGN GOALS

The three-axis hydrofluidic stability augmentation system is made up of three individual pitch-, roll-, and yaw-axis controllers. These controllers were designed to meet the following basic guidelines specified at the beginning of the hardware design phase:

- Make each controller as small as practical.
- Use common parts.
- Provide null adjust and built-in-test (BIT) capability.
- Make providions to interconnect pitch and roll controllers without additional tubing (this goal was later rejected).

The pitch-axis controller is shown in Figure 5, the roll-axis controller in Figure 6, and the yaw-axis controller in Figure 7. Hardware schematics of the three controllers are shown in Figure 8. An exploded view of the yaw-axis controller is shown in Figure 9.

CONTROLLER PACKAGES

Pitch Axis

The pitch-axis controller (Figure 5) consists of a vortex rate sensor (built integrally into the manifold), four hydrofluidic amplifiers (one located underneath the controller), a lead-lag, and a high-pass network. Null adjust and BIT buttons are also located underneath the controller and thus are not visible.

The signal and reference ports connect tc the servoactuator.

Roll Axis

The roll-axis controller (Figure 6) is the least complex of the three axes. It consists of a vortex rate sensor, two hydrofluidic amplifiers, and a high-pass network. The large high-pass capacitor volume required to provide the proper high-pass time constant (10 seconds) prevented the package from being much smaller than the pitch-axis controller. The BIT button is shown.

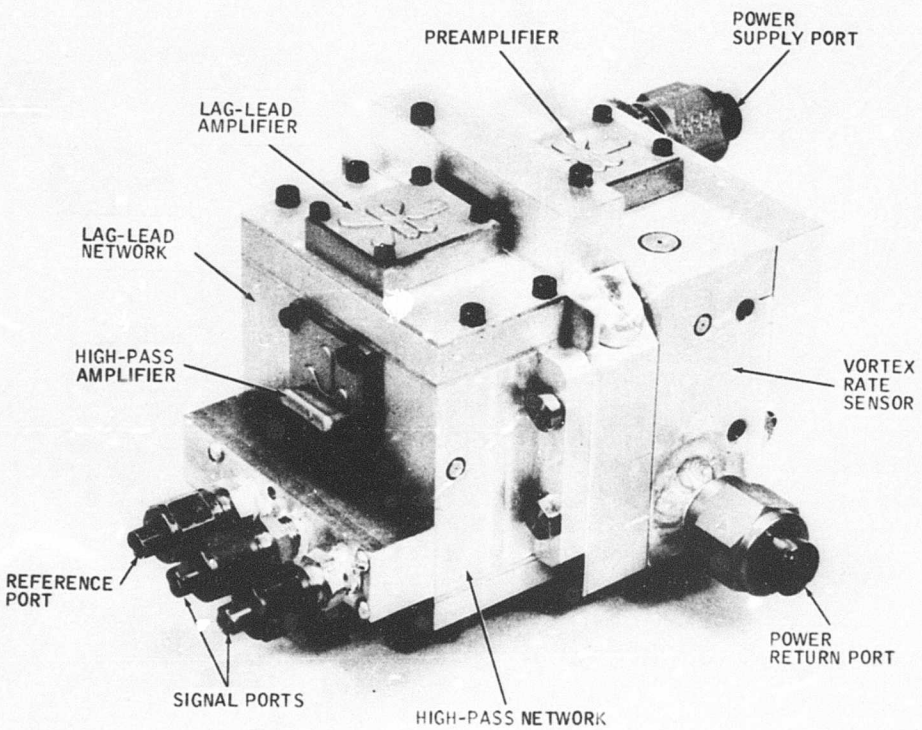

Figure 5. Pitch-Axis Controller.

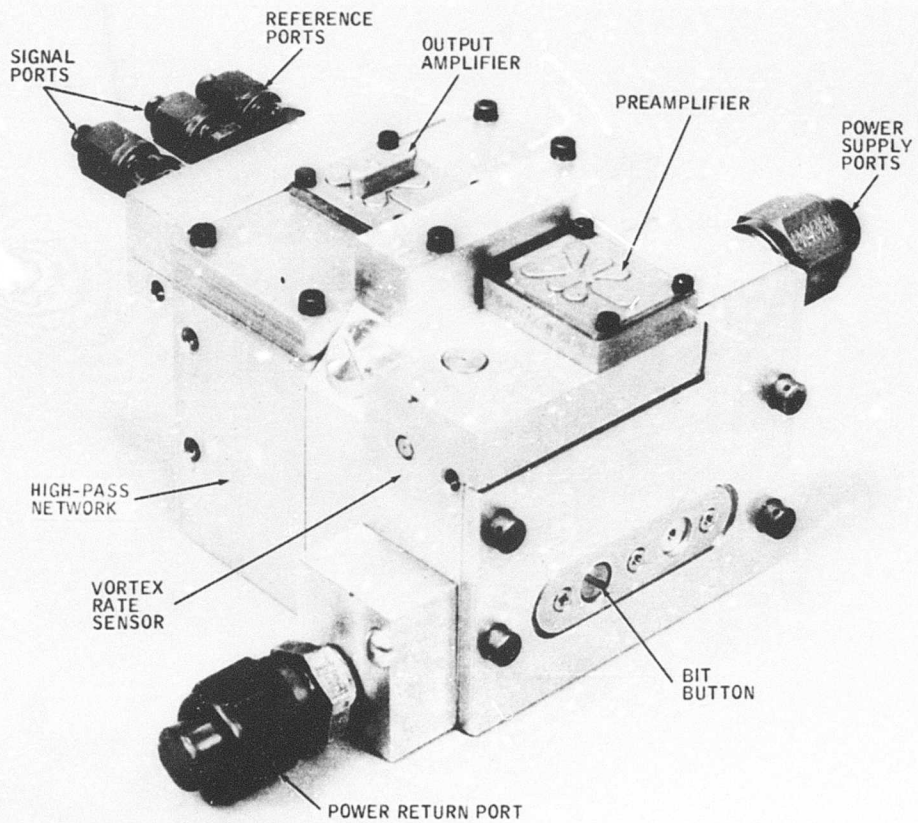

Figure 6. Roll-Axis Controller.

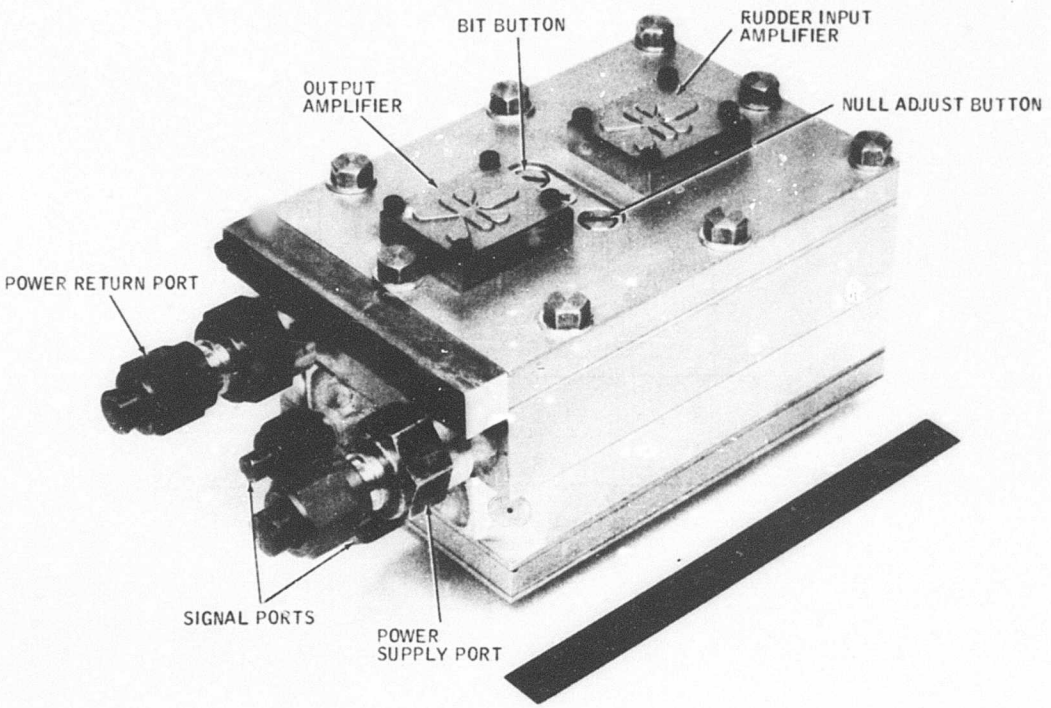

Figure 7. Yaw-Axis Controller.

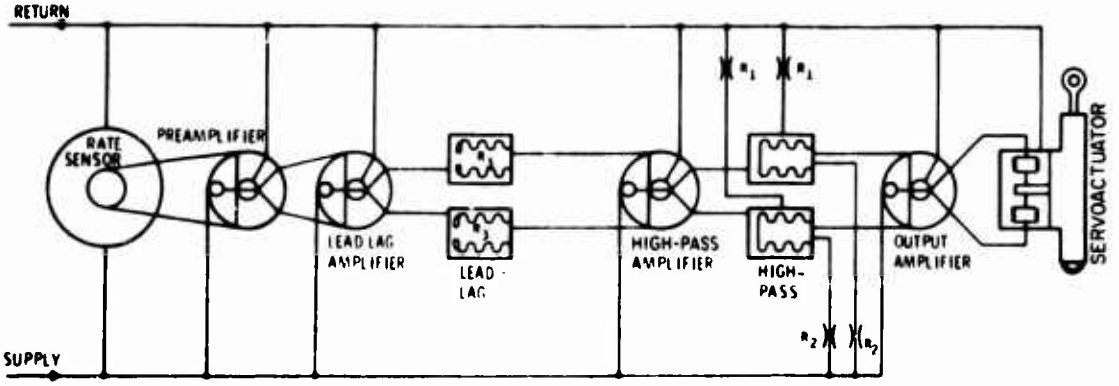

A. PITCH AXIS

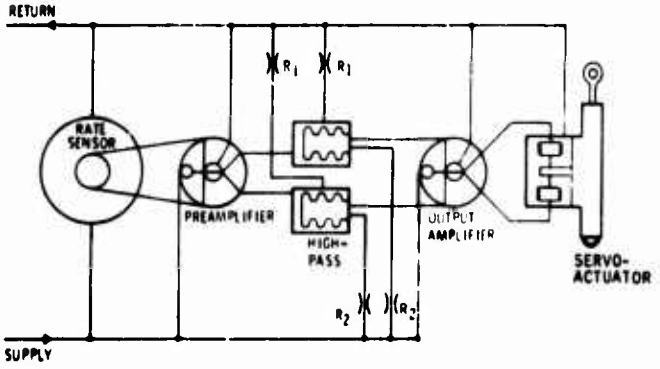

B. ROLL AXIS

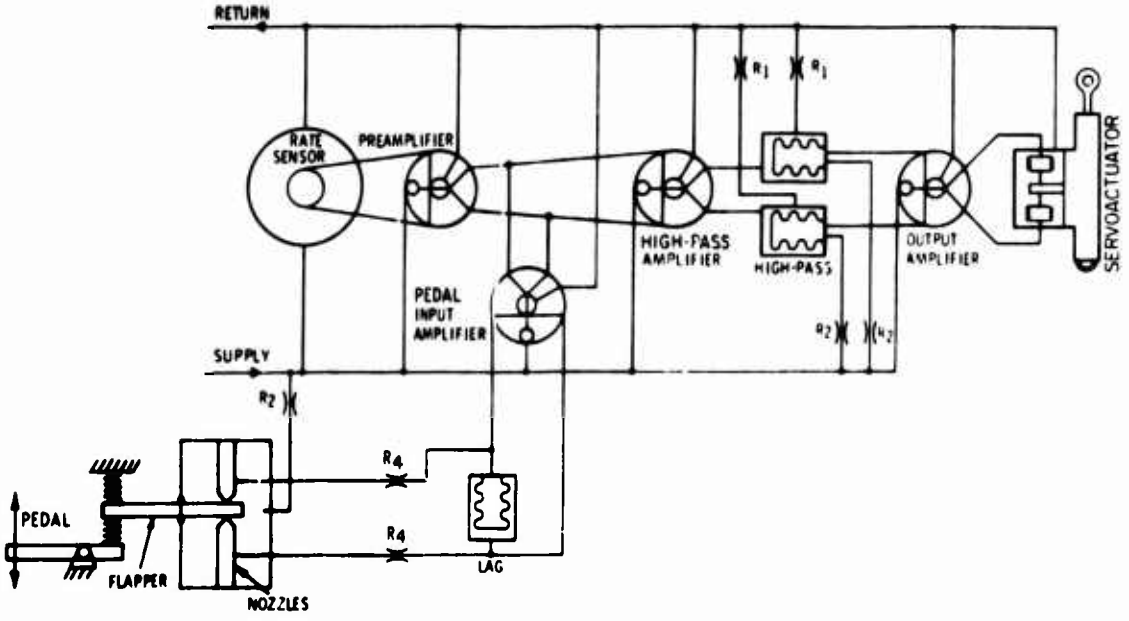

C. YAW AXIS

Figure 8. Hardware Schematics.

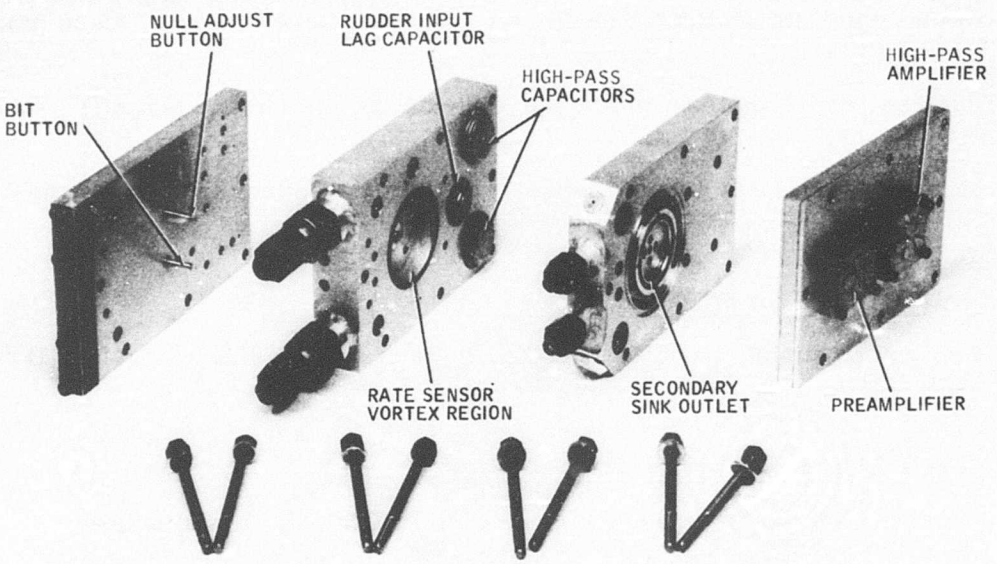

Figure 9. Yaw-Axis Controller -- Exploded View.

Yaw Axis

The yaw-axis controller (Figure 7) is very much like the roll axis, containing a vortex rate sensor, three hydrofluidic amplifiers, a high-pass and a lag network, and the pedal input transducer (shown in Figure 1). The null adjust and BIT buttons can be seen between the two amplifiers.

The exploded view of the yaw-axis controller (Figure 9) typifies the fabrication and packaging techniques used.

The top and bottom cover plates are of a sandwich construction. These cover plates have a center core with channels on each side. Thin sheets of metal are bonded to the center core, resulting in permanently sealed manifold plates. The fluidic amplifiers are bolted to these manifolds.

The two center plates contain the vortex rate sensor and shaping networks.

External sealing is accomplished with O-rings and/or by permanent bonding. Packaging details are discussed later.

SYSTEM POWER SUPPLY

Two power supply circuits were considered during this program. Both were mechanized using standard off-the-shelf components.

Parallel Circuit (Spool Valve Servoactuators)

Figure 10 shows the circuit proposed for flight testing the system using the spool valve servoactuators. The 1500-psi aircraft supply will power the three controller packages in series and the servoactuator in parallel with the three controllers.

A flow control valve was used to regulate 2.3 gpm through the controllers. A relief valve was set at 500 psi so that the controllers could be designed to withstand a proof pressure of 750 psi instead of 2250 psi; this allowed the controllers to be built smaller and lighter.

A back-pressure regulator was used to isolate the controllers from return line surges caused by other aircraft components and servoactuator motions. This circuit was used throughout the test program when using the spool valve servoactuators.

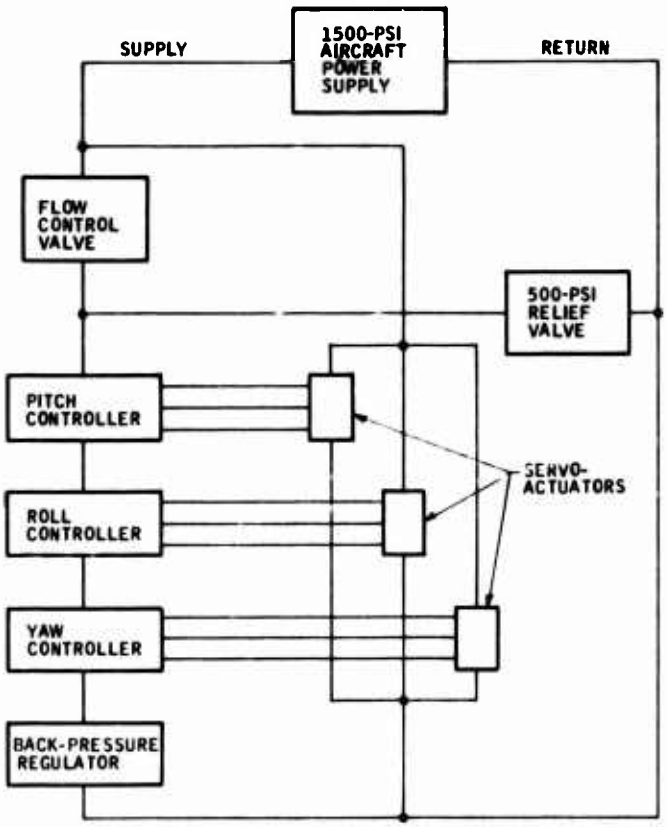

Figure 10. Parallel Power Supply Circuit.

Series Circuit (Vortex Valve Servoactuators)

Later in the program, a second power supply circuit was designed to provide for future flight testing of the fluidic system using vortex valve servoactuators. These servoactuators* used fluidic vortex valves as the servovalve second-stage amplifier instead of the conventionally-used spool valve. The vortex valve servoactuator requires a larger steady-state flow than the spool valve servoactuator. The total controller-actuators' required flow (4 gpm) exceeded that available from the aircraft supply when operated in parallel. Therefore, the series circuit shown in Figure 11 was designed.

The controllers were placed "upstream" of the vortex valve servoactuators to eliminate the effects of their nonconstant discharge flow. The 1200-psi relief valve will eliminate any effects due to the nonconstant servoactuator flow demand.

*Described in detail in USAAVLABS Technical Report 70-52, "Fluidic Servoactuators for Three-Axis Fluidic Stability Augmentation System," September 1970, Contract DAAJ02-70-C-0007.

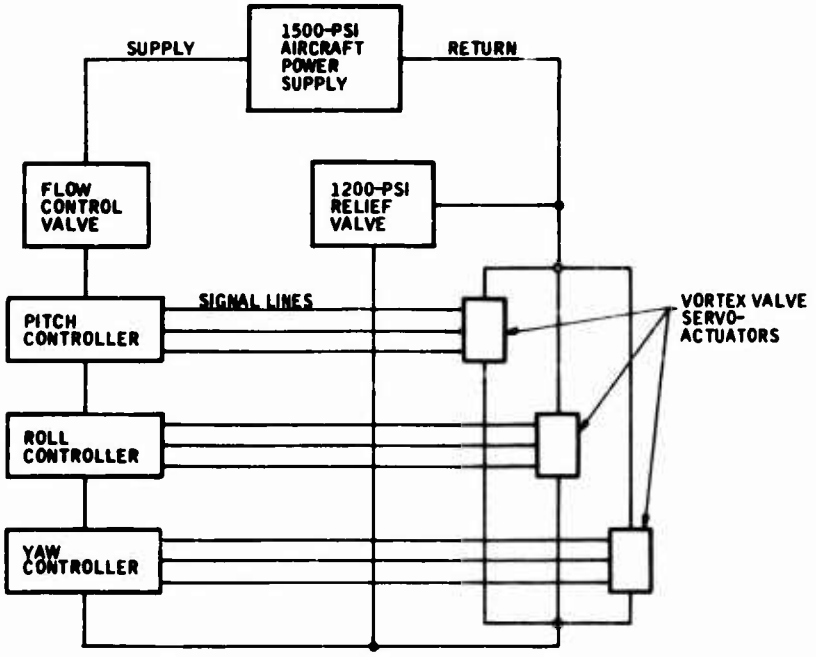

Figure 11. Series Power Supply Circuit.

This mechanization, as shown in Figure 11, now required the controller packages to withstand the higher 2250-psi proof-pressure testing, so manifold strengthening was required. This development effort is described in Section IV.

PACKAGING DETAILS

Size

Two major hardware mechanization considerations that involve a large volume in any hydrofluidic design are O-rings and the tube fittings for supplying the oil from the power supply. Smaller O-ring use would allow the overall size of the controllers to be reduced. Because the channels should be kept large to eliminate unwanted temperature effects due to viscosity losses, the only way the O-ring size could be reduced was to use an O-ring with a smaller cross section. Two nonstandard O-rings were selected on the basis of the amplifier port sizes used on previous systems. The internal diameters were 0.156 in. and 0.187 in. The cross sections were 0.038 in. and 0.040 in., respectively. This reduced the outside diameter from 0.316 in. (standard) to 0.230 in. for the small one and from 0.348 in. (standard) to 0.260 in. for the large one.

This size reduction allowed the power and control ports of an amplifier to be in a different hardware block than the return output ports. As can

be seen in Figure 12, the separation line (between individual blocks) would have passed through a seal point using the standard O-ring cross section.

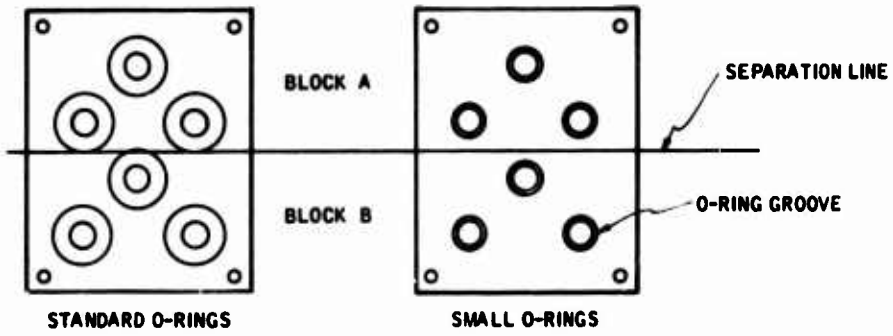

Figure 12. Use of Nonstandard O-Rings.

The size of the tube fittings which screw into a block for 2.5-gpm flow is comparatively large. This can be seen in Figures 5, 6, and 7. To reduce the depth, diameter, and clearance for a wrench, most of the tube fittings were welded onto the controllers. Because the lines to the servoactuators are small, the savings by welding these to the controllers were not considered sufficient to warrant the effort.

Manifolding

The manifolds to supply the power and signal ports to the amplifiers and capacitor were made by milling the necessary channels in the top half and/or bottom half of an aluminum plate. This allowed the channels to be routed close together and, as needed, to cross one another. The channels were sealed by bonding a 1/16-in. aluminum plate to the channel plate with an epoxy tape. This technique made for a very compact manifold as compared with drilling and plugging a solid block of aluminum. It also was smaller than if a gasket were used to seal the channels and screws were used to join the plates together. The epoxy served both functions, sealing and joining.

Another deviation from past practice was to mount the amplifiers on other than the top surface. All previous controllers had the amplifiers on the top to bleed off any air that might enter the amplifiers. Experience had shown that this was not necessary. Allowing the amplifiers to be mounted in any orientation gave much more latitude in arranging the circuit into a compact unit. The only restraint on orientation was that of the capacitors. They were mounted so that any air that entered them would rise to the top and would exhaust out to the return line. This makes the controllers self-purging, eliminating any need for special filling techniques.

Common Parts

To reduce the cost of this fabrication effort and future efforts, as many common parts as possible were designed into the three-axis system. The rate sensor for the pitch axis needed a 0.020-sec emptying time (rate sensor volume/flow rate), while the roll-axis and yaw-axis rate sensors needed only a 0.050-sec emptying time. It was decided to make all three identical with a 0.020-sec emptying time. This allowed the same coupling element, pickoff, and coupling plate to be used in all three sensors. All three controllers used the same amplifiers. The amplifiers could be used on any controller and in any location on each controller.

The yaw-axis controller configuration was unique as compared with the pitch and roll controllers. The yaw-axis controller had to have the input axis vertical as compared with the roll-axis and pitch-axis controllers, which had their input axes horizontal. The yaw-axis controller also had a pilot input mechanism. Because of these items, the yaw-axis controller did not have as many common parts as the roll-axis and pitch-axis controllers. However, the complete rate sensors for the roll and pitch axes were identical.

Connection of Roll-Axis and Pitch-Axis Controllers

For possible elimination of two tube fittings, one on the roll controller and one on the pitch controller, the controllers were designed so that they could be joined with an O-ring seal. This meant that the power outlet of the roll axis would have to line up with the power inlet of the pitch axis. By using an adapter plate with a fitting attached, the units could be run separately.

Null Adjust and BIT Button

Previous testing had shown that it was practical to add a null adjust vane in the vortex chamber of the rate sensor without increasing noise. A shaft with a blade on the end equal to the height of the vortex chamber was designed into the rate sensor. By turning the shaft, the null of the rate sensor could be adjusted to zero output differential pressure.

The BIT button was made almost identical to the null adjust except that it was made so that the blade could be inserted into or retracted from the vortex chamber of the rate sensor. By pushing the blade into the vortex chamber (see Figure 9), a bias was created that appeared at the pickoff like a turning rate. The force to retract the blade was produced by the internal pressure in the vortex chamber. The BIT button simulates a step input to the rate sensor, allowing a convenient means of checking on the performance of the controller and servoactuator without physically moving the controller.

COMPONENT DETAILS

Vortex Rate Sensor

The vortex rate sensor was quite similar in design to sensors built in the past. The pickoff was identical in configuration to past pickoffs except the number of bends in the ports from the pickoff to the first-stage amplifier was reduced. From the 0.017-in. by 0.035-in. pickoff ports, the flow made only one bend into a 0.156-in.-diameter port right to the amplifier. Figure 13 shows a cross section of the roll-axis controller and shows this straight run to the amplifier.

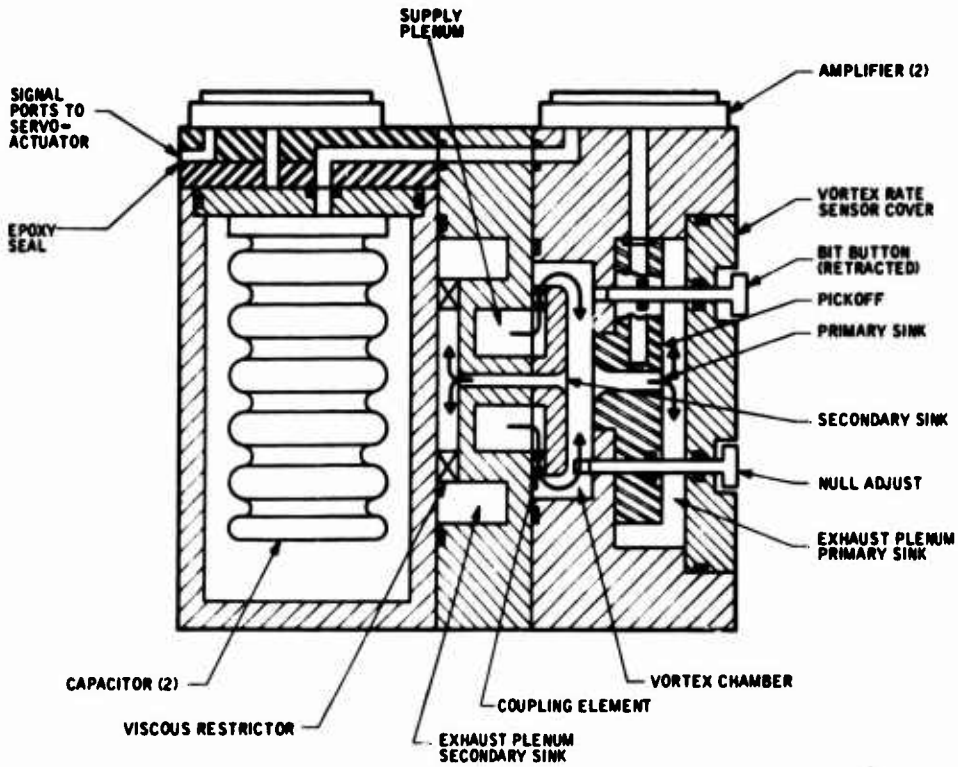

Figure 13. Roll Axis -- Cutaway View.

As shown, the coupling element on these sensors was essentially folded around so that the flow was from the inside to the outside and then around into the vortex chamber. Previous units had the flow passing from a plenum around the outside of the coupling element through the element from outside to inside and into the vortex chamber. The design used here makes the rate sensor a little thicker, but it reduces its diameter considerably. This configuration was also compatible, volume-wise, with the capacitor bellows.

To get the desired 0.020-sec emptying time, it was necessary to use 2.2 gpm of oil. To stay below a Reynolds number of 2000 in the primary sink, for noise reasons, and to keep the gain high (a small primary sink diameter), the sensor was designed with two sinks. Because the flow through each sink was different, the viscous losses through each were different. This caused the flow split (ratio of flow through the secondary to primary sinks) to vary with temperature, which, in turn, caused the gain of the rate sensor to vary with temperature. By placing a viscous restriction in the secondary sink flow path, the flow split could be kept almost constant over the design temperature range. If necessary, the rate sensor could be overcompensated to correct for gain changes in other elements such as the amplifiers. This is discussed in Section IV.

Shaping Networks

All three controllers contained high-pass circuits with different time constants. The pitch controller also contained a lead-lag circuit, and the yaw controller, in conjunction with the pilot input device, contained a lag circuit. The capacitor sizes were calculated using the input and output impedances of the amplifiers as the resistances in the various equations for a lag, high-pass, and lead-lag. The actual physical sizes of the capacitors were then determined on the basis of the bellows available from the vendor.

Amplifiers

The amplifiers were of the type previously developed and improved under the study phase contract. The amplifiers, designated FG1001-AA09, were made by the electroformed conductive wax (ECW) process. An injection mold was machined for the FG1001AA09-type amplifier. Using this mold and a baseplate, conductive wax was injected into the mold. Nickel was then electrodeposited onto the resulting wax mandrel and baseplate. The wax was then removed, leaving a cavity that is the amplifier. This process produces a very repeatable unit, leaktight both internally and externally, and capable of high internal pressure (3000 psi).

Pedal Input Device

The pedal input device, which was part of the yaw controller, was a mechanical (rudder pedal motion)-to-fluidic transducer. The motion of the pedal was transferred to a push-pull cable that ran from the rudder pedals back to the controller. At the controller, the cable operated a motion-reducing arm. The other end of the arm operated against a

spring, which, in turn, pushed on a flex pivot similar to that in a servovalve. This linkage reduced rudder pedal motion from ±3.25 inches to plus or minus a few thousandths of an inch. The end of the flex pivot varied the opening to two nozzles which were connected to an amplifier. A schematic of this device is shown in Figure 14.

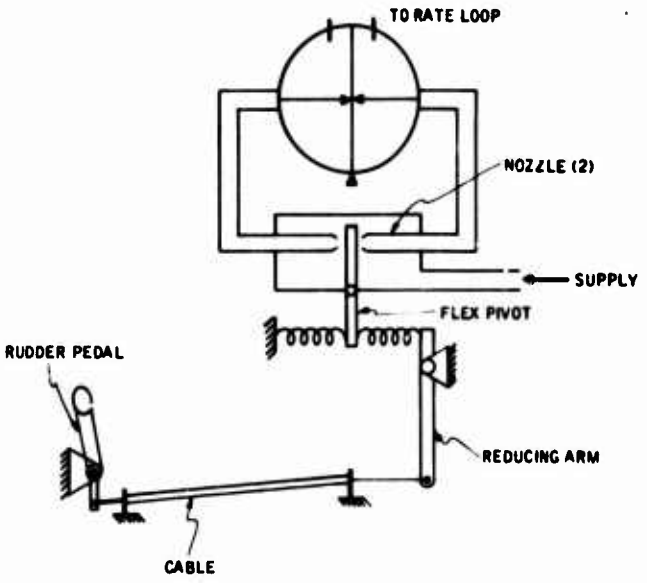

Figure 14. Pedal Input Device Schematic.

SECTION IV
DEVELOPMENT TESTING

This section discusses the development testing conducted on the individual components and circuits of the three-axis system. Fmphasis is given to the various problems encountered and their resolution.

OBJECTIVES

Initial objectives of the development testing phase of this program were to:

- Uncover any fabrication deficiencies.
- Operate rate sensors with a flow of 2.2 gpm in order to obtain a 0.020-sec time delay. This is a substantial advancement over the 0.050-sec-delay sensor used in the previous program.
- Solve noise problems which may be introduced by the higher response, temperature compensation, new manifold design, BIT and null adjust vanes, power supply, and close proximity of other axes.
- Reduce system sensitivity to small changes in flow. (Interaction between axes or between a single axis and its servoactuator is likely if controller output changes drastically with supply flow.)
- Demonstrate operation of the complete three-axis system using a single power supply. (System includes three controllers, two regulators, three servoactuators, a filter, a relief valve, four solenoid valves, and plumbing.)
- Demonstrate BIT and adjust its angle to provide the appropriate step rate signal in each axis.
- Adjust gains and time constants to provide required frequency response.
- Incorporate temperature compensation to minimize gain changes over the temperature range from 60°F to 185°F.

COMPONENT DEVELOPMENT

Amplifiers

Previous Amplifiers

Figure 15 shows the performance of the amplifers used in a previous flight test program (Contract DAAJ02-67-C-0056). These amplifiers were operated at a lower supply flow and nearly dead-ended during the flight test program, which allowed suitable performance "across center." Even at lower flows, these amplifiers experienced some nonlinearities, as shown in Figure 15A, when flow-loaded (an amplifier of the same type used as a load).

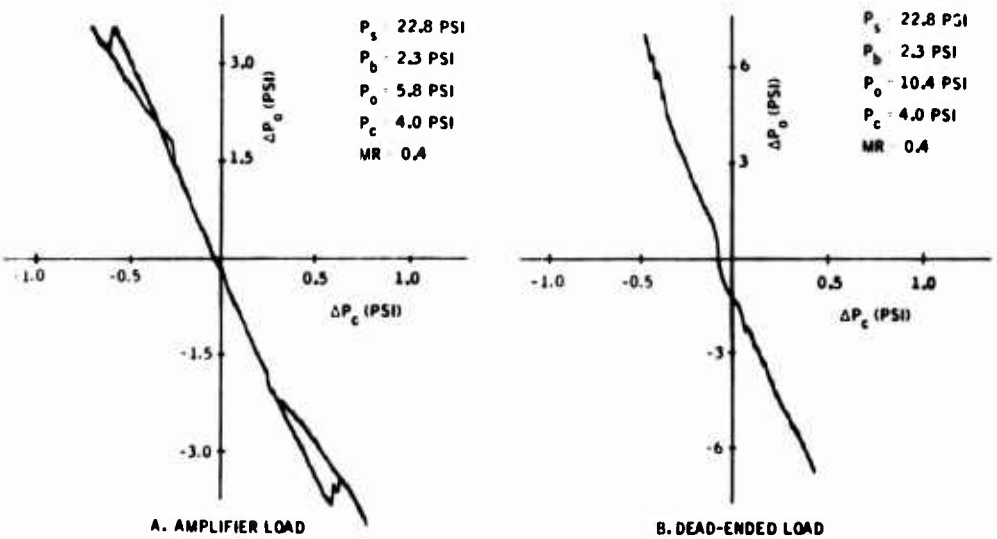

Figure 15. Original Amplifier Performance.

Present Configurations

Amplifier improvement was accomplished through large-scale model studies on Contract DAAJ02-68-C-0039. Two types of molds (for future electroforming) were fabricated. The low-profile design can be seen in Figure 16, where the two top amplifiers are relatively flat. With this amplifier, the crossover is milled into the thick baseplate. Also shown in Figure 16 is the second design with the crossover milled into the mold. This second design with the protruding crossover is shown electroformed on a thin baseplate which does not contain a crossover. The protruding crossover design was also electroformed over a thick baseplate to provide an amplifier with both an upper and a lower crossover.

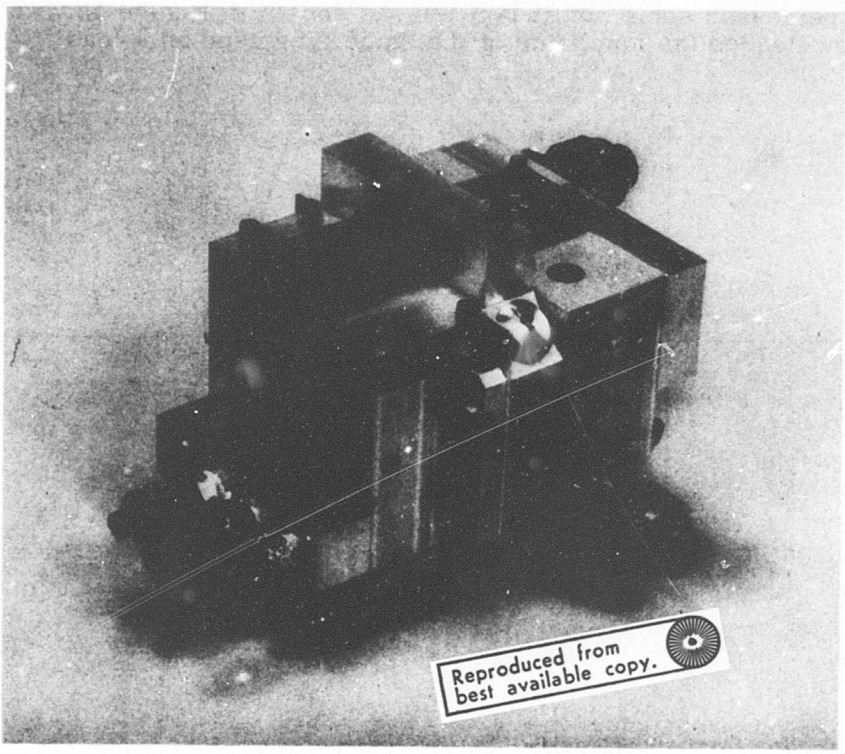

Figure 16. Controller Showing Amplifier Types.

Initial development tests were conducted with the molds before the amplifiers were fabricated. Molds were bolted to baseplates and tested as amplifiers. Although test results were reasonable, they were not conclusive, since there was significant external "weepage" from the "pseudo" amplifier, with the possibility of internal leakage.

Performance characteristics of the low-profile amplifiers (top of pitch axis in Figure 16) are shown in Figure 17. Nonlinearities are extended well outside the normal operating range, and overall performance, including noise, improves substantially at lower flows.

Curves of the thin-baseplate amplifier with the protruding crossover (front face of pitch axis in Figure 16) are shown in Figure 18. Flow-loaded characteristics of this amplifier appear superior to those of the other designs.

Later systems tested at lower flows showed that both the low-profile design and the protruding crossover design have excellent performance, with neither being distinctly better than the other. The old design (Figure 15) is definitely unsatisfactory for the wide range of loadings and temperatures encountered in this program.

Flow Straightener Use

Restrictors were placed under the power ports of amplifiers during development tests to reduce flow and thereby reduce system noise. Initial tests showed an increase in noise which appeared to be generated by the restrictor. A flow straightener shown in Figure 19 was designed to provide an orifice restriction and several layers of filter screen to eliminate any vortices which might be shed by the restrictor. This flow straightener was a major contribution to the reduction of system noise.

Proof-Pressure Tests

Proof-pressure tests of the first electroformed amplifiers showed serious bonding problems in the 1000- to 1400-psi range. Investigations uncovered inadequacies in the electroforming process, resulting in a poor bond between the amplifier and the baseplate. The sensitizing process was revised, and one resultant test amplifier was pressurized to 4000 psi. All other amplifiers have been cycled 10 times up to a pressure of 2250 psi without failure. Proof pressure was marked on the side of each amplifier after proof test to prevent use of untested amplifiers.

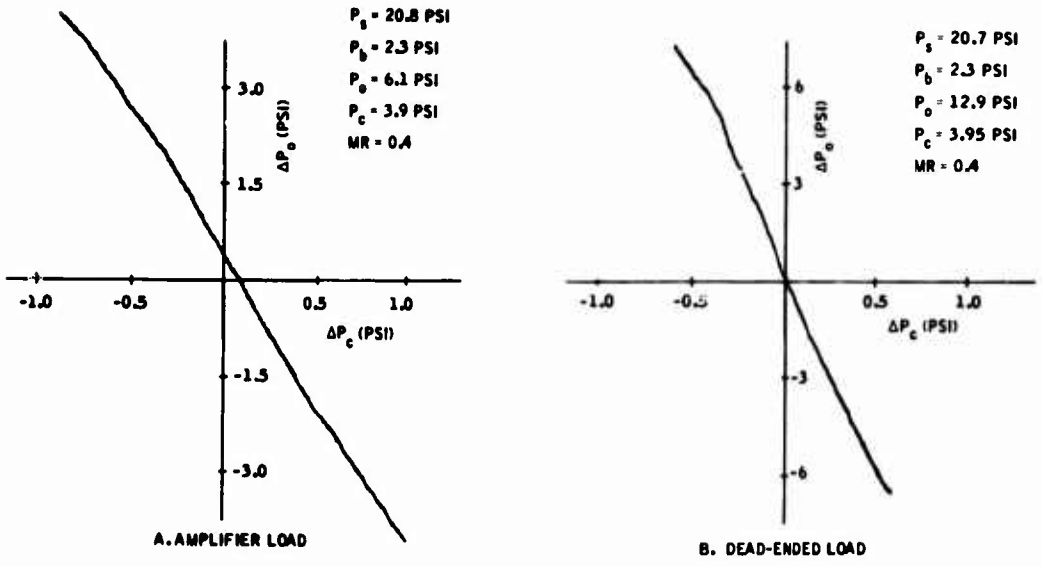

Figure 17. Low-Profile Amplifier Performance After Redesign.

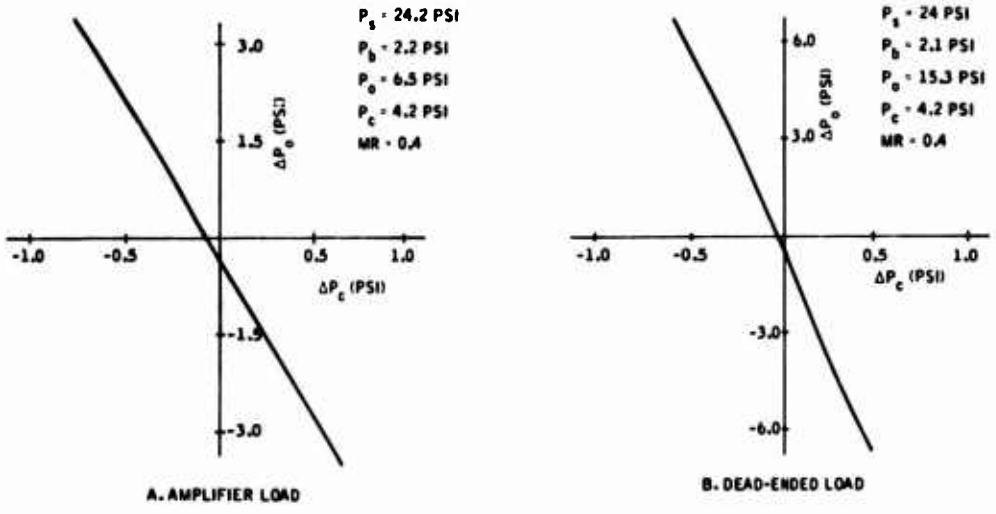

Figure 18. Normal Amplifier Performance After Redesign.

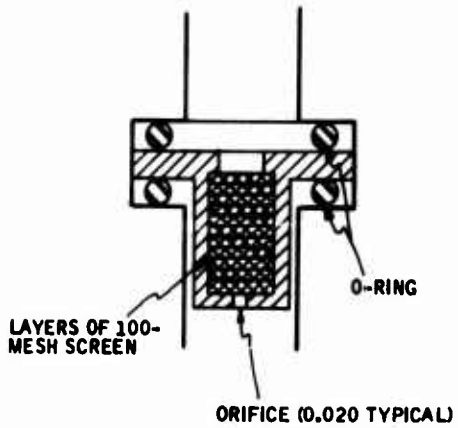

Figure 19. Flow Straightener.

Rate Sensor

Configuration

A cutaway view of the vortex rate sensor is shown in Figure 13. Flow from the supply passes through the coupling element and into the vortex chamber (pancake region). Approximately 20 percent of the flow passes through the primary sink into the exhaust plenum primary sink and returns to the supply reservoir. The remaining 80 percent of the flow passes through the secondary sink, the viscous restrictor (for temperature compensation), and the exhaust plenum secondary sink, and returns to the supply reservoir.

This sensor was designed for a large flow rate of 2.2 gpm in order to obtain a time delay as low as 0.020 sec. The primary sink was small to obtain a large scale factor, and the secondary sink was large to reduce emptying time (to obtain fast response). Flow split was 8:1 for this sensor as compared with 4:1 for the previous flight test sensor.

Testing

Development testing of the rate sensor concentrated on minimizing noise while obtaining a high response. The large flow split between secondary and primary sinks resulted in a scalefactor substantially lower than that predicted. Performance was also

somewhat erratic and unpredictable. Two approaches were investigated to eliminate the high flow split: (1) operate at a higher pressure to increase primary sink flow and then reduce the size of the secondary sink;(2) add a third outlet which would be a bleed annulus around the primary sink.

Dead-ended single-sink performance tests were conducted to determine the limiting Reynolds number (N_R) where noise becomes excessive. Noise was converted to units of degrees per second, since both noise and scale factor increase with flow. Initially, the rate sensor output was dead-ended into a transducer and operated with primary sink Reynolds number in excess of 6000. When dead-ended, the sensor output signal-to-noise ratio tended to be the best at the higher Reynolds number.

Results were less satisfactory when the sensor pickoff was loaded into an amplifier. Tests at 120°F showed that noise increased sharply at a pressure of about 25 psi (N_R = 2700).

Figure 20 shows the bleed annulus incorporated into the pickoff. This annulus has an area of 0.008 in.^{2}, more than twice that of the primary sink. Flow splits are approximately 0.6 gpm for primary and secondary sinks and 1.0 gpm for the bleed annulus. At 120°F and 2.2 gpm, the sensor pressure drop was 25 psi with the annulus and 75 psi without the annulus. Testing substantiated that use of the bleed annulus was a satisfactory solution.

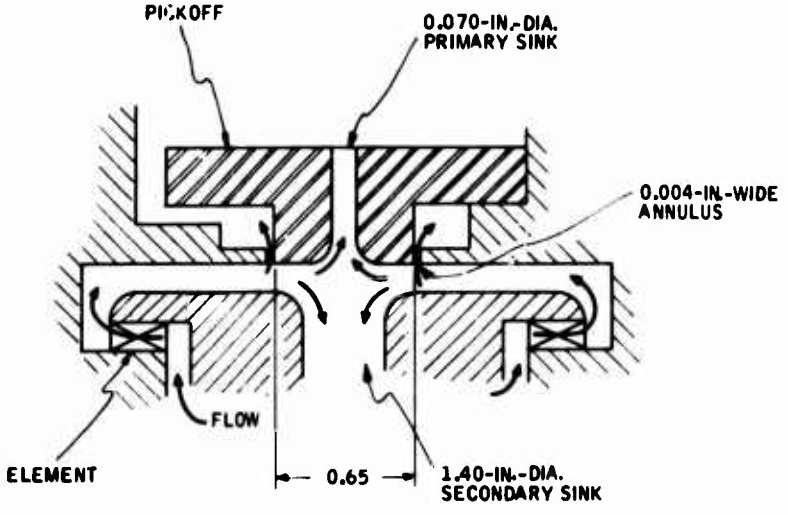

Figure 20. Bleed Annulus.

The final sensor configuration included a compromise: primary sink flow was increased and the bleed annulus was added.

Amplifier - Sensor Monitoring

Concurrent with the investigation of return line noise and back-pressure studies (discussed later) was a study to determine the best method of matching the amplifier to the rate sensor; typically, scale factor would drop by more than half and noise would increase by a factor of two, reducing signal-to-noise ratio by a factor of about 5. Figure 21 shows three approaches to minimizing this problem. All of these circuits were considered on the premise that drawing flow from the pickoff (as in Figure 21A) will create a disturbance in the primary sink which results in the increased noise levels. The circuit in Figure 21B is the most complex but appears to have the greatest advantage in reducing noise. Bias flow through restrictors R_1 supplies flow to the amplifier, eliminating or reducing flow from the pickoff. A high flow through R_1 would also increase the input impedance of the amplifier while reducing the output impedance of the pickoff. This bias flow technique minimizes the flow disturbance in the primary sink while improving the impedance match and increasing scale factor.

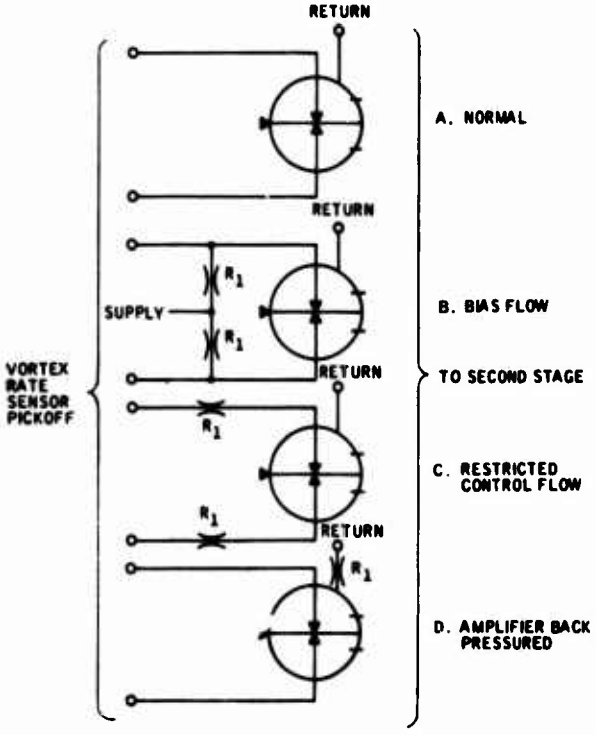

Figure 21. Vortex Rate Sensor - Amplifier Matching Techniques.

Figure 21C shows a circuit which restricts the amplifier control ports to reduce the flow disturbance in the primary sink. Reduction of scale factor is the major drawback. Providing the amplifier with a back pressure by restricting its return as shown in Figure 21D is another solution. This technique also has the disadvantage of reducing the effective amplifier input impedance.

Test results showed that the use of bias flow (as in Figure 21B) increased scale factor and in most cases reduced noise. Tests on other circuits (Figures 21C and 21D) showed no advantage. Results of these tests are not conclusive, since these tests were performed before the return line noise problem (discussed later) was isolated. Matching techniques, such as the use of bias flow, were not required in the final hardware configuration, but were presented here for future consideration.

Final performance data obtained on the vortex rate sensor using the normal matching technique is shown in Table II.

TABLE II. VORTEX RATE SENSOR FINAL PERFORMANCE DATA

Load	Flow* (gpm)	Pressure (psi)	Pickoff Static Level (psi)	Gain (psi/deg/sec)	Noise (psi) Peak-to-Peak	
					Unfiltered**	Filtered at 5 Hz
Ports Blocked	2.2	24.0	13.5	0.013	0.0060	-
With Amplifier Load	2.2	24.0	8.0	0.005	0.0075	0.00013

*Temperature 120°F.

**Contains all noise frequencies up to Sanborn Recorder limit of about 50 Hz.

Networks

Most shaping networks were designed with time constants larger than required. Adjustment was made by first running frequency response tests to determine the amount of change required. If the time constant required a 25-percent reduction, length of the bellows would be reduced by 25 percent. This method accomplished the required change without the repeated iterations associated with alternate methods. Adjustment by reducing the bellows length was used whenever the time constant was

excessive. Adjustment with restrictors (such as bias restrictors) was used whenever it was necessary to increase time constants.

High-Pass Network Example

The mechanization of a high-pass circuit (see Figure 22) is discussed here as an example. The transfer function of this circuit is

$$\frac{\Delta P_o}{\Delta P_c} = \frac{TS}{TS + 1}$$

where

$T = (R_o' + R_i')\,C$

R_o' = Effective amplifier output impedance $\frac{R_o R_3}{R_o + R_3}$ $\left(\frac{\text{lb-sec}}{\text{in.}^5}\right)$

R_i' = Effective amplifier input impedance $\frac{R_i R_2}{R_i + R_2}$ $\left(\frac{\text{lb-sec}}{\text{in.}^5}\right)$

C = Bellows capacitance $\left(\frac{\text{in.}^5}{\text{lb}}\right)$

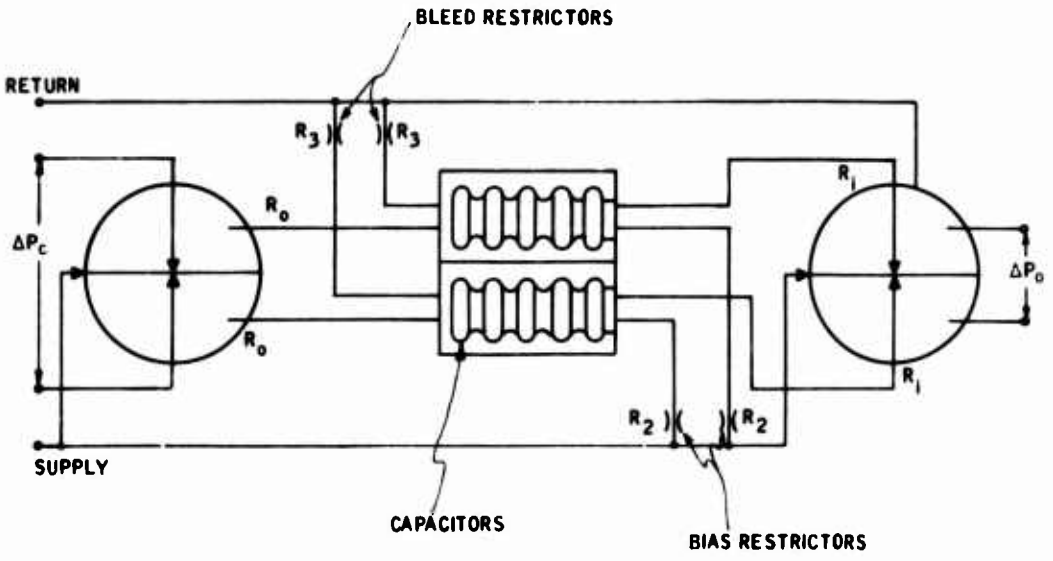

Figure 22. High-Pass Circuit Schematic.

Bias restrictors, R_2, are usually small and have an impedance of about 200 lb-sec/in.^{5}. The amplifier input impedance (R_i) will be about 20 lb-sec/in.^{5} under these conditions, resulting in an effective amplifier input impedance, R_i', of about 18 lb-sec/in.^{5}. Increasing the size of R_2 will increase the bias flow without substantially reducing its resistance.

This increase in bias flow will greatly increase amplifier input impedance R_i as well as R_i'. Effective amplifier input impedance, R_i', can therefore be increased by enlarging the size of bias restrictor R_2. This trend will continue until the area of bias restrictor R_2 approaches that of the amplifier control port. A typical method for increasing the high-pass time constant would be to increase effective amplifier input impedance, R_i', by increasing the physical size of bias restrictor R_2.

Nonlinear Bellows Effect

Early tests on the pitch-axis controller showed the need for increasing the high-pass time constant. Increasing the size of bias restrictor R2 did not increase the high-pass time constant as expected. Further investigations showed that a nonlinear bellows was responsible.

Characteristics of the pitch-axis controller high-pass bellows are shown in Figure 23. When bias flow was small, the bellows

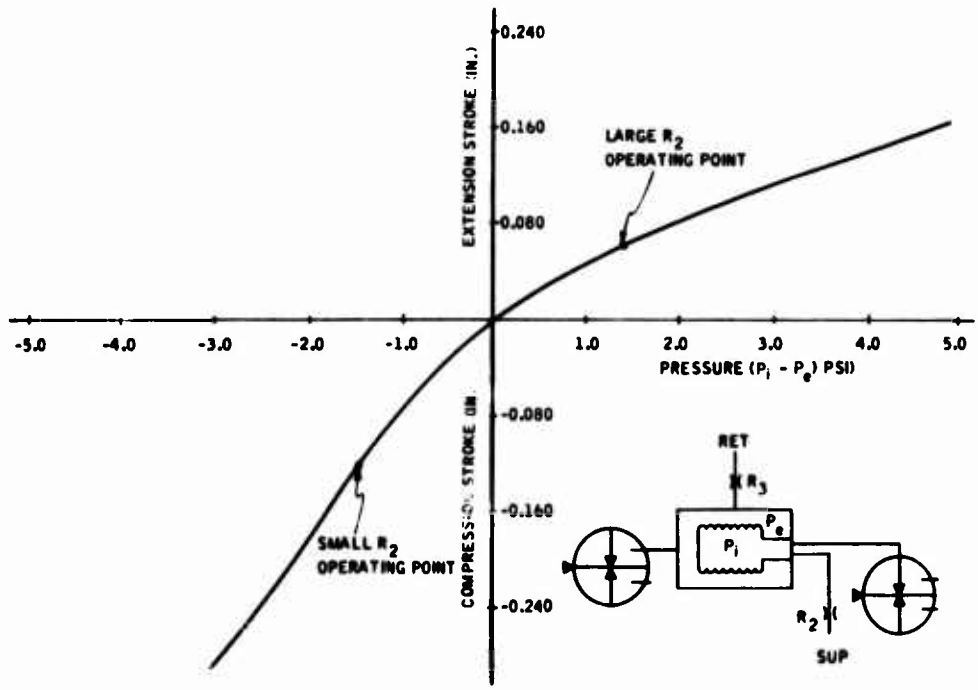

Figure 23. Performance Characteristics of Pitch-Axis Controller High-Pass Bellows (Original Bellows).

were operating in compression, where the external pressure (P_e) was greater than the internal pressure (P_i). It can be seen that the bellows were more flexible at this condition, and therefore their capacitance was high. When the physical size of R_2 was increased (R_i' increased), the bellows were in tension and relatively stiff, resulting in low capacitance. It can be seen that changes in fluid temperature would also vary the capacitance; temperature (viscosity) changes cause static pressure level changes which shift the operation point.

Alternate off-the-shelf designs were selected, tested by the vendor, and supplied as replacements for the nonlinear design. A characteristic curve of the replacement bellows for the pitch-axis controller is shown in Figure 24.

Although nonlinear bellows create a problem when a system is initially adjusted, this effect could be an advantage in future systems, since nonlinear bellows could provide a method for automatically changing time constant as part of temperature compensation, or to change system dynamics as a function of preselected flight conditions.

Servoactuators

Two types of fluidic servoactuators were used during this development program: the spool valve type, which uses force capsules with a nozzle flapper for the first stage and a spool valve for the second stage, and a vortex valve type using a nozzle flapper for the first stage and vortex valves for the second stage. A photograph and schematic of the spool valve-type servoactuator are shown in Figures 25 and 26. A photograph and schematic of the vortex valve-type servoactuator are shown in Figures 27 and 28.

The performance of the two types of servoactuators is summarized in Table III, and a graph of frequency response is shown in Figure 29.

Force Capsules

The most significant problem with the spool valve servoactuators was loss of the pin and/or destruction of the force capsules (see Figure 30) during pressure transients. When the solenoid valve is turned on, the pressures in all three signal lines increase by about 200 psi. If the pressure in one line builds up faster than it does in another, a substantial differential pressure may occur across the force capsule, causing either pin dropout or force capsule destruction. In early testing, the amplifier output impedance was equivalent to a 0.22-in.-diameter orifice; however, the reference

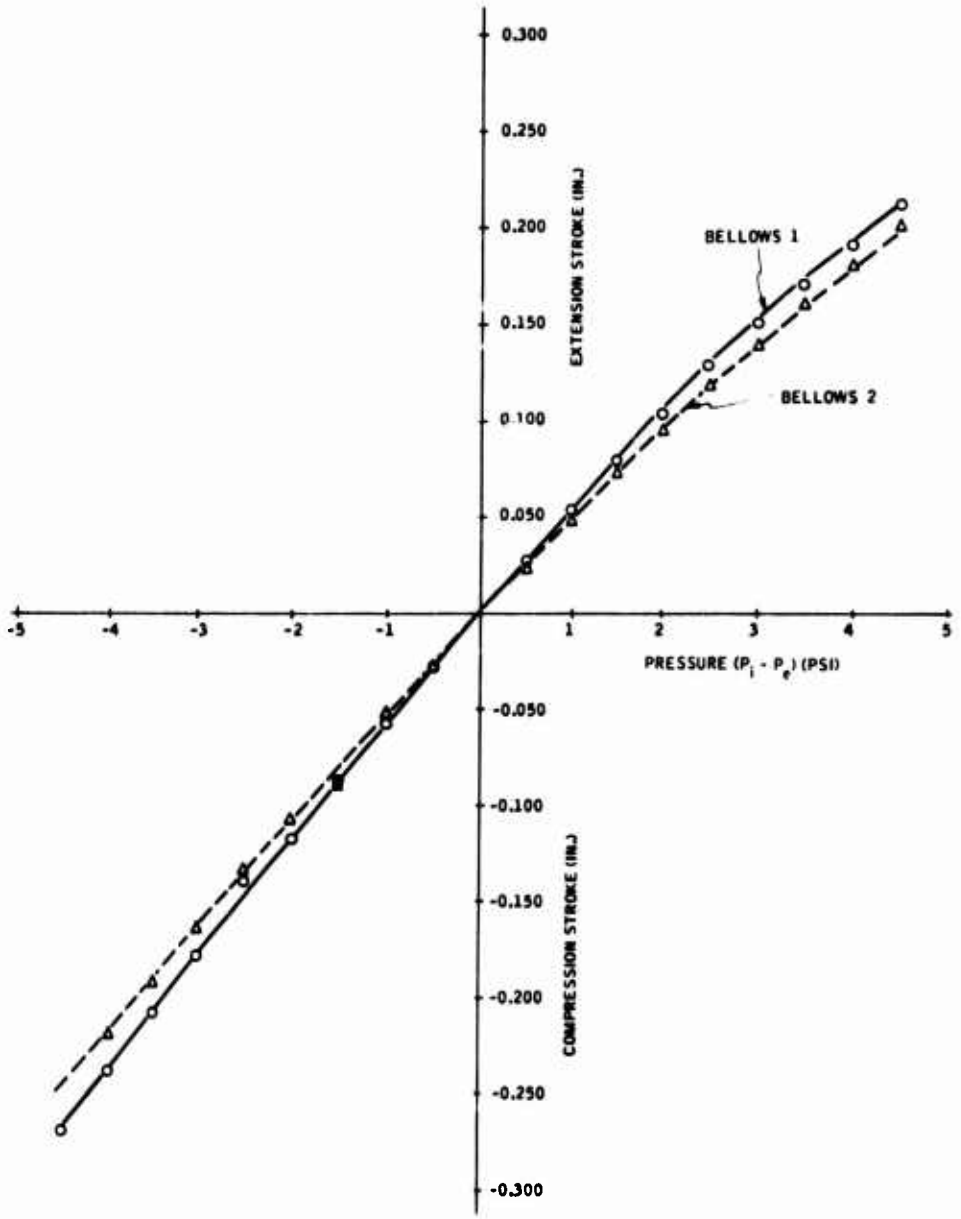

Figure 24. Performance Characteristics of Pitch-Axis Controller Replacement Bellows.

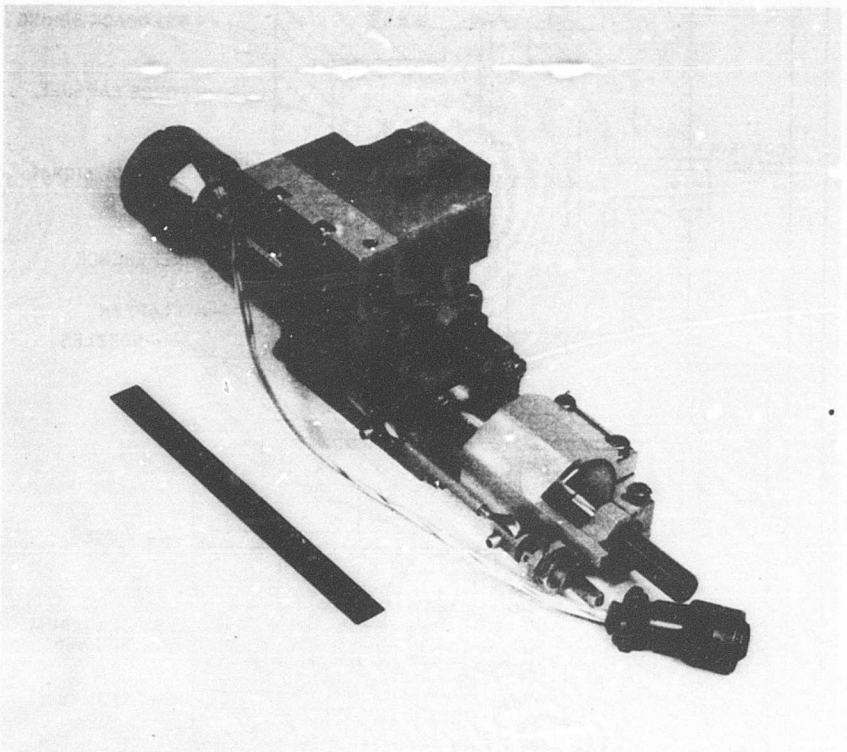

Figure 25. Spool Valve Servoactuator.

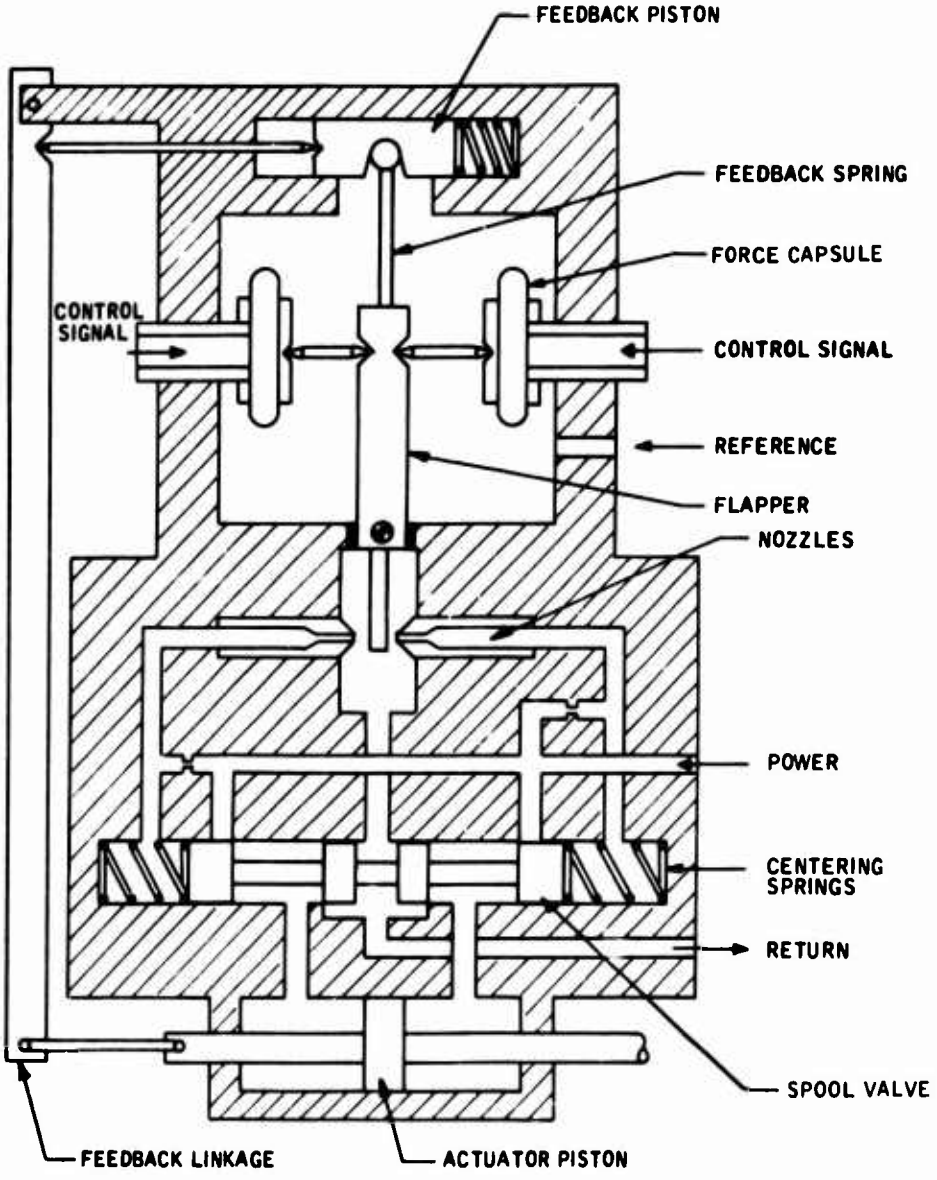

Figure 26. Spool Valve Servoactuator Schematic.

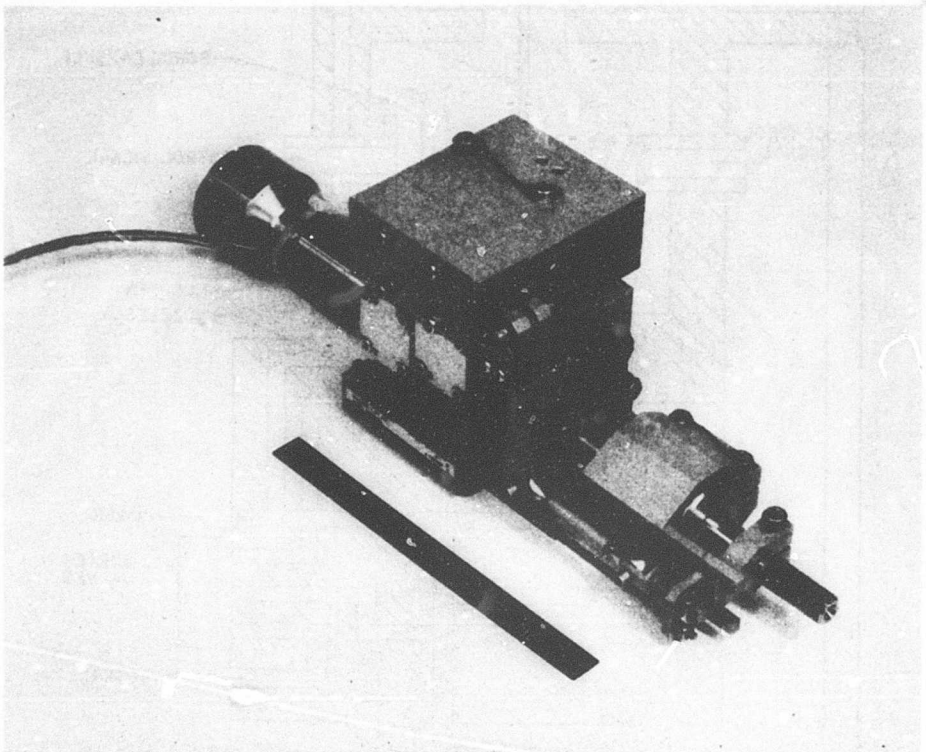

Figure 27. Vortex Valve Servoactuator.

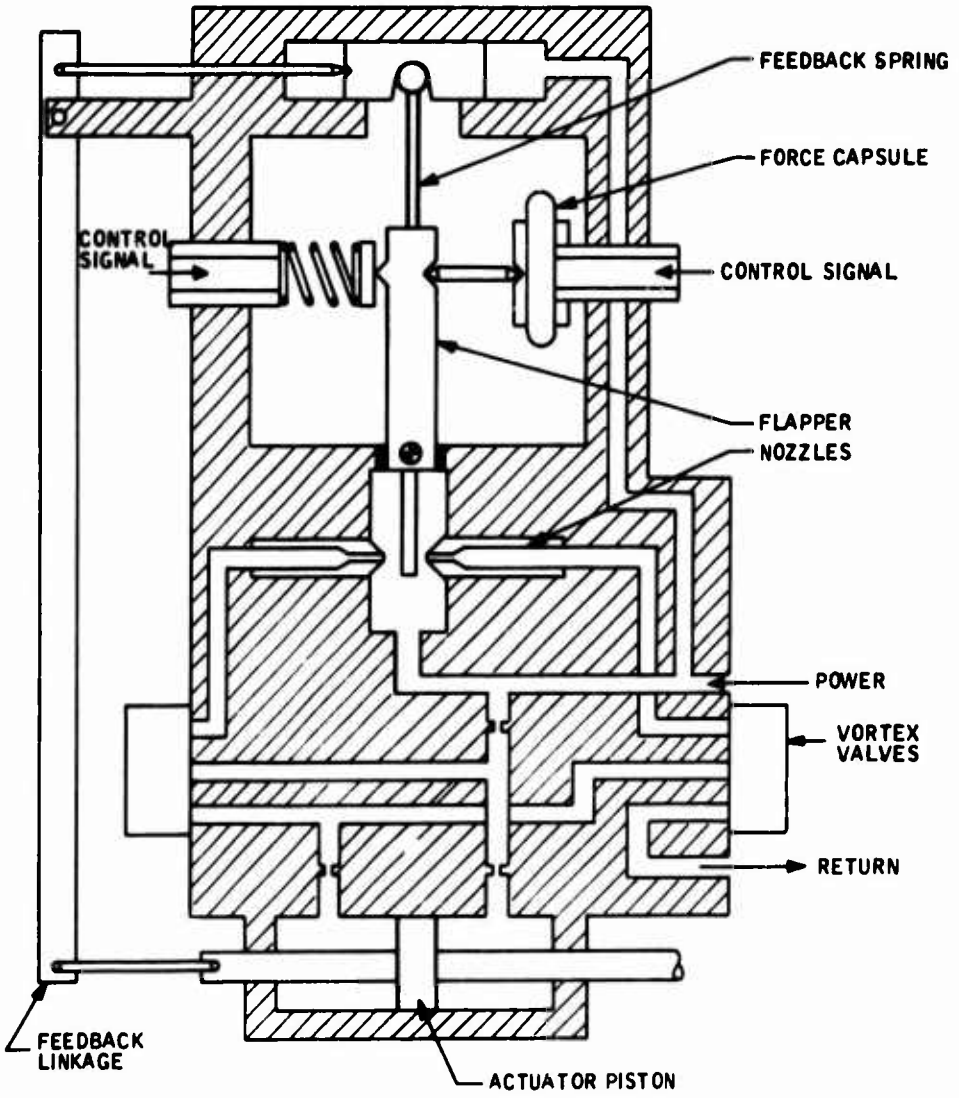

Figure 28. Vortex Valve Servoactuator Schematic.

TABLE III. SUMMARY OF SERVOACTUATOR PERFORMANCE			
Type	Gain (in./psi)	Threshold (psi)	Null (in.)
Spool Valve	0.090	0.018	0.016
Vortex Valve	0.112	0.055	0.001

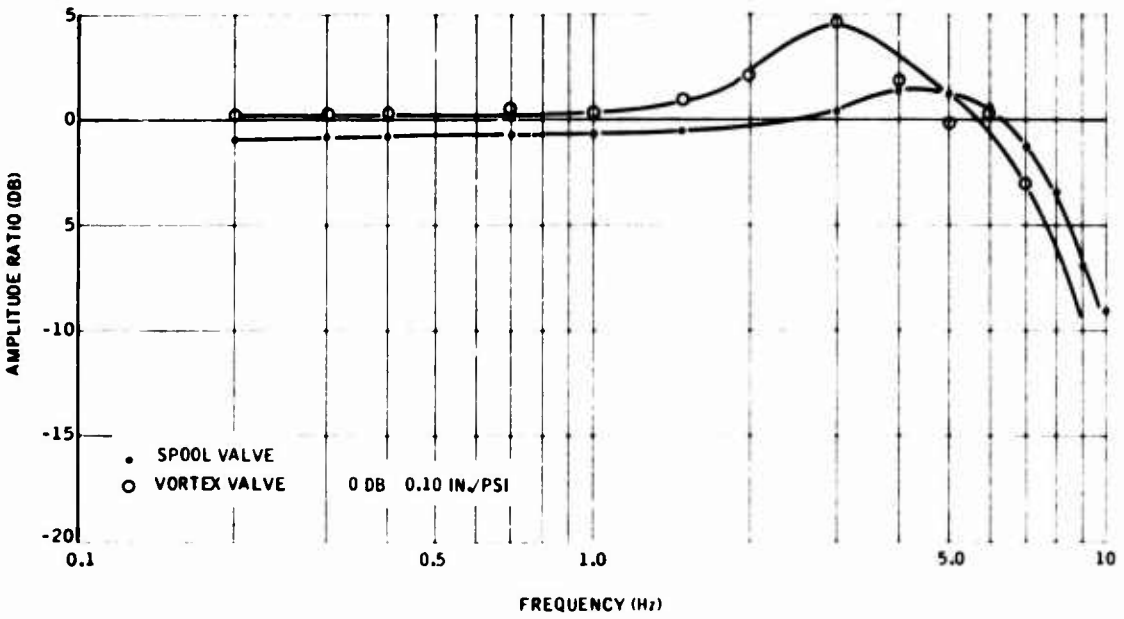

Figure 29. Frequency Response of Spool Valve and Vortex Valve Servoactuators.

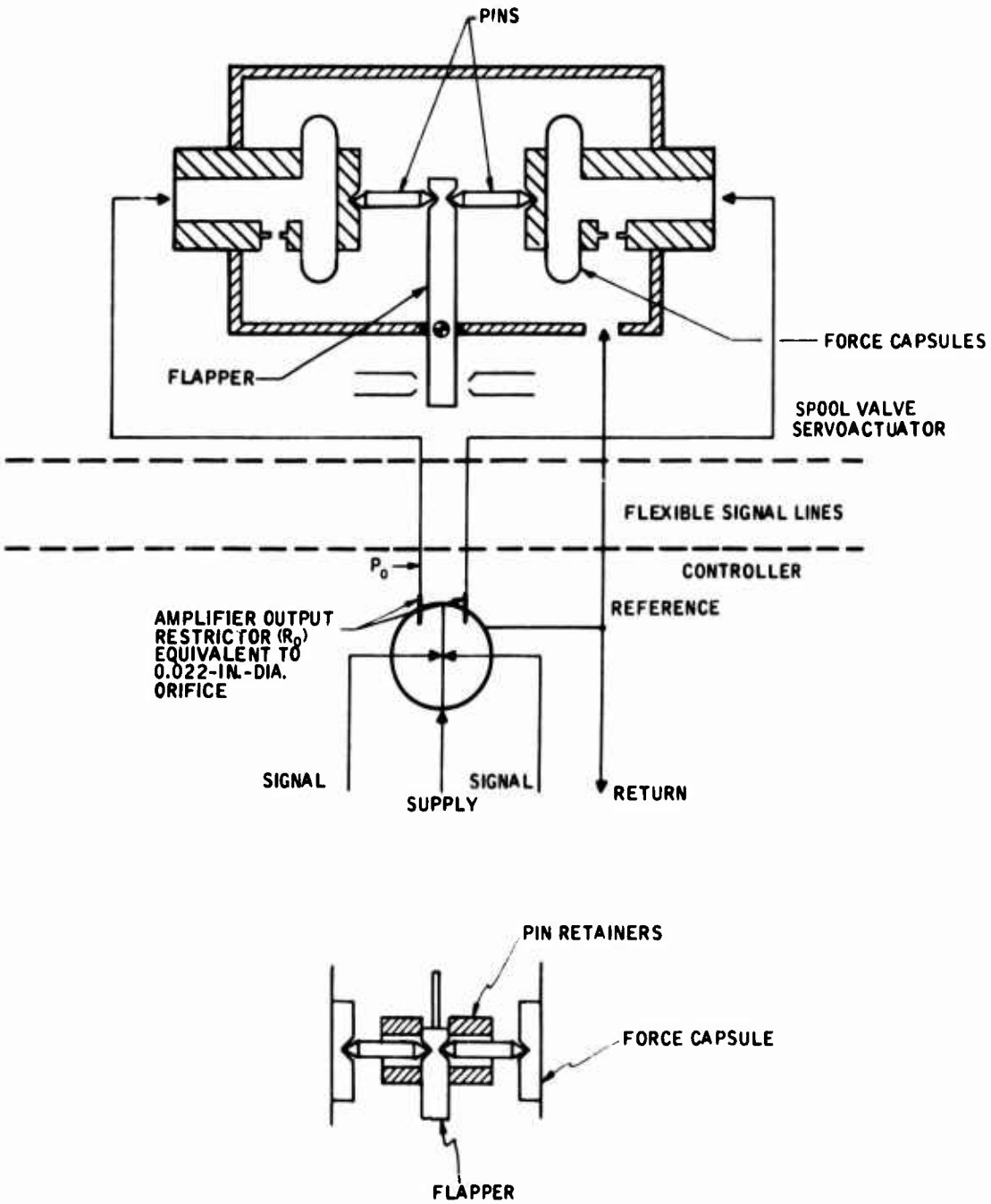

Figure 30. Spool Valve Servoactuator Schematic -- Final Configuration.

pressure line did not have a significant restriction. If the signal lines expand or if air is trapped in the force capsules, the reference pressure will reach 200 psi almost immediately, while the R-C network in the signal lines (about 0.01 sec) prevents the force capsules from charging, thus resulting in trouble. To prevent this, a 0.022-in.-diameter restrictor was placed in the reference pressure line to obtain an equivalent time constant in all three regions. However, if there is air in the reference chamber of the servoactuators, this solution will tend to create the problem in the opposite direction instead of solving the transient pressure problem. In the final configuration, the spool valve servoactuators contained the retainer shown at the bottom of Figure 30. This retainer prevented the loss of pins but did not prevent destruction of the force capsules if very large transients were encountered.

A long-term solution to this problem may not be necessary, since the pressure transients described here are created by solenoid valve cycling. The valves involved are not required in most prototype applications. The normal slow buildup of pressure with an engine-mounted pump is not likely to cause problems. However, if transients are expected, the use of stronger force capsules, along with flapper changes, may be the best low-cost approach to the problem.

Force capsule problems were not experienced with the vortex valve servoactuators. The major reason for this is that transients were avoided during testing of these servoactuators. Their single-capsule design (Figure 28) also appears less susceptible to transients if air is not allowed to collect in this area. However, the lack of a self-bleeding feature could result in air accumulation.

Feedback Piston

The feedback piston (for spool valve servoactuators) as shown in Figure 26 is driven in one direction by the feedback pin and in the other direction by a spring. The reference chamber is sealed by O-rings on this piston. During initial testing of the controllers, it was found necessary at one time to increase the reference pressure to over 100 psi. This increased reference pressure increased the load on the feedback piston O-rings. The force was high enough to cause the piston to hang up when only the spring was trying to move the piston. This caused the servoactuator to perform erratically. Backup rings and a stiffer spring were used to alleviate this problem. The vortex valve servoactuator used the supply pressure in place of the spring (see Figure 28); therefore, it did not experience this problem.

Peaking

During testing to determine the capacitance of the input force capsule mechanism on servoactuators developed for a previous USAAVLABS program (Contract DAAJ02-67-C-0056), it was discovered that the capacitance decreased by 20 percent when the servoactuator was operating. Figure 31 is a schematic of this mechanism; it should be noted that the feedback spring is located below the flapper. The reduction in capacitance when operating closed-loop can be visualized in the following manner. If the left force capsule were pressurized to 1 psi, the flex pivot would move to the right. In this process it would require about 0.0005 in.^{3} of oil to expand the force capsule the required amount. If the servoactuator is operating, the feedback will move in order to null the signal at the flapper, which in turn will tend to restore the flex pivot and force capsule to their original position. Capacitance tests showed that this restoring motion is only 20 percent of the original motion; i.e., only 0.0001 in.^{3} of the 0.0005 in.^{3} would be returned from the force capsule as the servoactuator moves to its commanded position.

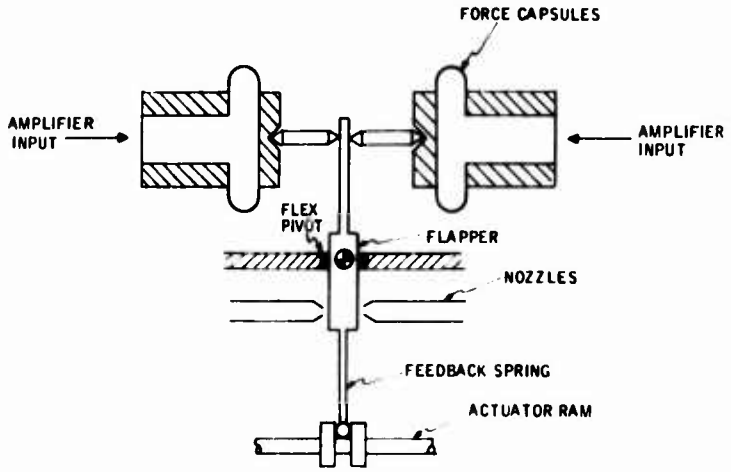

Figure 31. Spool Valve Servoactuator Feedback Techniques -- Feedback Spring Located Below Flapper.

Present servoactuators have a different feedback design, which is shown in Figure 32. Since the feedback spring is above the force capsules, closed-loop capacitance will be nearly zero. However, closed-loop operation is different and can be visualized as follows. Increasing pressure in the left-hand force capsule by 1 psi will require 0.0005 in.^{3} of oil as the flex pivot is displaced as before. Error signals from the flapper will move the servoactuator ram

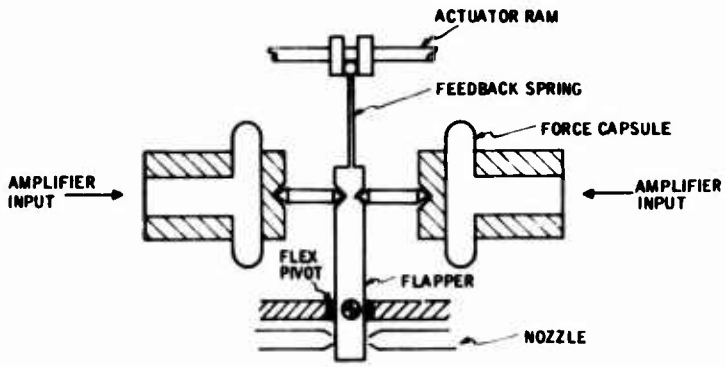

Figure 32. Spool Valve Servoactuator Feedback Techniques -- Feedback Spring Located Above Flapper.

and feedback piston until the force capsules are restored to their original position. Now, the force capsules will have to expel the the full 0.0005 in.^{3}. This causes a phenomenon called "peaking."

Operation of the servoactuator with an amplifier is shown in Figure 30. Assume that the amplifier has unity gain and that actions occur in sequence rather than simultaneously. An input signal of 1 psi results in an output pressure which builds up to 1 psi as the force capsule expands. The flexibility of the force capsule mechanism (capacitance) and the amplifier output impedance determine the time constant for this buildup in pressure. Commands from the nozzle flapper move the servoactuator to restore the flapper (and the force capsule). Compression of the force capsule expels flow through R_o, increasing pressure (P_o). This increase in P_o is in effect a command for the servoactuator to move beyond its original commanded position. This reaction between the servoactuator and amplifier could be described as positive velocity feedback, which is destabilizing.

Peaking of the frequency response curve will occur near the servoactuator crossover frequency when it is driven by an amplifier. This resonant peaking can be detected at the output of the amplifier as well as at the output of the servoactuator. This problem did not occur with previous servoactuators because the mechanization of the feedback/capsule arrangement resulted in a true capacitance (accepts flow while being charged but does not expel flow as secondary action occurs).

One servoactuator was modified to include compensation shown in Figure 33. The flow expelled by the force capsule was received by the expanding feedback cavity, eliminating an increase in P_o. This compensation is effectively negative velocity feedback, since it reduces the command when the servoactuator velocity is high.

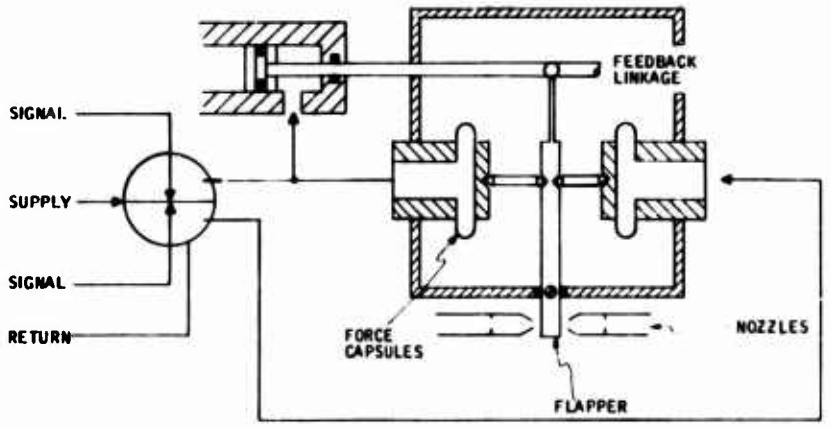

Figure 33. Negative Velocity Feedback Technique.

Performance showed this to be an adequate solution, but it increased envelope and cost. Also, high transient pressures could be induced into the force capsules if a hardover servoactuator were quickly deenergized.

The solution selected was to operate the servoactuator at a lower supply pressure where its loop gain would be lower. Peaking was 3 db or less at a supply pressure of 700 psi. Later in the program when the vendor fabricated additional servoactuators, he made them with a substantially stiffer flex pivot to reduce loop gain as well as its input capacitance. These fixes were also incorporated into the two remaining servoactuators. This modification enables the servoactuator supply pressure to be increased from 700 psi to 1000 psi with a resultant performance improvement (response).

The vortex valve servoactuators also experienced peaking when driven by an amplifier.

In addition, some unusual behavior of the vortex valve servoactuators was experienced at 120°F and about 3 Hz when operating with low-amplitude input signals of 0.06 in. peak-to-peak and an inertial load. Peaking of 7 db would occur as frequency was increased to 3 Hz, and then the output amplitude decreased to nearly zero at 10 Hz. When the input frequency was then decreased from 10 Hz to 3 Hz, the peaking did not reoccur; applying forces to the servoactuator ram would result in high peaking for tension force or nearly zero output for a compression force. This behavior cannot be adequately explained at this time.

Results of flightworthiness tests on the servoactuators are described in Appendixes III and IV.

SYSTEM DEVELOPMENT

Plumbing and Its Effect on Noise

System return-line plumbing was changed several times during development to add a tee for pressure instrumentation, to add heat exchangers, etc. Noise performance seemed to change with each setup. Data were not repeatable, and it became obvious that the return-line plumbing was a major contributor to system noise, with elbow fittings the greatest offender.

A venturi-shaped restrictor was placed downstream of the rate sensor, resulting in a dramatic noise reduction at the higher system Reynolds numbers. Internal return-flow passages in the rate sensor also contained "elbows," resulting in flow velocities of about 15 ft/sec. The sensor was modified to reduce these velocities to less than 7 ft/sec, resulting in additional noise improvement.

During tests to establish the relationship between noise and primary sink flow, it was noticed that an abrupt change in signal noise was accompanied by a change in the audible noise emitted from the sensor. Audible noise is indicative of cavitation, and tests were conducted to determine the effect of back pressure on noise. Results showed that noise decreased with increasing back pressure. Increasing back pressure above 120 psig did not result in further improvement.

Later tests were conducted with back pressures of at least 160 psi to supply a margin of safety between the set back pressure and the minimum back pressure to eliminate this noise source. With higher back pressures, performance remained consistent even when the system was moved from one test setup to another.

Null Adjustment

All sensors have some offset when fabricated, and various techniques have been used to compensate for or eliminate this offset. In this program the sensor was fabricated with a vane in the vortex chamber which could be rotated to generate a "compensating swirl."

The null adjust could also minimize system sensitivity to small changes in supply flow. Insensitivity to supply flow is a prerequisite to eliminating interactions between controllers and servoactuators. A test setup similar to that shown in Figure 34 was used to investigate roll-axis sensitivity to changes in supply flow. Since the system contains a high-pass circuit, very little change would be expected from slow steady-state changes, and therefore it was necessary to make these changes at a higher frequency: about 0.2 Hz for roll, 0.4 Hz for yaw, and 1.5 Hz for pitch. At these frequencies, system gains are the greatest. Tests on the roll-axis controller, where flow was varied by about ±5 percent, demonstrated a sensitivity of only 0.035 deg/sec/percent flow at 0.2 Hz. Minimum sensitivity was experienced when the sensor was nearly nulled.

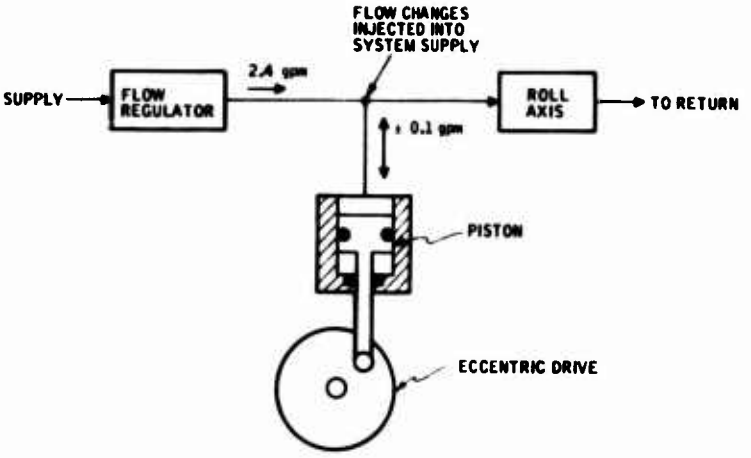

Figure 34. Flow Sensitivity Test Setup.

Built-in-Test Button

BIT (built-in-test) is another vane (similar to the null adjust) which creates a vortex in the rate sensor chamber when depressed. This vane is "locked" to an angular position where its effect, when depressed, will be equivalent of a specified angular rate. BIT in the roll-axis controller was adjusted to an equivalent of 25 deg/sec (about 0.2-in. servoactuator travel). The output characteristic resulting from BIT is shown in Figure 35. Observing the output provides a check on system performance. If system gain is low, the magnitude of the output will be less. Shaping characteristics, for a high-pass circuit in this case, can also be checked by observing the time that it takes for the system output to decay by 63 percent. BIT has been helpful in showing changes in gain and changes in time constant, and in defining polarities.

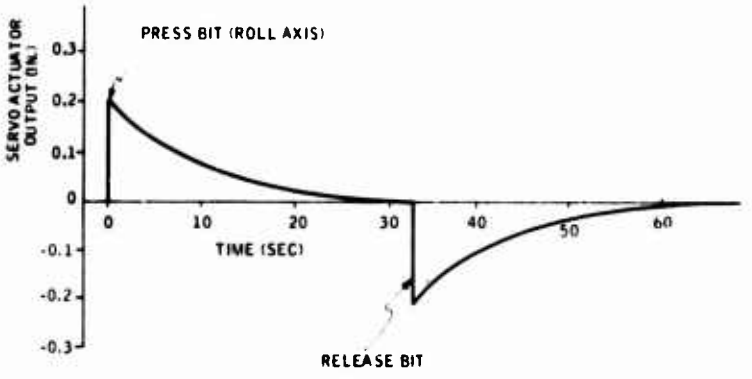

Figure 35. Controller Output for BIT Input.

In the yaw-axis controller, BIT was adjusted to a smaller angle to provide an equivalent of 13.5 deg/sec. Since the yaw system gain is higher, it is necessary to use a smaller rate step to prevent complete saturation of the servoactuator.

The pitch-axis controller has the highest gain; therefore, the size of the BIT vane was decreased to make it less sensitive. This vane was then adjusted to provide an equivalent of 6.2 deg/sec.

Temperature Compensation

A viscosity-sensitive restrictor in the rate sensor secondary sink (see Figure 13) is the major provision for temperature compensation of the system. Rate sensor scale factor increases with an increasing primary sink flow (contains pickoff). Efficiency of the rate sensor (and its scale factor) is lowest when fluid viscosity is high. The restrictor provides for increased primary sink flow when fluid viscosity is high in order to compensate for a decreased sensor inefficiency. The amount of compensation is varied by changing the characteristic of the viscous compensation element. For example, an element with a single passage 0.010 in. high would provide less compensation than an element with four passages each 0.005 in. high. The compensation element with four passages will have a higher viscous pressure drop because of the close spacing (even when actual velocity is lower). Therefore, it will allow greater primary sink flow at cold temperatures. At high temperatures, where the viscous drop is small, the larger open area of the four-passage element will allow it to bypass more flow (less primary sink flow) than the single-passage element, resulting in a constant sensor gain for various oil temperatures.

In each controller, the amplifiers share a common supply with their associated rate sensor. Sensor compensation, therefore, also results in an increased amplifier supply pressure at cold temperatures and decreased pressure at hot temperatures. This pressure relationship tends to make amplifier gain more constant with temperature.

The roll-axis controller had been compensated early in the development testing phase. Other controllers were then fabricated with the same compensation. Tests conducted later in the program (when the systems were being checked prior to flightworthiness testing) showed that pitch-axis and roll-axis controller gain varied with temperature as shown in Figure 36. The pitch-axis controller was by far the more sensitive, which was probably due to its having more stages of amplification. The pitch-axis controller compensating restrictor was modified to make it more sensitive to viscosity. Performance of the modified pitch-axis controller is also shown in Figure 36.

The yaw-axis controller compensation was also modified. The before and after performances are shown in Figure 37.

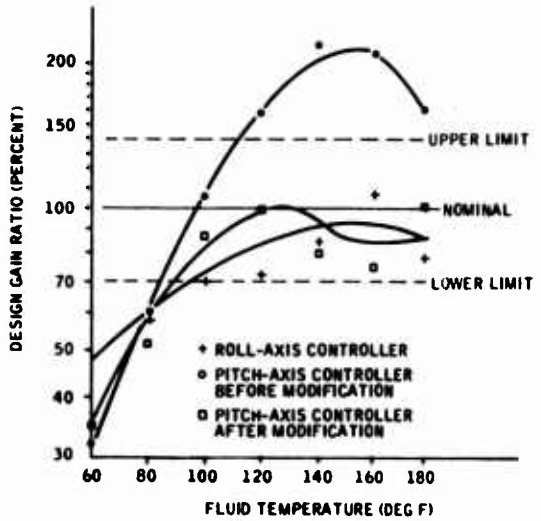

Figure 36. Pitch- and Roll-Axis Controller Temperature Compensation.

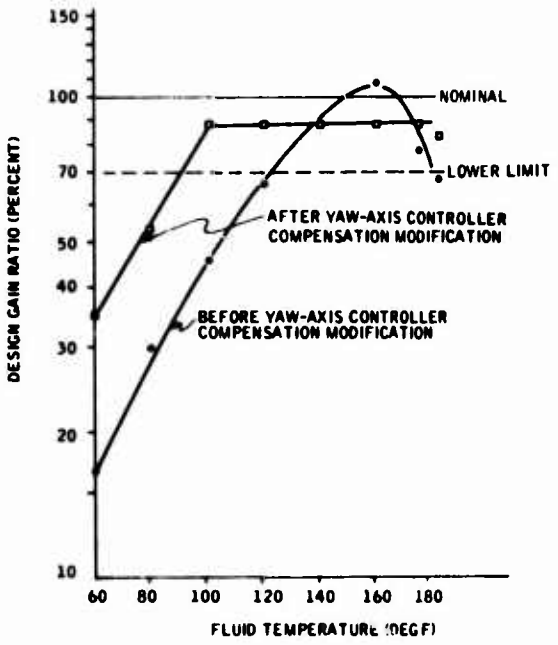

Figure 37. Yaw-Axis Controller Temperature Compensation.

As presently compensated, the three-axis system meets the design goals over the temperature range from 90°F to 160°F. Below 90°F, gains were low by 30 percent; above 160°F, noise of the pitch-axis controller exceeded the specification requirements. Operation outside this range, however, would not result in an unsafe flight condition. Time constraints prevented further effort; however, it is felt that future systems could be compensated to meet specification requirements over a lesser temperature range, if required.

System Performance

Table IV presents data regarding scale factor null offsets and noise and how they build up throughout the individual controller packages (refer to Figures 2, 3, and 4). Typical system (including servoactuators) response data are shown in Figure 38. Comparing these curves with the nominal response curve demonstrates the effect of servoactuator peaking as well as the absence of other system lags projected in the Phase I analysis. The system in this configuration was given temperature and vibration flightworthiness testing (see Section V) prior to final gain adjustment. Final system nulls are given in Section V, Table V. Closed-loop testing indicated that no additional effort on shaping at the higher frequencies was required.

GENERAL SYSTEM PROBLEM AREAS

Manifolds and Bonding

The manifolding technique used was satisfactory. However, much difficulty was encountered with the epoxy bonding technique used. One manifold difficulty occurred because of a marginal design. In one area a tapped hole was located near a channel in the manifold. The manifold channel in the area of the tapped hole was closely inspected before the cover was bonded. A break between the tapped hole and the channel after bonding occurred when a screw was inserted in the hole. Forces from the screw expanded the Helicoil insert,and it broke through the thin wall into the channel.

Bonding problems were first encountered when the 0.01-in.-thick epoxy bonding tape extruded into one of the manifold channels, closing it off. This was caused by the high holding force used in the bonding process and also by the fact that the bonded surface was large with only a few channels. Thinner tape (0.005 in.) was later used and the problem was eliminated.

The most significant bonding problems occurred later in the program when the scope was changed to require proof-pressure testing to 2250 psia (previously 750 psia). A small manifold on the roll axis controller (see Figure 39) was the first to fail.

TABLE IV. CONTROLLER DATA AT 120°F

Axis	Vortex Rate Sensor			Preamplifier			Output[b]		
	Scale Factor (psi/deg/sec)	Noise[a] (deg/sec) (peak-to-peak)	Null (psi)	Scale Factor (psi/deg/sec)	Noise[a] (deg/sec) (peak-to-peak)	Null (psi)	Scale Factor (psi/deg/sec)	Noise[a] (deg/sec) (peak-to-peak)	Null (psi)
Pitch	0.0055	0.73	+0.001	0.007	-	+0.032	0.43/0.90[d]	0.22	-0.85
Roll	0.0042	0.25	-0.014	0.020	1.0	-0.100	0.068	0.74	-0.20
Yaw	0.0048	0.40	-0.160	0.008	-	-0.010[c]	0.320	0.64	-0.05

[a]Noise filtered with 5-Hz filter.

[b]Output loaded with 0.014-in. orifice.

[c]Rudder input device nulled to obtain preamplifier null.

[d]Low-frequency/high-frequency scale factor due to lead-lag network.

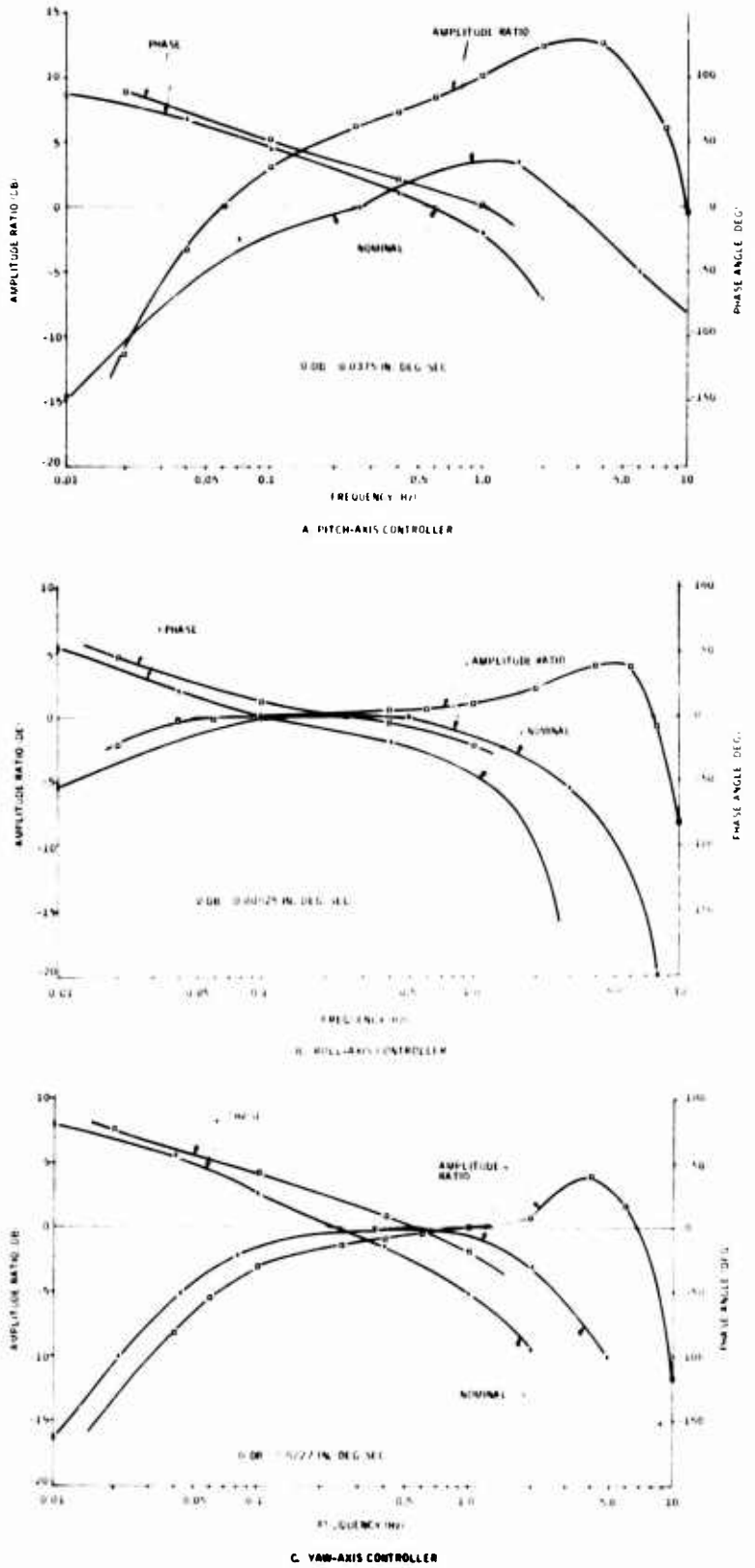

Figure 38. System Response.

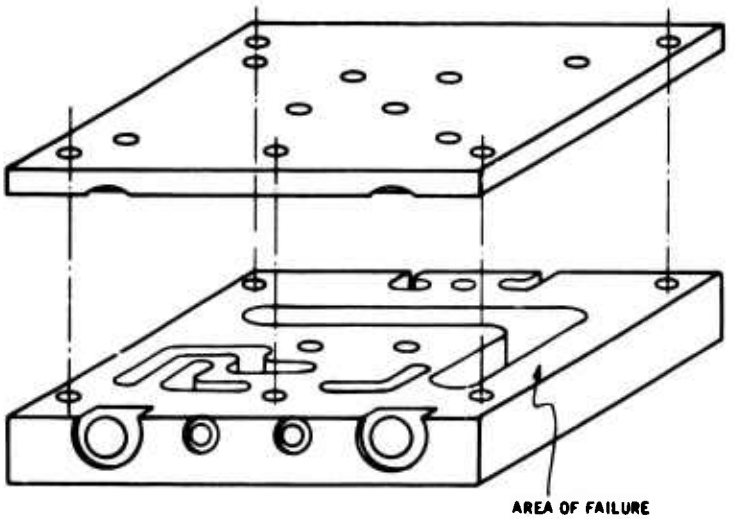

Figure 39. Roll-Axis Controller Manifold.

Two solutions to this problem were investigated simultaneously. Diffusion bonding of the aluminum manifold showed that the process was unsatisfactory without additional engineerirg development effort. The manifold was also redesigned to minimize the length of channels and to locate them farther from the outer edges. This redesigned manifold was bonded with epoxy tape, installed in the roll-axis controller, and proof-pressure tested to 2250 psi without failure.

Proof testing of the yaw-axis controller resulted in several manifold failures. These failures were attributed to an inadequate "peel" strength of the bond. Thickness of the outer cover was increased to reduce the flexing which resulted in the peeling tendency. The yaw axis-controller was then able to withstand the 2250-psi proof pressure.

The pitch-axis controller was modified similar to the yaw-axis controller. It then withstood the 2250-psi proof pressure.

Amplifier bonding problems were discussed under amplifiers in this section.

External Leakage

Considerable effort was spent in reducing external leakage. Most of the external leakage problems, which involved O-ring seals, became apparent and were examined after the program scope change increased system proof pressure from 750 psia to 2250 psia.

A special seal was used under the amplifiers to provide additional design flexibility. These O-rings have a cross-section diameter of only 0.040 in. as compared with 0.070 in. for the conventional design. Figure 12 shows the two O-ring groove patterns and how the smaller rings would allow the amplifier to "bridge" across parting lines in a system. Final design for the three-axis system did not include any of these parting lines, and the small O-ring design was not required. The design was not changed, since the O-ring grooves are milled into the baseplate of the amplifier before electroforming and considerable effort would have been required to increase the size of the grooves. Centers of the holes are at the same location on both designs. Future amplifiers will probably not contain O-ring grooves, but special plates will be used between the manifold and the amplifier that will contain the O-ring. These O-ring plates would make it possible to change O-ring sizes without modifying the amplifier.

Difficulty was experienced in sealing areas where the small-cross-section (0.040-in.) O-rings were used. The problem was greatest where restrictors were used in conjunction with the O-rings such as shown in Figure 19. Even with large O-rings, problems were experienced with orifice disks as shown in Figure 40A. Reverse pressure transients would permanently deform the O-ring, resulting in leakage. Retainers shown in Figure 40B were used to correct this problem.

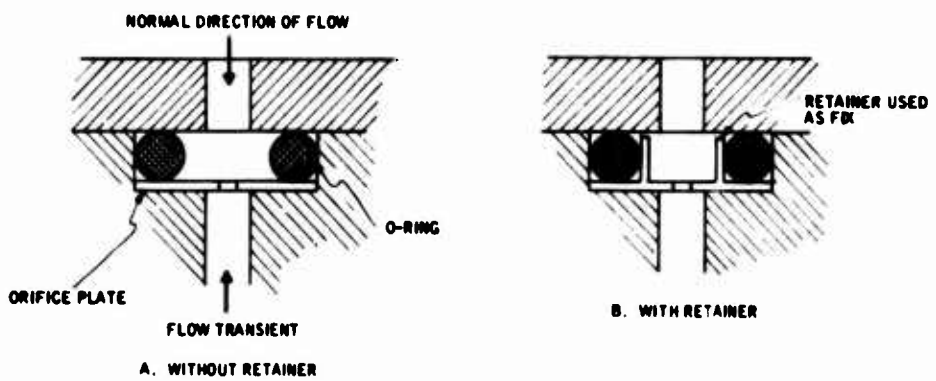

Figure 40. Flow Transient Problem on O-Ring -- Orifice Combination.

Manifolds such as those used on the yaw-axis controller have large flat surfaces with more than 10 O-ring seals. Maintaining flatness, closely controlling the depth of O-ring grooves, and proper prestressing of bolts are necessary to obtain good seals.

Pressure forces are a significant factor, creating material deflections which induce leakage. Figure 41 shows the roll-axis manifold with perpendicular sealing surfaces. Bolts held the manifold and the rate sensor to the capacitor block. Pressure forces on the manifold from the rate sensor side would cause it to slide across the capacitor block. Locating pins were placed in the location shown to prevent this shifting.

Contamination

Intermittent and unusual phenomena are usually diagnosed to be the result of contamination. A number of cases of suspected contamination have occurred where the "problem particle" was apparently dislodged during attempts to isolate the problem. In most cases the particle and/or the source of contamination was found.

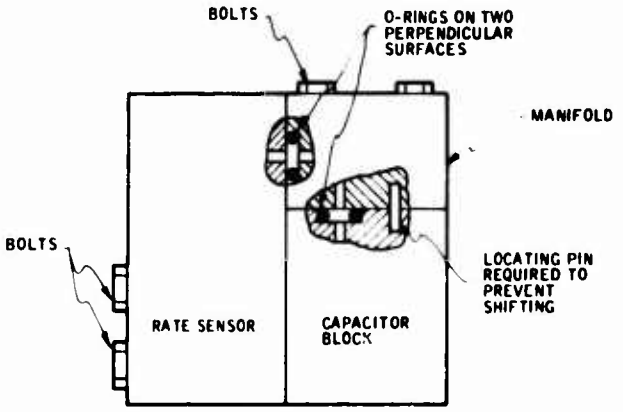

Figure 41. Perpendicular O-Ring Seals.

The smallest restriction in the fluidic controllers is larger than 200 microns (0.009 in.). Amplifiers are even larger, with the smallest dimension being over 400 microns (0.016 in.). Most of the system flow passes through the rate sensor sink, which is nearly 2000 microns in diameter. Overall, the system appears to be relatively tolerant of contamination. Problems experienced were associated with large quantities of internally- and externally-generated contaminants which were larger than 0.01 in.

During assembly of the rate sensor BIT and null adjust vanes, sharp edges would shave pieces of the O-rings into the vortex chamber. Since this is a blind assembly, the problem was not noticed until the large particles blocked critical orifices. Figure 42 shows how these vanes were modified to eliminate this problem when reasonable care was exercised in assembly.

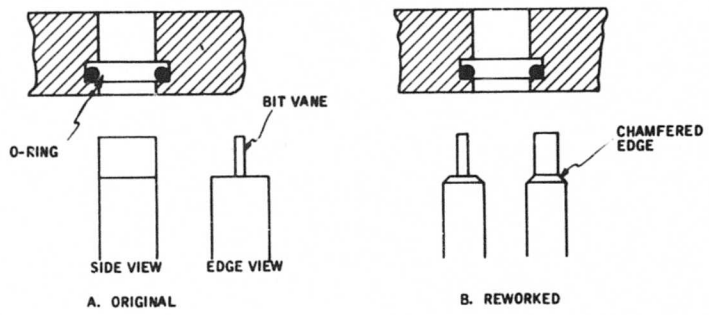

Figure 42. BIT Configuration Change.

Contamination has also entered the system from the assembly and disassembly that occurs during development testing. The test area was not a "clean room," allowing the entry of contamination from the room. Shavings from screw threads or the threads on hydraulic fittings must be carefully controlled.

During system flight testing, filter screens (about 100 microns) will be placed ahead of each controller to minimize contamination problems. There is concern that some particles may still be lodged in the corners of low-velocity manifold channels and will become unlodged at a later date.

Contamination is not expected to be a serious problem in the future if systems are designed to prevent the generation of contaminants (in assembly or use).

SECTION V
ACCEPTANCE TESTING

The final acceptance testing consisted of conducting closed-loop testing of the three-axis system and comparing the results with those acquired in the previous analytical study (see Appendix I). Prior to acceptance testing, flightworthiness testing was conducted, consisting of vibration and temperature environmental operation of the controller packages and servoactuators.

FLIGHTWORTHINESS TESTING

The system, using the spool valve servoactuators, was installed on a vibration fixture (Figure 43), with the power supply circuit and connections simulating the actual aircraft installation as nearly as practicable.

The system was tested per the detailed specification (see Appendix I) at oil temperatures of 60°F, 120°F, and 180°F. The system was then subjected to 15-minute vibration scans per Figure 514-2, curve A, of MIL-STD-810A, in each of the three mutually perpendicular axes. Nulls were monitored during vibration. The system was then retested at the above temperatures. Appendix II presents the flightworthiness test report.

Both the spool valve and vortex valve servoactuators underwent individual flightworthiness testing. Appendixes III and IV present the test reports.

CLOSED-LOOP ACCEPTANCE TESTING

Prior to conducting closed-loop acceptance testing, system parameters were adjusted to the values shown in Table V. Final performance of the three-axis hydrofluidic SAS was then verified by evaluating system transient response behavior.

Test Setup

The closed-loop test setup checked the pitch and lateral-directional axes separately. Analog computer simulations represented the uncoupled pitch and lateral-directional equations of motion of the UH-1B helicopter at representative forward speeds ranging from hover to 130 kn. A rate table provided appropriate motion inputs to the rate sensors. The three-axis hydrofluidic SAS was mounted on the rate table and used to drive the hydrofluidic servoactuators. Thus, the closed-loop tests are functionally equivalent to those anticipated from flight testing except for any nonlinear characteristic present in the primary control system of the UH-1C helicopter. A typical test setup is shown schematically in Figure 44.

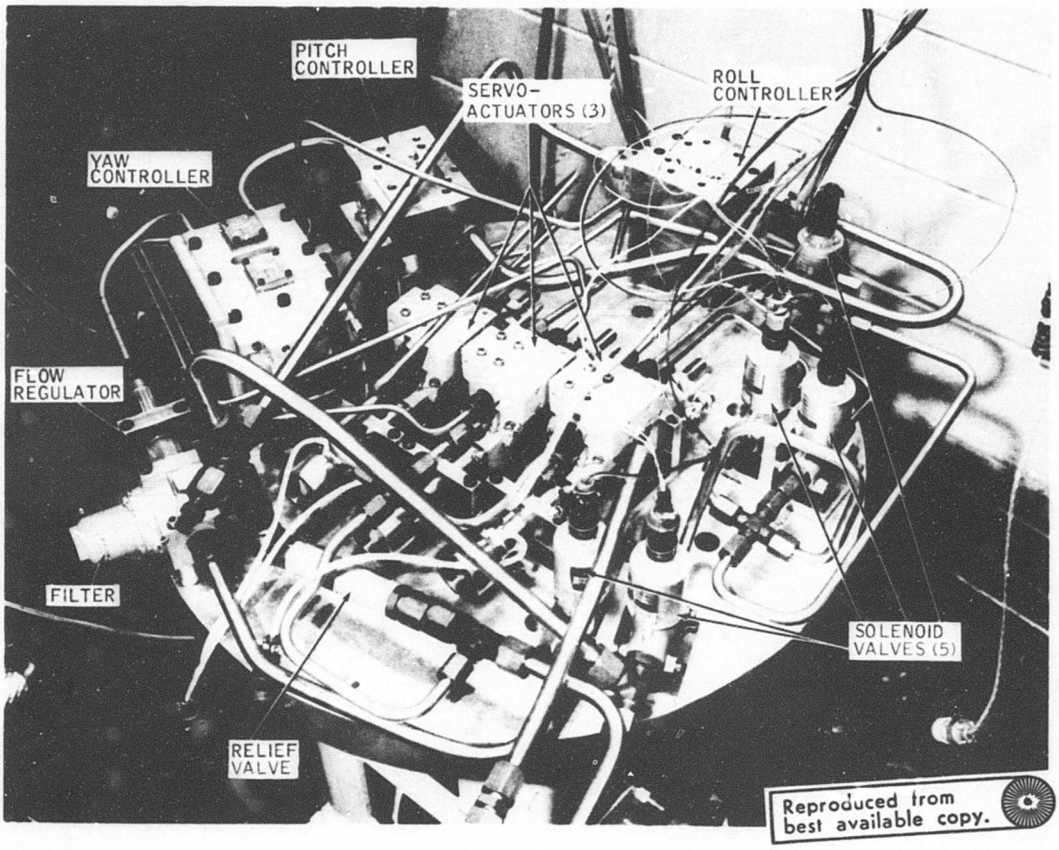

Figure 43. Three-Axis Closed-Loop Test Setup.

TABLE V. SUMMARY OF FSAS PERFORMANCE

Axis	Temperature (°F)	Gain (in./deg/sec)	Noise* (in.)	Threshold (deg/sec)	Null (in.)
Pitch	120	0.0420	0.028	< 0.5	0.005
	60	0.0096	0.010	< 0.5	0.005
	185	0.0240	0.140	< 0.5	0.020
Roll	120	0.0064	0.005	< 0.5	0.020
	60	0.0016	0.020	1.7	0.020
	185	0.0044	0.010	<0.5	0.010
Yaw	120	0.0216	0.028	< 0.5	0.040
	60	0.0100	0.022	< 0.5	0.022
	185	0.0120	0.024	< 0.5	0.030

*Peak-to-Peak

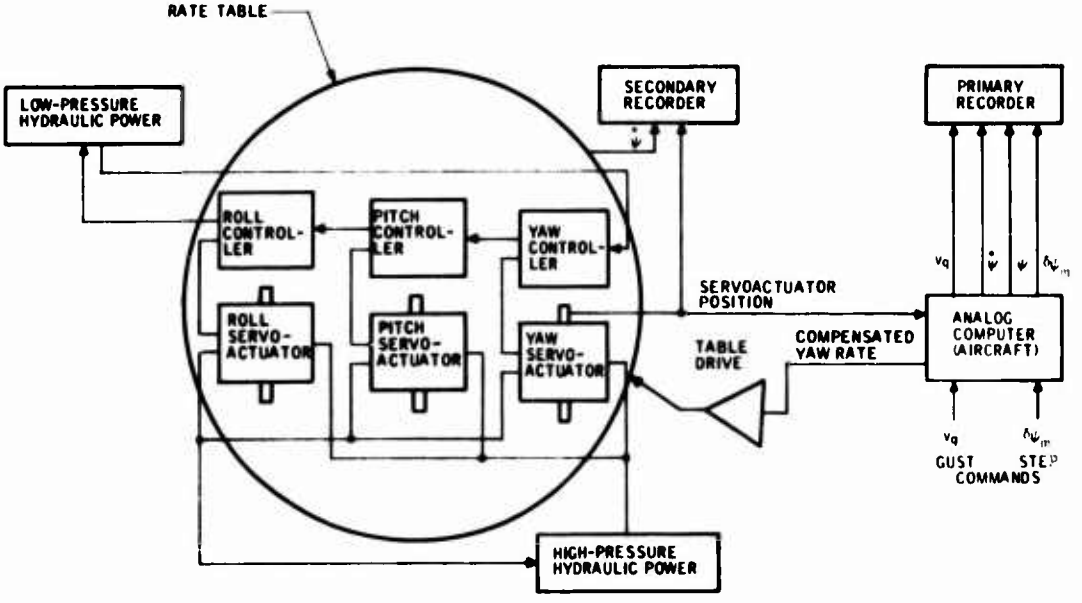

Figure 44. Closed-Loop Test Setup Schematic.

Test Procedures

The various airspeed and temperature test conditions used during the tests are summarized in Table VI.

Test inputs set up in the analog computer simulation were vertical gusts (10 ft/sec) and pitch cyclic inputs (1 in.) to check vehicle short-period damping and control power in the pitch axis. Corresponding yaw-axis inputs were side gusts (10 or 30 ft/sec) and pedal inputs (1 in.) to check dutch roll damping and yaw control power. Roll cyclic inputs (0.1 in. and 0.5 in.) were used to check roll control power. Closed-loop performance of the FSAS was obtained by evaluating transient responses to test inputs at the various test conditions. Recordings were made of six significant parameters in each axis.

Test Results

Transient responses showing closed-loop system performance of the three-axis hydrofluidic SAS are presented in Figures 45 through 62. The effects of oil temperature variations on nominal pitch and lateral-directional damping, noise levels, and control power are summarized below.

Pitch Axis

Pitch-axis SAS damping of gust inputs is compared with that for the free aircraft in Table VII.

The nominal pitch SAS response data at the 120°F temperature are nearly identical to those obtained in the analog developmental studies (Appendix I) shown in the right-hand column. The effect of oil temperatures on the short-period response is not apparent for the high-speed (130-kn) case. This is due to the fact that the short-period response is well-damped and slow and is similar for either the free or the augmented vehicle at the lower speeds, whereas damping augmentation is needed at higher speeds. At the 130-kn speed, the low temperature (60°F) reduced pitch damping to gusts and cyclic inputs to nearly that of the free aircraft, as noted in Table VII and shown in Figure 50. The high temperature (185°F) does not affect damping but does result in a greatly increased system noise level, as shown by the boost trace in Figure 52.

The high noise level would be undesirable, since it would induce excessive wear in the mechanical linkages. However, in actual operation, the oil temperature is not expected to reach 180°F. The resulting vertical acceleration shown in the trace of Figure 52 is about ±0.1 g at frequencies of 5 to 10 Hz. If this level of vibration were felt by the pilot in flight, it would be rated disagreeable.

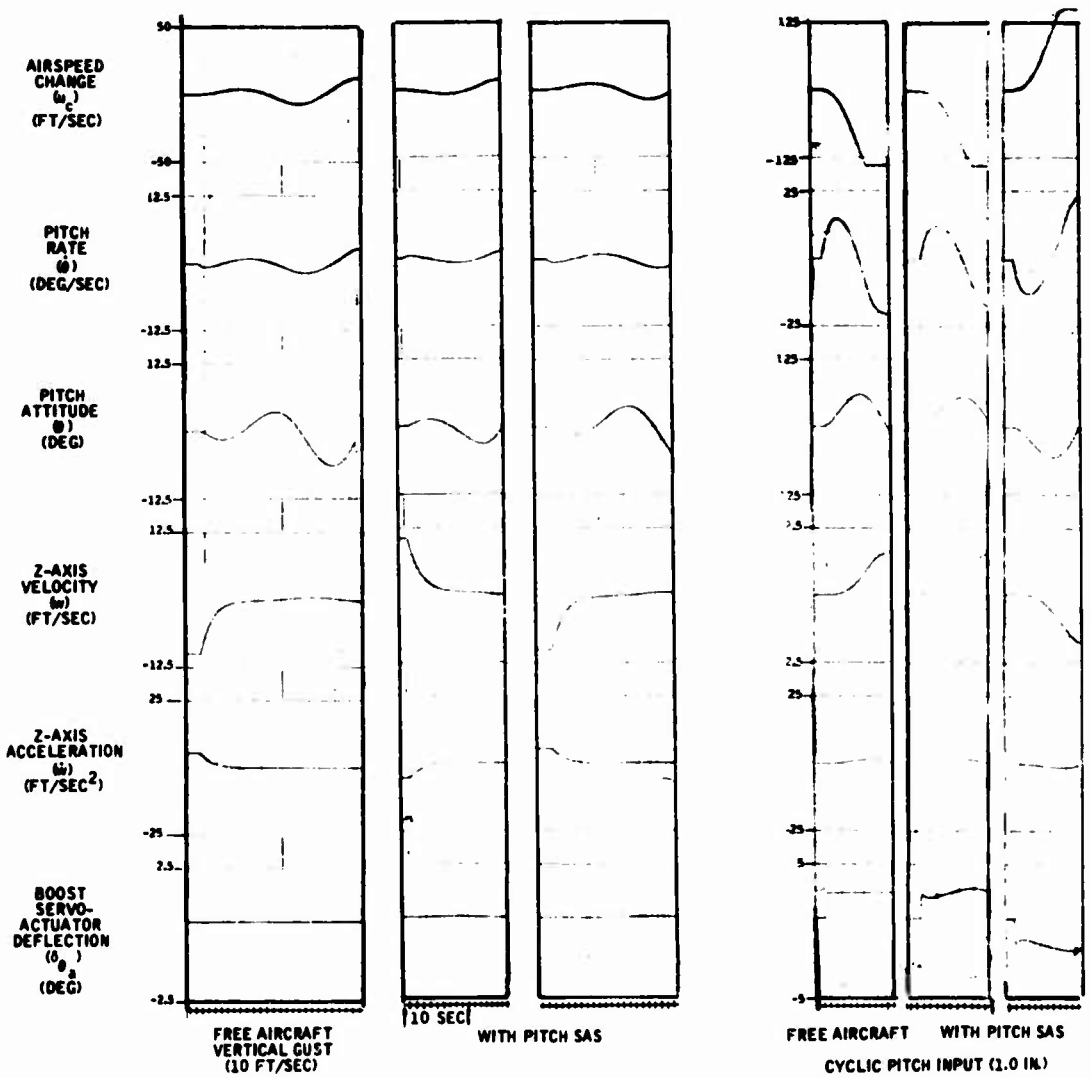

Figure 45. Pitch-Axis Responses at Hover, Oil Temperature = 60°F.

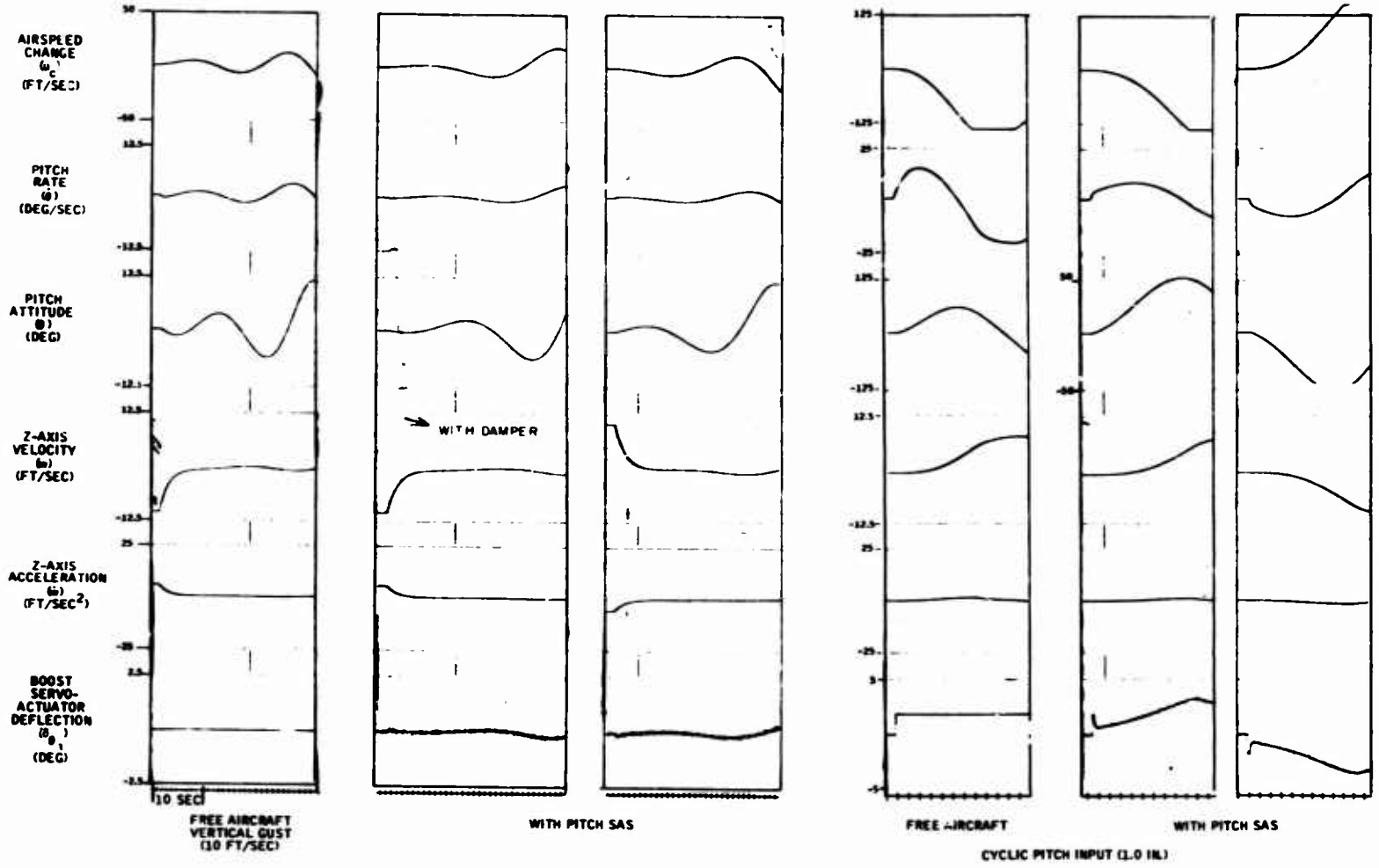

Figure 46. Pitch-Axis Responses at Hover, Oil Temperature = 120°F.

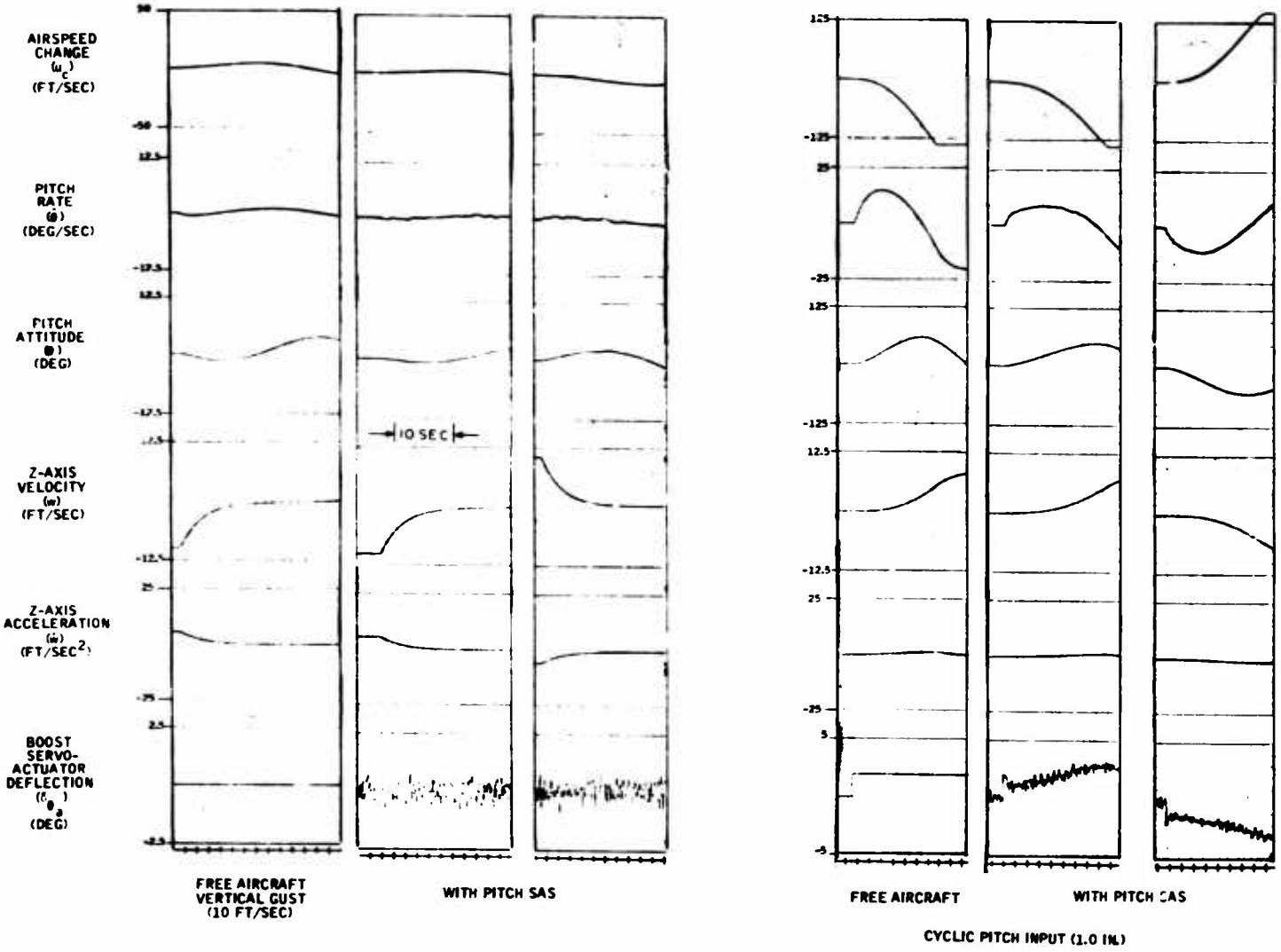

Figure 47. Pitch-Axis Responses at Hover, Oil Temperature = 185°F.

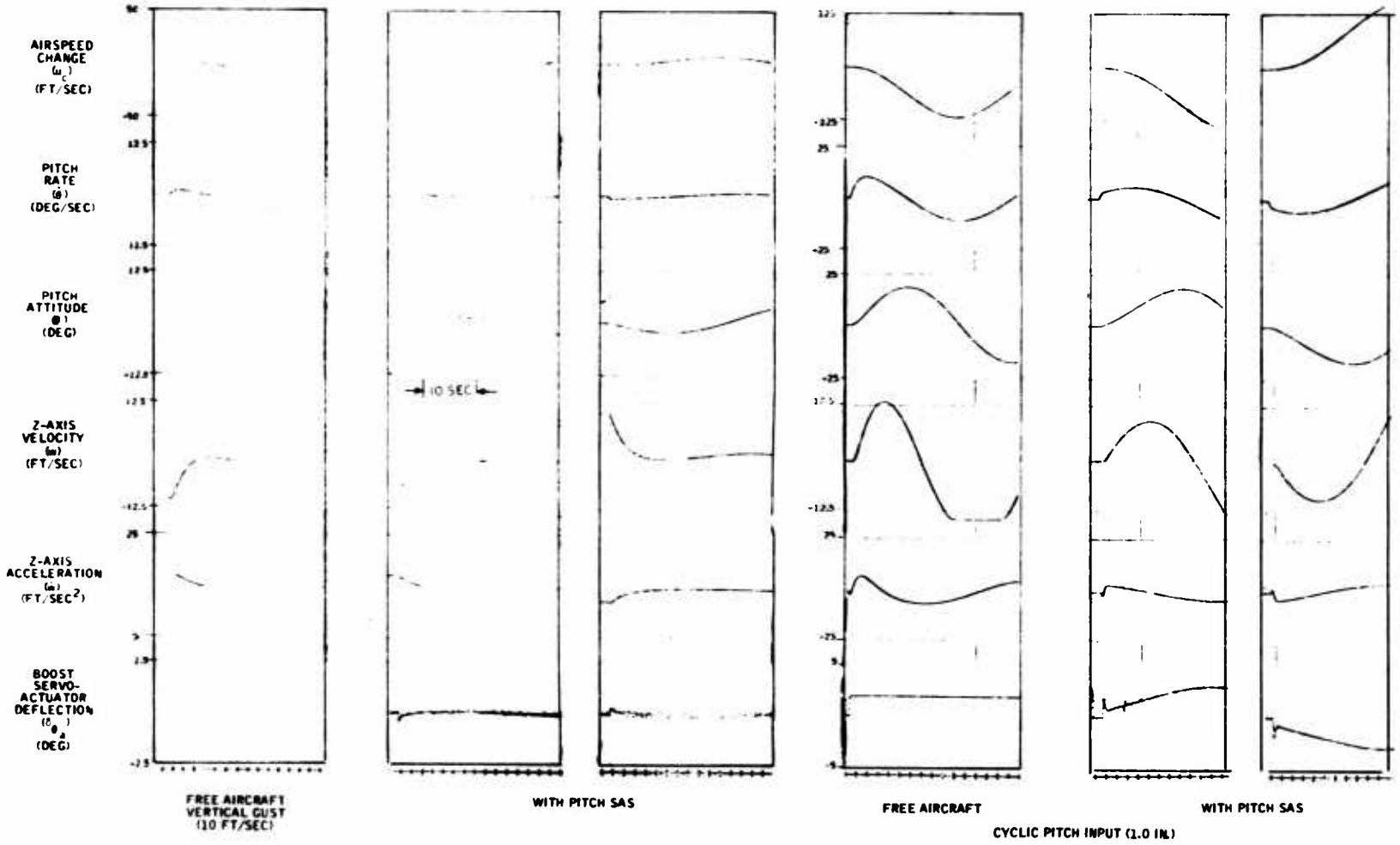

Figure 48. Pitch-Axis Responses at V = 45 Knots, Oil Temperature = 120°F.

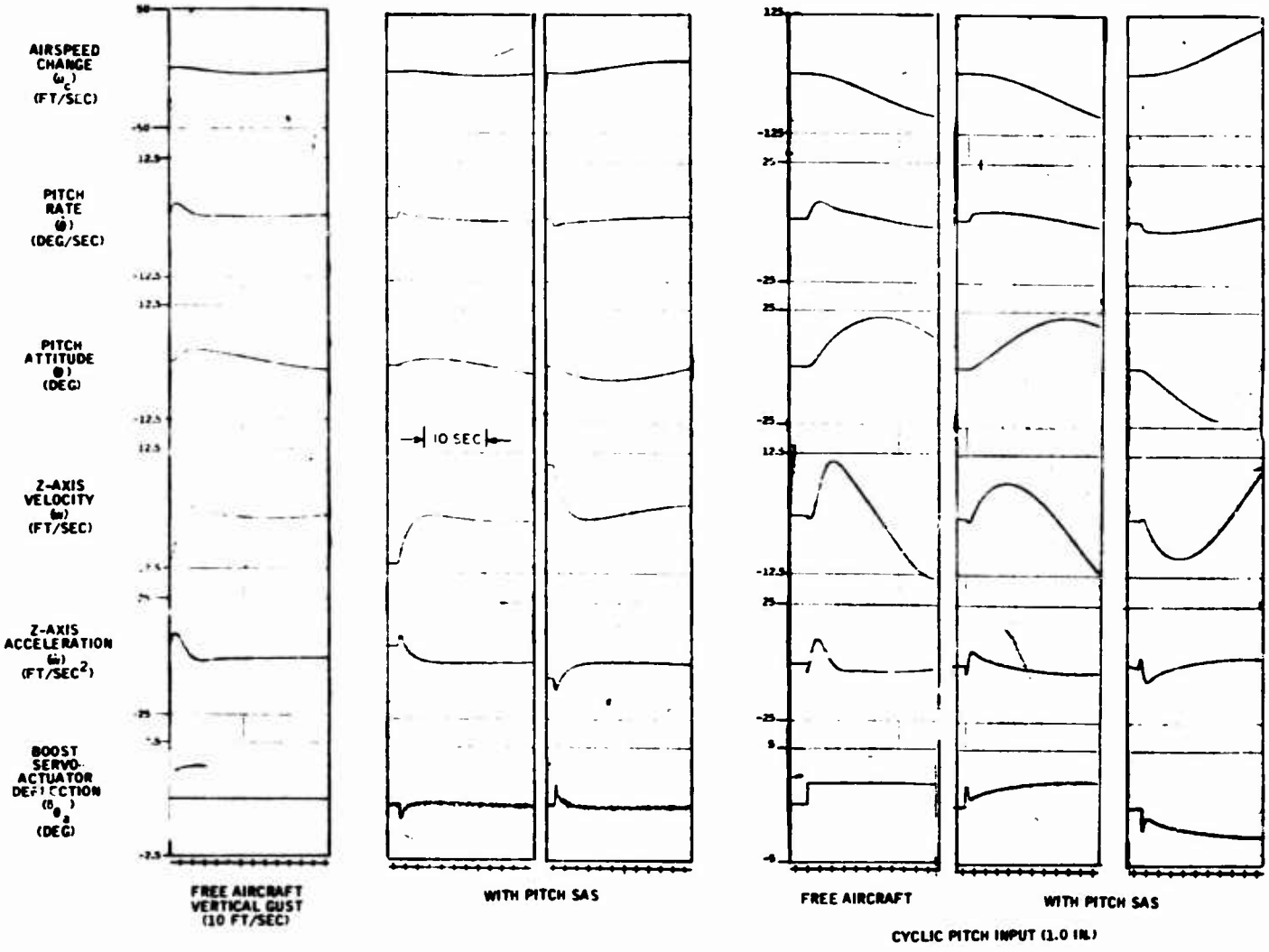

Figure 49. Pitch-Axis Responses at V = 85 Knots, Oil Temperature = 120°F.

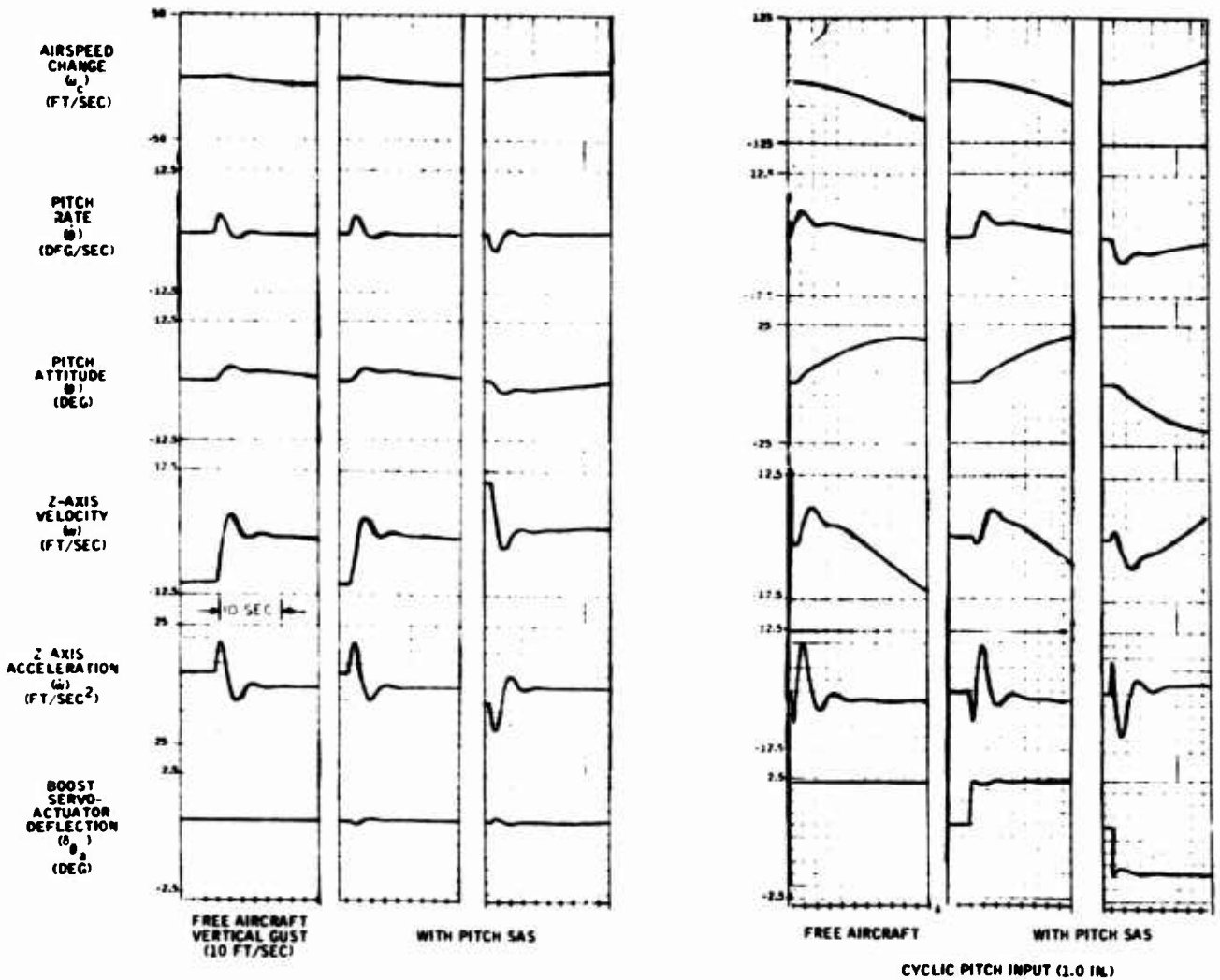

Figure 50. Pitch-Axis Responses at V = 130 Knots, Oil Temperature = 60°F.

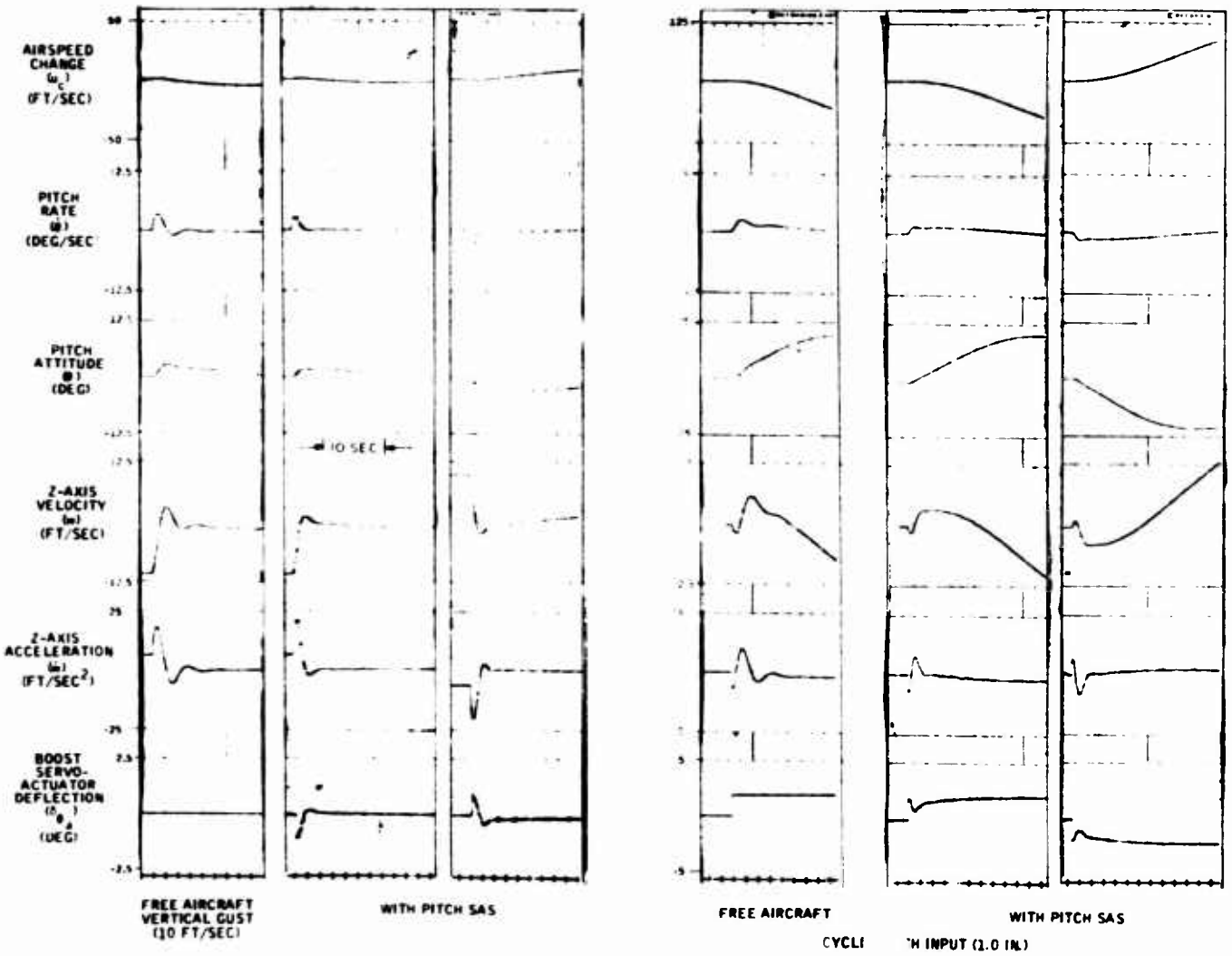

Figure 51. Pitch-Axis Responses at V = 130 Knots, Oil Temperature = 120°F.

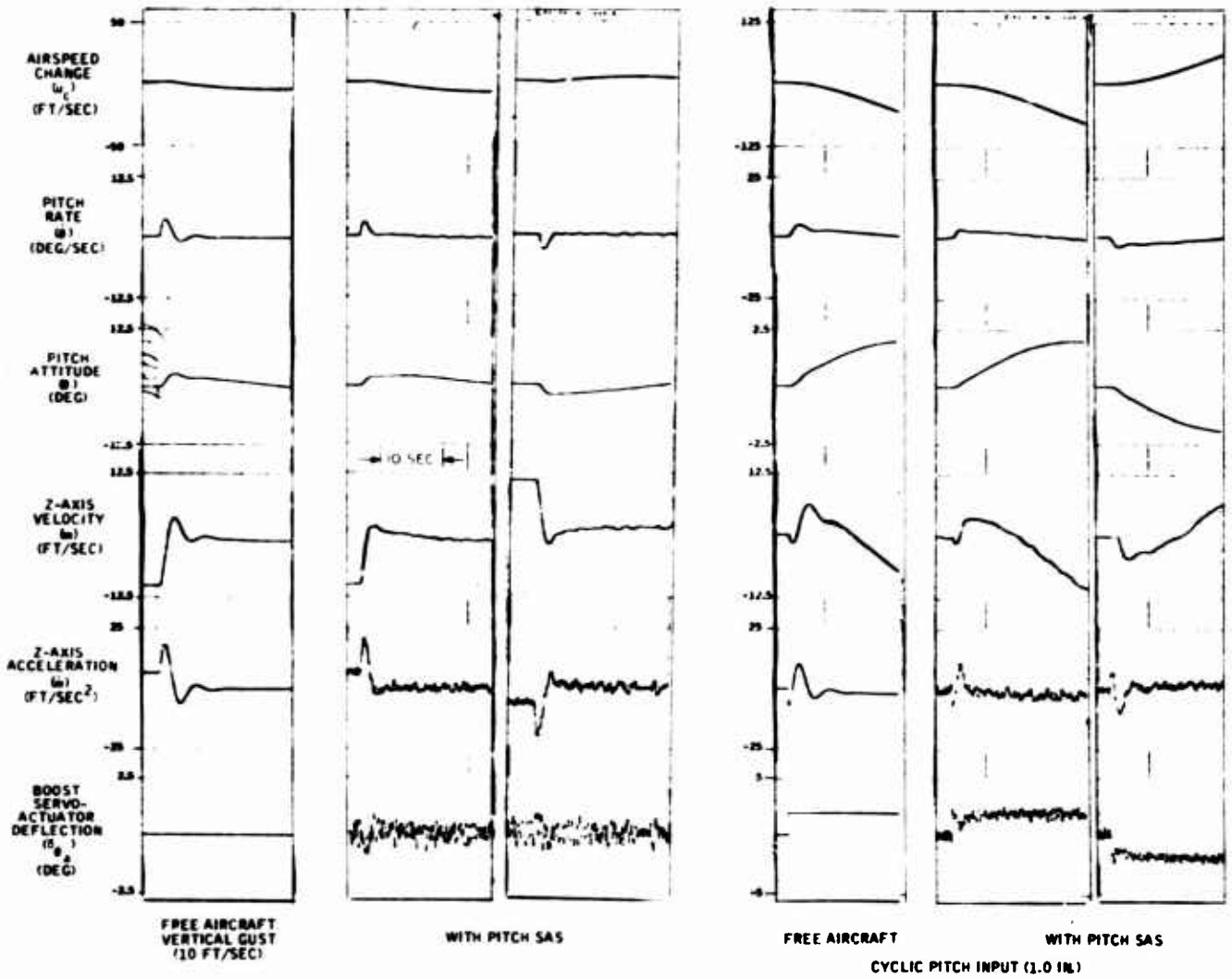

Figure 52. Pitch-Axis Responses at V = 130 Knots, Oil Temperature = 185°F.

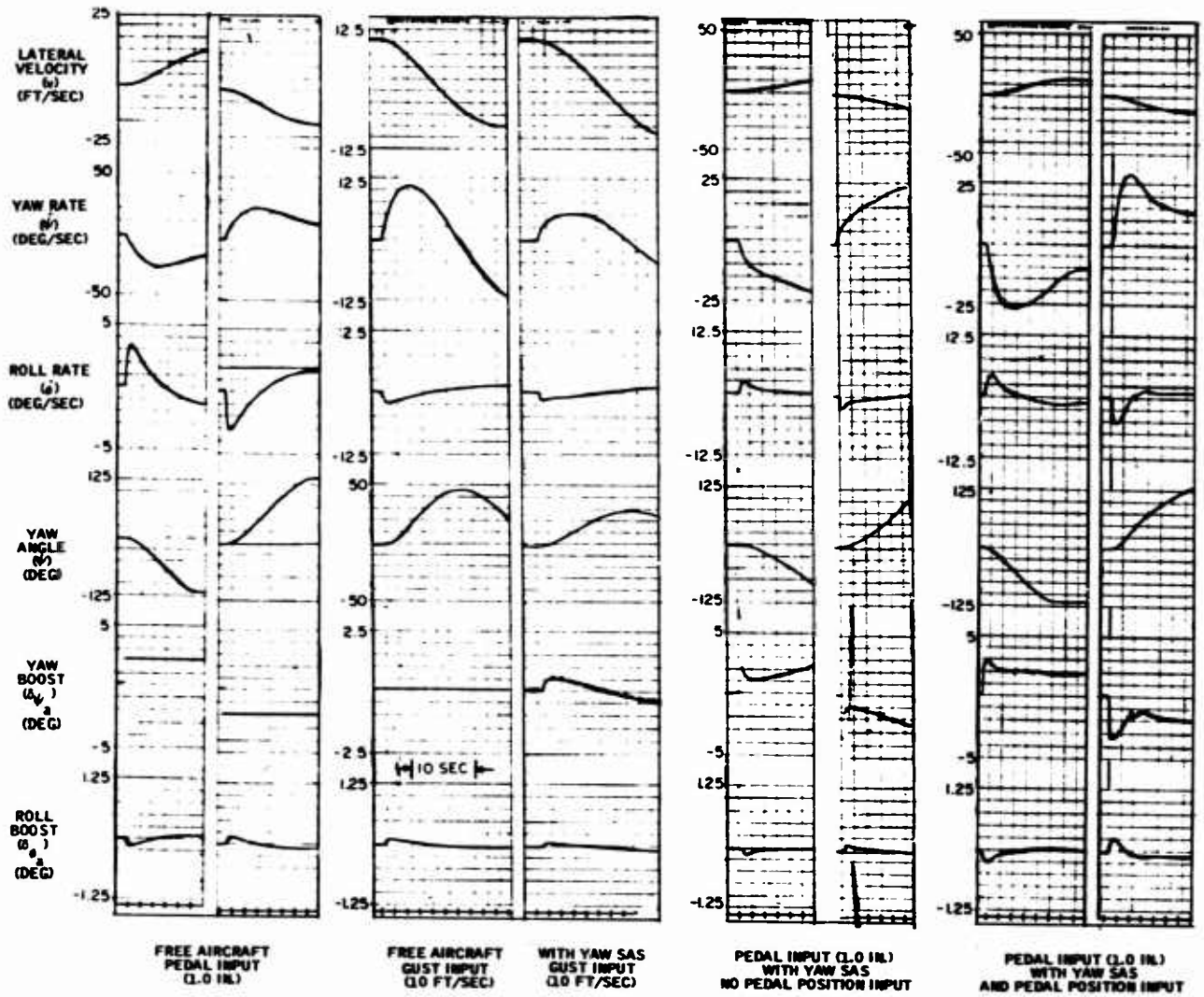

Figure 53. Yaw-Axis Responses at Hover, Oil Temperature = 120°F.

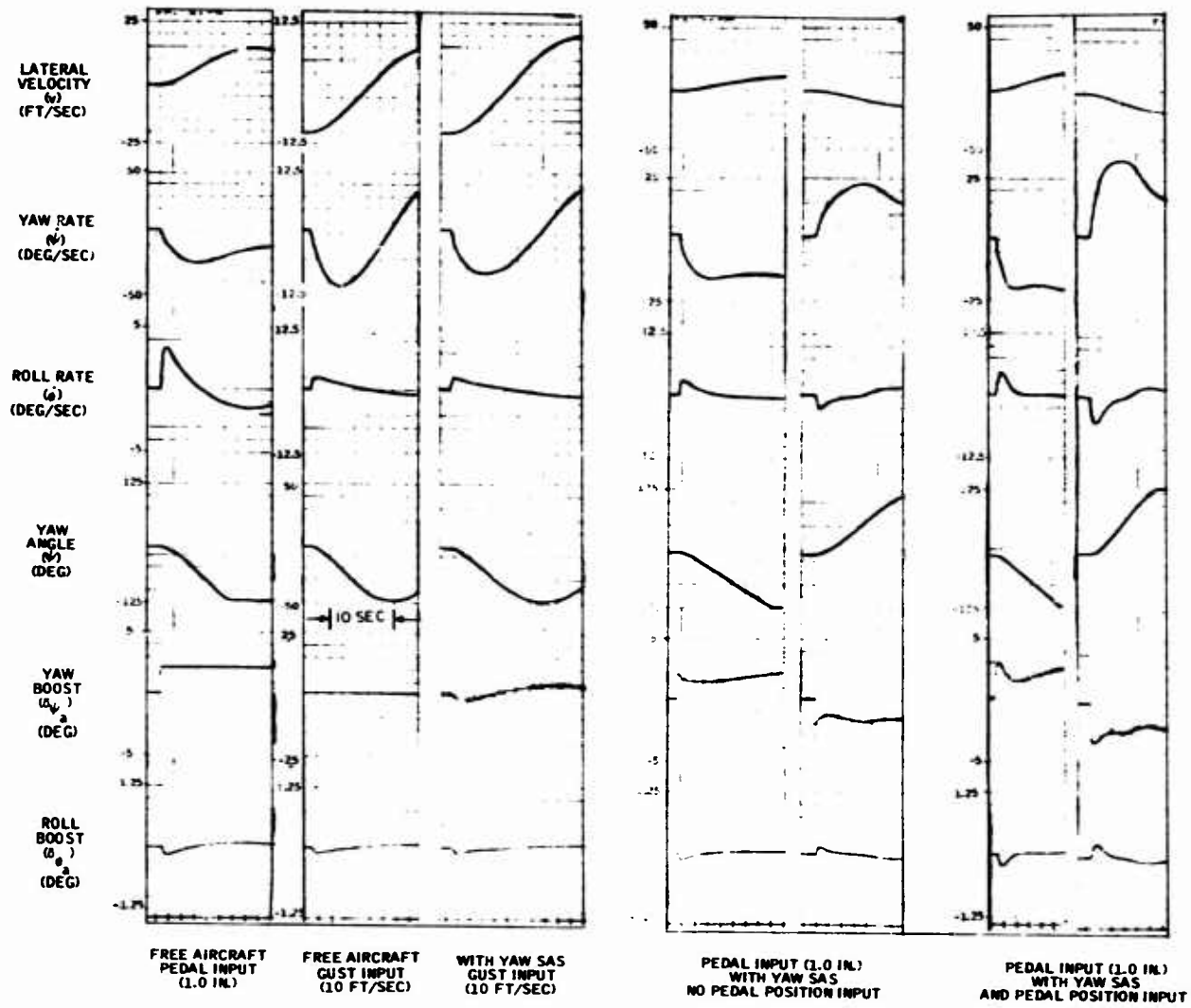

Figure 54. Yaw-Axis Responses at Hover, Oil Temperature = 185°F.

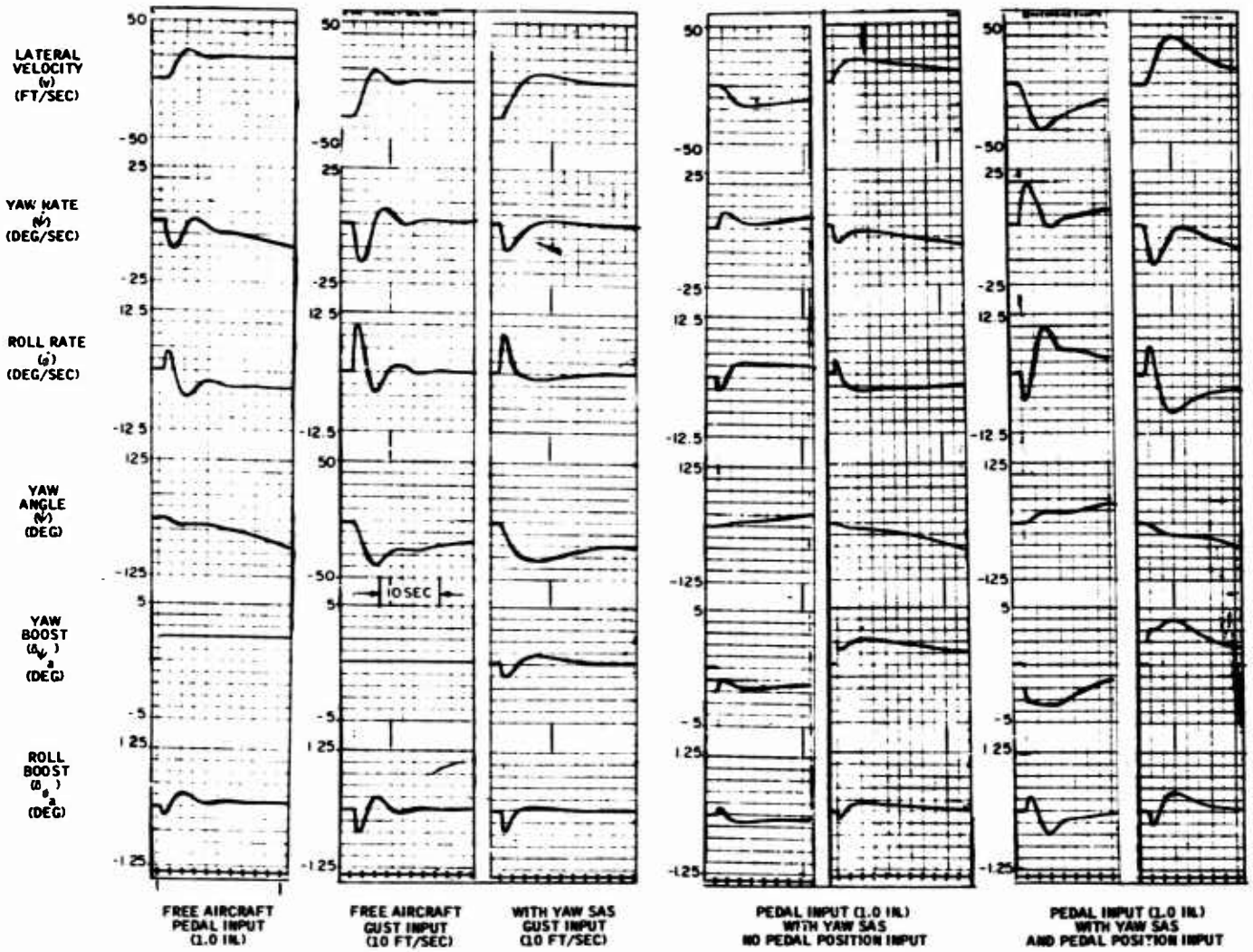

Figure 55. Yaw-Axis Responses at V = 60 Knots, Oil Temperature = 120°F.

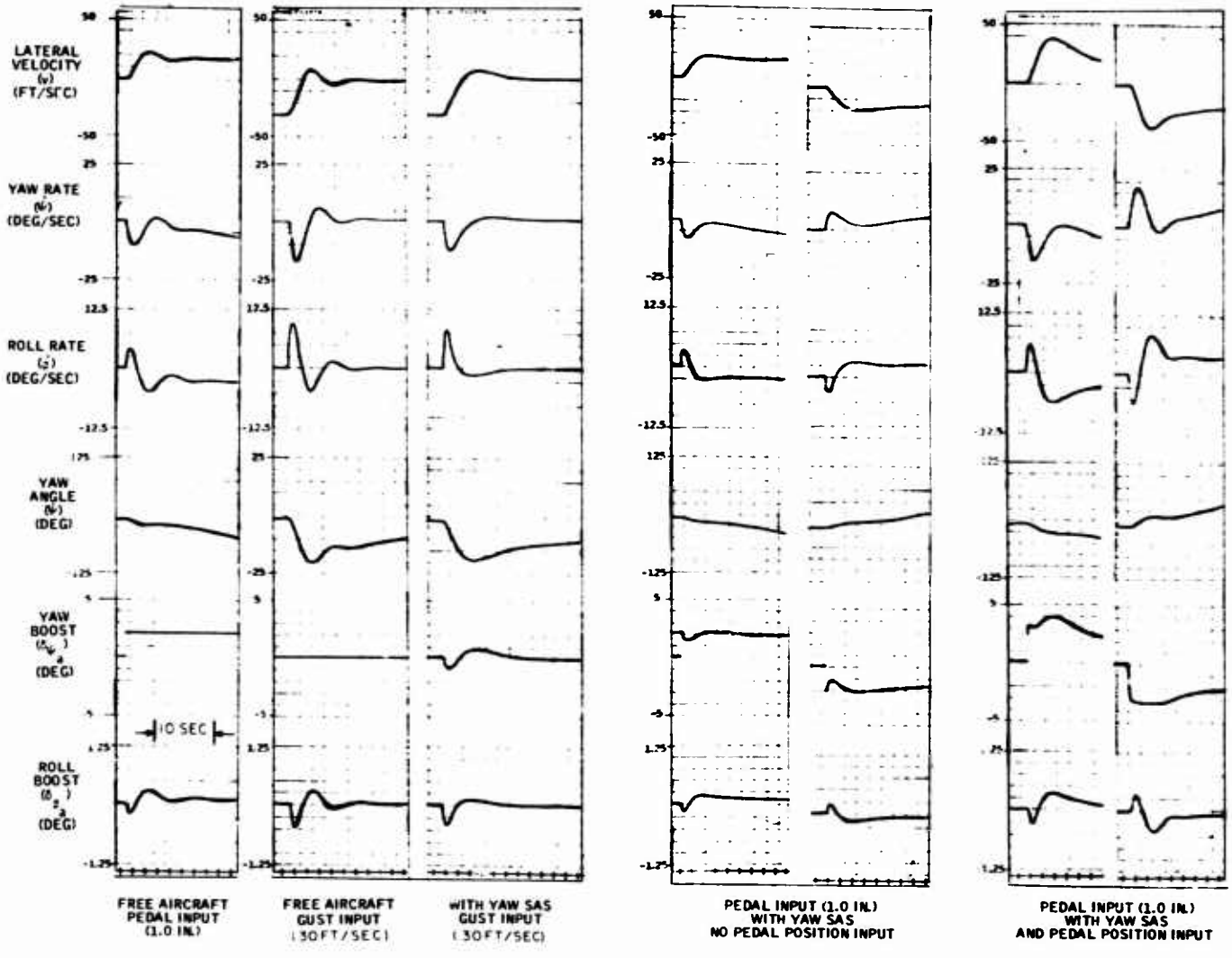

Figure 56. Yaw-Axis Responses at V = 60 Knots, Oil Temperature = 185°F.

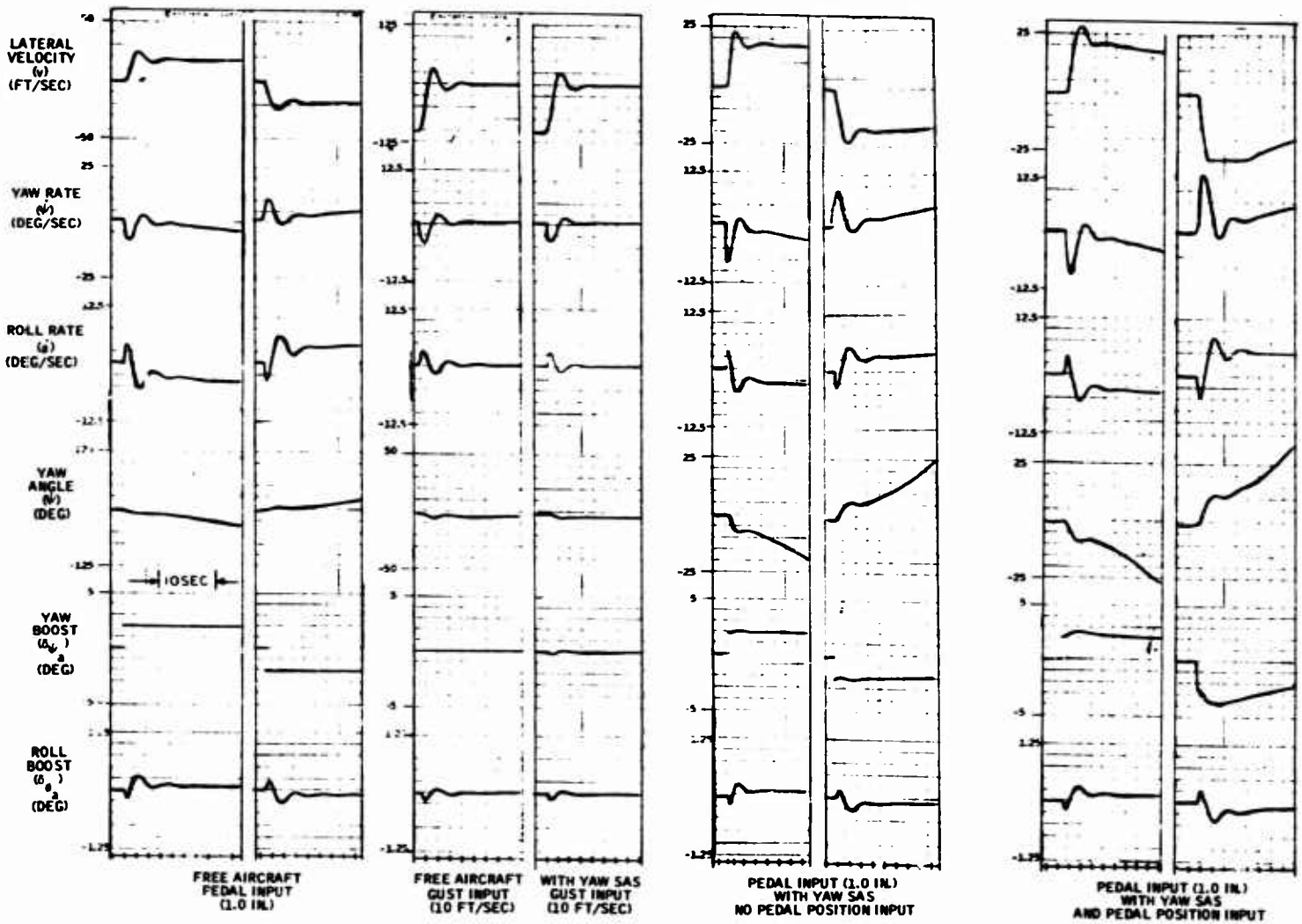

Figure 57. Yaw-Axis Responses at V = 120 Knots, Oil Temperature = 60°F.

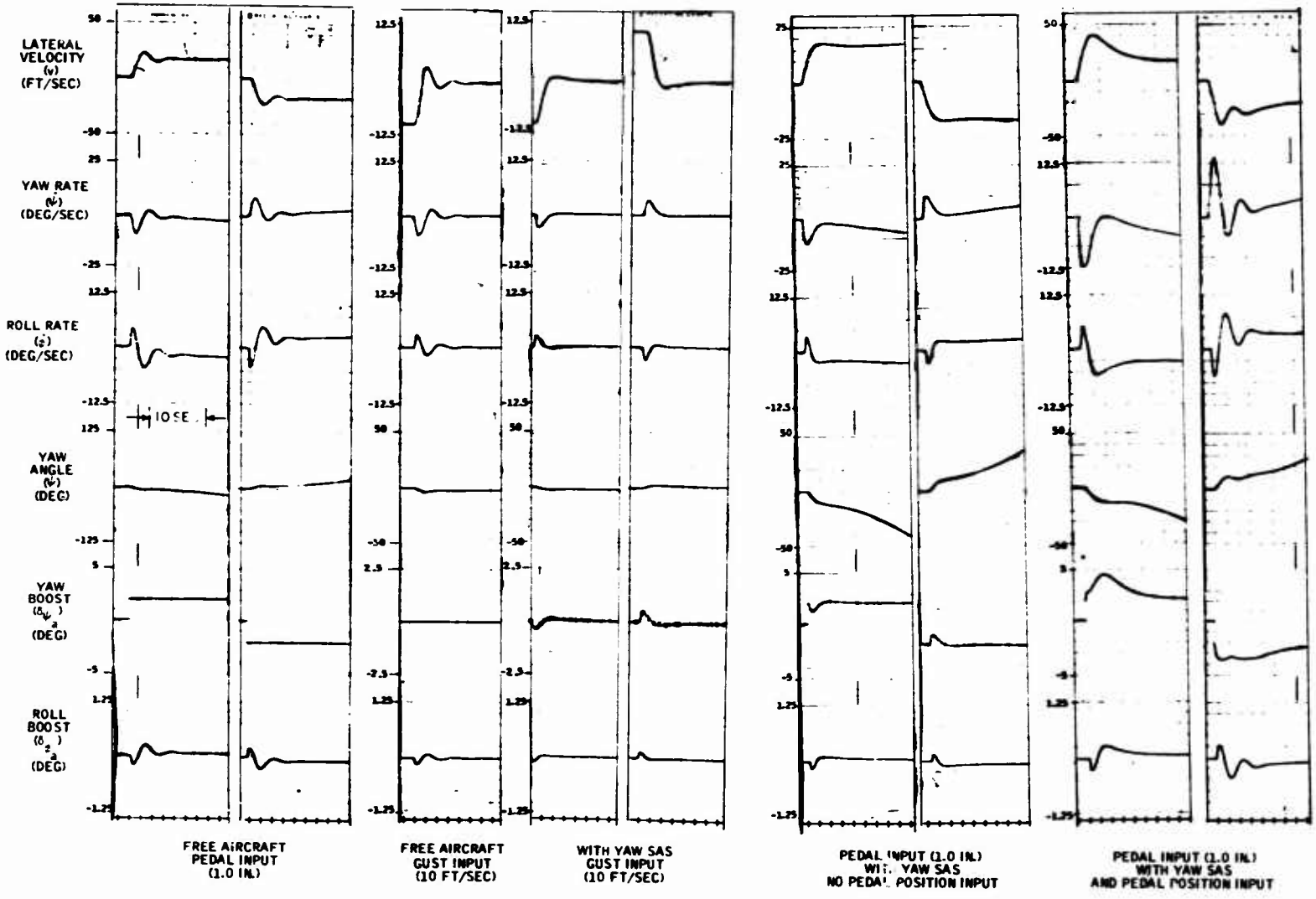

Figure 58. Yaw-Axis Responses at V = 120 Knots, Oil Temperature = 120°F.

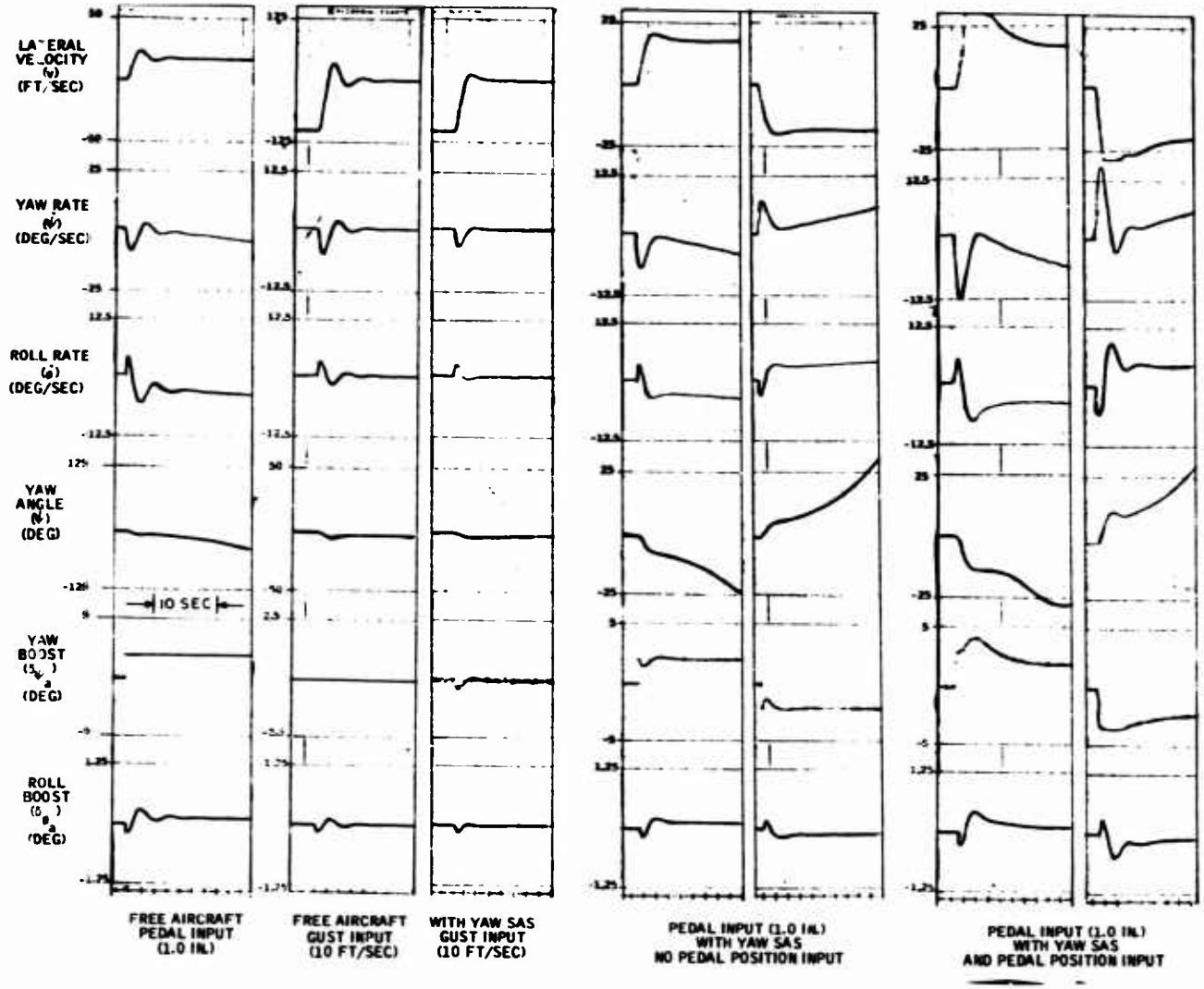

Figure 59. Yaw-Axis Responses at V = 120 Knots, Oil Temperature = 185°F.

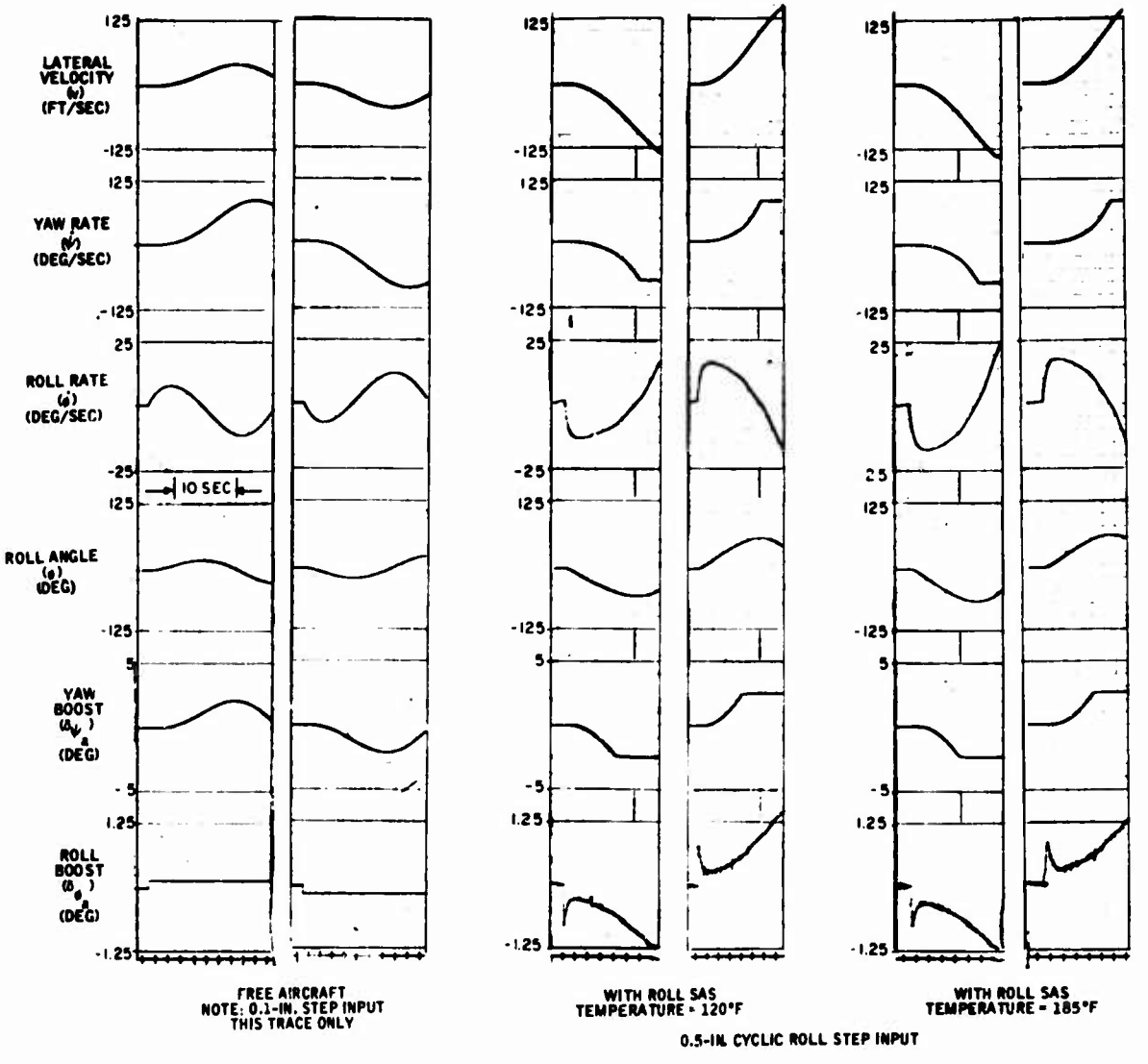

Figure 60. Roll-Axis Responses at Hover.

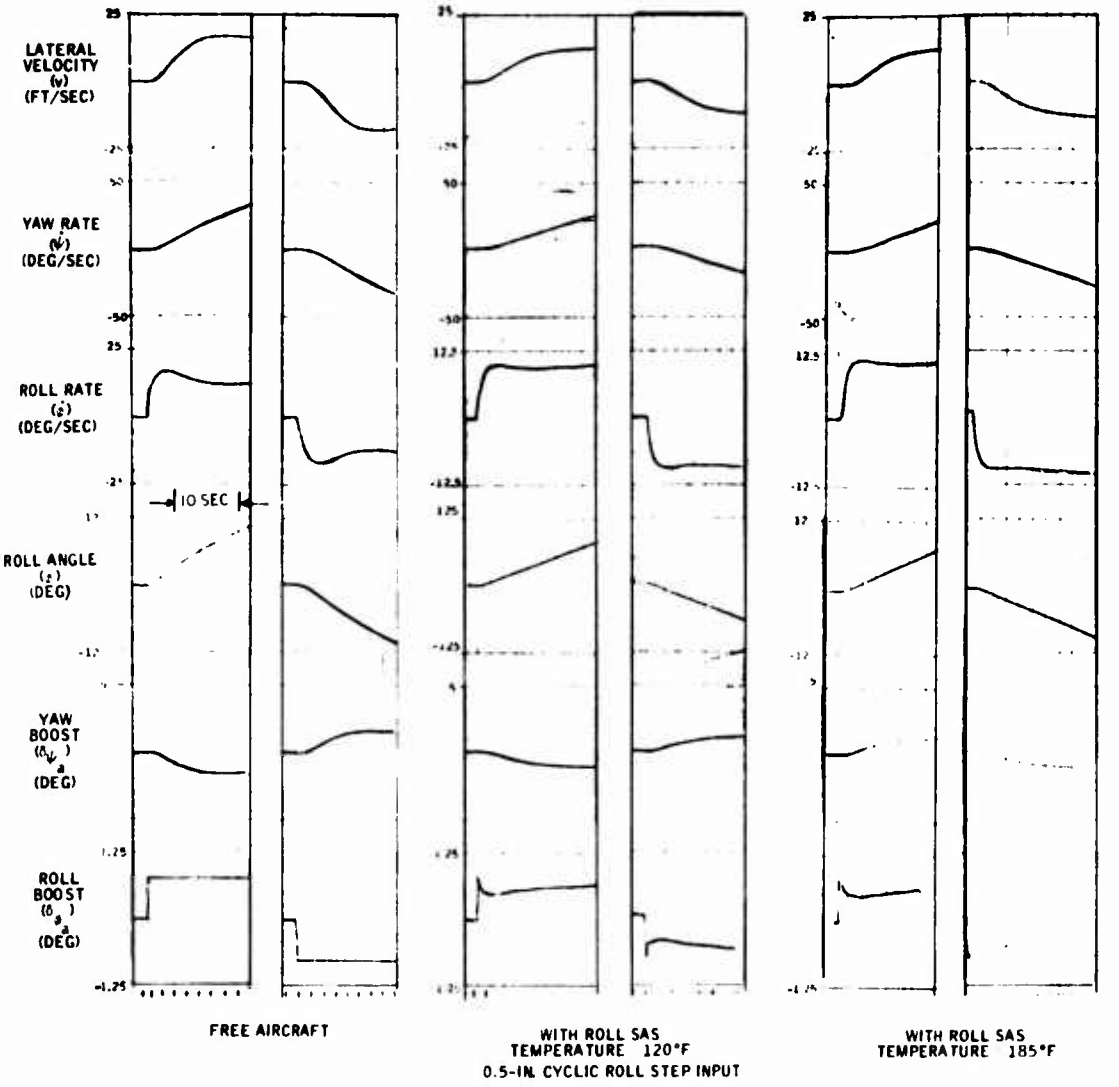

Figure 61. Roll-Axis Responses at V = 60 Knots.

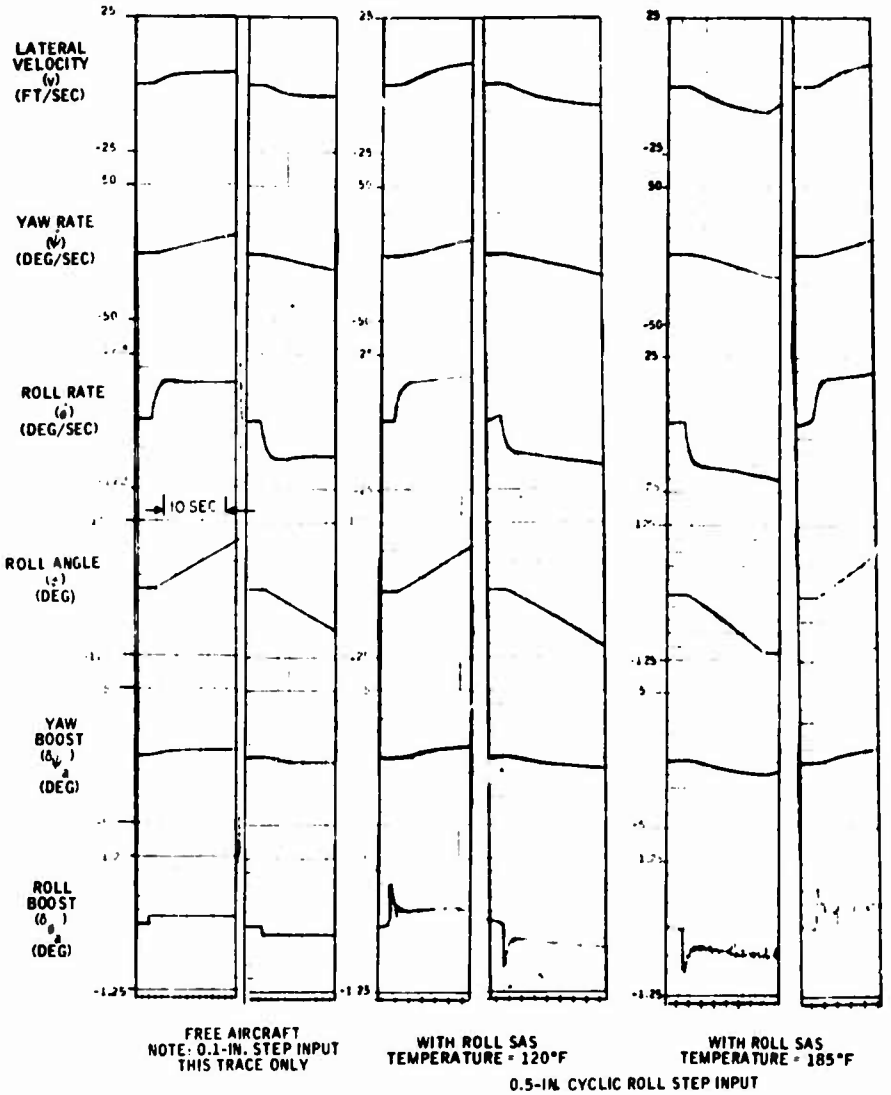

Figure 62. Roll-Axis Responses at V = 120 Knots.

TABLE VI. TEST CONDITIONS

Axis	Speed (kn)	Temperature (°F)
Pitch	Hover, 130	60
	Hover, 45, 85, 130	120
	Hover, 130	185
Yaw	Hover, 120	60
	Hover, 60, 120	120
	Hover, 60, 120	185
Roll	Hover, 60, 120	120
	Hover, 60, 120	185

TABLE VII. SUMMARY OF PITCH-AXIS GUST RESPONSES

Flight Condition	Free Aircraft	Pitch SAS Temperature 60°F	Pitch SAS Temperature 120°F	Pitch SAS Temperature 185°F	Analysis Results
Hover					
O/SH (%)	0.0	0.0	-	0.0	0.0
$t_{90\%}$(sec)	4.2	4.2	-	4.0	4.4
45 kn					
O/SH (%)	0.0	-	0.0	-	0.0
$t_{90\%}$(sec)	2.0	-	2.6	-	2.8
85 kn					
O/SH (%)	10.0	-	5.0	-	5.0
$t_{90\%}$ (sec)	1.0	-	1.5	-	1.4
130 kn					
O/SH (%)	35.0	32.0	17.0	20.0	17.0
$t_{90\%}$(sec)	0.5	0.5	0.5	0.5	0.7

Note, however, that the high noise level at hover does not couple into the acceleration trace in Figure 47. This is explained by the fact that acceleration is a function of airspeed:

$$\dot{W} = \frac{U}{g}\dot{\theta} - \frac{W}{g}$$

and

$$U = 0 \text{ at hover}$$

Pitch-axis control power is evaluated by measuring the amount of pitch deflection, θ, obtainable at 1 sec after a cyclic step input of 1 in. Results obtained from closed-loop responses are similar to those obtained in the analog study and were found to be insensitive to temperature variations.

Yaw Axis

Yaw-axis SAS damping of gust inputs is compared with that of the free aircraft in Table VIII.

Yaw gust responses are similar to those of the analysis study but have slightly more overshoot. The effect of oil temperatures on yaw-axis damping is similar. Dutch roll damping approaches that of the free aircraft at the low (60°F) temperature for the high-speed case (120 kn), as shown in Figure 57. The effect of temperature on yaw system noise is much less than that for pitch. A comparison of responses with 120°F (Figure 58) and 185°F (Figure 59) shows equivalent noise levels in the yaw boost trace.

Yaw control power was evaluated by measuring the amount of heading deflection (yaw angle), ψ, obtainable at 1 sec after applying a 1-inch pedal input. Results of the closed-loop tests are summarized in Table IX. The values are averages for right and left pedal inputs and do not precisely match the results of analog studies. Right and left pedal responses are sometimes quite different in both amplitude and damping, as shown in Figures 53 through 59. The difference may be due to the pedal input device, which could cause the summing amplifier to saturate in one direction if the device is not precisely nulled. However, the results in Table IX indicate that the use of a pedal position input consistently increases yaw control power by a significant amount.

Roll Axis

Roll-axis damping (dutch roll mode) is primarily a function of the yaw-axis SAS, as previously described. Roll-axis control power is evaluated by measuring roll angle, ϕ, at 1 sec after applying a roll cyclic input. The roll rate and roll angle values summarized in Table X have been normalized to represent a 1-inch input.

TABLE VIII. SUMMARY OF YAW-AXIS GUST RESPONSES

Flight Condition	Free Aircraft	Yaw SAS Temperature 60°F	Yaw SAS Temperature 120°F	Yaw SAS Temperature 185°F	Analysis Results
60 kn					
O/SH (%)	26.0	-	23.0	23.0	14.0
$t_{90\%}$ (sec)	2.6	-	5.2	4.6	5.2
120 kn					
O/SH (%)	35.0	25.0	10.0	10.0	7.0
$t_{90\%}$ (sec)	1.7	1.5	0.7	0.8	1.0

TABLE IX. YAW-AXIS CONTROL POWER FOR 1-IN. PEDAL INPUT

Flight Condition	Free Aircraft	Yaw SAS Temperature 60°F No PI	60°F PI	120°F No PI	120°F PI	185°F No PI	185°F PI	Analysis Results No PI	Analysis Results PI
Hover									
ψ (deg) at 1 sec	9.0	-	-	7.0	13.0	8.0	12.0	7.0	10.0
60 kn									
ψ (deg) at 1 sec	7.0	-	-	6.0	13.0	6.0	11.0	6.0	8.0
120 kn									
ψ (deg) at 1 sec	6.5	7.0	9.0	8.0	9.0	6.5	11.0	5.0	7.3

*PI = Pedal Input

TABLE X. SUMMARY OF ROLL-AXIS RESULTS FOR 1-IN. CYCLIC INPUT

Flight Condition	Free Aircraft	Roll SAS Temperature 120°F	Roll SAS Temperature 185°F	Analysis Results
Hover				
$\dot{\phi}$ ss* (deg/sec)	-	-	-	24
ϕ (deg) at 1 sec	40	20	24	24
60 kn				
$\dot{\phi}$ ss (deg/sec)	25	20	22	17
ϕ (deg) at 1 sec	18	14	15	12
120 kn				
$\dot{\phi}$ ss (deg/sec)	68	24	30	20
ϕ (deg) at 1 sec	30	16	20	14

*ss = Steady State

The actual input values were 0.1 or 0.5 inch as marked on the traces in Figures 60 through 62. The roll rate and roll angle values are slightly higher than those obtained in the Phase I studies. The response shapes and trends are similar and are not overly sensitive to temperature changes.

Roll-axis noise levels are only slightly increased at the 185°F temperature.

SUMMARY

Closed-loop simulation results obtained on the three-axis hydrofluidic SAS indicate that nominal transient response performance is nearly equivalent to that indicated in the Phase I studies (see Appendix I).

The following items should be considered during flight tests of the FSAS:

1. Recordings of helicopter responses with stabilizer bar are desired for comparing operation of the FSAS with that of the stabilizer bar.

2. The phugoid mode of the helicopter without stabilizer bar is not stability-augmented by the FSAS. Analysis results indicate that the phugoid mode in hover has divergent damping for the free aircraft and aircraft plus FSAS with a period of 20 seconds or longer. Thus, hover control in flight may be somewhat marginal depending on the validity of the analytical model of the helicopter without stabilizer bar.

SECTION VI
CONCLUSIONS AND RECOMMENDATIONS

CONCLUSIONS

This program represents a significant milestone in the development of a major fluidic system. It is significant because the development was carried through system hardware without going through a breadboard phase. In addition, in designing to an "operational"-type specification, many beneficial as well as adverse hardware conditions were uncovered that could aid the designer in future hardware programs. This section presents conclusions in three categories: (1) general program conclusions; (2) items to be incorporated in future designs; and (3) items that should be avoided in future designs.

General Conclusions

The following general conclusions are presented:

- Analysis to Hardware - Although the specification was not completely met in terms of compensation over the entire temperature range, and some deficiencies were uncovered in the area of servoactuator peaking, it was shown to be possible to develop final hardware from analytical study specifications without going through a system breadboard phase.

- Size Reductions - A hydrofluidic system can be packaged in a compact envelope competitive with conventional systems on a volume and weight basis.

- Temperature Compensation - Future hydrofluidic systems can be compensated for temperature variations over a desired temperature range without adding significantly to hardware complexity. For simple systems it is possible, with proper design of the vortex rate sensor alone, to compensate the system for temperature variations from 90°F to 160°F.

- Built-in Test - It was demonstrated that hydrofluidic systems can incorporate BIT capability without complex circuitry.

- Power Supply - Testing demonstrated that the three-axis hydrofluidic system can be mechanized into an aircraft-type power system without interaction between the various systems. The use of standard available pressure regulation hardware will result in satisfactory system performance.

For Future Design Use

The following items should be incorporated in the design of future systems:

- System Back Pressure - Hydrofluidic systems should be back-pressured to at least 100 psi when the pressure drop across the system is approximately 20 psi. This eliminates effects of downstream plumbing and reduces the noise generated by cavitation within the system. Whether the back pressure can be changed for different system pressure drops was not determined.

- Orifice in Series With Amplifier Power Port - An orifice directly under the power nozzle of an amplifier increases amplifier noise considerably. It was found that by placing a number of layers of screen between the orifice and amplifier, the noise was greatly reduced. This technique offers a convenient means of reducing individual amplifier pressures without increasing amplifier output noise.

- Flow Split in Vortex Rate Sensor - It was found that the flow split and secondary-to-primary sink diameter ratio in the vortex rate sensor could not be larger than approximately 3-to-1. Larger ratios degraded sensor performance. A solution to this problem was to add an annulus-type outlet just before the flow reached the primary sink inlet radius. This technique can be used wherever it is necessary to obtain a high-response rate sensor.

- Nonlinearity of Bellows - It had been assumed originally that standard bellows have a linear characteristic between displacement and applied force. This was found to be erroneous. With special forming and heat treating, it is possible to obtain bellows with linear characteristics. All future purchases of bellows should have a specification as to the linearity required.

- Servoactuator Deficiencies - Deficiencies were noted in both the spool valve and vortex valve servoactuators used in the program. Both types have problems in the area of the force capsules that are presently used; they can be damaged quite easily by pressure surges that can be encountered during system startup. In addition, the vortex valve servoactuator force capsules were susceptible to air entrapment, as no "bleeds" were incorporated.

  Both types exhibited underdamped operation when run with a hydrofluidic amplifier (peaking). In addition, the vortex valve servoactuator exhibited peaking and nonrepeatable performance at low-amplitude input signals. The method

of applying the feedback to the flapper could be changed, or possibly a stiffer flapper-force capsule combination would solve both the force capsule and peaking problems. It is felt that a higher pressure gain would solve the vortex valve servoactuator low-amplitude input problem.

Avoid in Future Design

The following items should be avoided in future designs:

- Nonstandard O-Rings - O-rings with a small cross section were used in this program to reduce the size of the system. The end result was a negligible effect on overall size, but a marked increase in difficulty of assembly, tolerance to variations such as orifice disks placed under the O-ring, availability, and sealing capability when used on large plates.

- Epoxy Tape for Sealing and Joining - For pressures over 1000 psi, it was found that using epoxy tape to seal and join a manifold is presently questionable. With more study it may become a usable technique. Study is needed to determine thickness of tape to use, the amount of load it can take, and how large a surface should be between channels and between the channels and edge of the manifold. Future systems will probably use the electroformed conductive wax (ECW) process, used to fabricate amplifiers for the present system, for the construction of most future manifolds.

- Orifice Disks Located Under O-Rings - The practice up to this time has been to install orifices in the system by placing 0.005-in.-thick disks under the appropriate O-ring. This creates two problems. One is a slight leak when the system is subject to a high back pressure (1000 psi), and the other is that the O-ring can be sucked out of shape when a large flow passes through the orifice at startup. A different technique of adding orifices should be used for the construction of most future manifolds.

- Large Plates With Many O-Rings - Large, flat plates with many O-rings located across the plates make assembly difficult. Also, when the plates are subjected to high internal forces, it is difficult to keep sufficient pressure on the O-rings to prevent leakage. This problem is aggravated by nonstandard cross-section O-rings.

RECOMMENDATIONS

Two major recommendations are submitted as a result of experience gained from this program:

1. On the basis of the performance demonstrated during the closed-loop tests, it is recommended that the three-axis fluidic stability augmentation system be flight-test evaluated in a UH-1-type helicopter. The flight test evaluation should include a comparison between aircraft performance with the stabilizer bar and that with the FSAS.

2. Further development effort should be applied in the areas of temperature compensation, resolving servoactuator deficiencies, and the use of the electroformed conductive wax (ECW) process for fabricating most manifolding.

APPENDIX I
THREE-AXIS FLUIDIC STABILITY AUGMENTATION SYSTEM FINAL REPORT (HONEYWELL DOCUMENT 21058-FR1, DECEMBER 1968)

Prepared by

Honeywell Inc.
Government and Aeronautical Products Division
Minneapolis, Minnesota

For

EUSTIS DIRECTORATE
U. S. ARMY AIR MOBILITY RESEARCH AND DEVELOPMENT LABORATORY
FORT EUSTIS, VIRGINIA

CONTRACT DAAJ02-68-C-0039

TABLE OF CONTENTS

TABLE OF CONTENTS (CONTINUED)

TABLE OF CONTENTS (CONCLUDED)

SECTION I
SUMMARY AND CONCLUSIONS

SUMMARY

This report summarizes the analysis, research, and development accomplished on Contract DAAJ02-68-C-0039.

The objective of this program was to establish the requirements for a three-axis fluidic stability augmentation system (FSAS) suitable for the UH-1 helicopter.

Major efforts on this program consisted of:

- Computer simulation studies of various control concepts
- Hardware and circuit studies to determine feasibility and expected performance of selected components or networks
- System design effort to define a three-axis hardware mechanization and an associated specification.

The program resulted in the following major accomplishments:

- System analysis efforts resulted in a control system which will substantially improve the handling qualities of the UH-1B helicopter without significantly changing the desirable free-vehicle characteristics. This system is compatible with the characteristics of hydrofluidic technology. The analysis efforts are described in detail in Section II.

- The simplified lag-lead circuit and the integrating rate sensor described in the Engineering Program Plans and Procedures document were fabricated and tested. Both of these devices were found to be superior to the standard lag-lead network. This lag-lead network was originally simulated as one vehicle response shaping scheme, but it was not used in the final FSAS configuration because its frequency characteristics caused the augmented vehicle to have handling qualities much different from those of the desired free-vehicle qualities.

- A pilot input device was fabricated and evaluated. The concept used was found to be suitable for the rudder input device, and to have the capability to provide a nonlinear gain characteristic.

- A "calibrate button" for the vortex rate sensor (to simulate a steady-state input rate) was tested and will be incorporated in the three-axis system to improve preflight checkout.

- Tests on a large-scale model of the hydrofluidic amplifier showed that specific changes in the amplifier geometry will improve its performance in regions where the present design exhibits a nonlinear gain curve.

- Results of system analysis and hardware studies were combined to select a mechanization for the three-axis FSAS. This mechanization and its requirements are described in Detail Specification DS 21565-01, which is presented in Section IV. Drawings showing the individual axes in schematic form, installation details, and the power supply mechanization are also presented.

CONCLUSIONS

- The computer analysis presented herein shows that it is feasible to develop an all-hydraulic control system (FSAS) to augment the damping and control response characteristics of the UH-1B helicopter.

- The defined FSAS augments response characteristics of the UH-1B in a manner that satisfies the requirements of the design goals.

- Nominal FSAS performance will be achieved with a hydrofluidic mechanization that exhibits typical off-design tolerances.

SECTION II
ANALYSIS REPORT ON THE THREE-AXIS FSAS FOR THE UH-1B HELICOPTER

INTRODUCTION

This report represents the results of a stability and control analysis of the UH-1B helicopter, using computer simulation techniques aimed at defining a simple three-axis fluidic stability augmentation system (FSAS) to provide adequate stabilized aircraft performance within the constraints imposed by the current state of the art in hydrofluidics. The analysis was directed at optimizing the damping versus control response performance of the UH-1B for the high-speed fire support mission. Control concepts were evaluated from the viewpoint of increasing vehicle damping and augmenting the free vehicle's short-term response characteristics to provide a rate response proportional to control stick inputs.

A performance demonstration is to be conducted using the UH-1B, without the stabilization bar, as the test vehicle.

SUMMARY

The objective of this analysis program was to define mathematically the system block diagrams for a simple fluidic stability augmentation system to augment the roll, pitch, and yaw axes of the UH-1B helicopter, using hydraulic fluid (hydrofluidics) as the control medium. No performance requirements were specified other than that the FSAS must improve vehicle damping and handling qualities of the UH-1B helicopter during the high-speed gun-firing mission. With these general requirements in mind, a set of detailed design goals was generated that permits FSAS performance to be evaluated in light of these self-imposed system requirements. The detailed analysis goals are presented in a later section.

Nominal FSAS performance was evaluated in light of the design goals, and the time histories and data show that design requirements were satisfied. FSAS performance is summarized briefly as follows:

- Yaw-axis damping was increased from 0.3 to approximately 0.6 or greater.
- The pedal position input loop eliminates the hover and low-speed problem of the yaw-axis damper fighting pilot input commands.

- Pitch-axis damping was increased from 0.3 to 0.5 or greater.
- Roll-axis control effectiveness was adjusted to provide a more controllable vehicle.
- Roll and pitch responses were designed for a rate response proportional to control stick deflection.

The parameter variation study results show that nominal FSAS performance may be achieved for ±20-percent tolerance variations. In some cases, parameters such as high-pass time constants and pedal position input gain are considered noncritical from the standpoint of stability, and larger tolerance variation from nominal may be allowed, so long as their effects on system transient response are taken into consideration.

An analysis of the effects of series servoactuator frequency response on system performance showed that the natural frequency, at the 90-deg phase lag point, should be 10 Hz or greater, with a damping of 0.7 to ensure nominal system performance. When the servoactuator natural frequency was set at 7 Hz, the data showed that the bandwidth of the system was decreased to a point where nominal system performance began to deteriorate slightly. Therefore, to avoid the problem of having the series servoactuator frequency characteristics act as a major contributor in establishing the stability margins of the system, the servoactuator's natural frequency should not be allowed to go below 8 Hz (at the 90-deg phase lag point) with a damping ratio of 0.7.

The primary goal of this analysis was to show three-axis hydrofluidic SAS feasibility using simplified control techniques. The use of flight path sensors was considered beyond the scope of the FSAS control system program.

The use of collective pitch and roll crossfeeds was considered during the "Fluid State Hydraulic Damper" program, under Contract DA 44-177-AMC-294(T), and was rejected for the following reasons:

- Airframe data to permit evaluation of a collective crossfeed were not available.
- Complexity of the system would be increased far beyond that necessary to demonstrate fluid system feasibility.

These control concepts were also considered during this analysis and were not pursued for reasons similar to those mentioned above.

The analysis results presented in the following sections show that a fixed-gain rate feedback system will be suitable to demonstrate the feasibility of using a hydrofluidic SAS to increase vehicle damping and produce a short-term rate response proportional to control stick deflection.

DISCUSSION

FSAS Description

Analytic block diagrams of the yaw, roll, and pitch axes of the FSAS are shown in Figures 63, 64, and 65, respectively. Each axis consists of a hydrofluidic vortex rate sensor with the fluid signal output amplified, shaped, and then fed directly to the series augmentation servoactuators. The feedback signal paths are high-passed to eliminate damper opposition to pilot input commands and also to minimize the effects of any component drift. Pedal position input is incorporated in the yaw SAS to eliminate the decrease in vehicle response to pedal inputs caused by the yaw damper. The pedal input transducer has a low gain over center to allow small trim-type tail rotor inputs to be made by the pilot. The transducer has a nonlinear null slope of approximately 0.5, increasing to a gain of 1.5 for moderately larger inputs.

Data and Assumptions

Six-degrees-of-freedom linear perturbation equations of motion were used during the analysis to mathematically represent the UH-1B helicopter. These equations are presented in Section III. The performance results of the stability augmentation system defined herein are those for the UH-1B helicopter defined by these equations of motion and aerodynamic data. Also presented in Section III are the UH-1B aerodynamic coefficient data for the four flight conditions studied, along with analog computer diagrams and potentiometer settings used during this analysis.

A servoactuator with a fluid interface having a natural frequency (90-deg phase lag point on amplitude response) of 10 Hz or greater and a damping ratio of 0.7 was initially specified. A frequency analysis showed that the natural frequency of the series servoactuator should be greater than 8 Hz to prevent the system's stability margins from being adversely affected.

All other system dynamics capable of generating gain or phase shift characteristics were assumed to be accounted for in a double-lagged transport delay as follows:

$$T(S) = \epsilon^{-\tau S}/(1 + 0.05S)^2$$

where

τ = Transport delay of 30 ms for yaw axis, 20 ms for roll axis, and 30 ms for pitch axis

S = Laplace operator

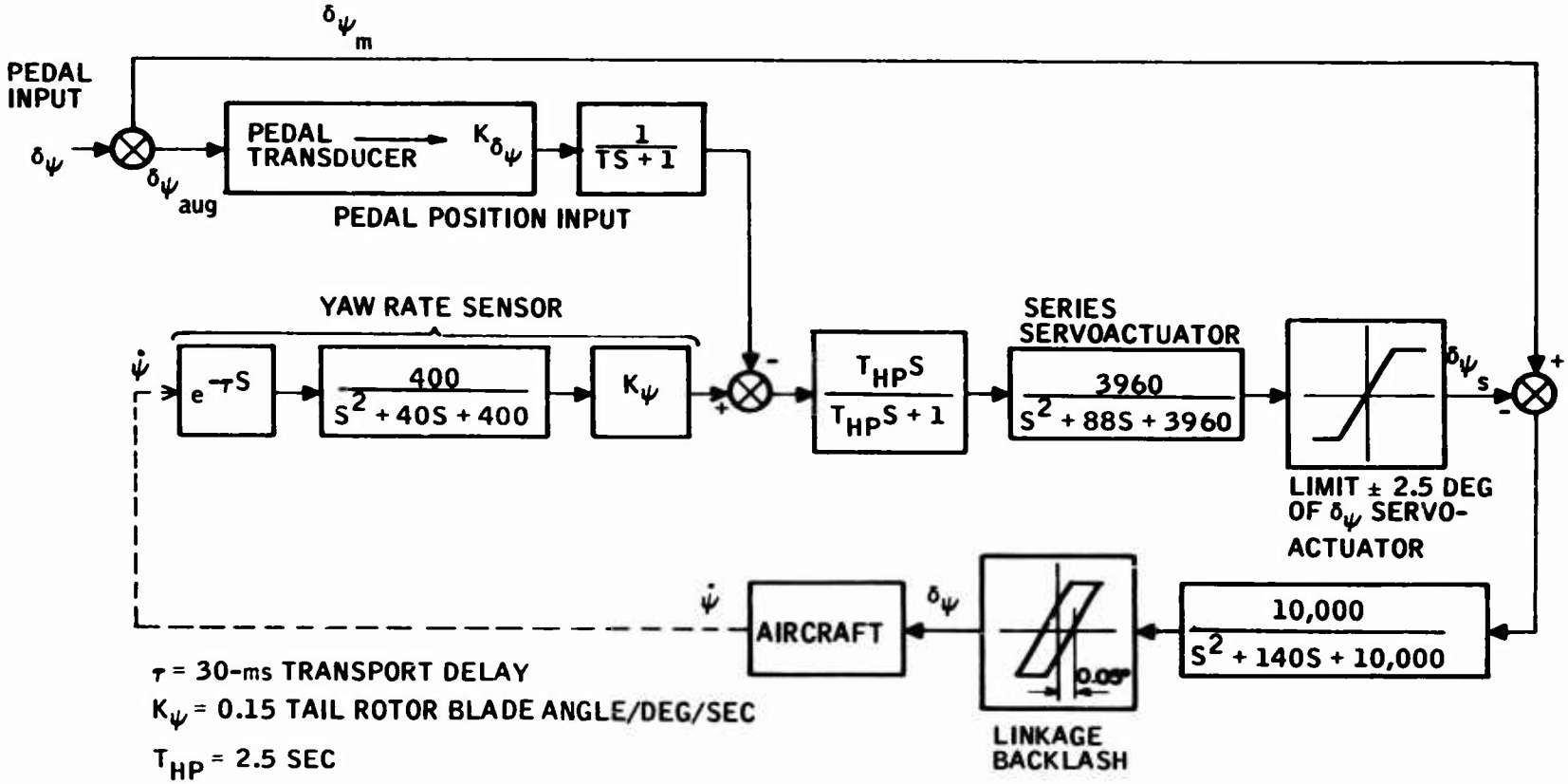

Figure 63. Analytic Block Diagram for UH-1B Yaw SAS.

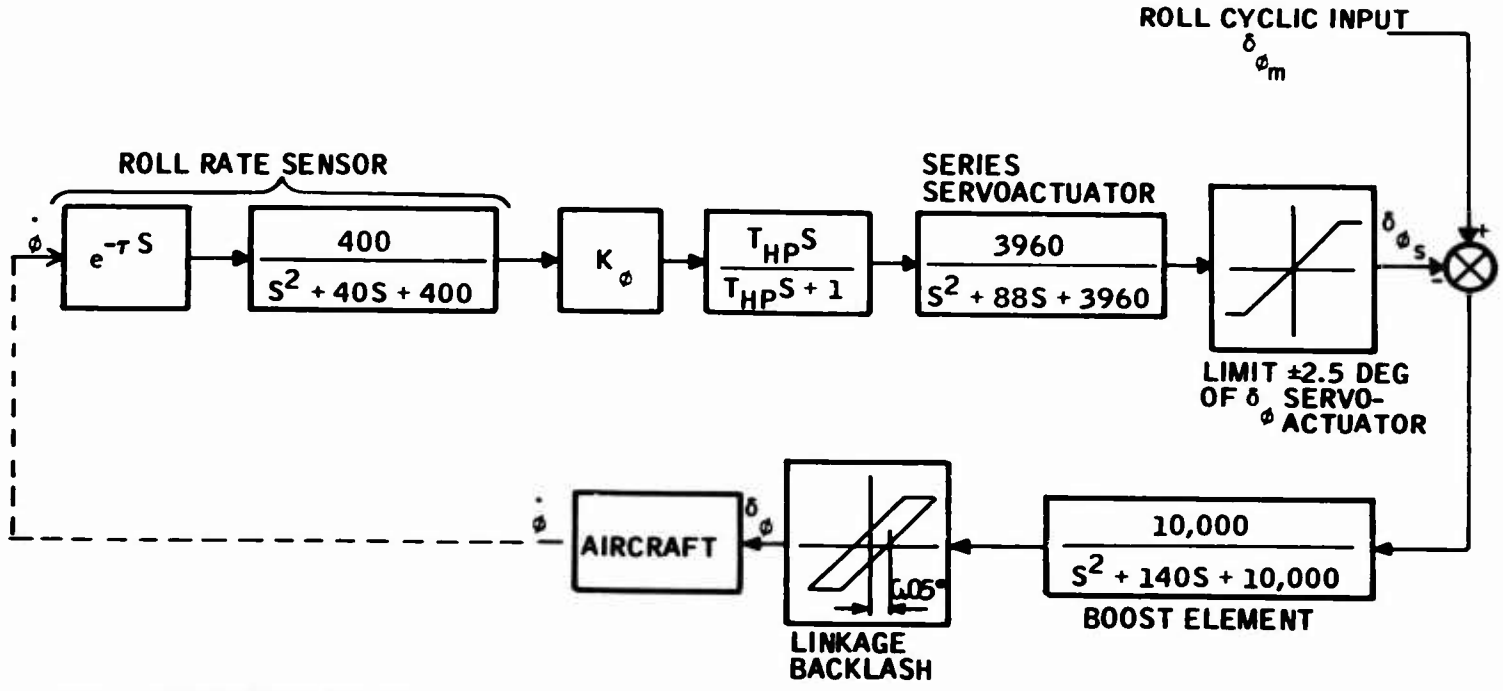

τ = 20-ms TRANSPORT DELAY

K_ϕ = 0.055 DEG LATERAL BLADE ANGLE/DEG/SEC

$T_{HP} \geq$ 10.0 SEC

LATERAL CYCLIC STICK SENSITIVITY = 1.54 DEG LATERAL BLADE ANGLE/IN. STICK

Figure 64. Analytic Block Diagram for UH-1B Roll SAS.

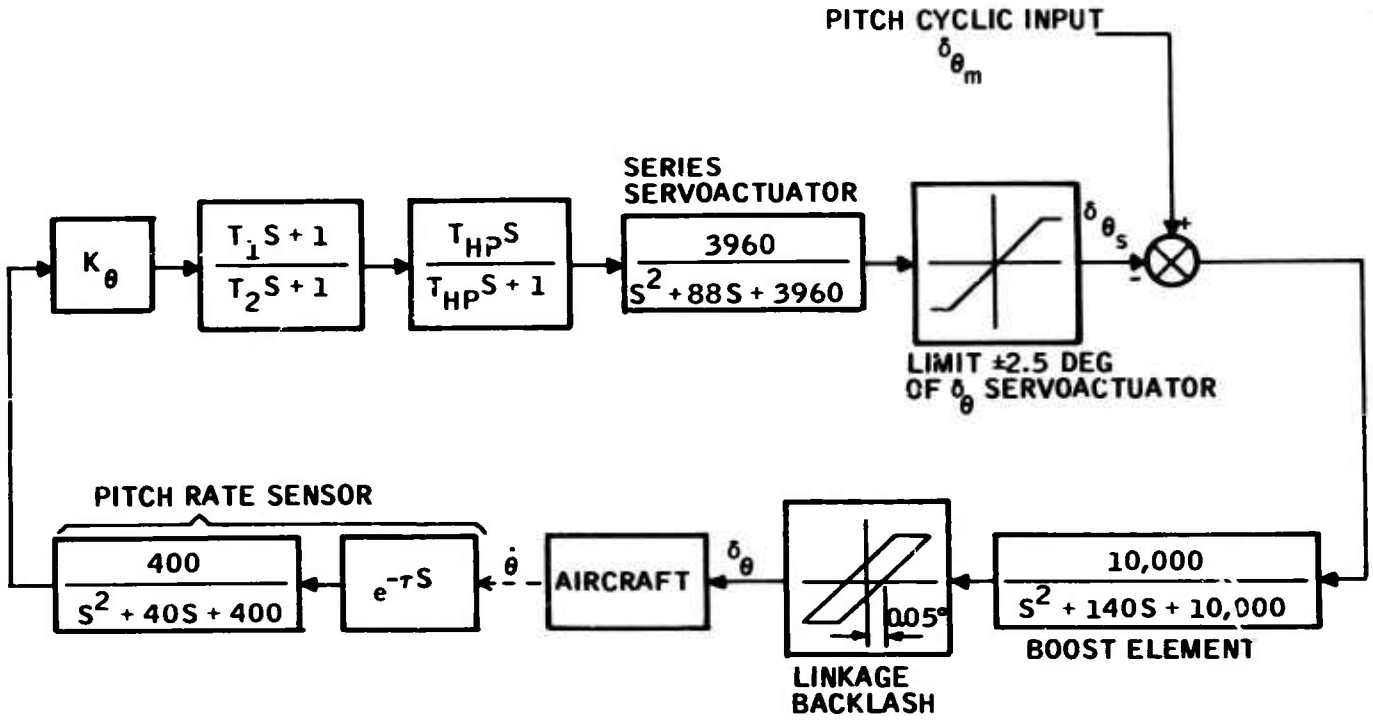

τ = 20-ms TRANSPORT DELAY

K_θ = 0.25 DEG LONGITUDINAL BLADE ANGLE/DEG/SEC

T_1 = 0.25 SEC

T_2 = 0.1 SEC

T_{HP} = 1.5 SEC

LONGITUDINAL CYCLIC STICK SENSITIVITY = 1.84 DEG LONGITUDINAL BLADE ANGLE/IN. STICK

Figure 65. Analytic Block Diagram for UH-1B Pitch SAS.

A fourth-order Pade approximation of the 20- and 30-ms transport delay was used as follows:

$$e^{-\tau S} = \left(\frac{S^2\tau^2 - 11.59\,\tau S + 36.53}{S^2\tau^2 + 11.59\,\tau S + 36.53}\right)\left(\frac{S^2\tau^2 - 8.42\,\tau S + 46.0}{S^2\tau^2 + 8.42\,\tau S + 46.0}\right)$$

This approximation of $e^{-\tau S}$ is valid for frequencies up to 20 Hz.

Tailboom bending, vibration modes, and small-amplitude linkage nonlinearities were not analyzed. Insufficient data exist to perform a detailed analysis of these higher-order characteristics. However, during this analysis, gains and time constants of the FSAS were defined to minimize the possibility of exciting these undesired modes.

DESIGN GOALS FOR THE FLUIDIC STABILITY AUGMENTATION SYSTEM

The design goals used as guidelines during this analysis to develop the FSAS control system are discussed in the subsections that follow. These design goals were generated to be in agreement with helicopter flying and ground handling-quality requirements detailed in Military Specification MIL-H-8501A.

The primary analysis guidelines were twofold: (1) The resulting FSAS must be a simple system and it must provide a more stable gun-firing platform for the high-speed UH-1B gun-firing mission. (2) The system must augment the vehicle in a manner presently accomplished by the mechanical stabilizer, the end result being to eliminate the need for a mechanical stabilizer.

FSAS performance will be demonstrated in light of these design goals.

Pitch-Axis Design Goals

The controls shall be free from objectionable transient forces in any direction following rapid pitch stick deflections.

There shall be no objectionable or excessive delay in the development of angular velocity in response to control displacement. The angular acceleration shall be in the proper direction within 0.2 sec after pitch control displacement.

The helicopter shall exhibit satisfactory dynamic stability characteristics following pitch disturbances in forward flight. Specifically, the stability characteristics shall be unacceptable if the following are not met for a single disturbance in smooth air:

- Any oscillation having a period of less than 5 sec shall damp to one-half amplitude in not more than 2 cycles, and there shall be no tendency for undamped small-amplitude oscillations to persist.

- Any oscillation having a period greater than 5 sec but less than 10 sec shall be at least lightly damped.

- Any oscillation having a period greater than 10 sec but less than 20 sec shall not achieve double amplitude in less than 10 sec.

Pitch control power shall be such that when the helicopter is hovering in still air at the maximum overload gross weight or at the rated power, a rapid 1-in. step displacement from trim of the pitch control shall produce an angular displacement at the end of 1 sec which is at least $45/(W_M + 1000)^{1/3}$ deg, where W_M represents the maximum overload gross weight of the helicopter in pounds.

Typical normal gross weight of the UH-1B helicopter was taken to be 9500 lb. This is the value recommended by the aircraft manufacturer. Therefore,

$$\theta = 45/\sqrt[3]{10,500} = 2.05 \text{ deg}$$

The gross weight used during this analysis is 5400 lb. This decreased weight over that of the recommended normal gross weight actually presents a more severe performance design goal. The resulting angular displacement using this value of gross weight is

$$\theta = 45/\sqrt[3]{6400} = 2.43 \text{ deg}$$

The pitch-axis damping ratio of the UH-1B helicopter shall be increased from approximately 0.3 to approximately 0.5, or greater, at or near the 100-kn flight condition. This design goal may be demonstrated by simulating a vertical gust input and measuring the aircraft performance in damping the gust.

The vertical gust input shall be damped to within 20 percent of its maximum value within 1.5 sec following the gust.

At the hover flight condition, the time to damp the gust may be significantly longer to account for the free-vehicle damping characteristics.

Yaw- and Roll-Axes Design Goals

Yaw control power shall be such that when the helicopter is hovering in still air at the maximum overload gross weight or at rated takeoff power, a rapid 1-in. step displacement from the trim of the yaw control shall produce a yaw displacement at the end of 1 sec which is at

least $110/\sqrt[3]{W_M + 1000}$ deg, where W_M represents the maximum overload gross weight of the helicopter in pounds.

Again, the typical normal gross weight of 9500 lb was used. Therefore,

$$\psi = 110/\sqrt[3]{W_M + 1000} = 5.03 \text{ deg}$$

The resulting angular displacement using 5400 lb as the gross weight is

$$\psi = 110/\sqrt[3]{6400} = 5.93 \text{ deg}$$

The response of the helicopter to yaw control deflection, as indicated by the maximum rate of yaw per inch of sudden pedal displacement from trim while hovering, shall not be so high as to cause a tendency for the pilot to overcontrol unintentionally. In any case, the sensitivity shall be considered excessive if the yaw displacement is greater than 50 deg in the first second following a sudden pedal displacement of 1 inch from trim while hovering at the highest normal service loading.

The controls shall be free from objectionable transient forces in any direction following rapid roll stick or pedal deflections. The response of the helicopter to roll control deflection, as indicated by the maximum rate of roll per inch of sudden control deflection from the trim setting, shall not be so high as to cause a tendency for the pilot to overcontrol unintentionally. In any case, at all flight speeds, including hovering, the control effectiveness shall be considered excessive if the maximum rate of roll per inch of stick displacement is greater than 20 deg/sec.

There shall be no objectionable or excessive delay in the development of angular velocity in response to roll or yaw control displacement. The angular acceleration shall be in the proper direction within 0.2 sec after the control displacement.

Roll control power shall be such that when the helicopter is hovering in still air at the maximum overload gross weight or at the rated power, a rapid 1-inch step displacement from trim of the lateral control shall produce an angular displacement at the end of 0.5 sec of at least $27/\sqrt[3]{W_M + 1000}$ deg, where W_M represents the maximum overload gross weight of the helicopter in pounds.

Again, assuming the typical normal gross weight of the UH-1B helicopter of 9500 lb, $\phi = 1.23$ deg.

Using the gross weight of 5400 lb, the resulting angular displacement is $\phi = 1.45$ deg.

The yaw-axis damping ratio of the UH-1B helicopter shall be increased from approximately 0.3 to approximately 0.6 or greater at the high-speed flight conditions. This design goal was demonstrated by simulating a roll gust input and measuring aircraft performance in damping the gust.

The roll gust input shall be damped to within 10 percent of its maximum value within 1 to 1.5 sec following the gust.

This design goal did not apply to the hover flight condition.

YAW-AXIS ANALYSIS

Yaw SAS Performance

The UH-1B yaw axis was analyzed to develop an augmentation system that increases the vehicle damping ratio and thus improves damping external flight path disturbances during steady maneuvers without opposing the pilot's commands. To accomplish this objective, the yaw SAS was analyzed in three phases:

- Stability augmentation system
- Pedal position input response
- Parameter variation study

The results of these analysis tasks are presented in the paragraphs that follow.

Yaw Stability Augmentation System

Yaw stability augmentation of the UH-1B was analyzed without the mechanical stabilizer as part of the basic vehicle. Results were obtained with and without roll coupling and with and without the linkage backlash hysteresis of the primary control system.

The stability augmentation system is a conventional high-passed yaw rate feedback as follows:

$$\delta_\psi = \delta_{\psi_m} - K_\psi \left(\frac{T_{HP} S}{T_{HP} S+1} \right) \dot{\psi}$$

where

K_ψ = 0.15 deg tail rotor/deg/sec

T_{HP} = 2.5 sec

$\dot{\psi}$ = Yaw rate, deg/sec

δ_{ψ_m} = Mechanical tail rotor command from pilot's pedals, deg

δ_{ψ} = Total tail rotor command

The yaw rate feedback is high-passed with a 2.5-sec network to allow steady turns without the SAS fighting the turn.

Transient response performance of the free aircraft and yaw SAS for all forward flight conditions is shown in Figures 66, 67, and 68. The control system and aircraft dynamics were analyzed with tail rotor commands and side velocity gust initial conditions. Yaw SAS performance was evaluated by examining the percentage of overshoot and response time of the system. These values were obtained from the lateral velocity traces of the referenced figures. Pertinent performance data taken from these time histories are presented in Table XI. The $T_{90\%}$ response times specified in the table are solution times for the lateral gust inputs. Solution time is defined as the time to reach and remain within 10 percent of the final value. For the tail rotor step input commands, $T_{90\%}$ refers to the time to reach 90 percent of the final value.

The data in Table XI show that, in all cases, the overshoot response to a gust input was substantially reduced with the augmentation system engaged. By assuming the initial portion of the responses to be second-order, this overshoot can be expressed as an increase in vehicle damping ratio. At 60 kn without hysteresis, a 14-percent overshoot is noted for the augmented vehicle. This is equivalent to a damping ratio of 0.53. For this same condition, it is further noted that the free vehicle overshoots 27.5 percent, which is equivalent to a damping ratio of 0.38. The yaw SAS increased the vehicle damping ratio by 40 percent at this flight condition.

The yaw SAS damping response was optimized for the 90- and 120-kn flight conditions. Overshoot data in Table XI show that the damping ratio is greater than 0.6 for these flight conditions and for the 60-kn flight condition when hysteresis is taken into consideration. It is reasonable to assume that some small level of hysteresis will be present in the actual vehicle primary control system. These time histories and tabulated data show that the design goals of the yaw axis were achieved.

High-passed yaw rate feedback acts to improve the damping in the yaw axis. However, as damping is improved, yaw stability suffers. The decrease in yaw stability presents itself as a loss of turn coordination.

The gains and time constants were adjusted to minimize the loss of turn coordination and improve damping. If, during flight test, turn coordination becomes a problem, yaw SAS gain can be reduced as a tradeoff between damping and turn coordination. Pedal position input gain should be reduced by the same ratio as yaw SAS gain.

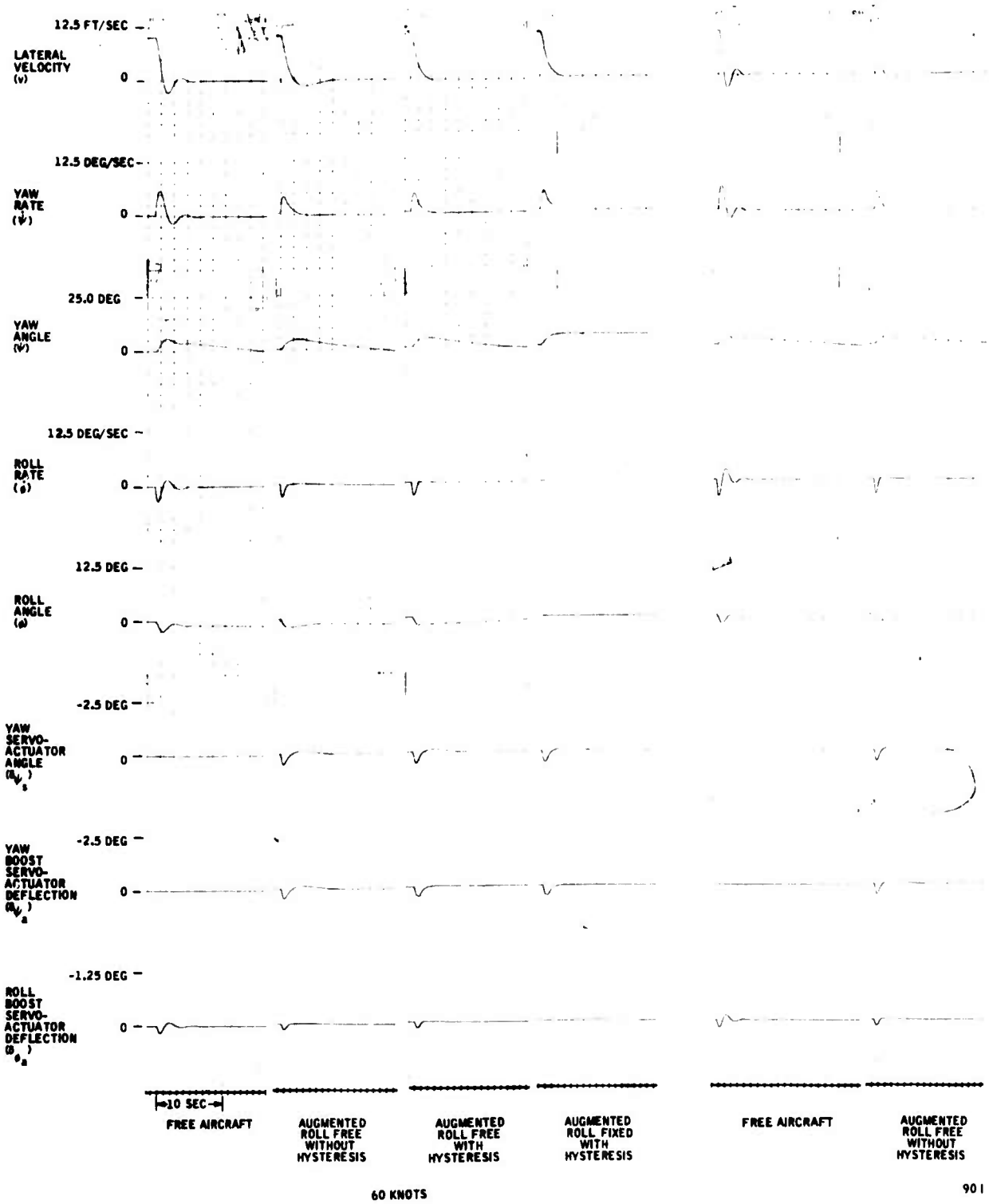

Figure 66. Free Aircraft and Yaw SAS Responses -- Lateral Gust Input (v_g = 10 Ft/Sec).

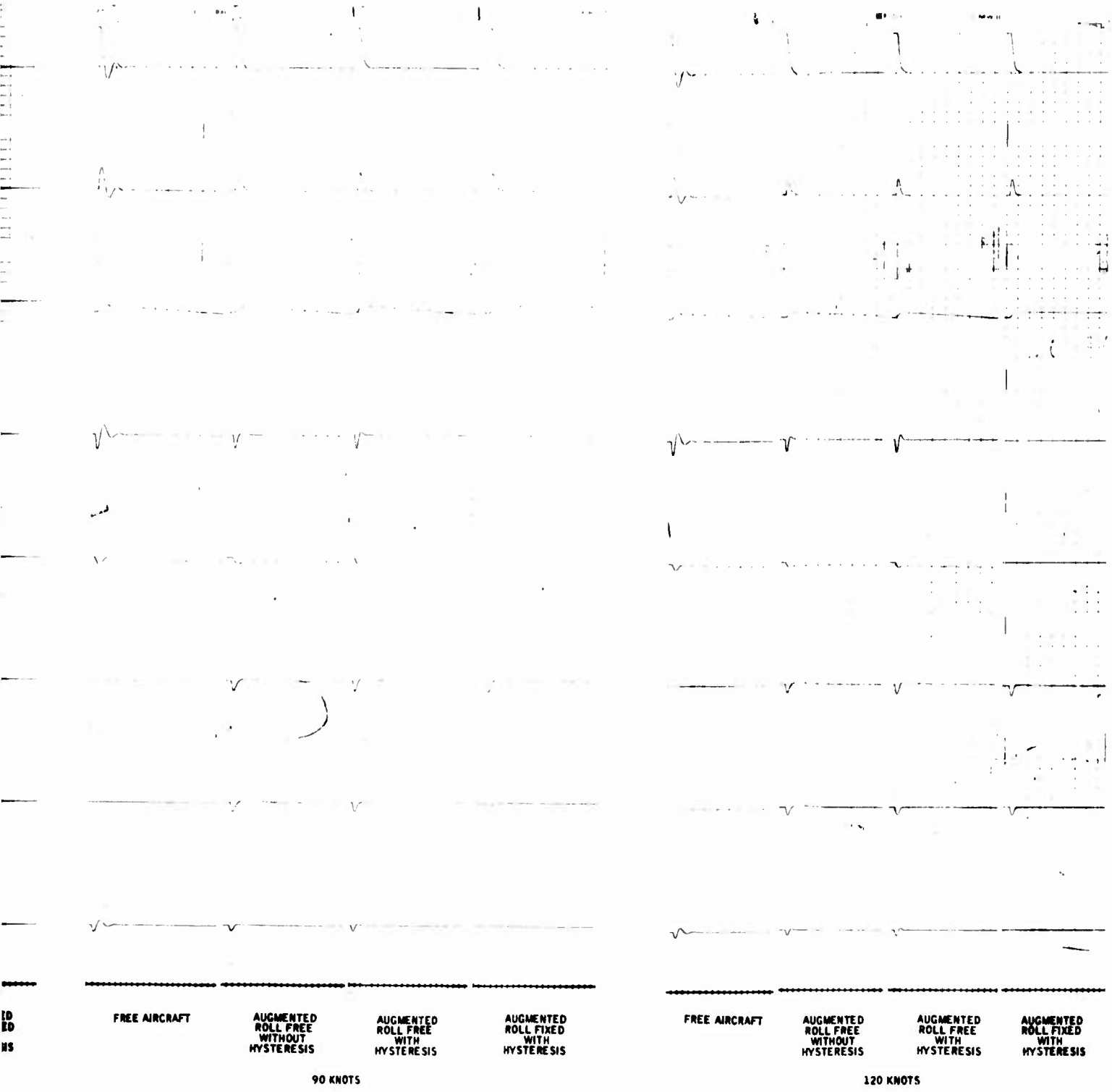

ponses -- Lateral

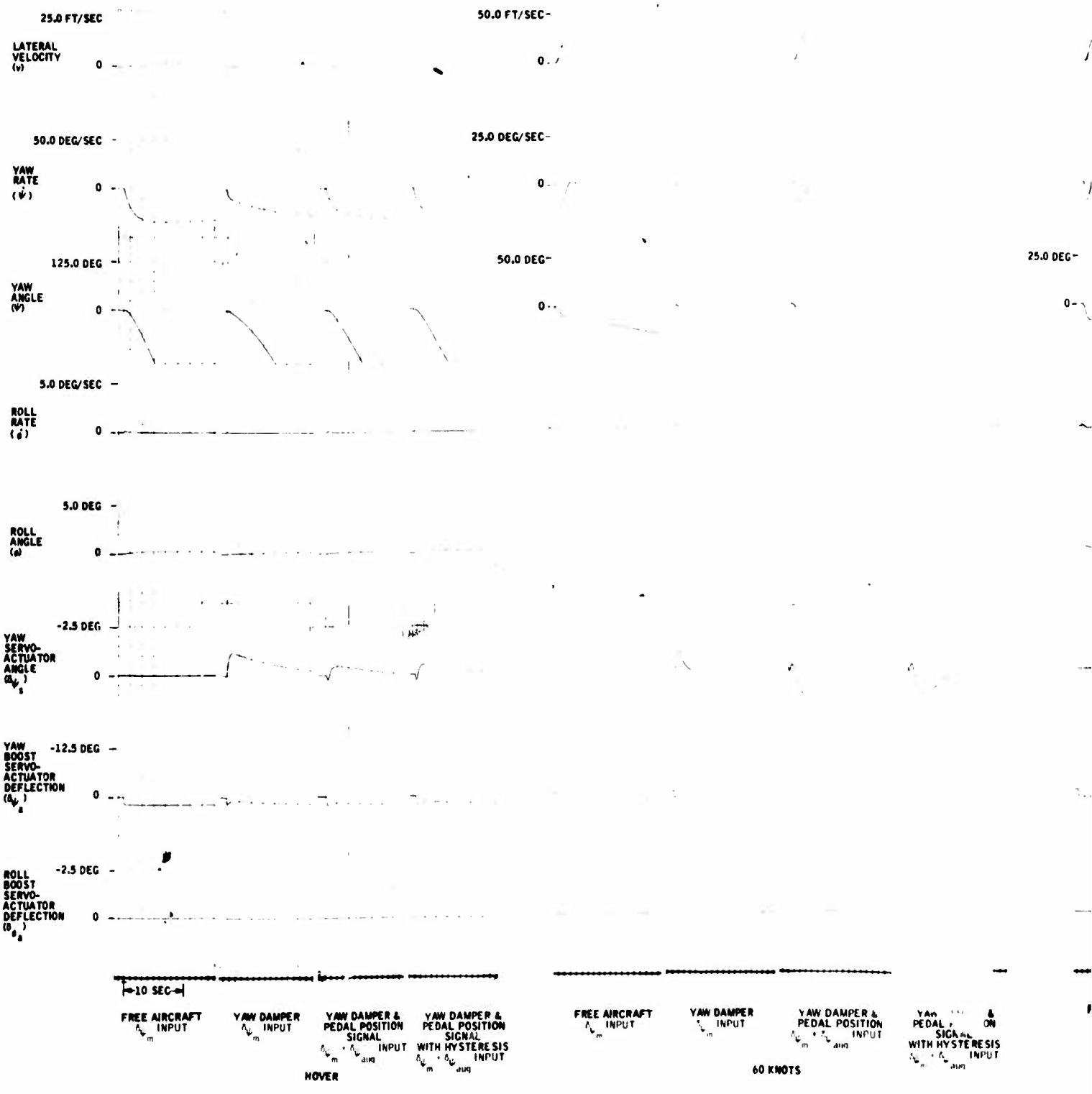

Figure 67. Free Aircraft and Yaw SAS Performance -- Pedal Position Input (δ_{ψ_m} = 2.0 Deg).

B

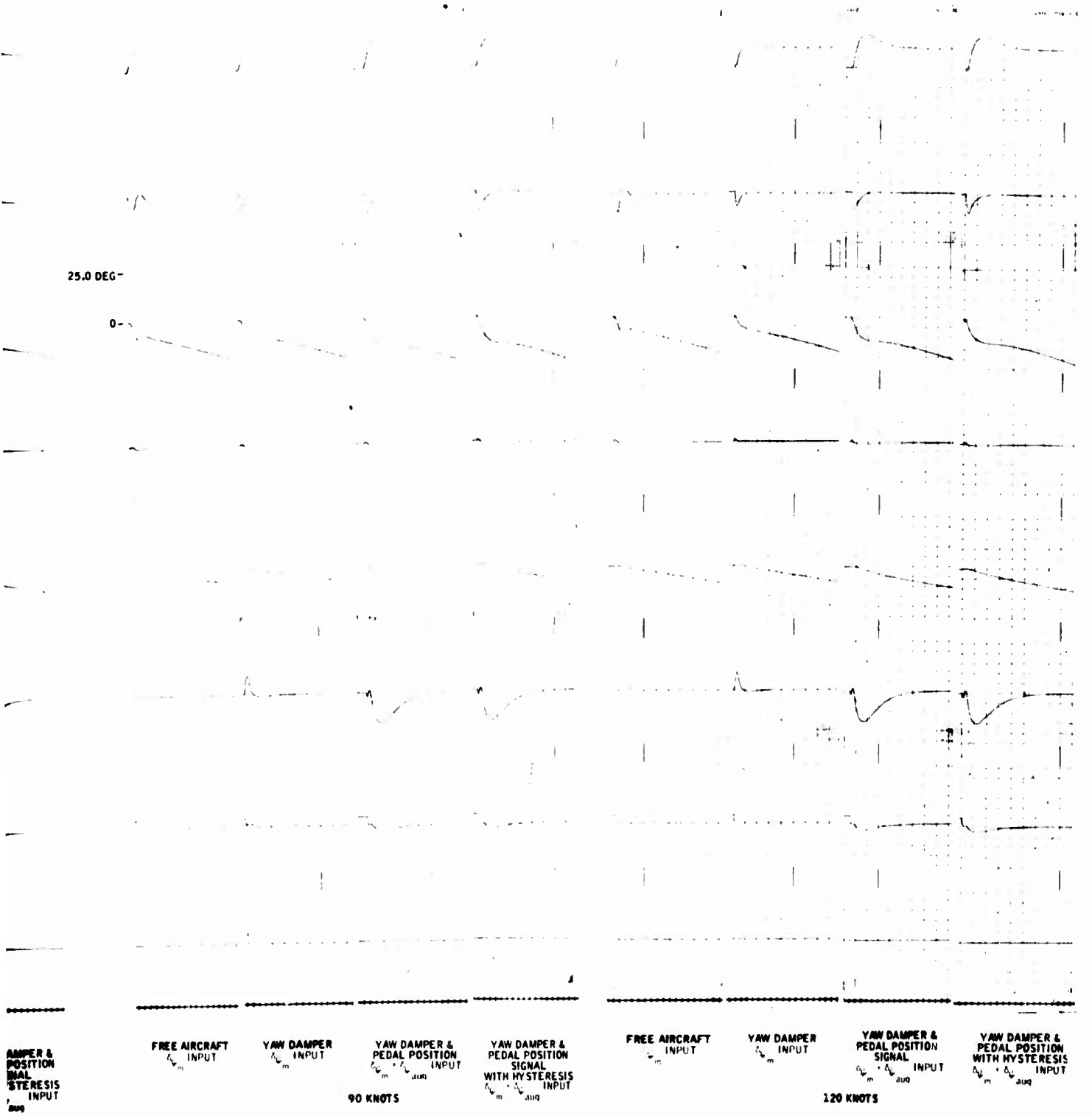
25.0 DEG
0
AMPER &
POSITION
NAL
STERESIS
INPUT
FREE AIRCRAFT
INPUT
YAW DAMPER
INPUT
YAW DAMPER &
PEDAL POSITION
INPUT
YAW DAMPER &
PEDAL POSITION
SIGNAL
WITH HYSTERESIS
INPUT
90 KNOTS
FREE AIRCRAFT
INPUT
YAW DAMPER
INPUT
YAW DAMPER &
PEDAL POSITION
SIGNAL
INPUT
YAW DAMPER &
PEDAL POSITION
WITH HYSTERESIS
INPUT
120 KNOTS

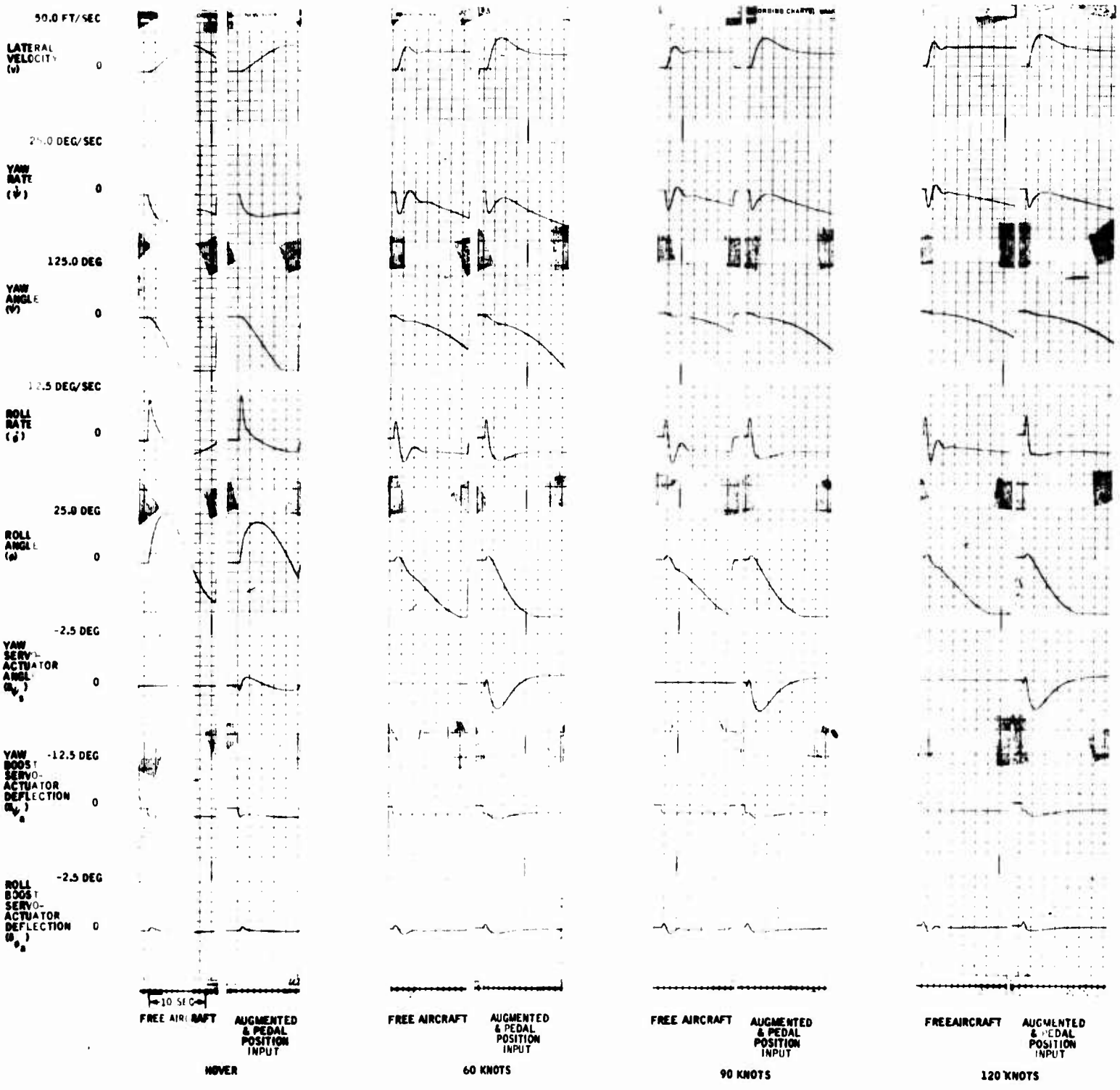

Figure 18. Yaw SAS Responses to a Pedal Position Input (δ_{ψ_m} = 2.0 Deg).

TABLE XI. NOMINAL YAW SAS PERFORMANCE

Flight Condition	Disturbance: Lateral Gust (v_g = 10 Ft/Sec)				Disturbance: Tail Rotor Step Input (δ_ψ = 1.0 In.)					
					Roll Axis					
	Free			Fixed	Fixed				Free	
		Augmentation On			Augmentation On					
	Off	Without Hysteresis	With Hysteresis	With Hysteresis	Augmentation Off	Without Hysteresis (δ_{ψ_m})	Without Hysteresis ($\delta_{\psi_m} + \delta_{\psi_{aug}}$)	With Hysteresis ($\delta_{\psi_m} + \delta_{\psi_{aug}}$)	δ_{ψ_m}	$\delta_{\psi_m} + \delta_{\psi_{aug}}$
Hover										
O/SH(%)	-	-	-	-	-	-	-	-	-	-
$T_{90\%}$ (sec)	-	-	-	-	-	-	-	-	-	-
ψ at 1 sec	-	-	-	-	7.0	7.0	10.0	7.0	7.5	7.5
60 Kn										
O/SH(%)	27.5	14.0	2.0	1.0	-	-	-	-	-	-
$T_{90\%}$ (sec)	2.72	5.2	1.8	1.8	1.02	1.9	1.12	1.2	1.0	0.6
ψ at 1 sec	-	-	-	-	8.0	6.0	8.0	7.5	6.0	10.0
90 Kn										
O/SH(%)	33.0	10.0	0.0	0.0	-	-	-	-	-	-
$T_{90\%}$ (sec)	2.7	1.0	1.0	1.0	0.72	1.28	0.8	0.8	0.68	0.6
ψ at 1 sec	-	-	-	-	7.0	5.0	7.5	7.5	6.0	6.0
120 Kn										
O/SH(%)	33.0	7.0	0.0	0.0	-	-	-	-	-	-
$T_{90\%}$ (sec)	2.4	1.0	1.0	1.0	0.7	1.0	0.6	0.6	0.6	0.6
ψ at 1 sec	-	-	-	-	6.5	5.0	7.3	6.2	6.0	6.0

Pedal Position Input Response

A pedal position input loop was analyzed as part of the yaw SAS. This pedal input eliminates the decreased vehicle response at the hover and low-speed flight conditions for pedal input commands caused by opposition from the yaw SAS.

Control of the yaw axis was analyzed with step inputs directly coupled to the vehicle's boost actuator element (δ_{ψ_m}) and with augmented pedal input commands to the series servoactuator plus inputs to the boost actuator ($\delta_{\psi_m} + \delta_{\psi_{aug}}$). Time histories for the free vehicle and yaw SAS with pedal position input are presented in Figure 67. During the recording of these time histories, it was assumed that the pilot would maneuver to a wings-level roll attitude and allow only small roll angles to develop.

The control equation used to augment the yaw pedal inputs is:

$$\delta_\psi = \delta_{\psi_m} + \left[K_{\delta_\psi} \left(\frac{1}{T_{lag}\, S+1} \right) \delta_{\psi_{aug}} - K_\psi \dot{\psi} \right] \left(\frac{T_{HP}\, S}{T_{HP}\, S+1} \right)$$

where

δ_{ψ_m} = Mechanical tail rotor command from pilot's pedals, deg

$\delta_{\psi_{aug}}$ = Augmented servoactuator command from pilot's pedals, deg

K_{δ_ψ} = 1.5 augmented servoactuator command per mechanical tail rotor command

K_{lag} = 1 sec

K_ψ = 0.15-deg tail rotor angle/deg/sec

$\dot{\psi}$ = Yaw rate, deg/sec

T_{HP} = 2.5 sec

An analytic block diagram of the yaw SAS and pedal position input augmentation is shown in Figure 63.

Including the pedal position input in the yaw SAS improved pedal input vehicle response significantly. Figure 67 shows that at the hover condition, for a 1-in. pedal input, the free-vehicle yaw rate is 16 deg/sec at the end of 1 sec and 26 deg/sec at the end of 2 sec. The yaw angle excursion is 6 deg at the end of 1 sec. The yaw rate response for an unaugmented pedal input is approximately one-third of these values. For augmented pedal input at the hover flight condition, yaw rate is 17 deg/sec at the end of 1 sec and 23 deg/sec at the end of 2 sec.

Yaw angle excursion is 8 deg at the end of 1 sec. These values show that with the stability loop adjusted to provide the correct damping, the inherent disadvantage of decreased pedal input response can be eliminated by including the pedal position input.

It should be noted that the peak yaw rate obtained for a 1-in. pedal input command to the free vehicle and to the vehicle augmented with the pedal position input is of similar magnitude at the 60-, 90-, and 120-kn flight conditions. This shows that the pedal position input does not appreciably change the vehicle response characteristics at the high-speed flight conditions. It should be further noted that the inclusion of linkage backlash hysteresis of 0.05 deg does not significantly affect performance response characteristics. The $T_{90\%}$ response times and yaw angle excursion at the end of 1 sec for a 1-in. pedal input are presented in Table XI. The $T_{90\%}$ response times are defined as the time required for the lateral velocity to reach 90 percent of its final value. The data in Table XI show that the yaw-axis control system complements the free-vehicle response, provides the desired damping and maneuver characteristics, and satisfies the design goal that the yaw-angle excursion should be greater than 5.9 deg at the end of 1 sec for a 1-in. pedal input command.

An important analysis guideline considered in selecting the gain and time constant for the pedal position input equation was that, for small pedal inputs, there must be sufficient series servoactuator travel left to provide the external disturbance damping function. A review of Figure 67 at the high-speed flight conditions shows that, for a 1-in. pedal input, the servoactuator traveled 1.5 deg of its allowable 2.5-deg range. The remaining 1 deg of servoactuator travel is considered to be a sufficient margin to perform the damping function, especially when it is considered that the pedals are used for minor trim-type inputs at speeds in excess of 60 kn. A 1-in. pedal input at speeds greater than 60 kn is considered a very severe and unrealistic input. One-inch pedal commands were performed on the analog simulation to demonstrate that there was sufficient servoactuator travel left to perform the damping function at high speeds.

Time histories at the four flight conditions studied, showing the free and augmented aircraft responses to pedal position inputs, with the roll axis unconstrained, are shown in Figure 68. These responses show that the yaw augmentation and pedal position input system provides a smooth and well-damped vehicle response to pedal input commands and does not show any evidence of an overcontrolled vehicle due to the augmented pedal inputs.

Pedal Position Input Transducer

During development of the fluidic pedal position input transducer, it was brought to the attention of the flight controls analyst that this device could be designed to provide a long-term pedal position trim

function, plus have a gain characteristic that is commonly called "low gain over center." However, to provide these desirable functions, the transducer must be designed to incorporate a high-pass network. The major disadvantage of a high-pass at this particular location in the yaw SAS is that it is a phase lead-producing device. Phase lag is the desired phase shift in a pedal position input mechanization. This is due to the fact that the augmented pedal input must be slowed down so that its effect on the aircraft is happening at approximately the same time as the unaugmented pedal input commands. If the phase difference between these commands is allowed to become relatively large, the pedal will feel jerky in response to pilot commands. Analog simulation results showed that if the high-pass can be designed to have a time constant of 20 sec or greater, the phase lead characteristic of the high-pass, at the frequency of interest, will have an insignificant effect on the short-term pedal input response characteristics.

During this program, a cross section of SEA combat-experienced helicopter pilots was interviewed, and it was learned that small trim-type pedal inputs by the pilots are difficult to make. This is due to the fact that the pedals on the UH-1 series helicopter are sensitive. That is, small inputs command relatively large vehicle responses. Providing a pedal transducer that has a low gain over center should alleviate this problem.

Yaw SAS Design Goal Compliance

The yaw-axis analysis results presented in time history and tabular form show that the final yaw SAS configuration satisfies the conditions of the design goals. These results are summarized as follows:

1. The results of Table XI show that the directional control power of the hovering helicopter is such that a rapid 1-in.-step pedal displacement produced greater than the specified 5.93 deg of yaw-angle displacement at the end of 1 sec.

2. The time histories of Figure 67 show that for a sudden pedal displacement (1 in.), the response of the helicopter while hovering is not so high as to cause the pilot to overcontrol unintentionally. The augmented vehicle achieves 17 deg/sec yaw rate at the end of 1 sec. The free-vehicle yaw rate is 16 deg/sec under similar conditions.

3. The time responses of Figure 67 show that the nominal system is free from objectionable transient forces following a rapid pedal deflection.

4. During this analysis, no objectionable or excessive delays in the development of an angular velocity in response to a pedal displacement were noted.

5. The yaw-axis damping ratio was increased from approximately 0.3 to approximately 0.6 at the high-speed flight conditions.

Yaw SAS Parameter Variation Study

During this analysis, a parameter variation study was conducted on each parameter of the yaw SAS and pedal position input control equation to determine their degree of sensitivity to off-design tolerance variations and to establish the degree of stability margins present in the yaw-axis control configuration. The parameters were varied over a sufficiently large range to show their effect on transient response and system stability. During this analysis, where a parameter variation was made on the pedal position input parameters, the roll axis was constrained. This was done to simulate a wings-level control of the roll axis by the pilot. As seen on these traces, the roll axis was allowed to make only small roll-angle excursions.

Pedal Position Gain Variation (K_{δ_ψ})

Figures 69, 70, 71 and 72 show the time histories for variations in the pedal position input gain (K_{δ_ψ}) at each of the four flight conditions. The time histories were recorded for gains of 0.5, 1.0, 1.5, and 2.0. In arriving at the desired pedal position input gain, the following five items were considered:

1. With the yaw SAS engaged, the vehicle's response to a pedal position input should be approximately that of the free aircraft.

2. The magnitude of the peak yaw rates for the free and augmented aircraft should be approximately the same.

3. The yaw-angle excursion for a 1-in. pedal input should be greater than 5.9 deg at the end of 1 sec.

4. There should be sufficient servoactuator travel left for nominal pedal input to perform the damping function. This analysis was performed for a yaw servoactuator travel providing 2.5-deg tail rotor blade angle. At the selected gain and for a 1-in. pedal input, the servoactuator traveled 1.5 deg to achieve the desired augmented vehicle response. This left a margin of 1 deg to perform the damping function.

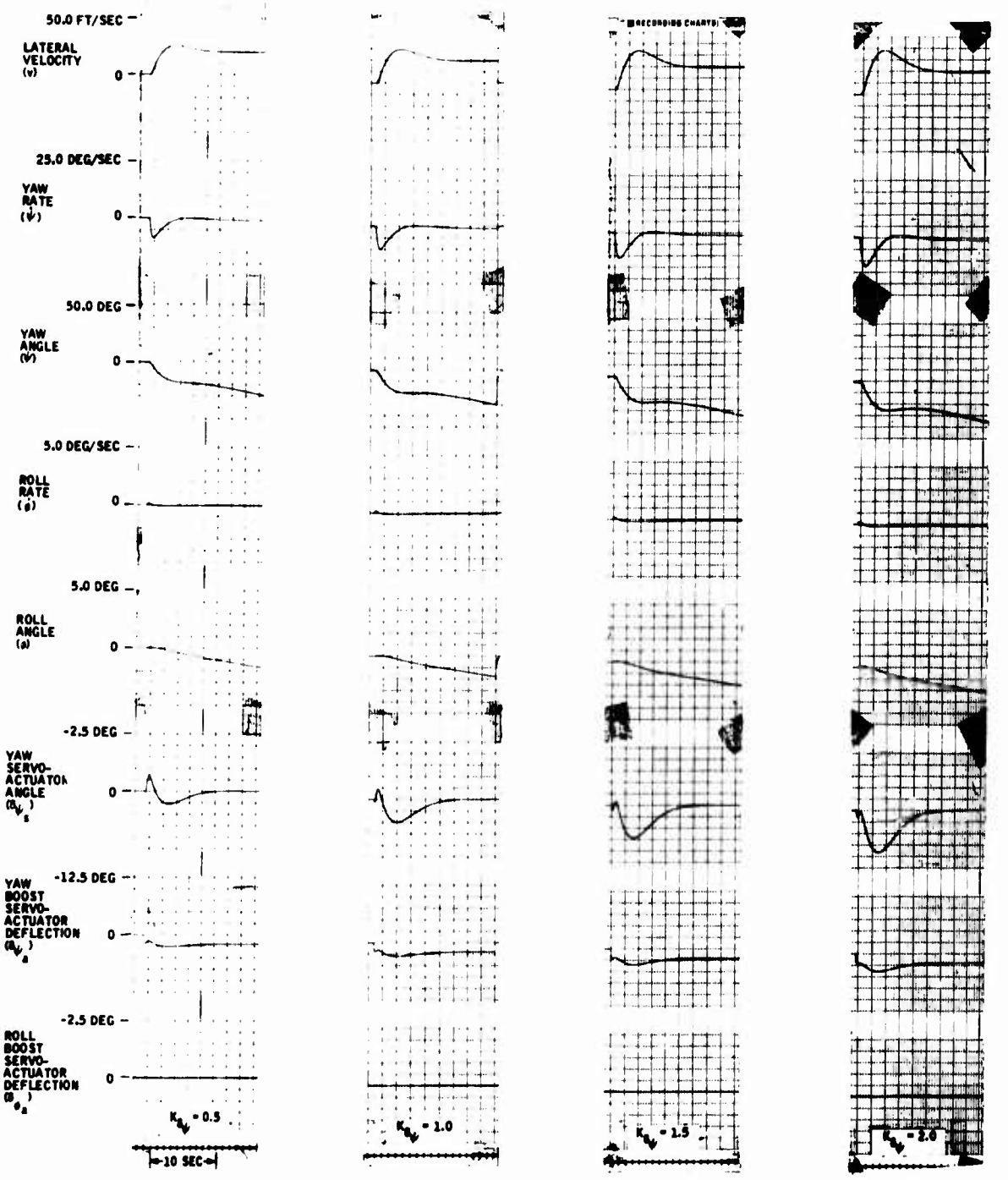

Figure 69. Yaw SAS Pedal Position Gain Variation -- Pedal Position Input (δ_{ψ_m} = 2.0 Deg) at 60 Knots.

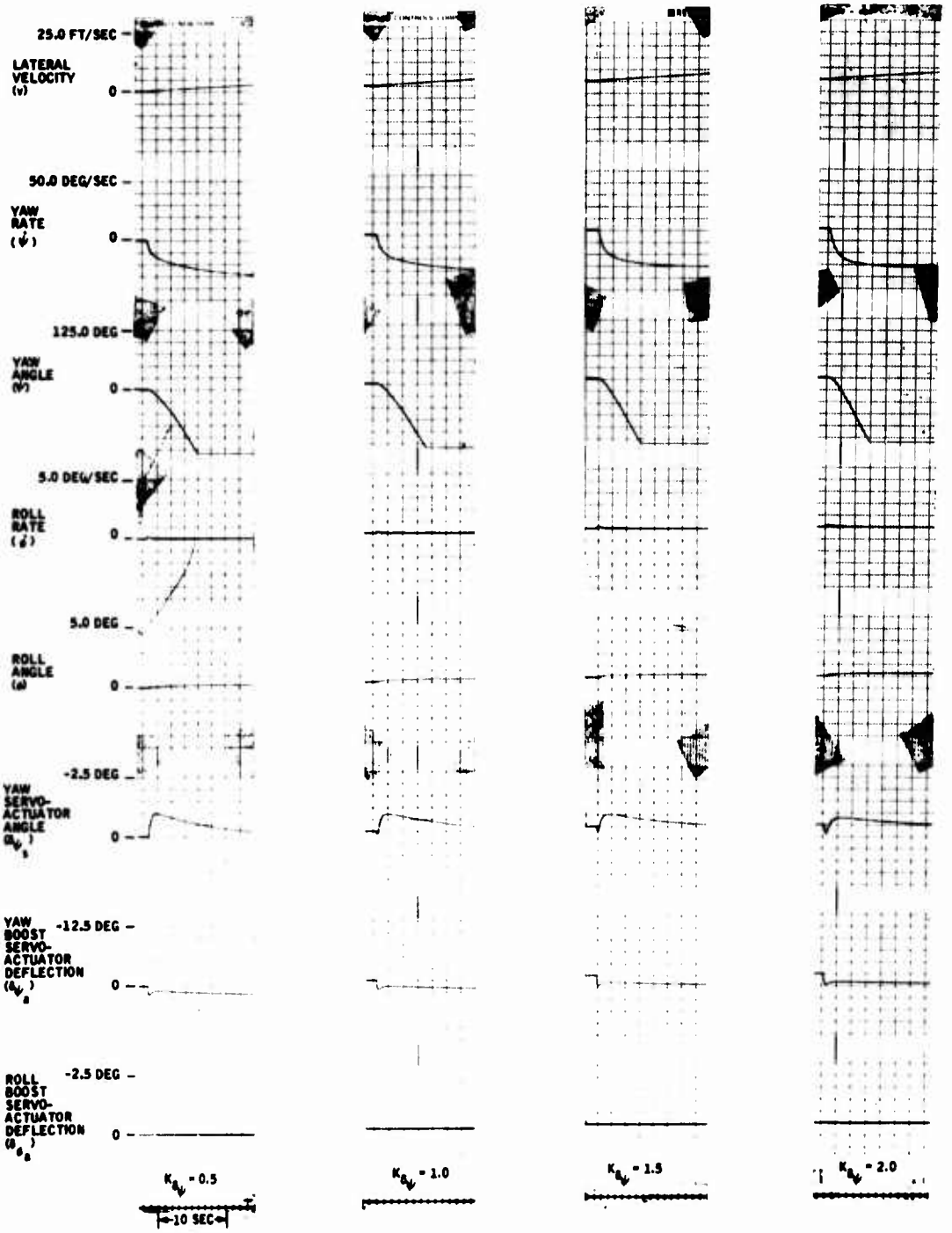

Figure 70. Yaw SAS Pedal Position Gain Variation -- Pedal Position Input (δ_{ψ_m} = 2.0 Deg) at Hover.

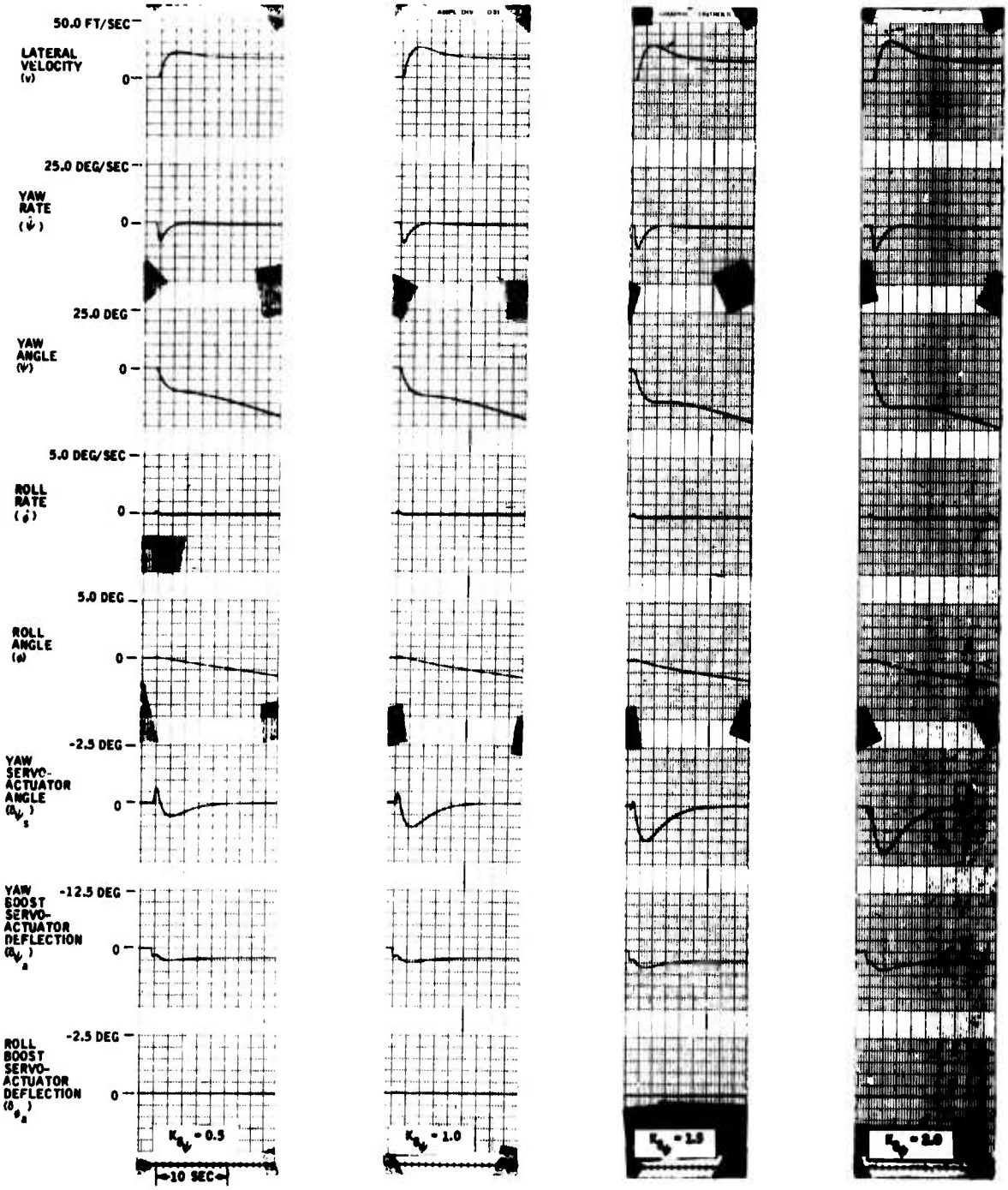

Figure 71. Yaw SAS Pedal Position Gain Variation -- Pedal Position Input (δ_{ψ_m} = 2.0 Deg) at 90 Knots.

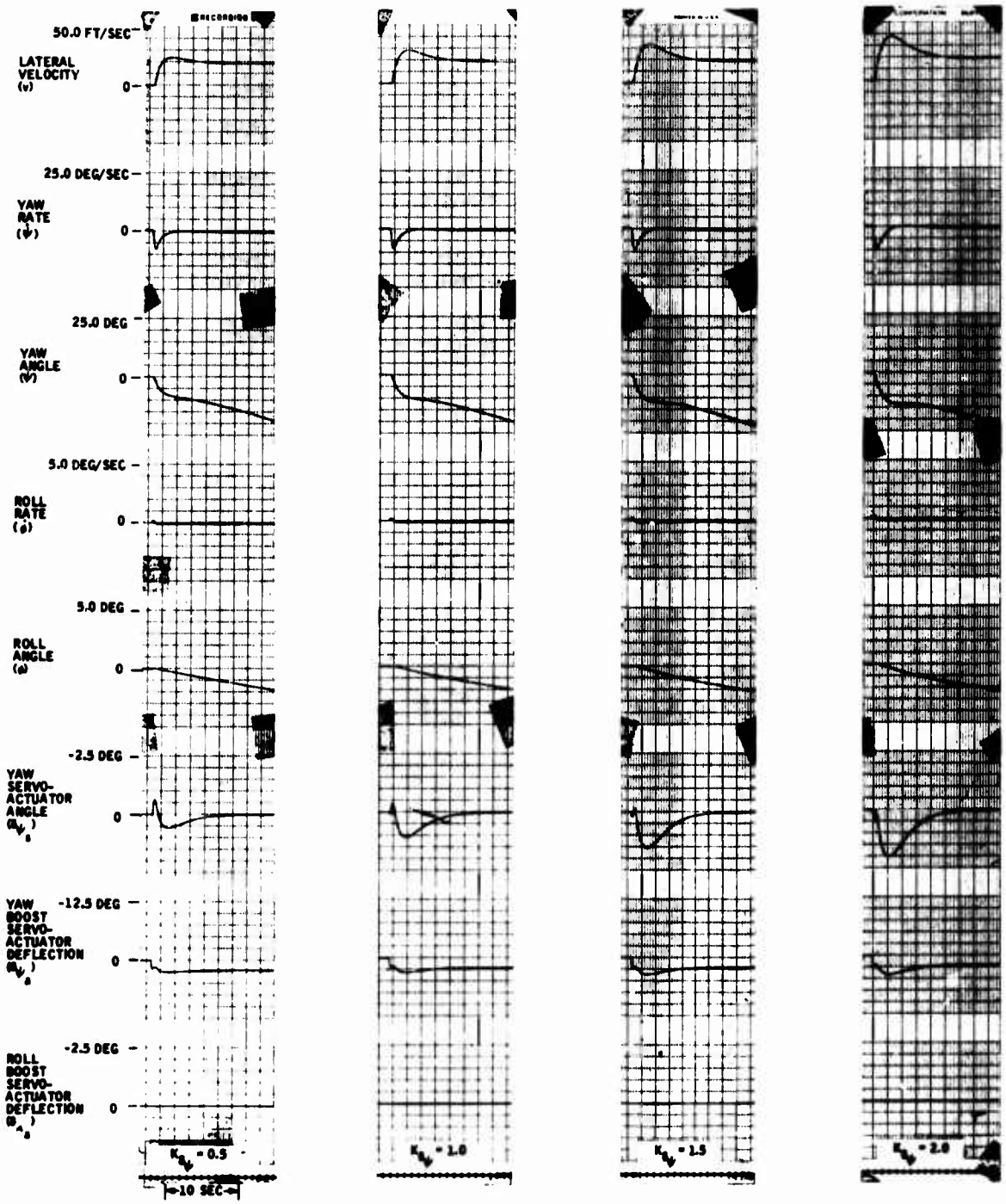

Figure 72. Yaw SAS Pedal Position Gain Variation -- Pedal Position Input (δ_{ψ_m} = 2.0 Deg) at 120 Knots.

5. A rapid servoactuator reversal, caused by the mechanical input and augmented input being slightly out of phase, should be restricted to as low a magnitude as reasonably possible.

A review of the time histories of Figures 69, 70, 71 and 72 shows that these analysis objectives were achieved.

The desired value of $K_{\delta\psi}$ was selected from a performance consideration rather than a stability consideration. Therefore, if it is desired to change the yaw SAS pedal input performance characteristics, this may be done within reason without affecting system stability.

Pedal Position Lag Time Constant Variation (T_{lag})

Figures 73, 74, 75, and 76 show the yaw-axis performance responses for variations of pedal position lag time constant (T_{lag}). These figures show that when the lag time constant is increased beyond the nominal value, the yaw-axis response is decreased significantly. When the time constant is much below the nominal value, the yaw rate becomes larger than that of the free aircraft, and the amount of initial servoactuator reversal becomes excessive. This implies that the unaugmented pedal commands are out of phase with the augmented pedal commands.

These figures show that a lag time constant of 1 sec is the optimum value for nominal yaw-axis performance. Near-nominal system performance may be achieved for a ±20-percent tolerance on this parameter.

Yaw SAS Gain Variation (K_{ψ})

Time histories for the yaw SAS gain variation were recorded at the 60-, 90-, and 120-kn flight conditions. These responses were recorded for an unconstrained roll axis and for a vertical gust input command equal to 10 ft/sec. Figures 77, 78, and 79 present the gain variation time histories with a linkage backlash hysteresis as part of the basic airframe. Figures 80, 81, and 82 were recorded without the linkage backlash hysteresis.

A review of the lateral velocity responses of Figures 77, 78, and 79 shows that near-nominal performance is maintained by a ±20-percent gain variation. As gain approaches 0.6 K_{ψ}, or a 40-percent decrease in gain, system response becomes slightly underdamped. If gain is increased by 40 percent, system response has a tendency to become sluggish at the 60-kn flight condition and a slight tendency toward instability at the 120-kn flight condition. Therefore, to achieve nominal system performance, the yaw SAS rate gain should be maintained within ±20 percent under normal environmental conditions.

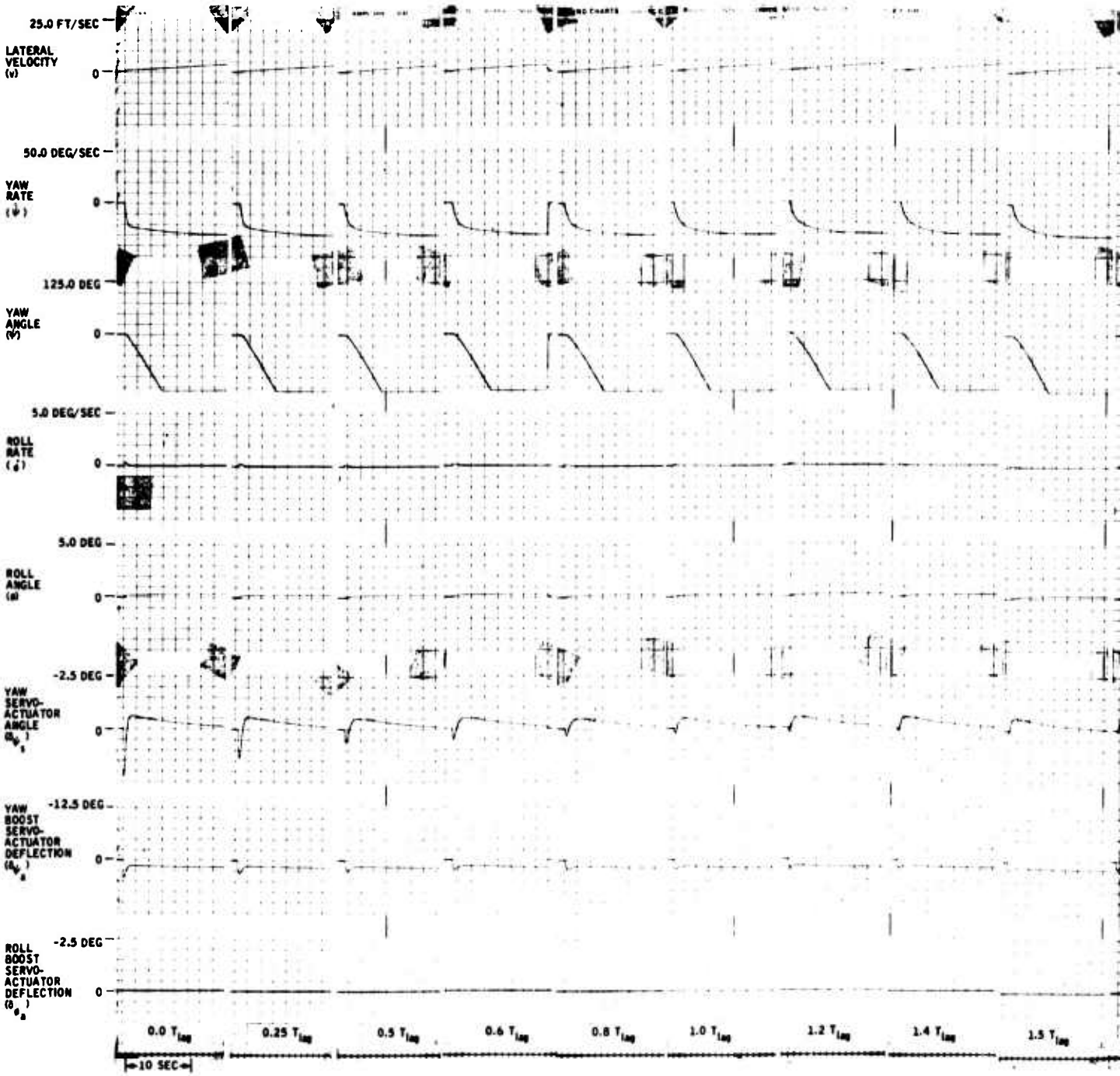

Figure 73. Yaw SAS Pedal Position Lag Time Constant Variation -- Pedal Position Input (δ_{ψ_m} = 2.0 Deg) at Hover.

B

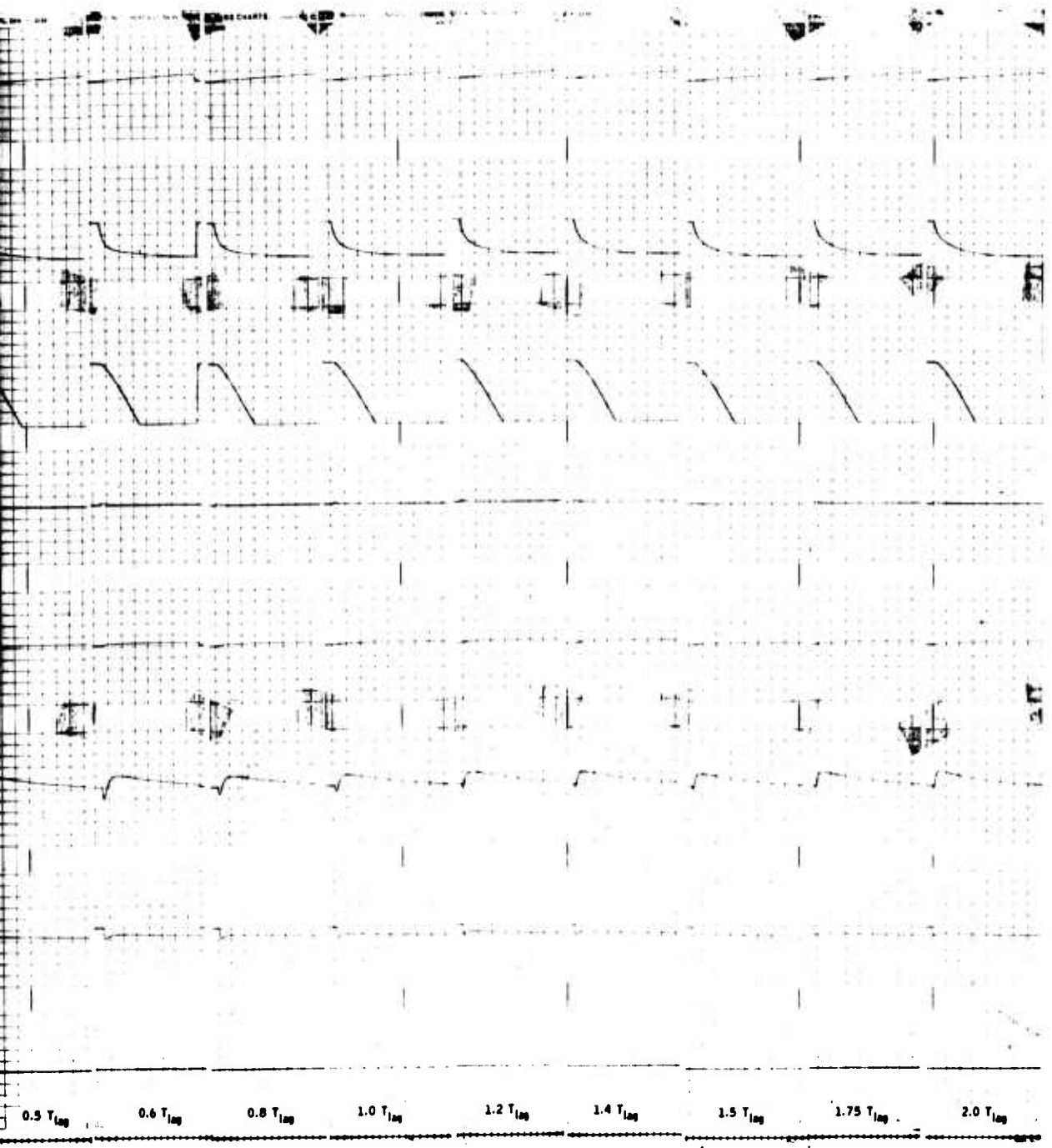

l Position Lag Time Constant Variation --
n Input (δ_{ψ_m} = 2.0 Deg) at Hover.

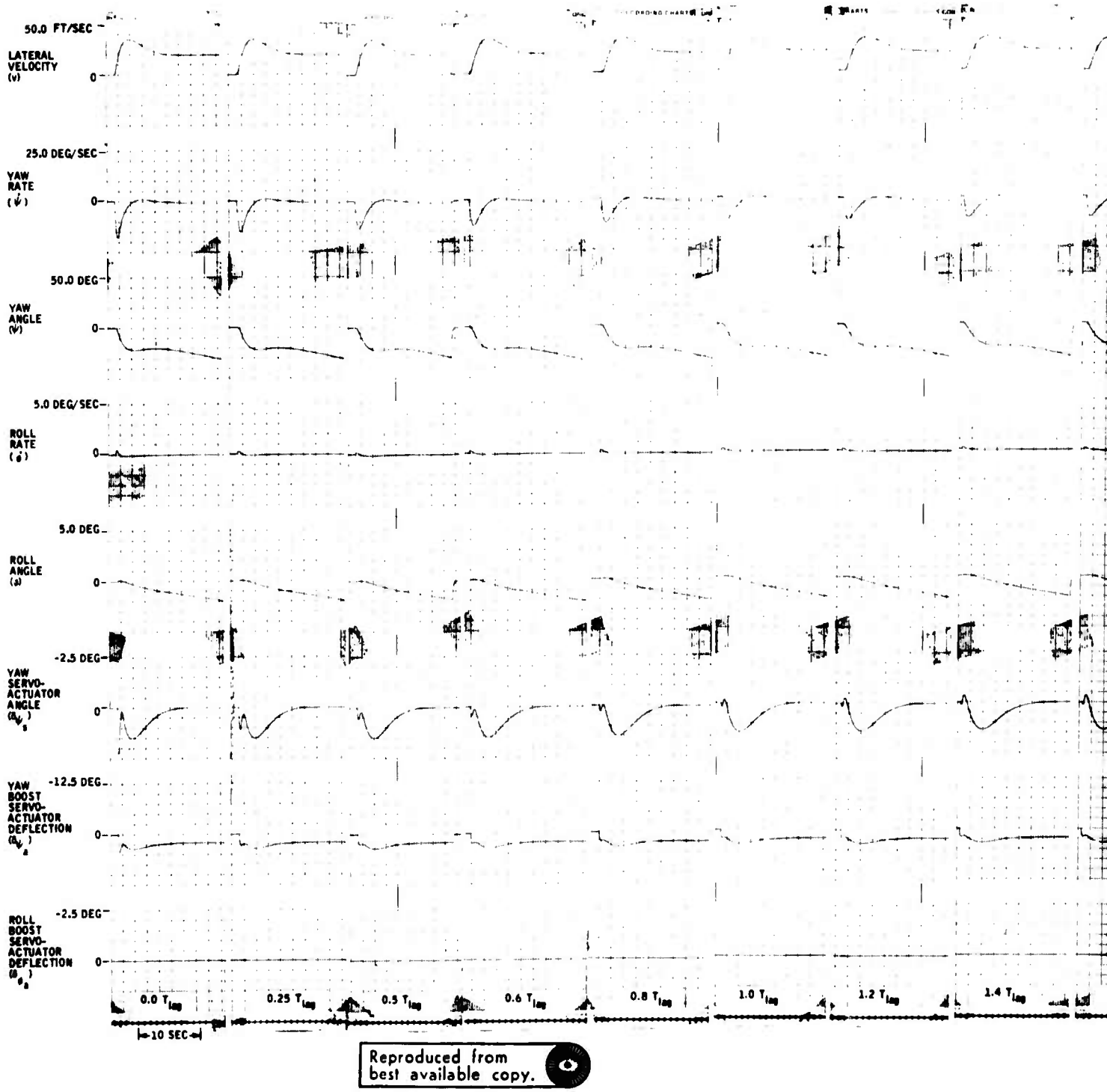

Figure 74. Yaw SAS Pedal Position Lag Time Constant Variation -- Pedal Position Input (δ_{ψ_m} = 2.0 Deg) at 60 Knots.

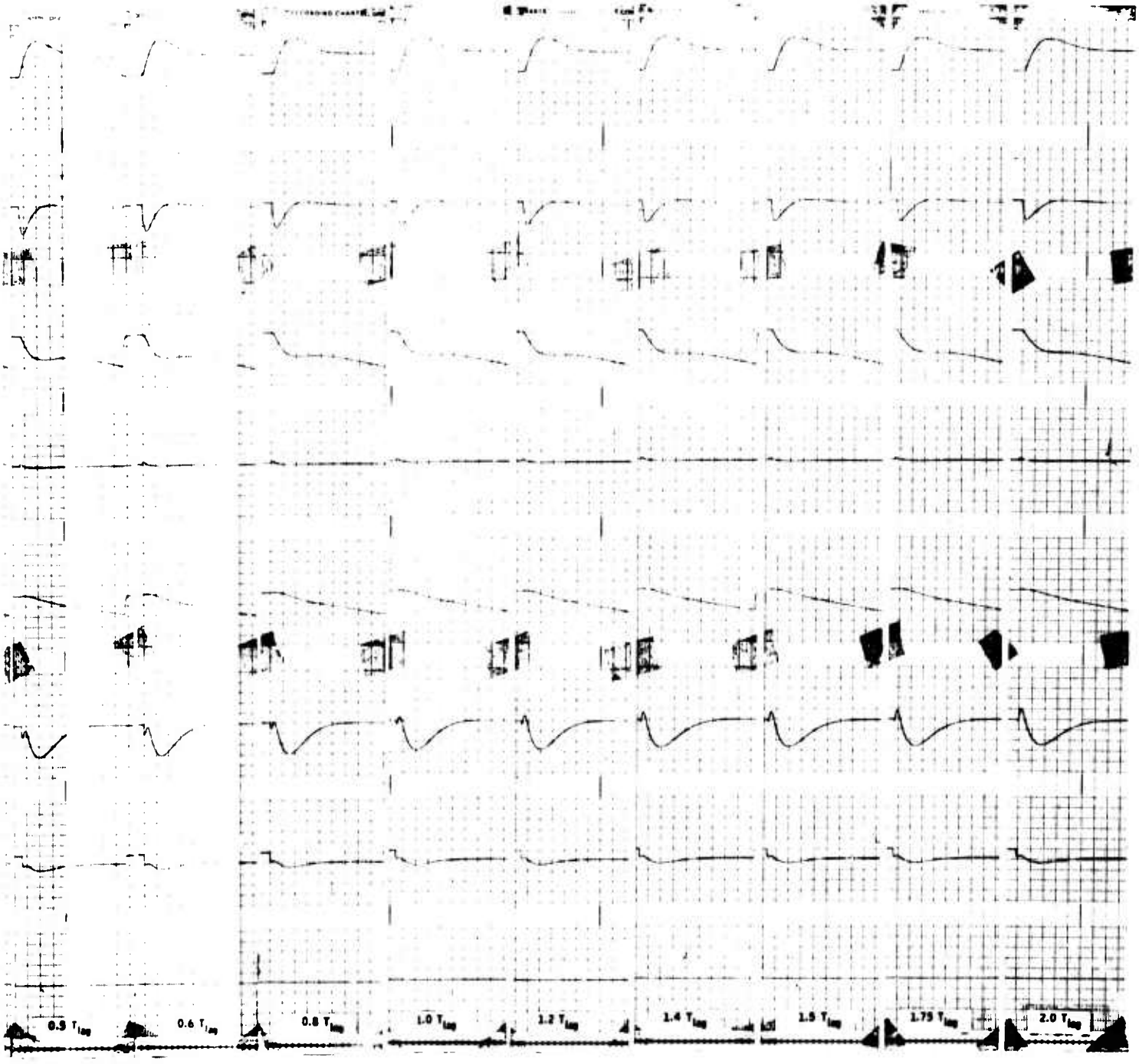

Position Lag Time Constant Variation -- Input (δ_{ψ_m} = 2.0 Deg) at 60 Knots.

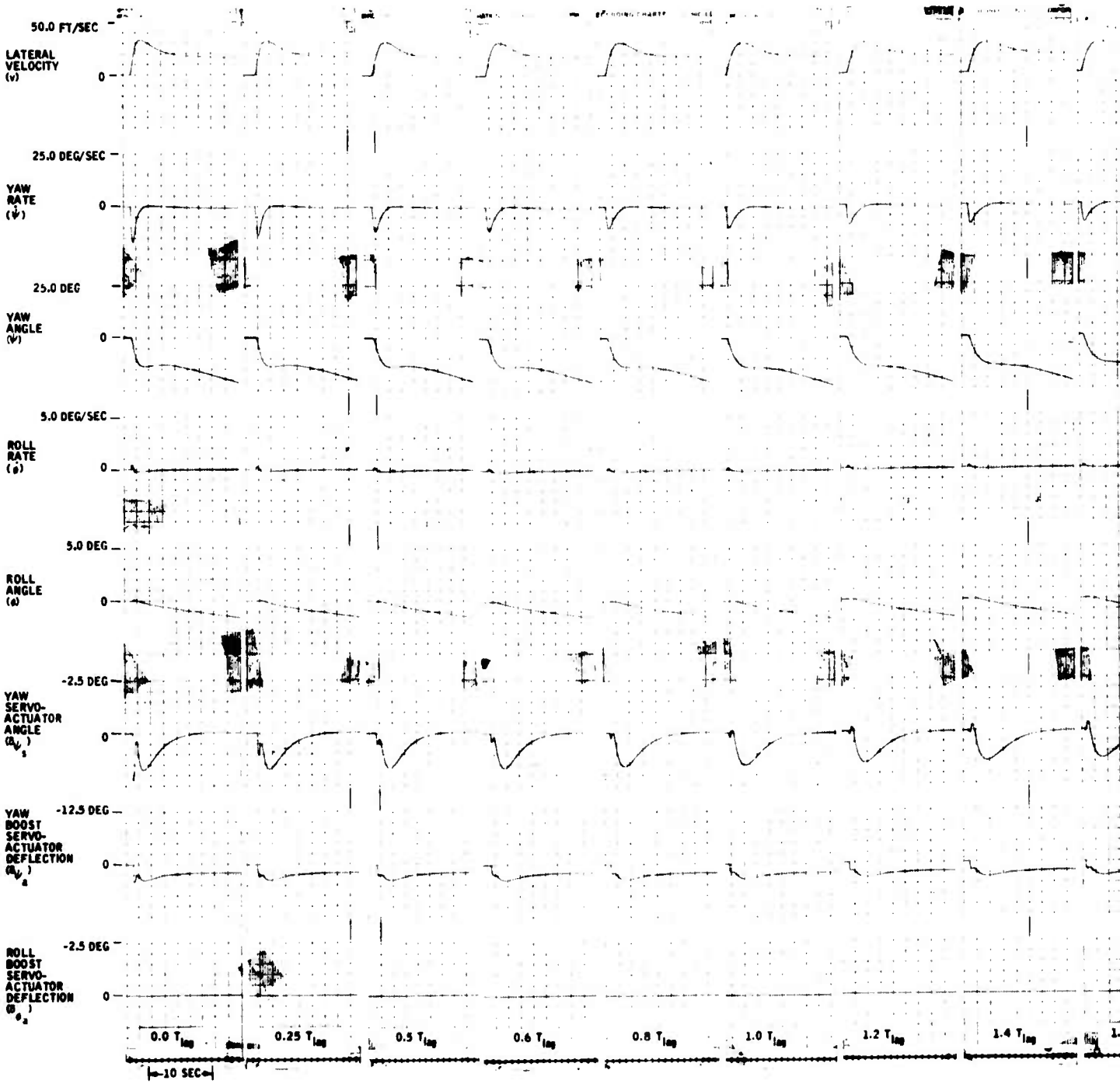

Figure 75. Pedal Position Lag Time Constant Variation -- Pedal Position Input (δ_{ψ_m} = 2.0 Deg) at 90 Knots.

B

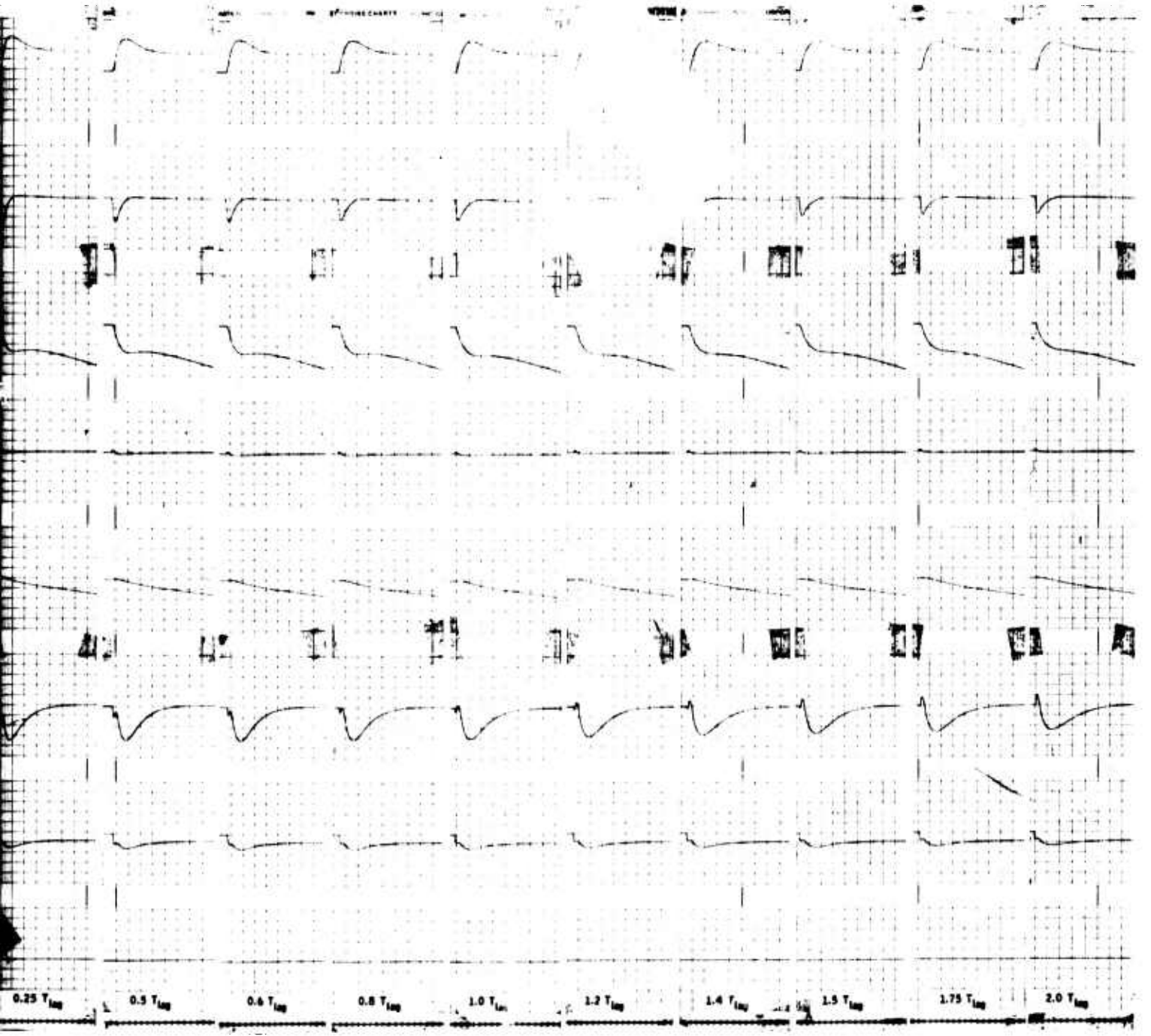

al Position Lag Time Constant Variation -- Pedal
tion Input (δ_{ψ_m} = 2.0 Deg) at 90 Knots.

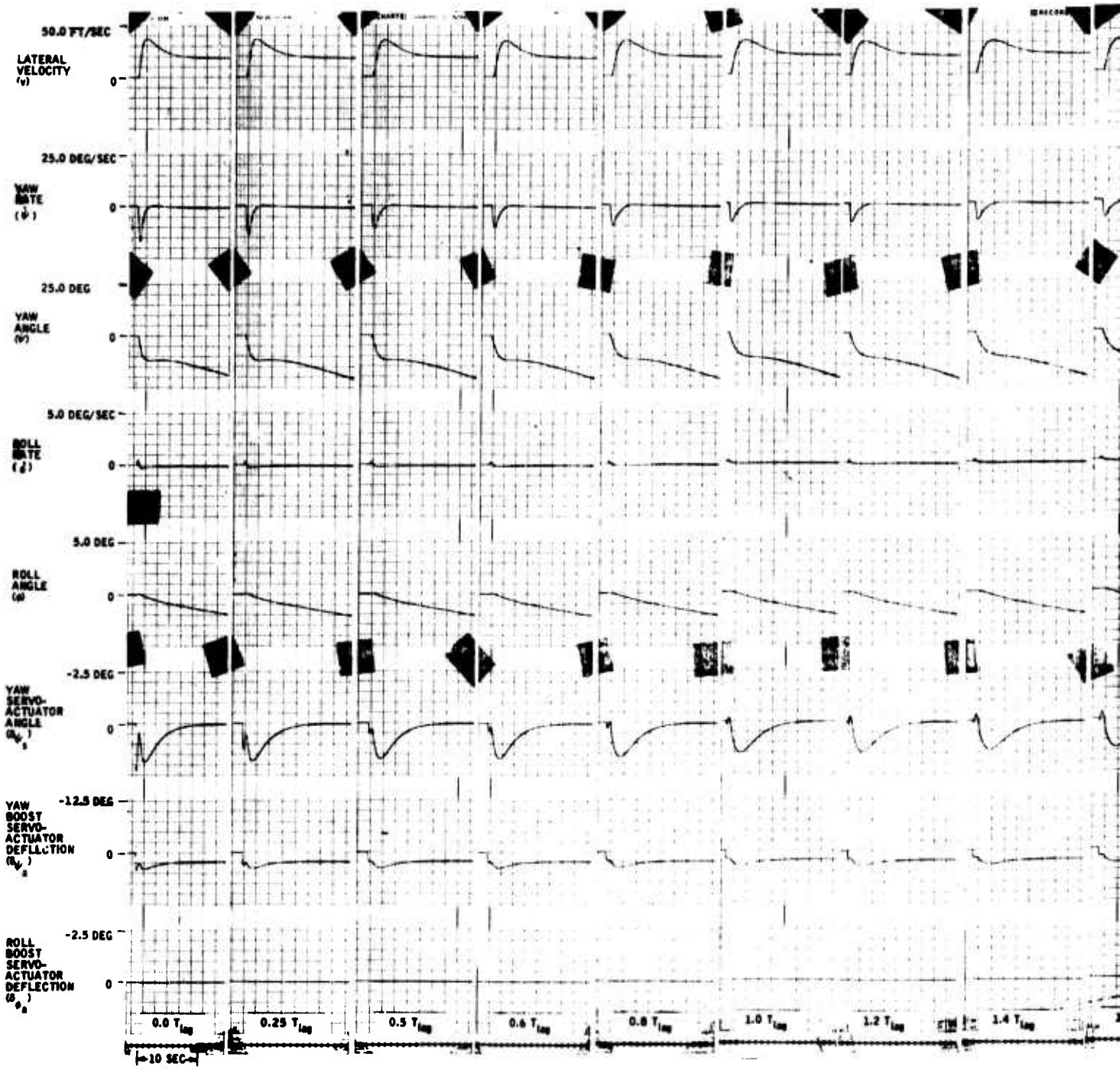

Figure 76. Pedal Position Lag Time Constant Variation -- Pedal Position Input (δ_{ψ_m} = 2.0 Deg) at 120 Knots.

B

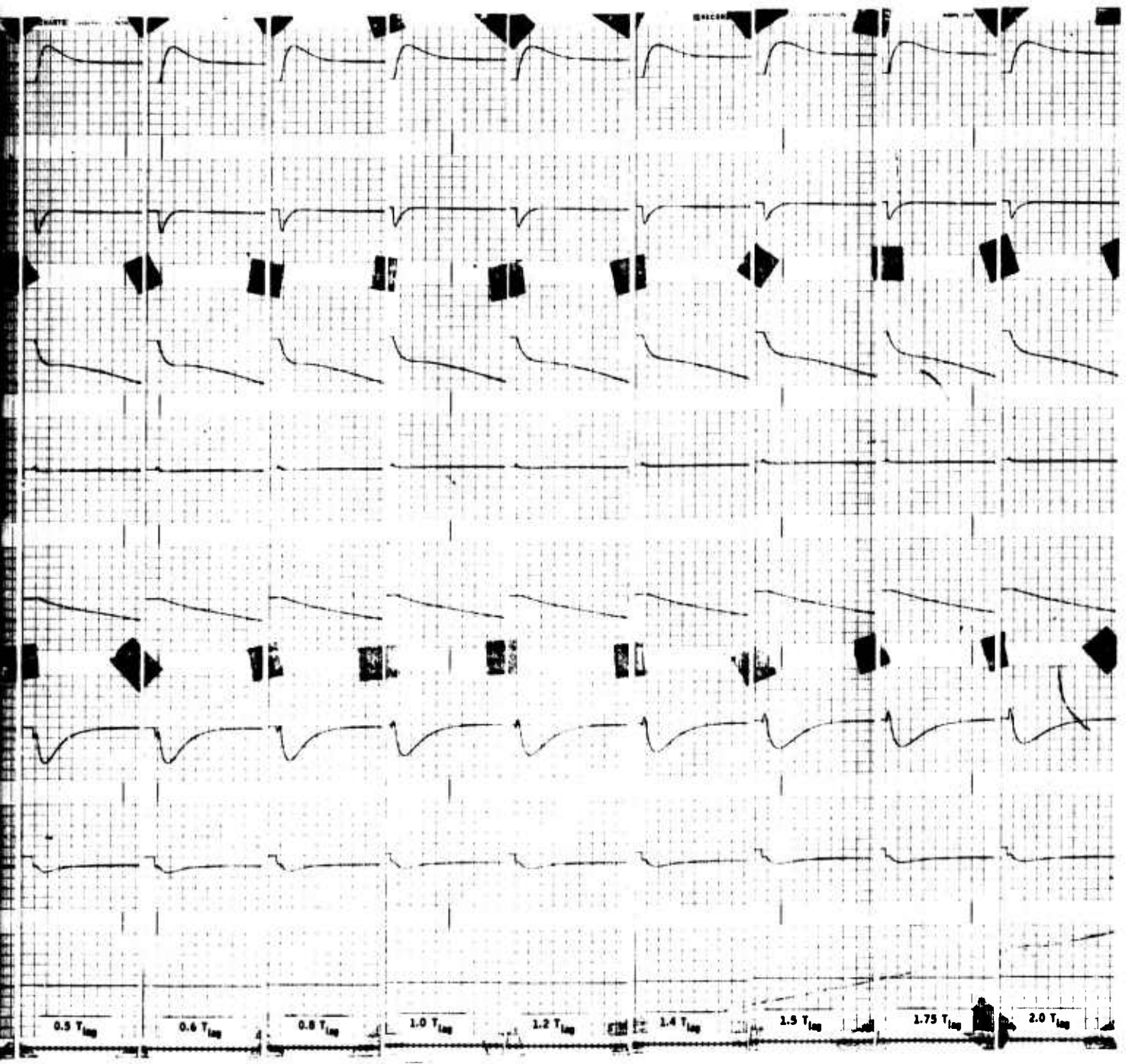

ition Lag Time Constant Variation -- Pedal
nput (δ_{ψ_m} = 2.0 Deg) at 120 Knots.

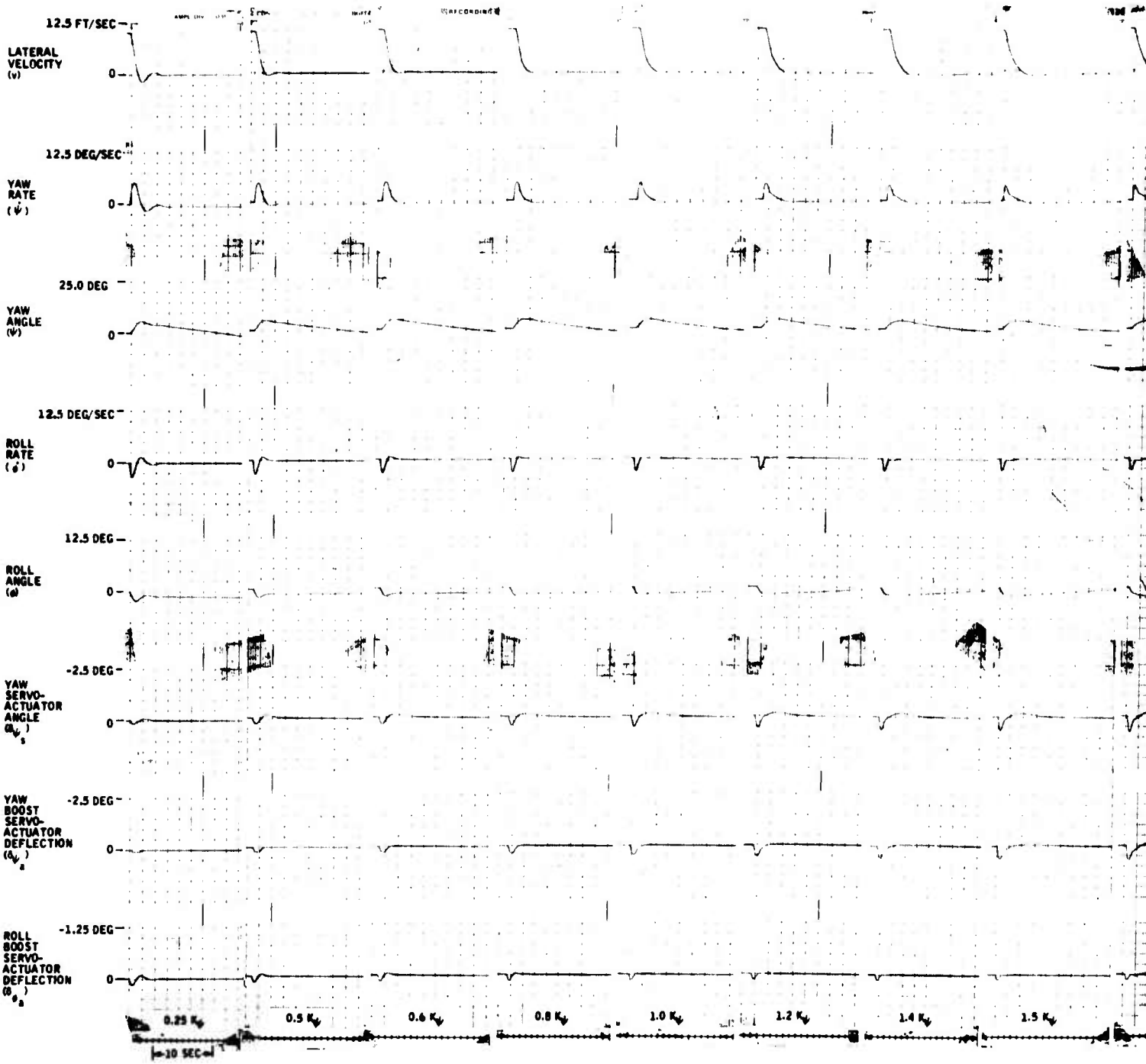

Figure 77. Yaw SAS Rate Gain Variation -- Lateral Gust Input (v_g = 10 Ft/Sec) at 60 Knots With Hysteresis.

B

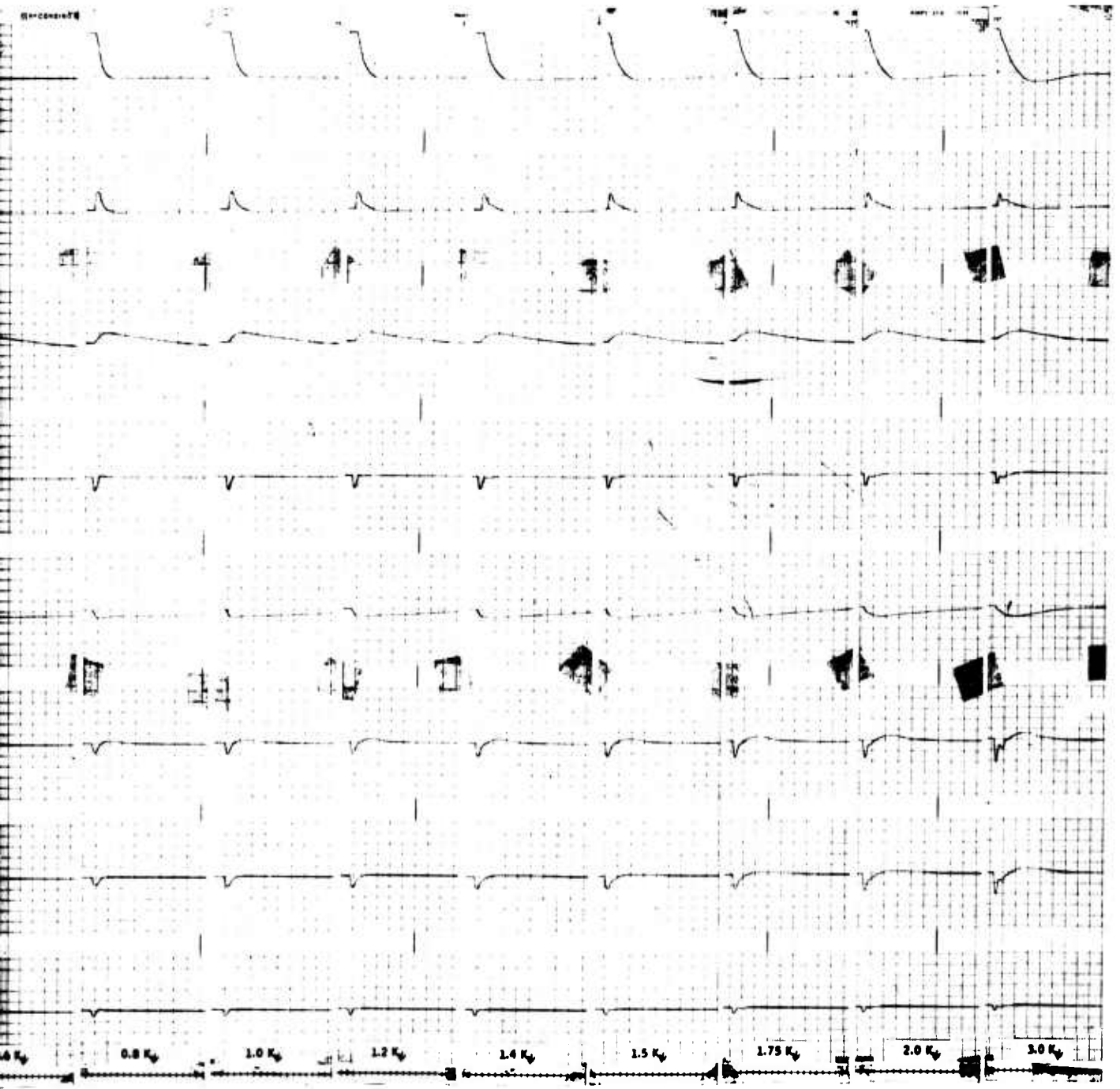

in Variation -- Lateral Gust Input
at 60 Knots With Hysteresis.

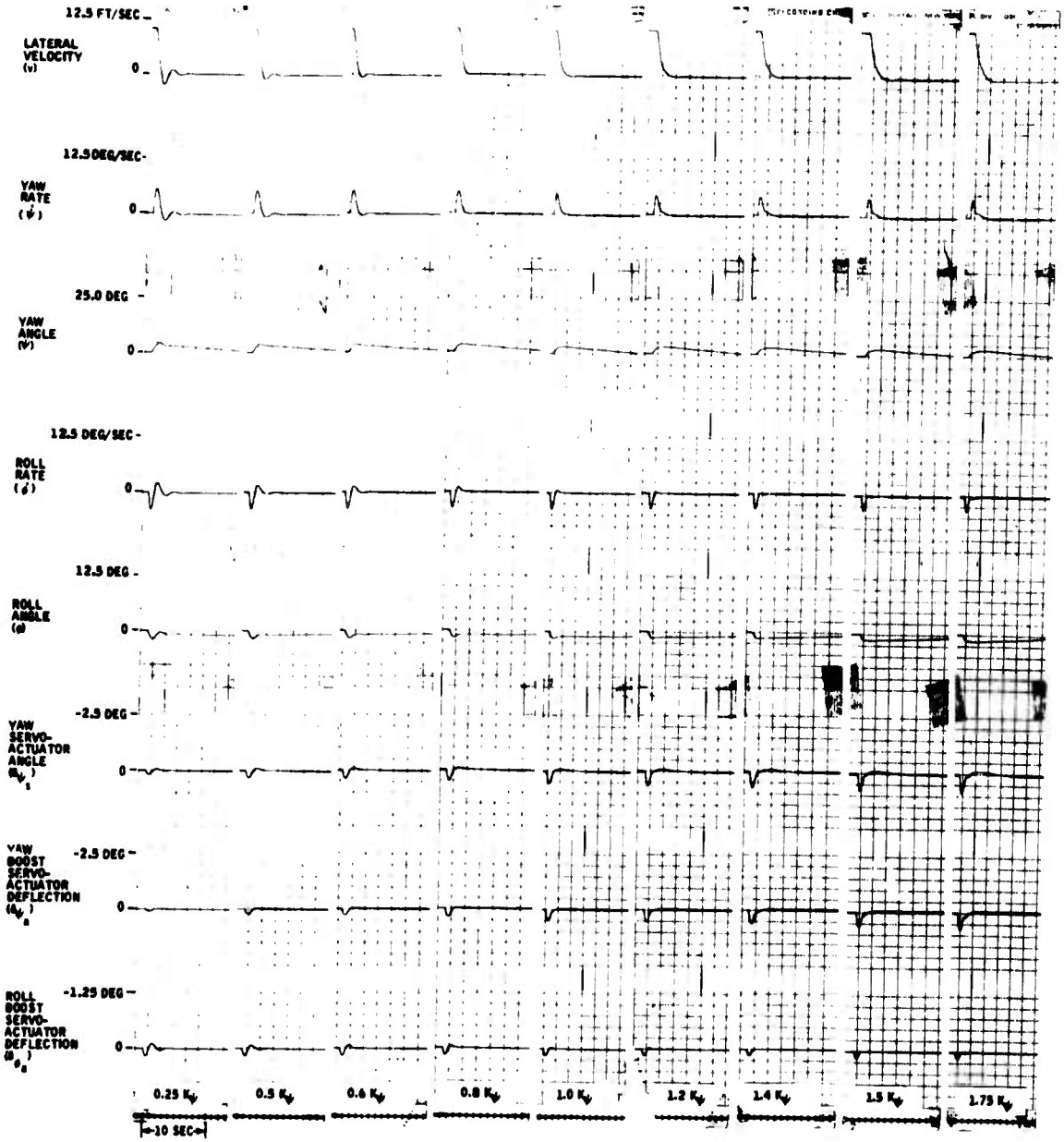

Figure 78. Yaw SAS Rate Gain Variation -- Lateral Gust Input (v_g = 10 Ft/Sec) at 90 Knots With Hysteresis.

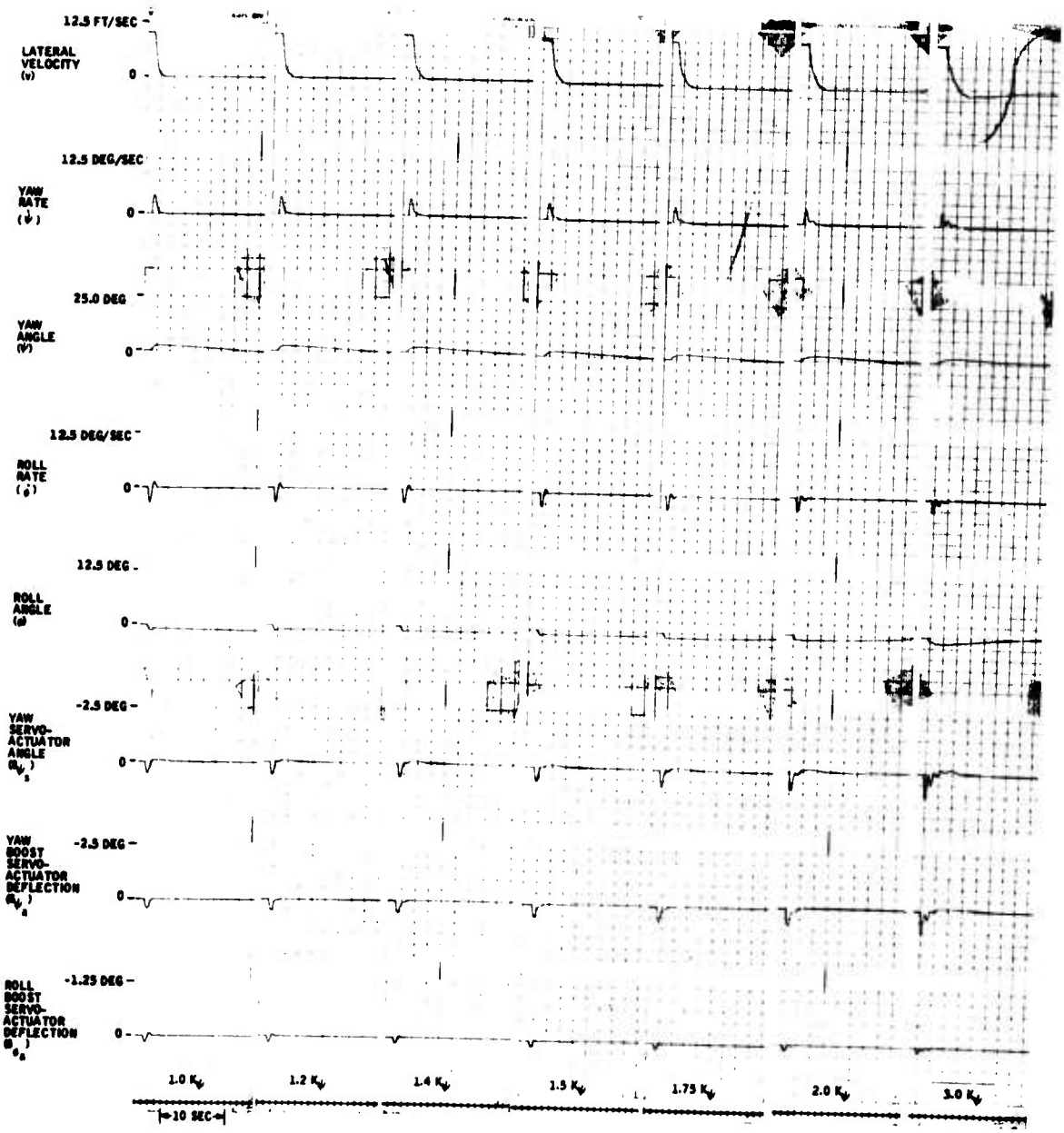

Figure 79. Yaw SAS Rate Gain Variation -- Lateral Gust Input (v_g = 10 Ft/Sec) at 120 Knots With Hysteresis.

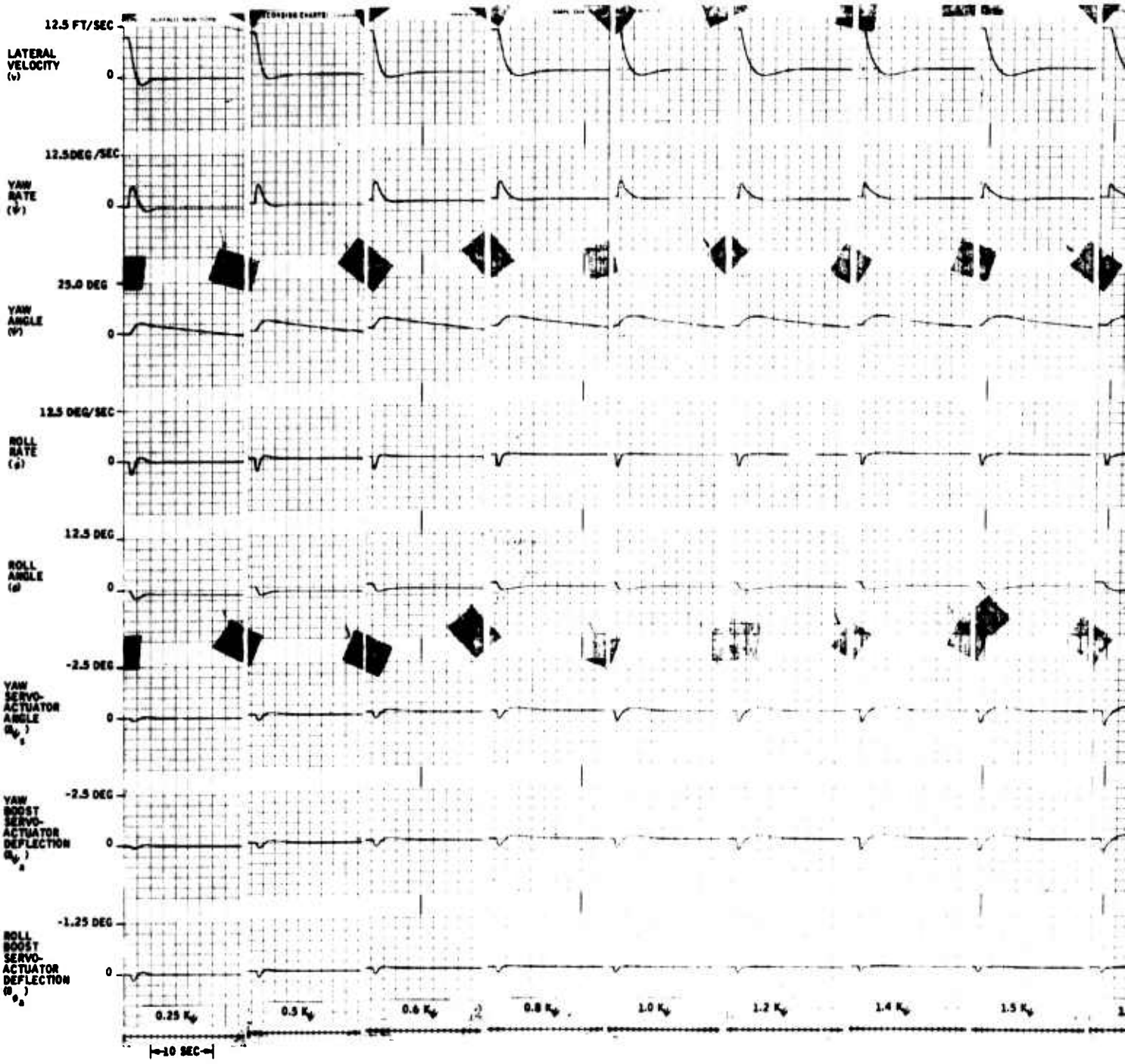

Figure 80. Yaw SAS Rate Gain Variation -- Lateral Gust Input (v_g = 10 Ft/Sec) at 60 Knots Without Hysteresis.

B

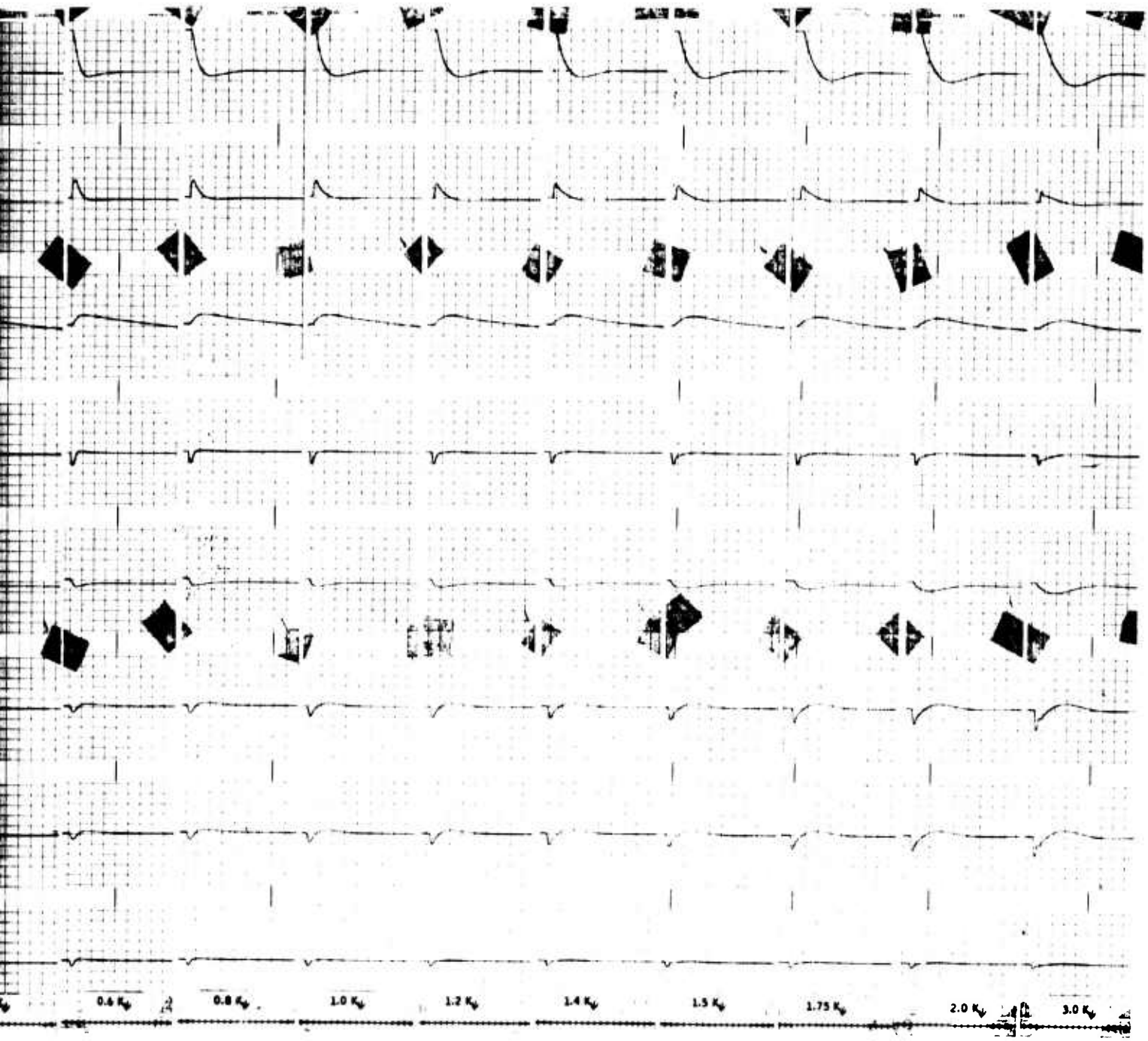

S Rate Gain Variation -- Lateral Gust Input
Ft/Sec) at 60 Knots Without Hysteresis.

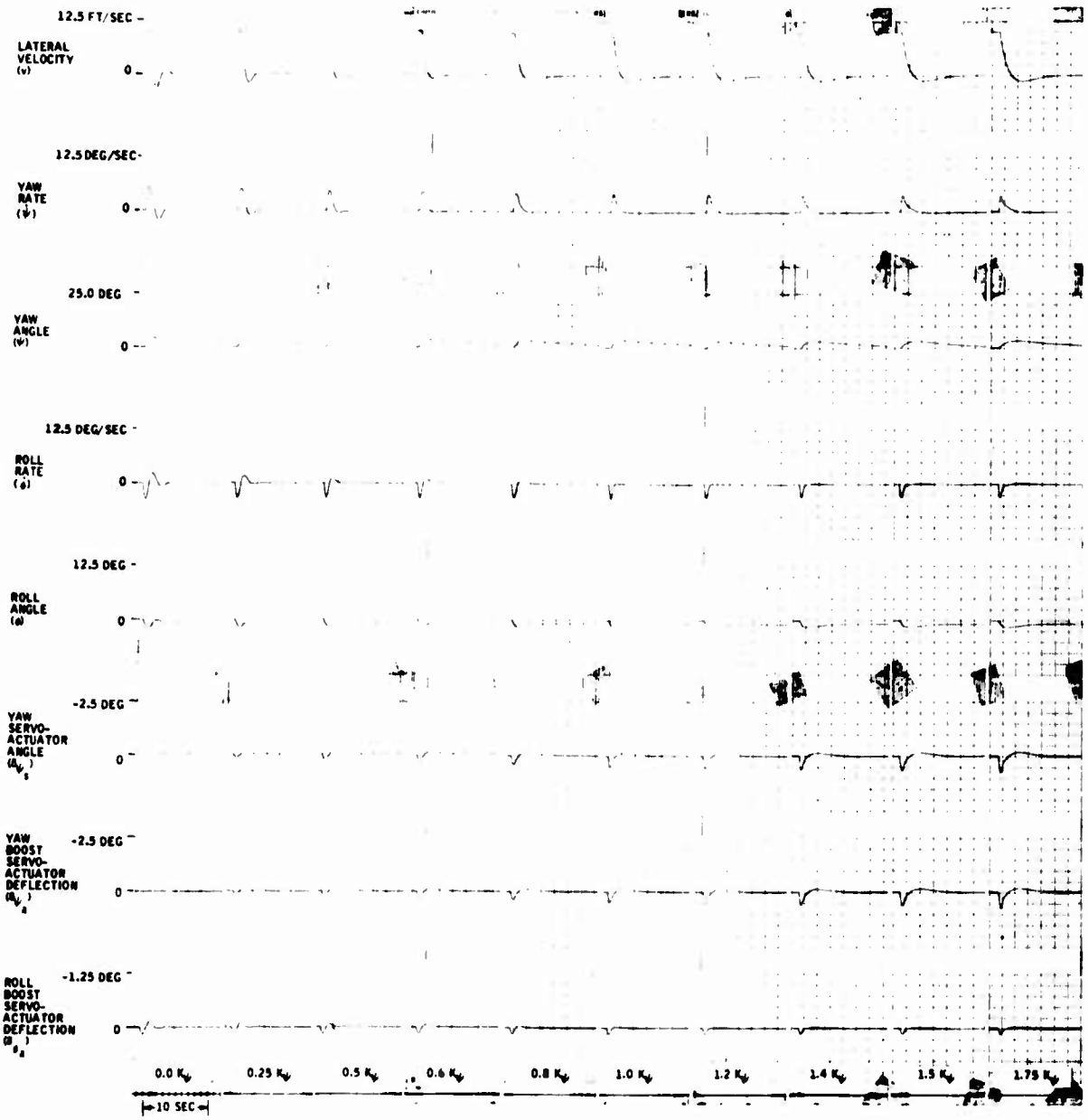

Figure 81. Yaw SAS Rate Gain Variation -- Lateral Gust Input (v_g = 10 Ft/Sec) at 90 Knots Without Hysteresis.

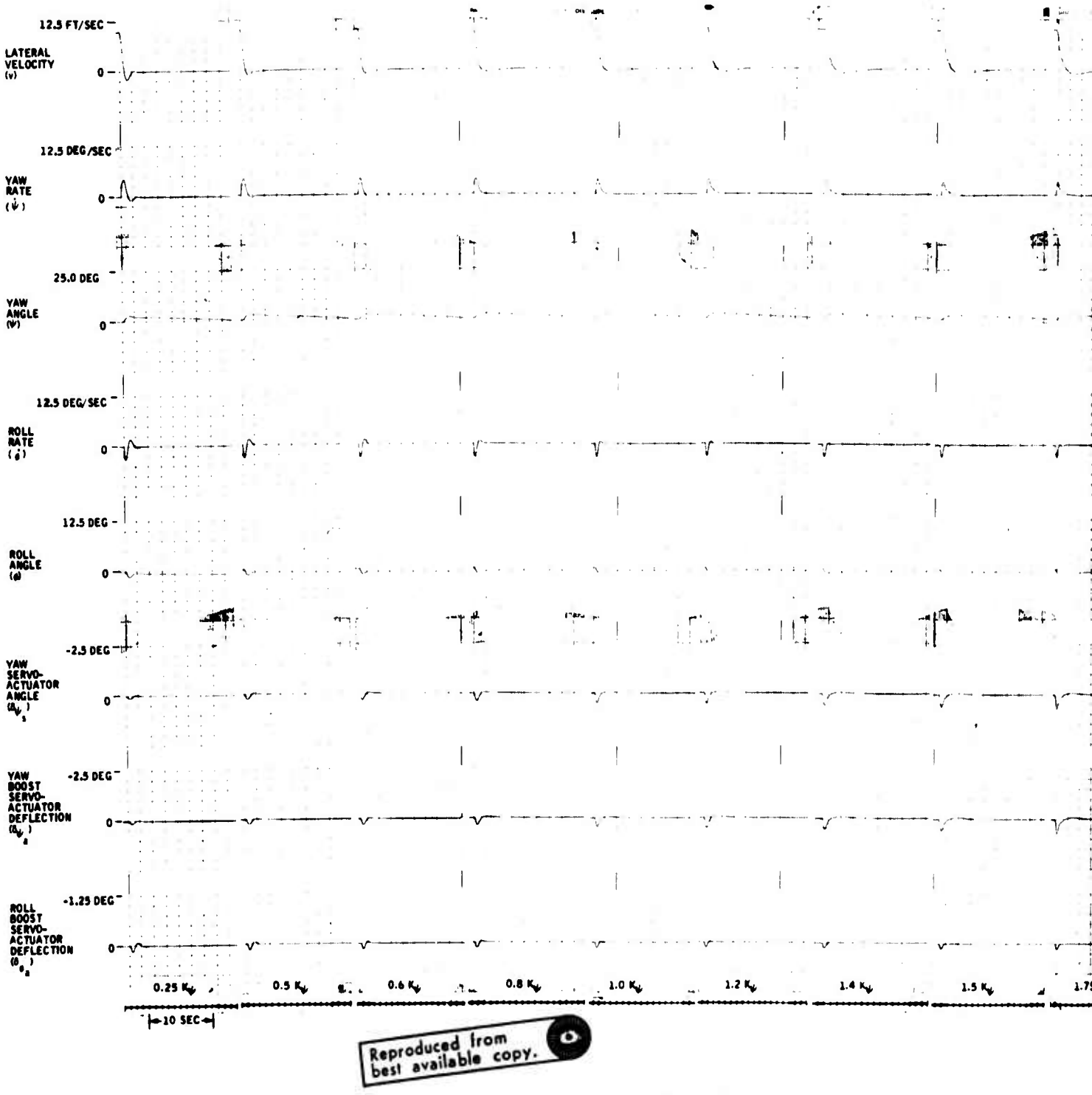

Figure 82. Yaw SAS Rate Gain Variation -- Lateral Gust Input (v_g = 10 Ft/Sec) at 120 Knots Without Hysteresis.

B

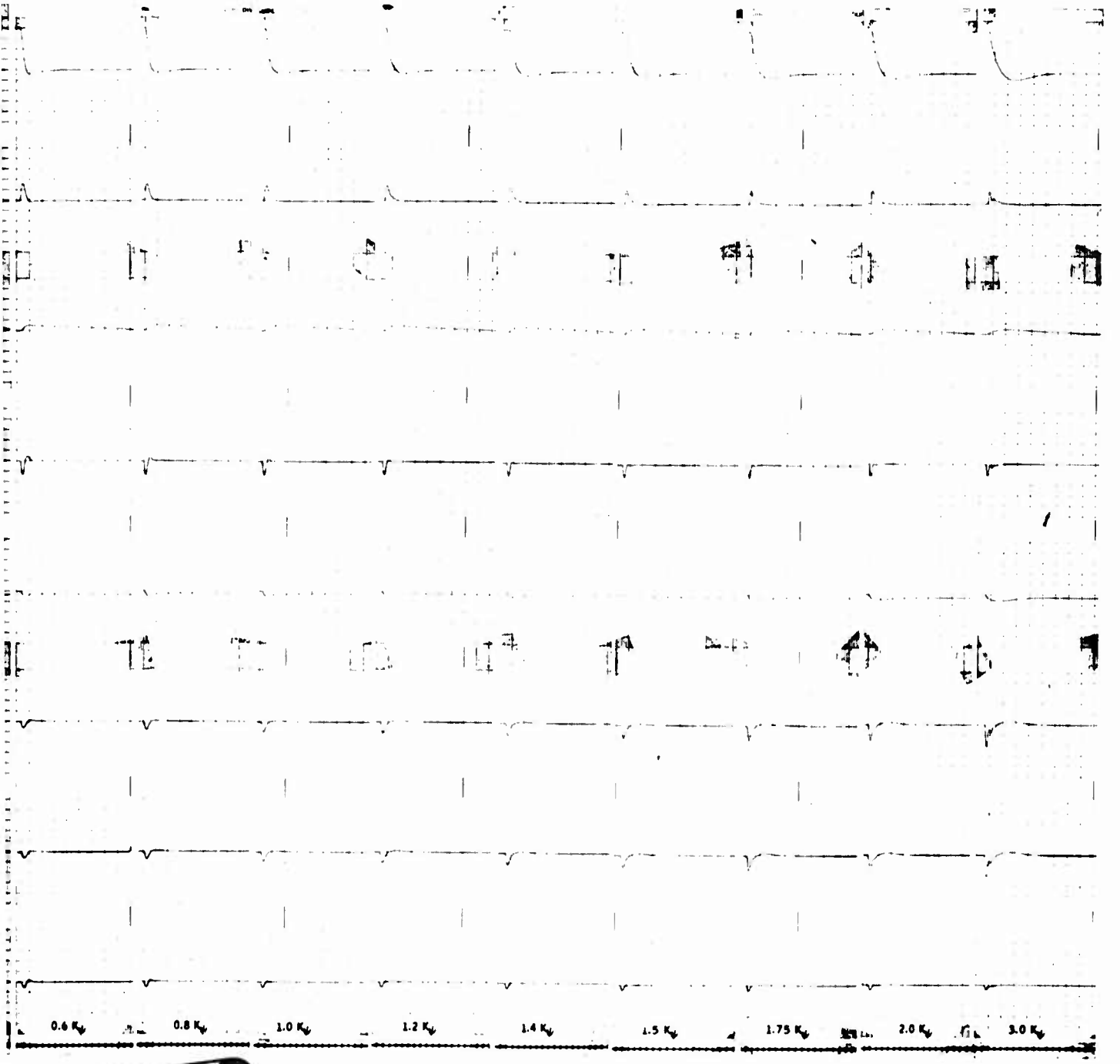

Gain Variation -- Lateral Gust Input
ec) at 120 Knots Without Hysteresis.

At the high-speed flight conditions (V>60 kn), yaw SAS gain was increased by a factor of 3, and the system was still relatively stable. This indicates that a gain margin of greater than 9.5 db exists for the nominal yaw SAS configuration.

The time histories of Figures 80, 81 and 82 were recorded without the linkage hysteresis backlash as part of the basic airframe. The lateral velocity responses show larger overshoots than those recorded with the linkage hysteresis backlash. This is due to the fact that the hysteresis acts as a deadband on the system and, as soon as signal levels are below the level of the hysteresis band, command signals are decreased to zero.

These figures also show that nominal performance can be achieved with a ±20-percent gain variation. If the gain is allowed to increase by 40 percent, the system response becomes sluggish at the 60-kn flight condition. A 40-percent decrease in the yaw SAS gain will result in a faster system response time that may result in an uncomfortable ride or jerky responses when damping external disturbances.

Yaw SAS High-Pass Time Constant Variation (T_{HP})

Yaw SAS high-pass time constant parameter variations at the 60-, 90-, and 120-kn flight conditions are shown in Figures 83, 84 and 85 with linkage backlash hysteresis as part of the basic airframe. Figures 86, 87 and 88 present the high-pass time constant variation without the linkage hysteresis backlash. These responses show that when linkage backlash hysteresis is included, relatively large variations in the high-pass time constant produce small changes in the performance of the yaw SAS when the vehicle is subjected to lateral gust inputs. The high-pass time constant may be varied as much as ±40 percent without significant changes in the yaw SAS performance.

In reviewing the responses of Figures 86, 87, and 88 without linkage hysteresis backlash, satisfactory lateral velocity gust response damping may be achieved within the bounds of the design goals for a ±20-percent variation in the high-pass time constant. These design goals specify that the lateral velocity overshoot should be 10 percent or less and the $T_{90\%}$ response time should be approximately 1.0 to 1.5 sec. Satisfactory damping performance may be obtained with slightly larger percentage variations in the high-pass time constant if the overshoot design goal is allowed to be greater than 10 percent and the response time is allowed to be longer than 1.5 sec. The gain of the system should not be allowed to decrease to a point where the $T_{90\%}$ response times are less than 1 sec. A rapid system response time will result in uncomfortable ride for the pilot and create maneuvering problems. Allowing the gain to become too large will result in a sluggish system.

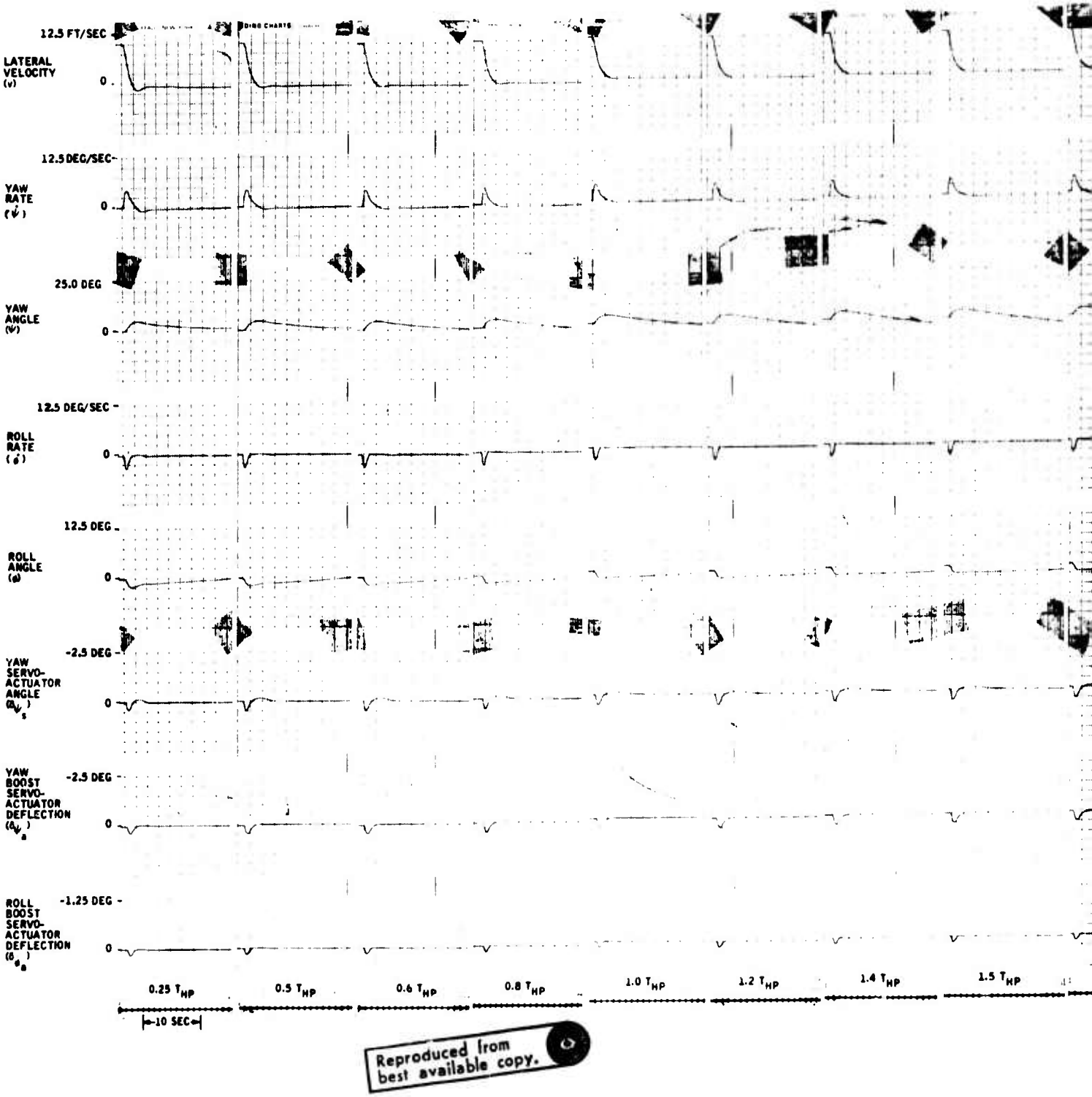

Figure 83. Yaw SAS High-Pass Time Constant Variation -- Lateral Gust Input (v_g = 10 Ft/Sec) at 60 Knots With Hysteresis.

B

Yaw SAS High-Pass Time Constant Variation -- Lateral Gust Input (v_g = 10 Ft/Sec) at 60 Knots With Hysteresis.

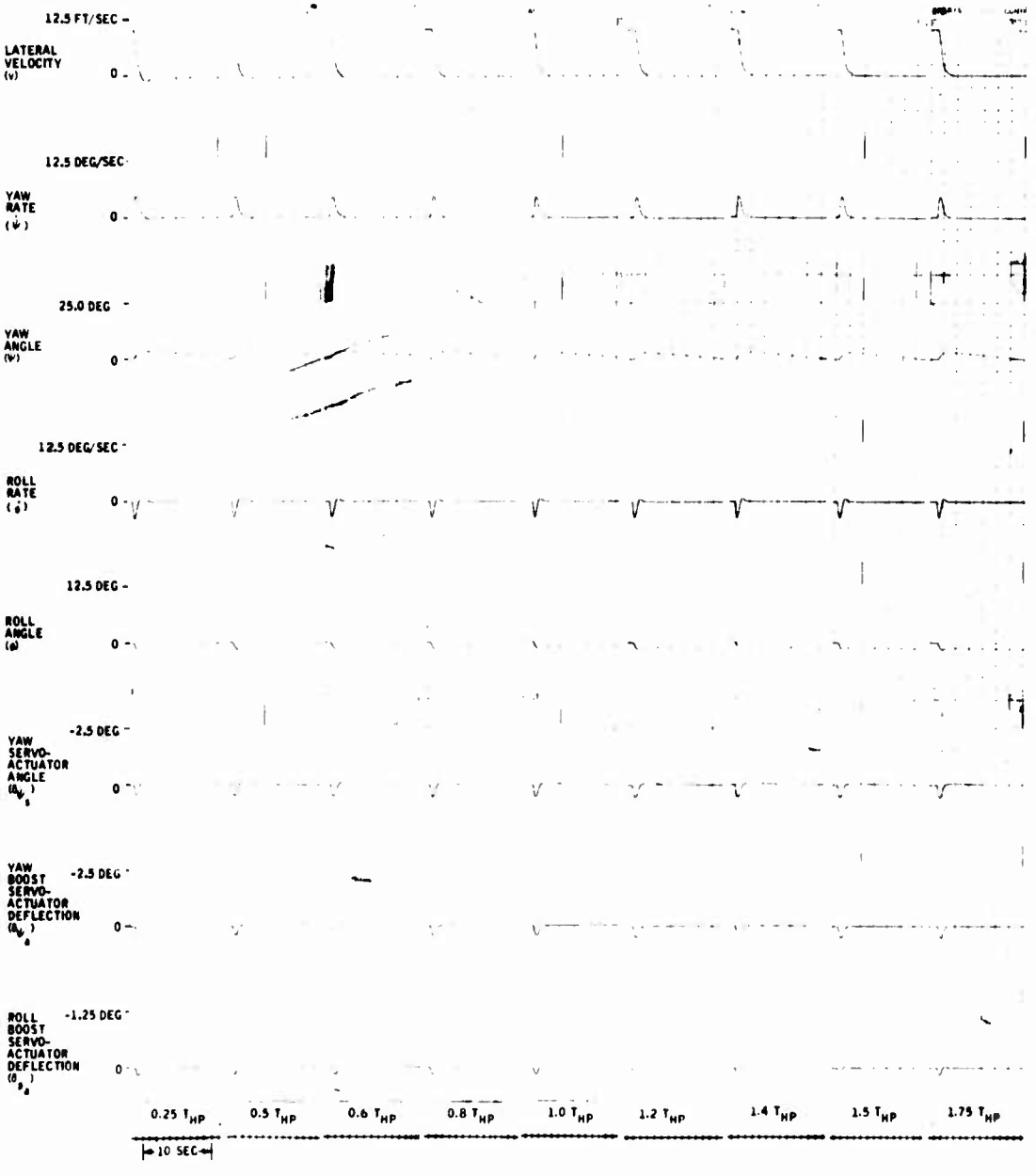

Figure 84. Yaw SAS High-Pass Time Constant Variation -- Vertical Gust Input (v_g = 10 Ft/Sec) at 90 Knots With Hysteresis.

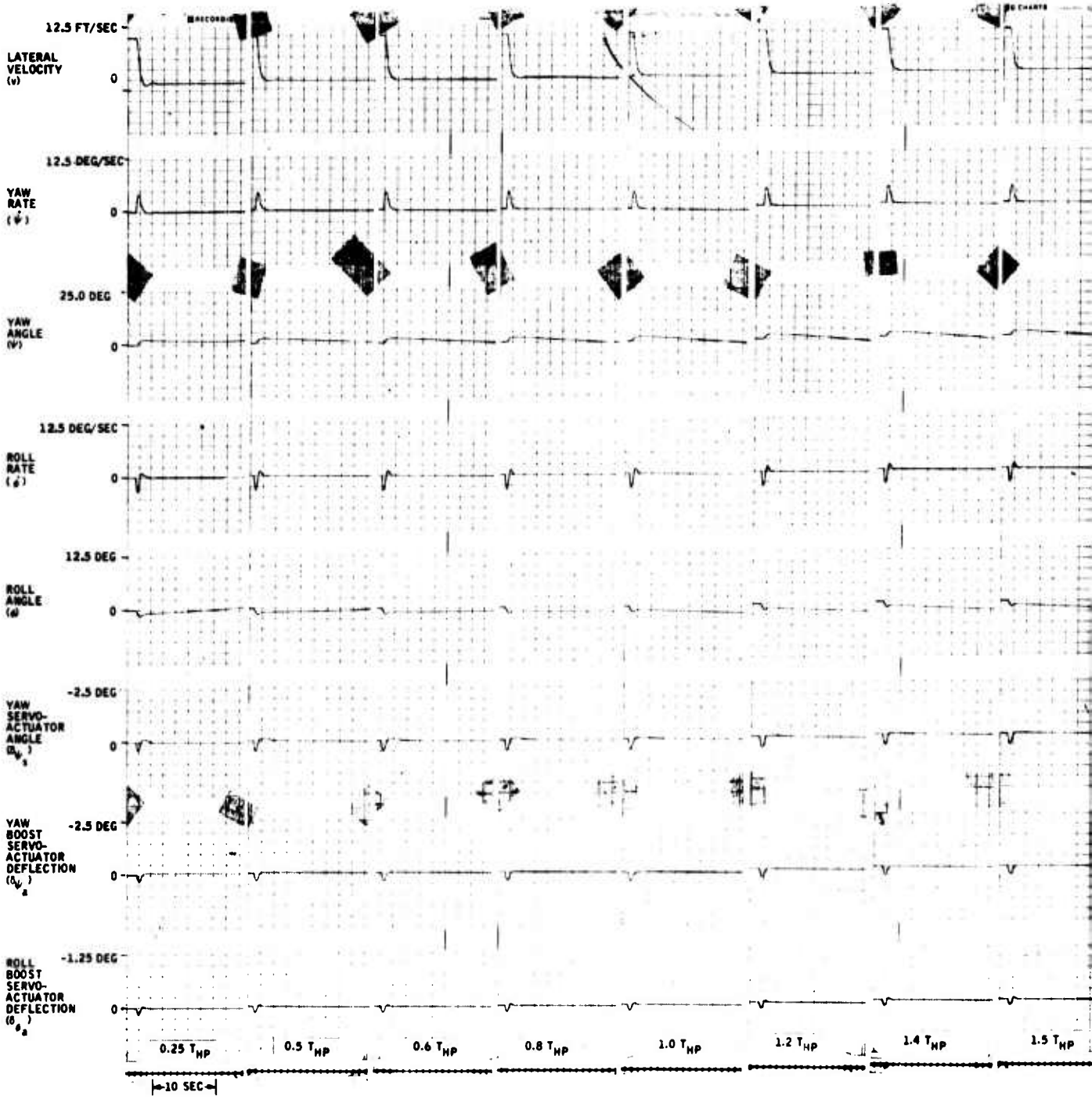

Figure 85. Yaw SAS High-Pass Time Constant Variation -- Lateral Gust Input (v_g = 10 Ft/Sec) at 120 Knots With Hysteresis.

B

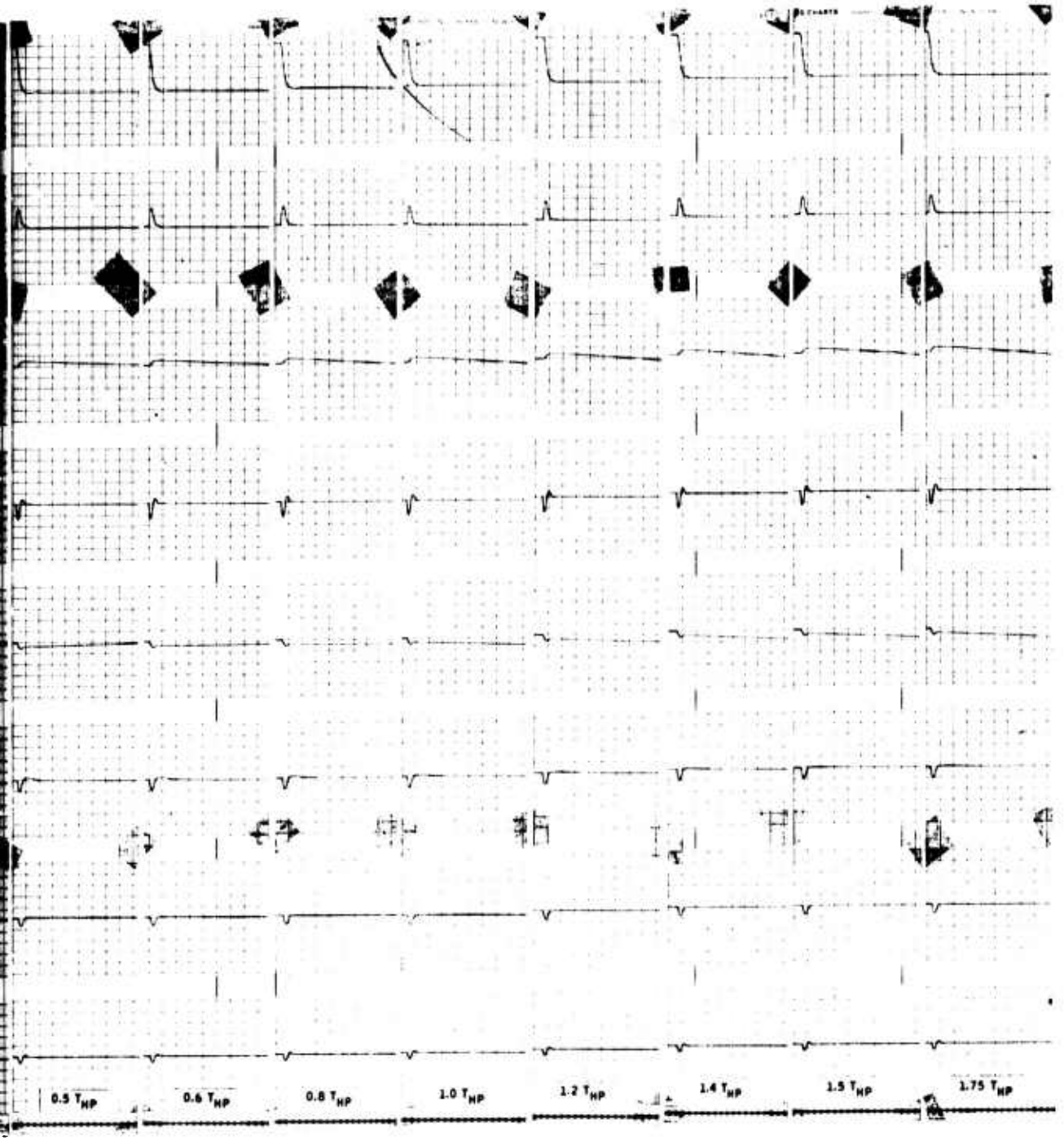

SAS High-Pass Time Constant Variation -- Lateral
t Input (v_g = 10 Ft/Sec) at 120 Knots With Hysteresis.

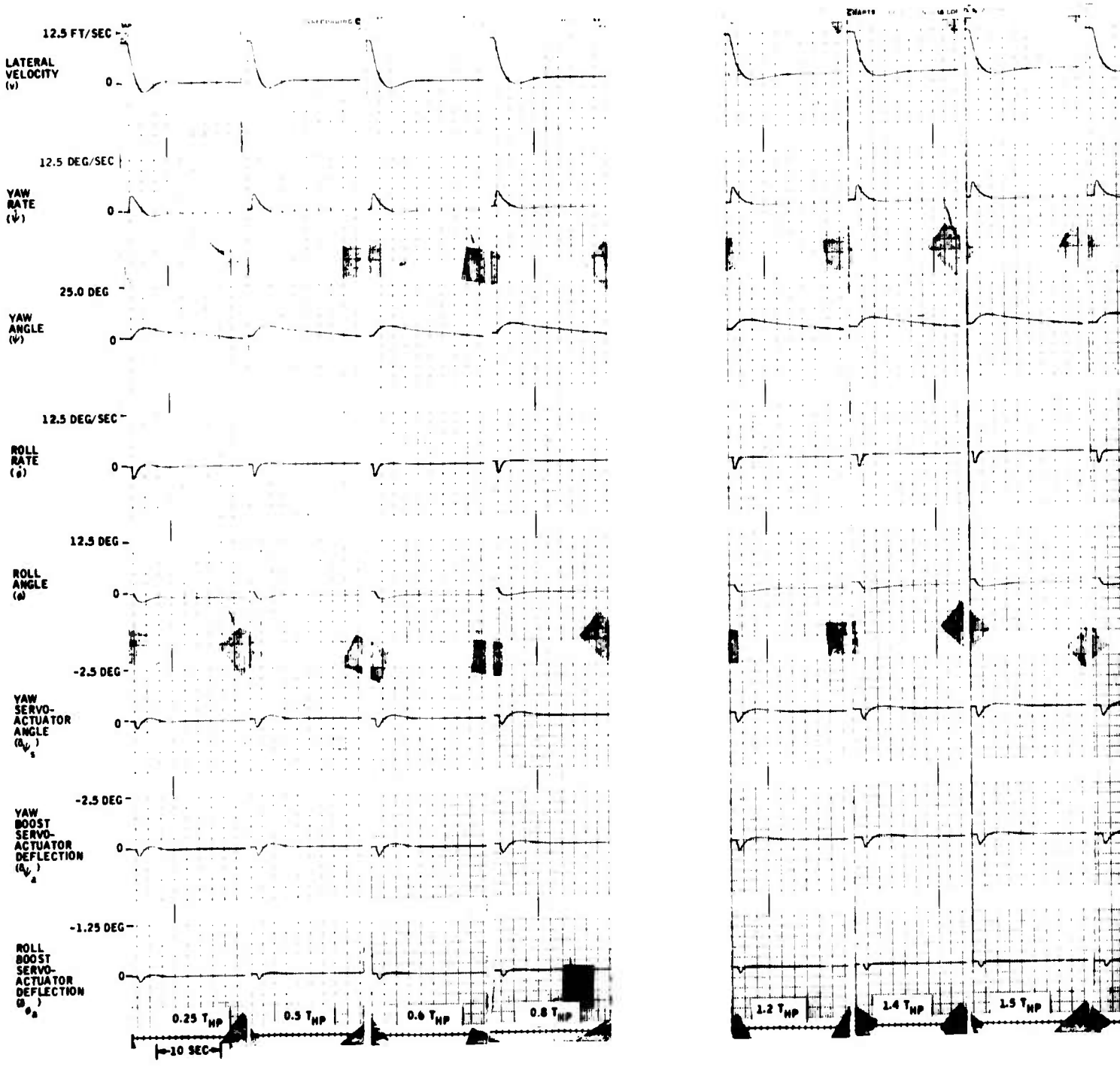

Figure 86. Yaw SAS High-Pass Time Constant Variation -- Lateral Gust Input (v_g = 10 Ft/Sec) at 60 Knots Without Hysteresis.

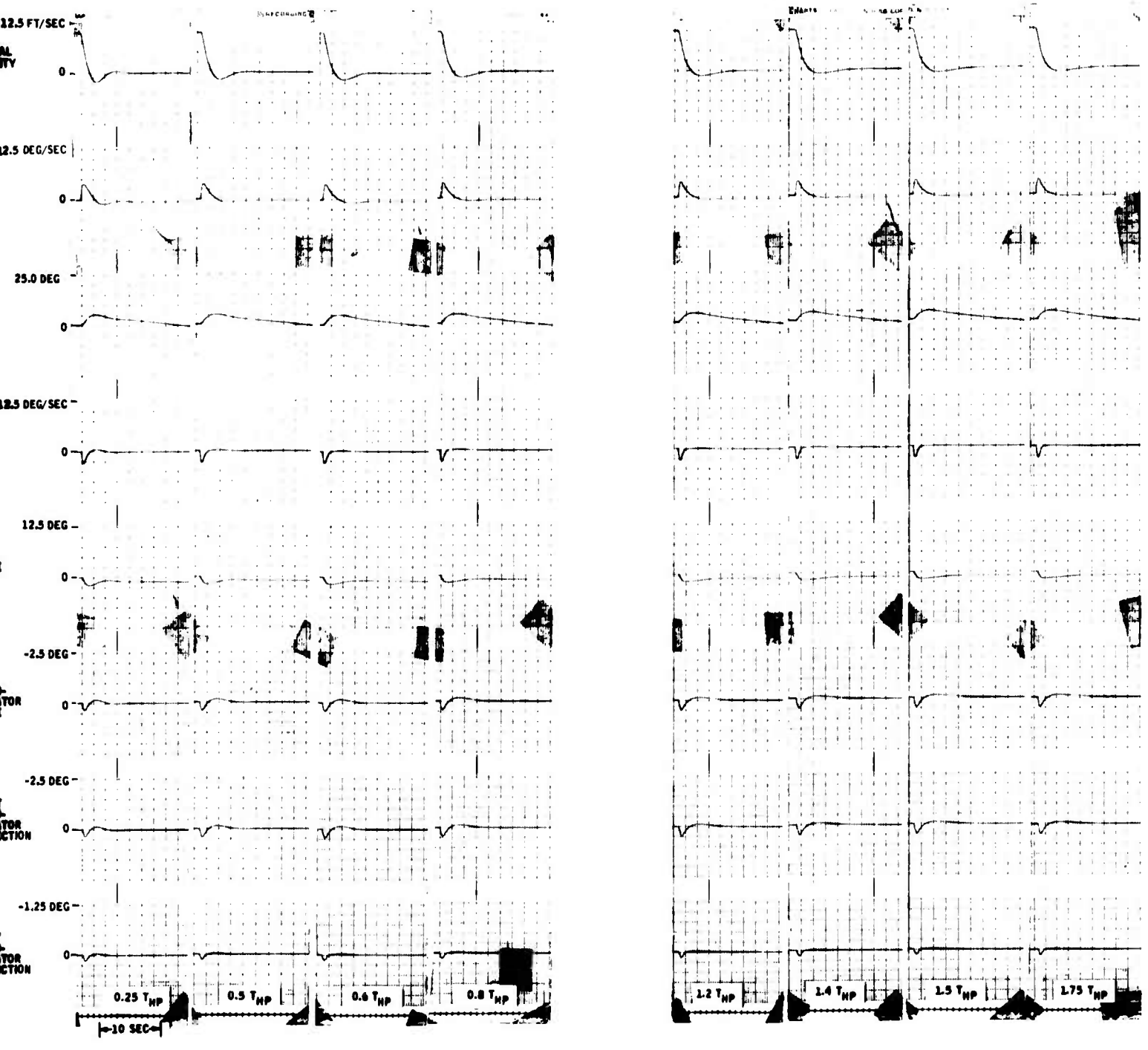

Figure 86. Yaw SAS High-Pass Time Constant Variation -- Lateral Gust Input (v_g = 10 Ft/Sec) at 60 Knots Without Hysteresis.

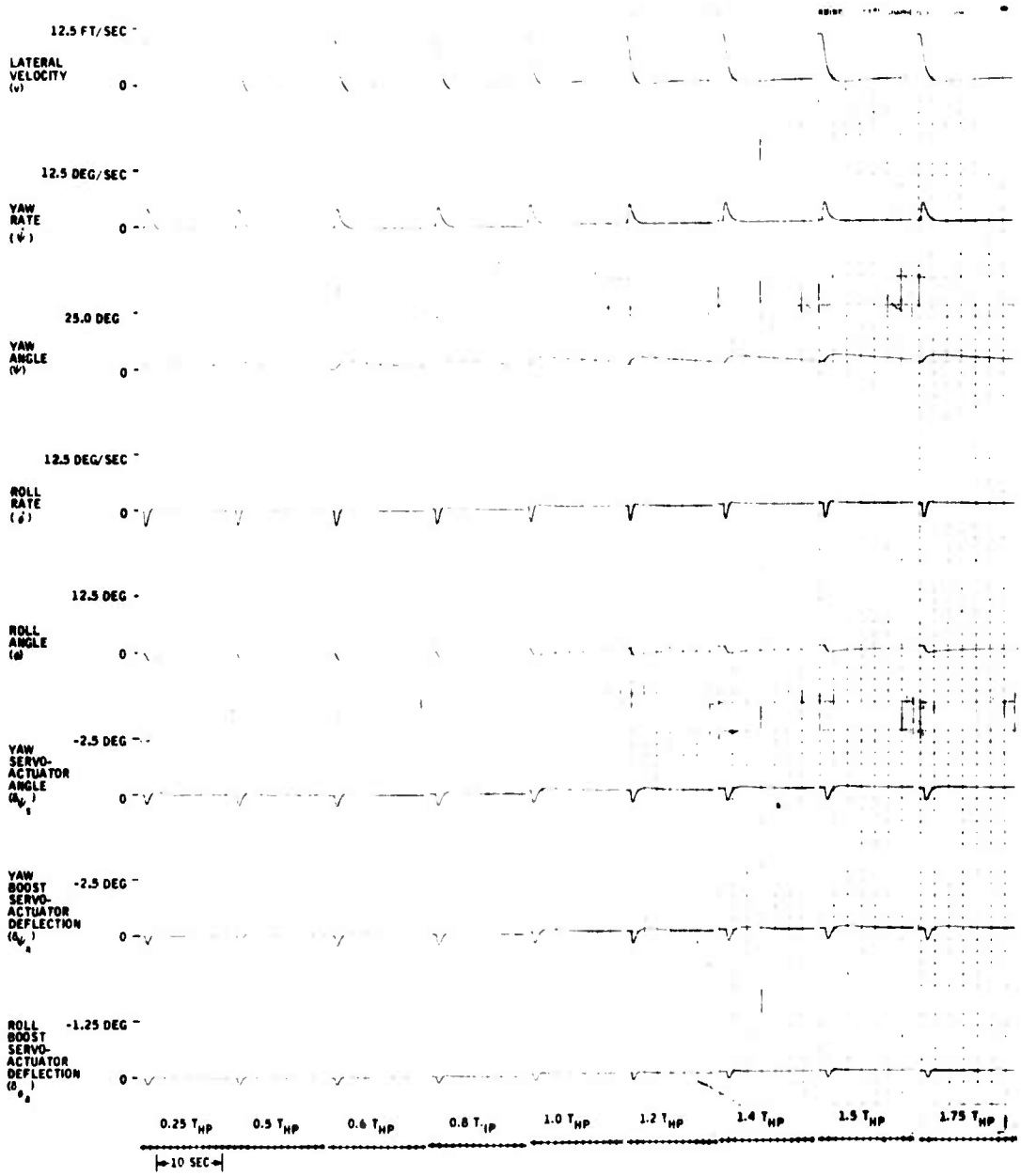

Figure 87. Yaw SAS High-Pass Time Constant Variation -- Lateral Gust Input (v_g = 10 Ft/Sec) at 90 Knots Without Hysteresis.

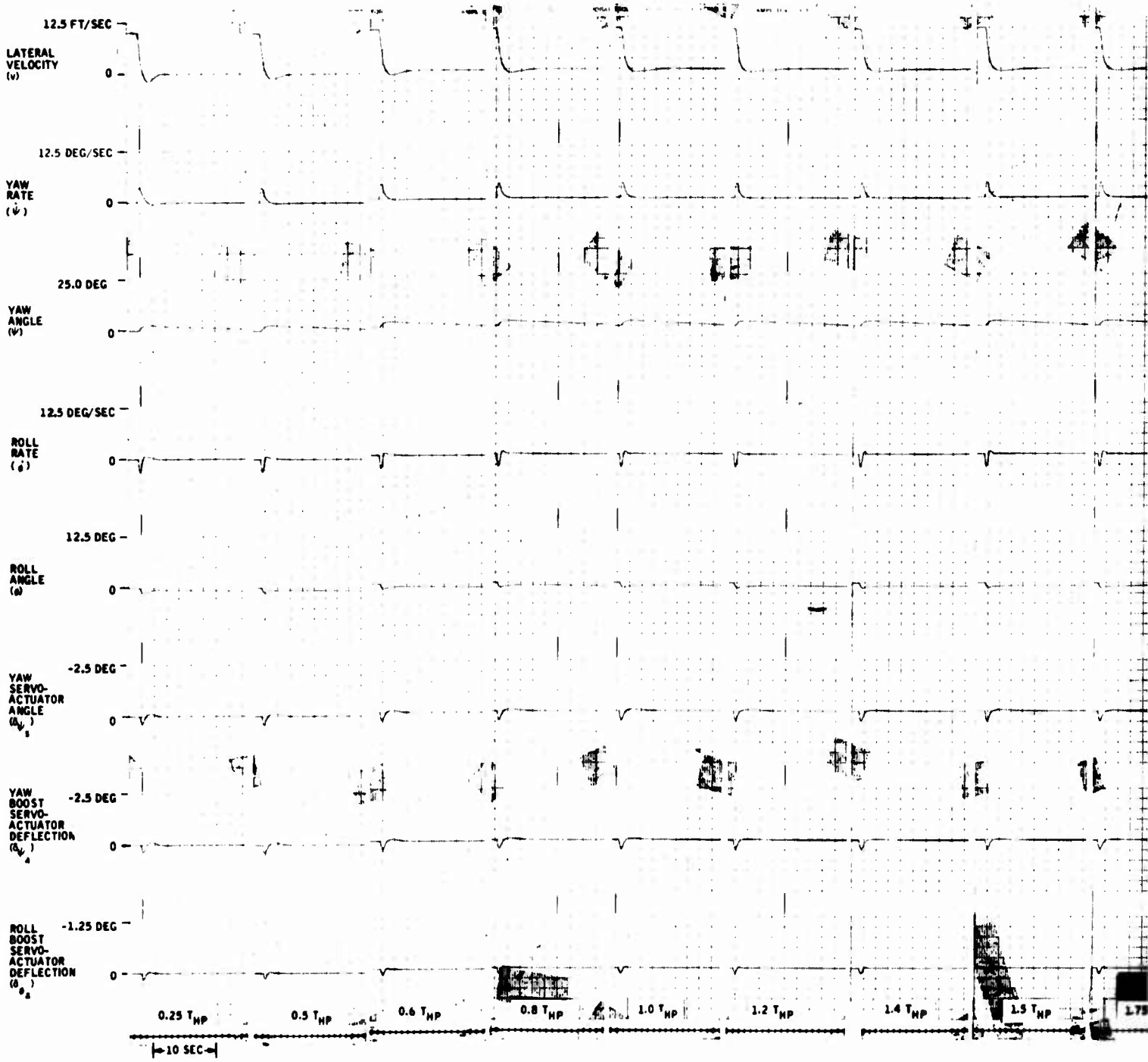

Figure 88. Yaw SAS High-Pass Time Constant Variation -- Lateral Gust Input (v_g = 10 Ft/Sec) at 120 Knots Without Hysteresis.

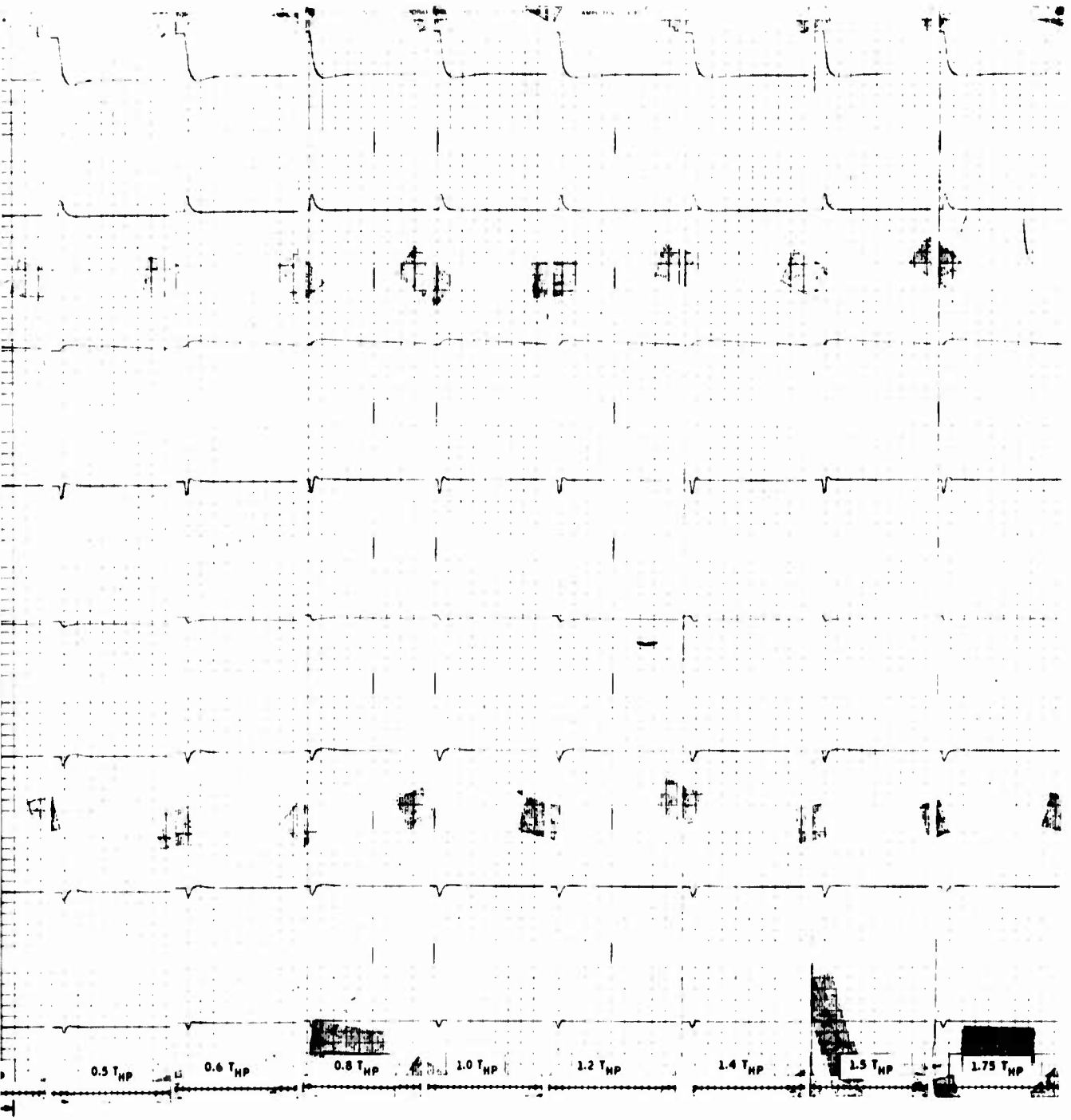

aw SAS High-Pass Time Constant Variation -- Lateral
ust Input (v_g = 10 Ft/Sec) at 120 Knots Without Hysteresis.

ROLL AXIS ANALYSIS

Roll Stability Augmentation System

Roll stability augmentation of the UH-1B was analyzed without the mechanical stabilizer as part of the basic vehicle. Results were obtained with and without the linkage backlash hysteresis of the primary control system.

The stability augmentation system defined during this analysis is a high-passed roll rate feedback as follows:

$$\delta_{\phi} = \delta_{\phi_m} - K_{\phi} \left(\frac{T_{HP}S}{T_{HP}S+1} \right) \dot{\phi}$$

where

K_{ϕ} = 0.055 deg roll cyclic blade angle/deg/sec

T_{HP} = 10 sec

δ_{ϕ_m} = Mechanical roll cyclic command from pilot's stick, deg

δ_{ϕ} = Total roll cyclic deflection, deg

$\dot{\phi}$ = Roll rate, deg/sec

An analytic block diagram of the final roll-axis control equation is shown in Figure 64. The roll rate feedback is high-passed with a 10-sec network to provide a long-term trim on the fluidic roll SAS feedback.

Transient response performance of the free aircraft and roll-SAS-augmented aircraft for all flight conditions is shown in Figure 89. The roll SAS and aircraft dynamics were analyzed with roll cyclic deflections. Roll SAS performance was evaluated by examining the steady-state roll rate response, $T_{90\%}$ roll rate response time (time to achieve 90 percent of final value), and roll-angle excursion. Pertinent performance data taken from Figure 89 are presented in Table XII.

The free-aircraft responses of Figure 89 recorded at the 60-, 90-, and 120-kn flight conditions show that the unaugmented vehicle characteristics are very well-behaved, and a simple roll rate feedback network provides the vehicle response characteristics to satisfy the design goals. The design goals observed during this analysis are briefly summarized as follows:

1. The control effectiveness shall be adjusted so that a 1-in. roll cyclic stick deflection produces a roll rate response of 20 deg/sec or less.

TABLE XII. ROLL SAS PERFORMANCE -- CYCLIC ROLL STEP INPUT (δ_{ϕ_m})

Flight Condition	Augmentation Off	Augmentation On	
		Without Hysteresis	With Hysteresis
Hover			
$\dot{\phi}$ s.s.*	70 (35)	24.0	24.0
$T_{90_{\dot{\phi}}}$ (sec)	1 (0.2)	0.2	0.2
ϕ at 1 sec**	40.0	24.0	24.0
ϕ at 0.5 sec	-	7.0	-
60 Kn			
$\dot{\phi}$ s.s.	25.0	17.0	17.0
$T_{90_{\phi}}$ (sec)	0.34	0.2	0.2
ϕ at 1 sec	17.0	12.0	12.0
90 Kn			
$\dot{\phi}$ s.s.	30.0	17.0	17.0
$T_{90_{\phi}}$ (sec)	1.0	0.25	0.25
ϕ at 1 sec	14.0	10.0	10.0
120 Kn			
$\dot{\phi}$ s.s.	62.5	20.0	20.0
$T_{90_{\phi}}$ (sec)	1.0	0.3	0.3
ϕ at 1 sec	20.0	14.0	14.0

* $\dot{\phi}$ s.s. = Steady-state rate, deg/sec
** = Roll angle, deg

2. At the hover flight condition, a rapid 1-in. roll cyclic deflection shall produce a roll-angle excursion of at least 1.45 deg at the end of 0.5 sec.

3. Free-vehicle characteristics shall not be changed to such a degree as to give the pilot a different vehicle to fly under emergency conditions.

Army helicopter pilots were interviewed to determine their viewpoints concerning the handling qualities of single-main-rotor helicopters. During this interview it was learned that all pilots felt the roll-axis control function of the UH-1B was nearly what they wanted. During this analysis, their viewpoints were kept in mind, and the roll SAS was designed to provide a vehicle that is easier to control and yet does not have the desired free-vehicle characteristics significantly altered.

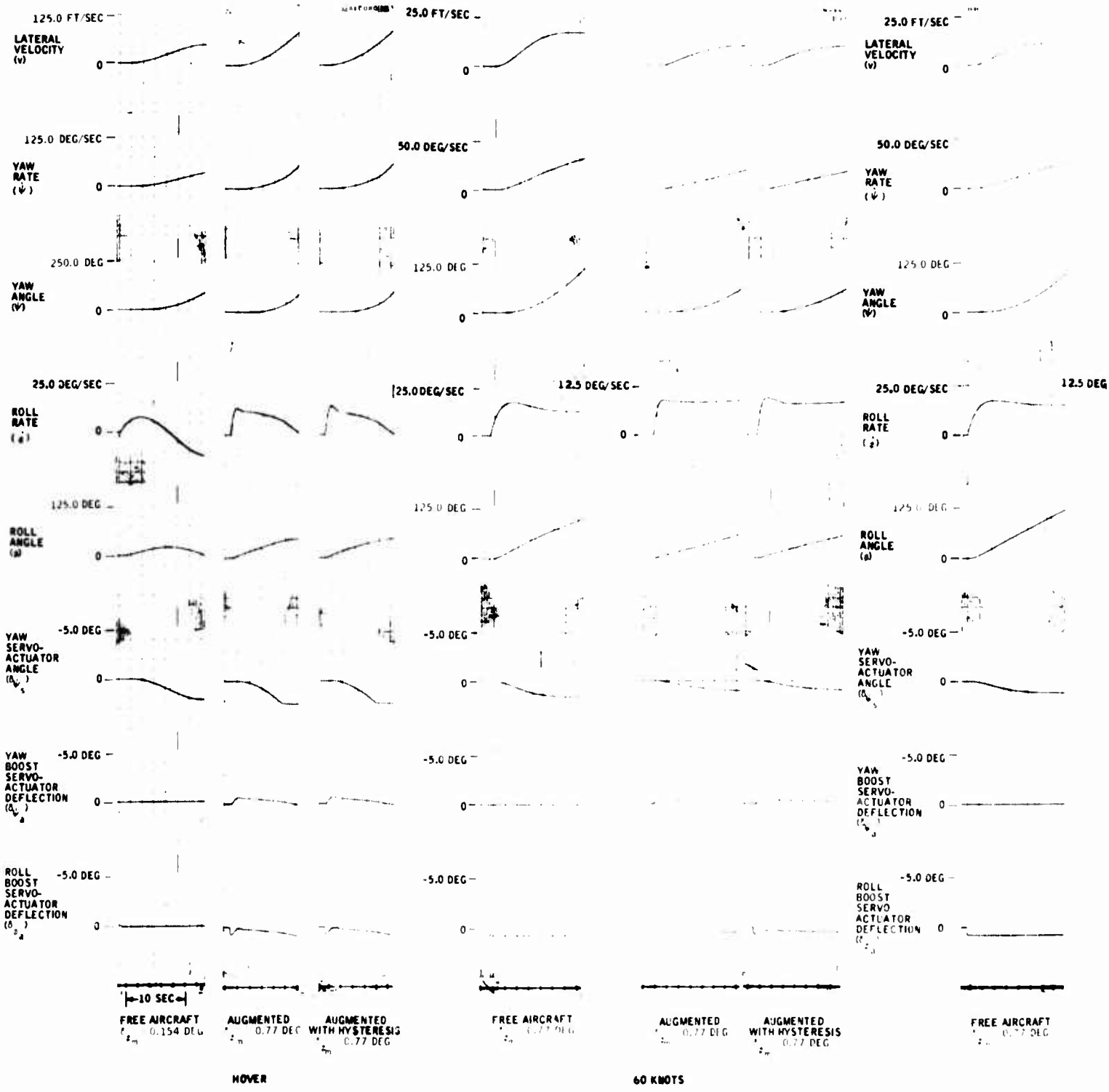

Figure 89. Free Aircraft and Roll SAS Performance Responses -- Cyclic Roll Step Input (δ_{c_m}).

B

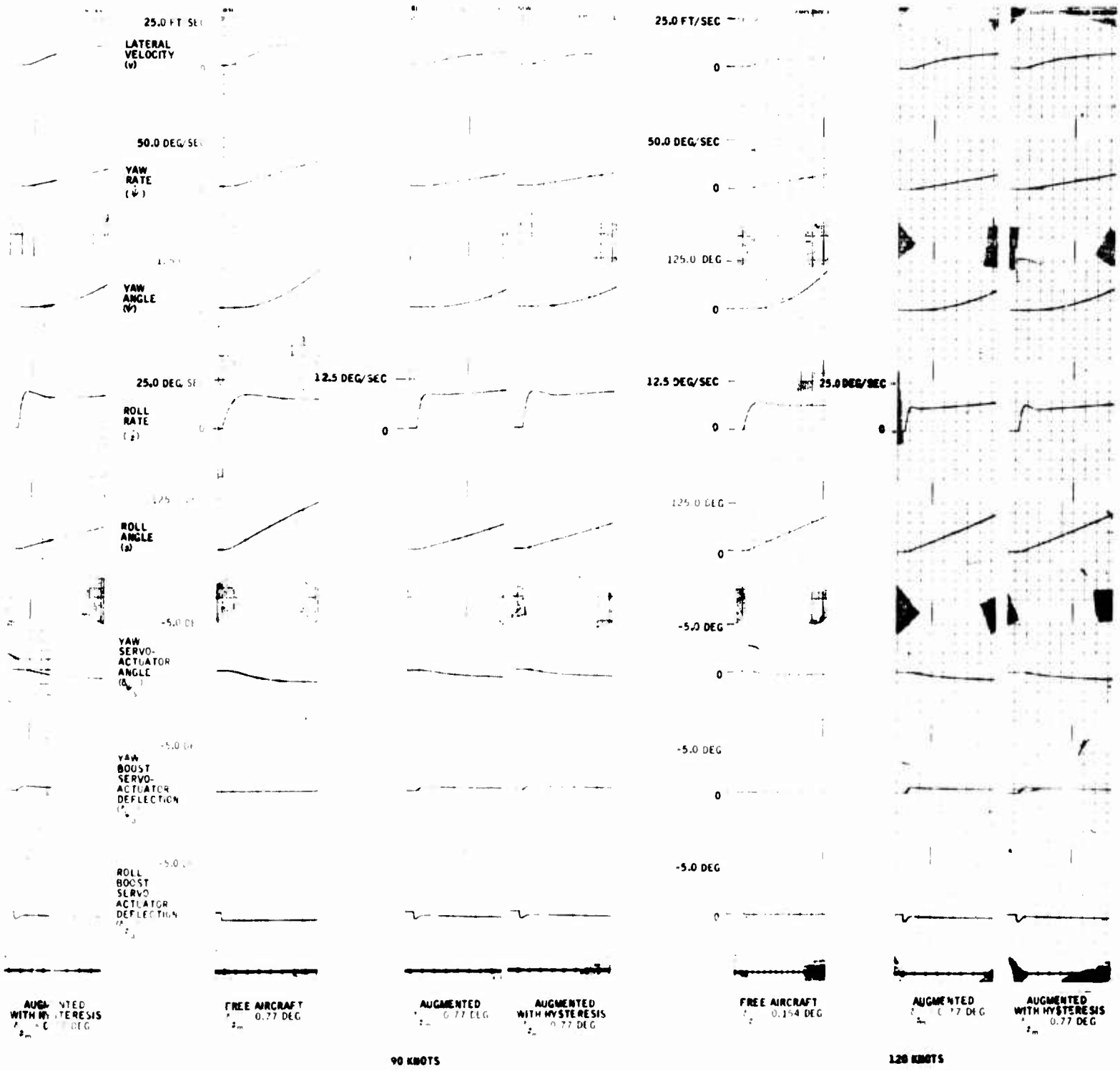
25.0 FT/SEC
LATERAL VELOCITY (v)
50.0 DEG/SEC
YAW RATE (ψ̇)
YAW ANGLE (ψ)
25.0 DEG/SEC
ROLL RATE (φ̇)
12.5 DEG/SEC
ROLL ANGLE (φ)
YAW SERVO-ACTUATOR ANGLE
YAW BOOST SERVO-ACTUATOR DEFLECTION
ROLL BOOST SERVO ACTUATOR DEFLECTION
0
-5.0 DEG
AUGMENTED WITH HYSTERESIS
FREE AIRCRAFT
0.77 DEG
AUGMENTED
AUGMENTED WITH HYSTERESIS
0.154 DEG
90 KNOTS
120 KNOTS

ses --

The transient responses given in Figure 89 show that the control effectiveness design goal was exceeded slightly at the hover flight condition. These data are summarized in Table XII. As shown, the hover control effectiveness was 24 deg/sec. The response time to achieve this rate was approximately 0.2 sec. The free aircraft during this same time period reaches 35 deg/sec. Based on this relative difference, the 24 deg/sec should not present a maneuver control problem to the pilots.

During this analysis, the gains were adjusted to achieve the best possible performance at the high-speed flight conditions. This resulted in the relatively high control effectiveness at the hover condition.

Roll SAS Parameter Variation Study

The roll SAS parameter variation study results are presented in Figures 90, 91, 92 and 93. During this analysis, only the roll rate gain ($K_{\dot{\phi}}$) was analyzed to determine its sensitivity to off-design tolerances. The 10-sec high-pass time constant is considered to be a noncritical parameter. Its purpose is to provide long-term sensor trim, and it is sufficient to say that the time constant should be equal to or greater than 10 sec.

Figure 90 presents the hover roll SAS parameter variation results. As shown, variations in the roll-rate gain have significant effects on the control effectiveness. A 40-percent decrease in the roll-rate gain results in a 45-percent increase in the control effectiveness. At the 90-kn flight condition, Figure 92, a 40-percent decrease in the roll rate gain produces a 29-percent change in the control effectiveness. It is therefore recommended that if environmental factors are anticipated that may result in relatively large roll-rate gain shifts, the nominal value of rate gain should be adjusted by the amount and opposite sign of the gain shift percentage. By making this adjustment in rate gain, the control effectiveness can be maintained at the desired level of 20 deg/sec/in. of lateral cyclic deflection. However, this may cause the control effectiveness to be too low under nominal conditions.

PITCH AXIS ANALYSIS

Pitch Stability Augmentation System

Pitch stability augmentation of the UH-1B was analyzed without the mechanical stabilizer as part of the basic vehicle. Results were obtained with and without the linkage backlash hysteresis of the primary control system.

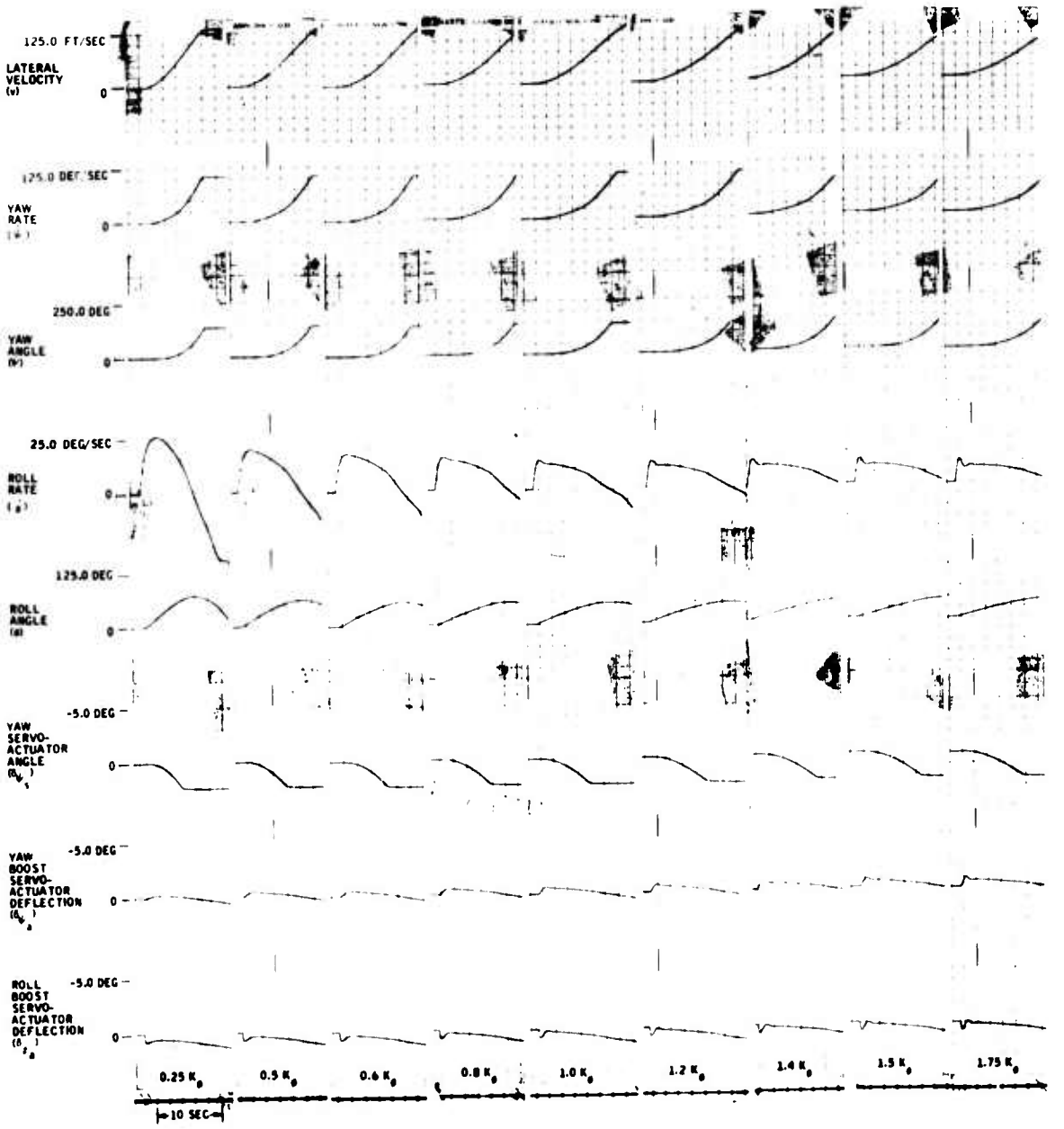

Figure 90. Roll SAS Rate Gain Variation -- Cyclic Roll Step Input (δ_{ϕ_m} = 0.77 Deg) at Hover.

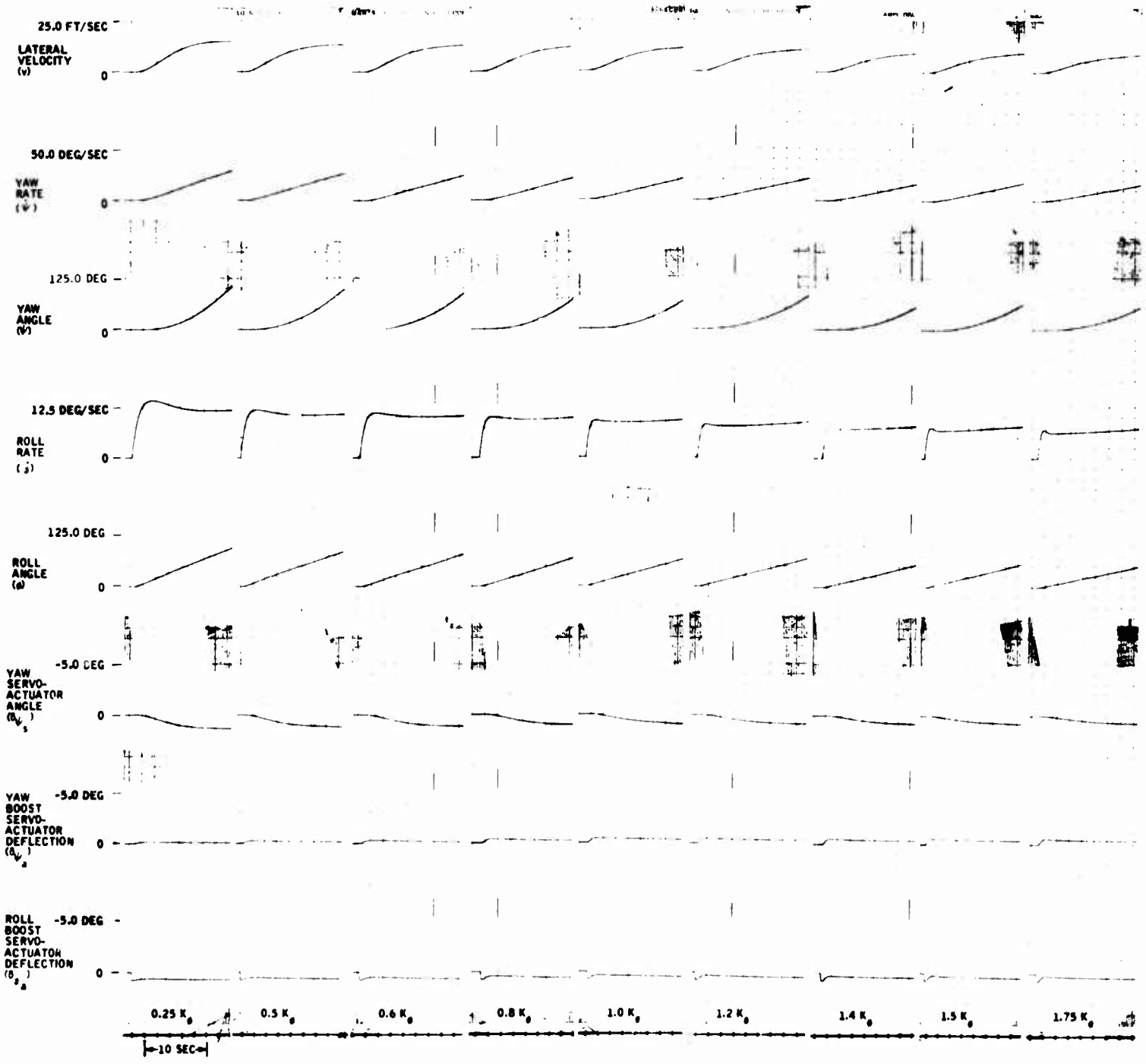

Figure 91. Roll SAS Rate Gain Variation -- Cyclic Roll Step Input (δ_{ϕ_m} = 0.77 Deg) at 60 Knots.

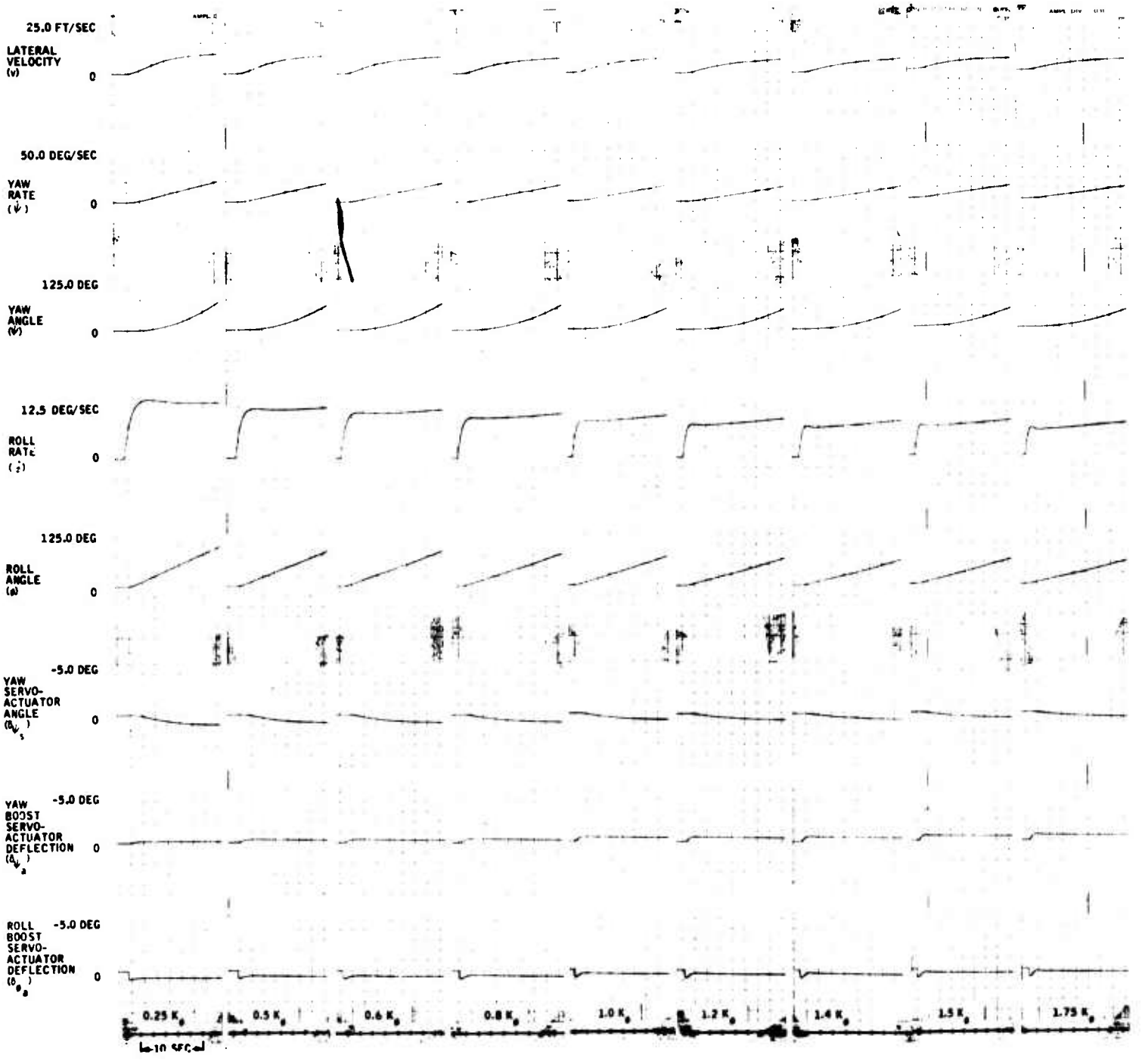

Figure 92. Roll SAS Rate Gain Variation -- Cyclic Roll Step Input (δ_{ϕ_m} = 0.77 Deg) at 90 Knots.

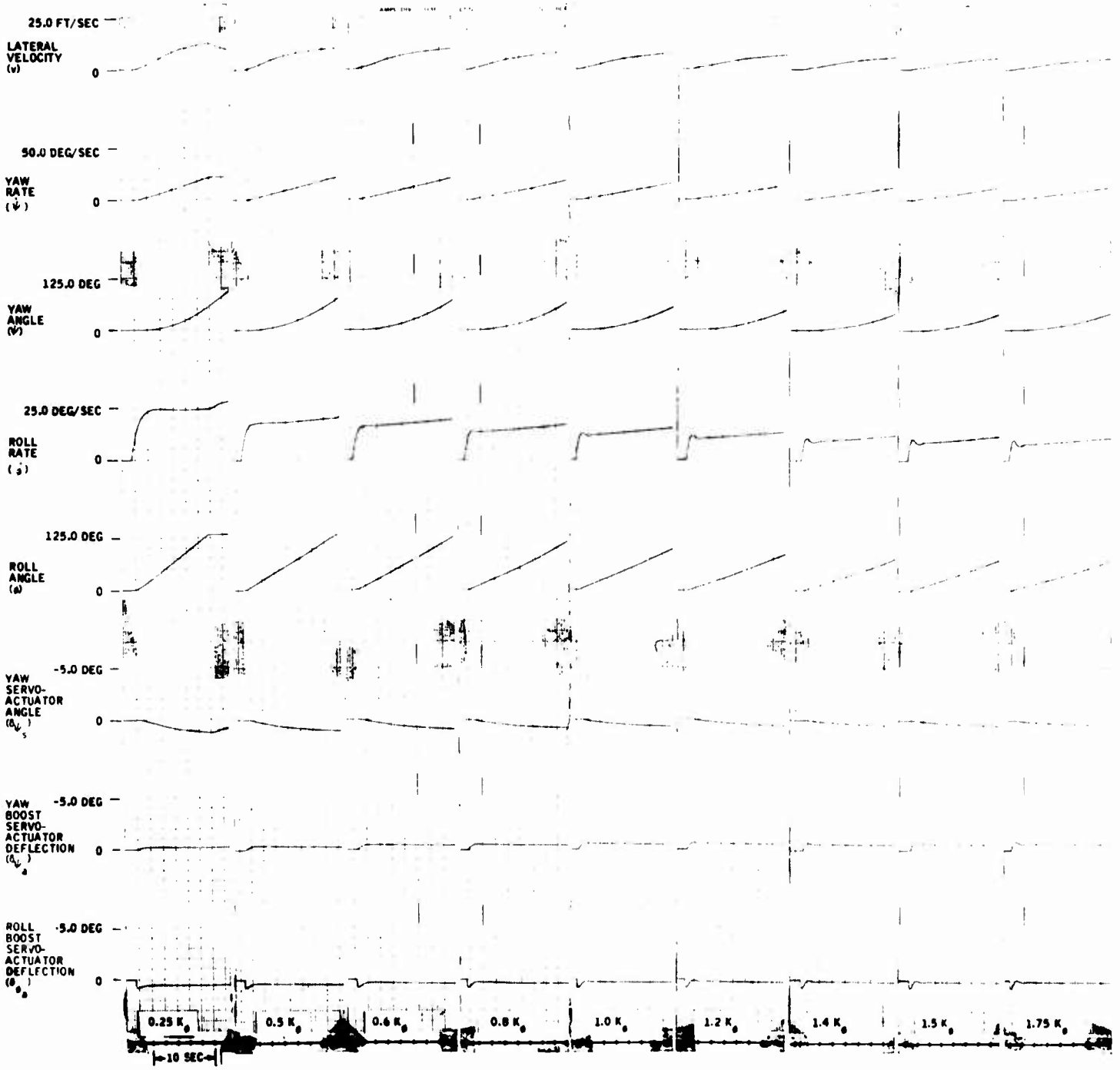

Figure 93. Roll SAS Rate Gain Variation -- Cyclic Roll Step Input (δ_{a_m} = 0.77 Deg) at 120 Knots.

The stability augmentation system defined during this analysis is expressed by the following control equation:

$$\delta_\theta = \delta_{\theta_m} - K_\theta \left(\frac{T_{HP} S}{T_{HP} S+1} \right) \left(\frac{T_1 S + 1}{T_2 S + 1} \right) \dot{\theta}$$

where

δ_θ = Total pitch cyclic deflection, deg

δ_{θ_m} = Mechanical pitch cyclic command from pilot's stick, deg

$\dot{\theta}$ = Pitch attitude rate, deg/sec

K_θ = 0.25 deg pitch cyclic blade angle/deg/sec

T_{HP} = 1.5 sec

T_1 = 0.25 sec

T_2 = 0.1 sec

An analytical block diagram of the final pitch SAS is shown in Figure 65.

The pitch rate feedback is high-passed to avoid damper opposition to the relatively low-frequency pilot inputs. The lead network is used to compensate for the inherent lag of the aircraft dynamics and the phase shift caused by the pure transport delay ($e^{-\tau S}$) of the fluidic rate sensor.

Time histories showing pitch SAS response to a pitch cyclic step input command are presented in Figure 94. These responses show that for the short time period, the pitch augmentation system changes the free-vehicle characteristics to provide the desired rate response proportional to cyclic stick deflection. Pertinent data used to show that the SAS does not adversely affect the helicopter's control power are shown in Tables XIII and XIV. The design goal regarding helicopter control power is briefly as follows: At the hovering flight condition, the pitch-angle excursion 1 sec after a rapid cyclic stick deflection of 1 in. shall be greater than 2.43 deg.

Time histories of the free and augmented aircraft with and without linkage backlash hysteresis are shown in Figure 95. These responses were recorded for a pitch cyclic step input command of 1 in.

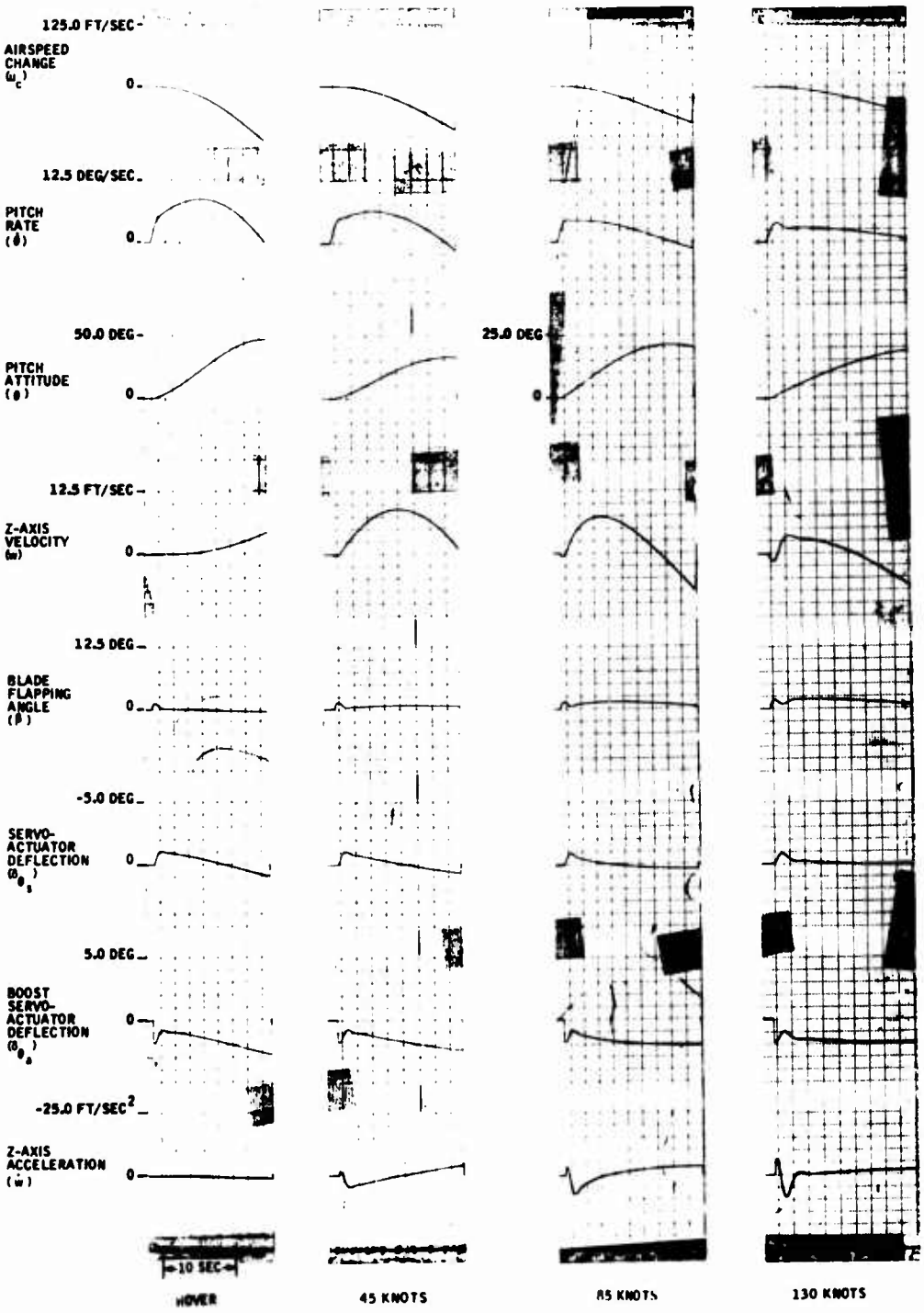

Figure 94. Pitch SAS Responses -- Cyclic Pitch Step Input (δ_{θ_m} = 1.84 Deg).

TABLE XIII. PITCH SAS PERFORMANCE--CYCLIC PITCH STEP INPUT ($\delta\theta_m$ = 0.77 DEG)

Flight Condition	Augmentation Off	Augmentation On	
		Without Hysteresis	With Hysteresis
Hover			
θ at 1 sec	4.0	3.0	3.0
45 Kn			
θ at 1 sec	3.7	3.0	3.0
85 Kn			
θ at 1 sec	3.5	2.7	2.7
130 Kn			
θ at 1 sec	2.0	2.0	2.0

*θ = Pitch angle, deg

TABLE XIV. PITCH SAS PERFORMANCE -- VERTICAL GUST INPUT (w_g = 10 FT/SEC)

Flight Condition	Augmentation Off	Augmentation On	
		Without Hysteresis	With Hysteresis
Hover			
O/SH (%)	0.0	0.0	0.0
$T_{90\%}$ (sec)	4.4	4.4	4.4
45 Kn			
O/SH (%)	0.0	0.0	0.0
$T_{90\%}$ (sec)	2.7	2.8	2.8
85 Kn			
O/SH (%)	10.0	5.0	0.0
$T_{90\%}$ (sec)	1.0	1.4	1.4
130 Kn			
O/SH (%)	30.0	17.0(ζ = 0.5)	18.0
$T_{90\%}$ (sec)	0.6	0.7	0.6

*ζ = Damping ratio

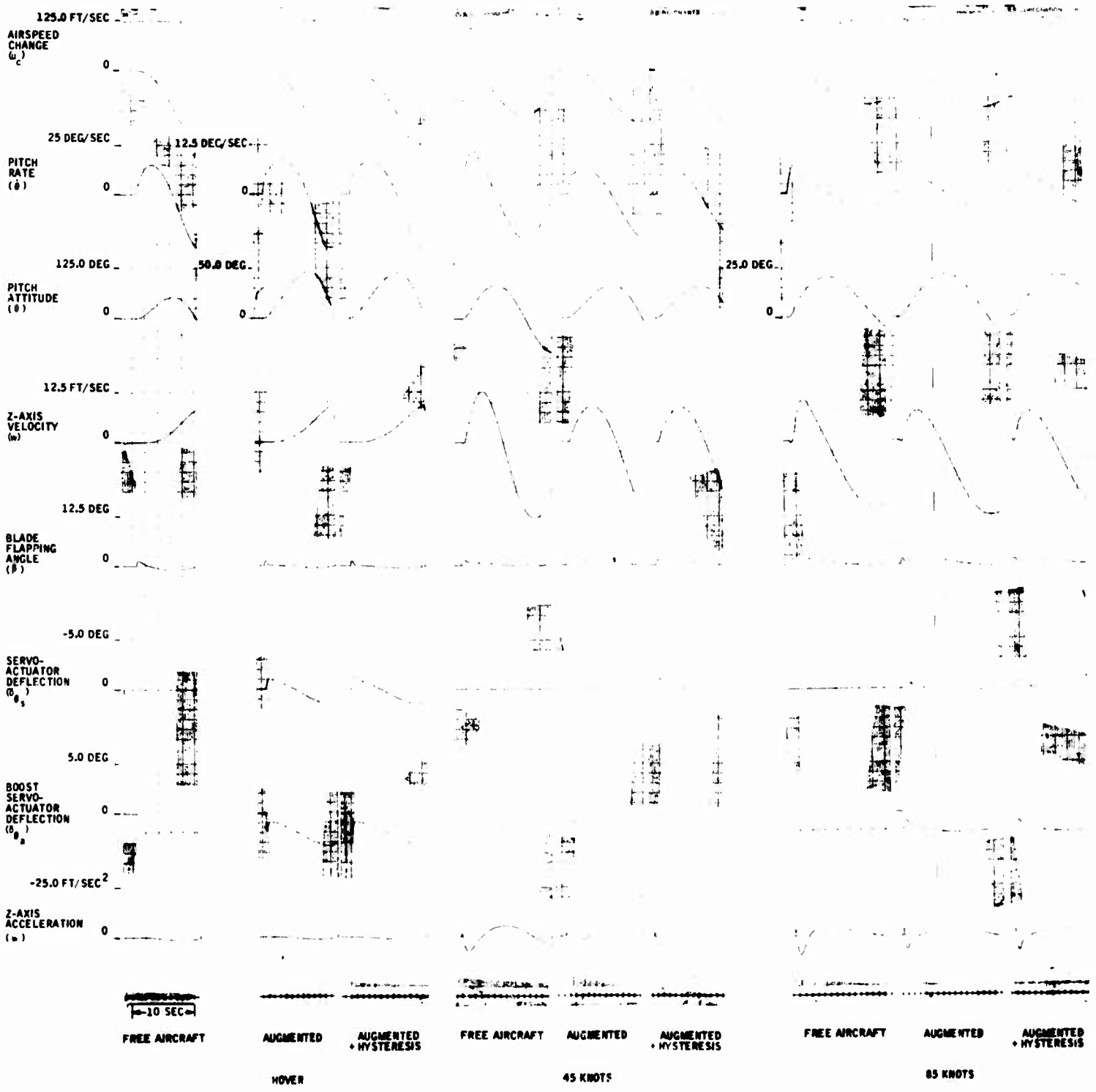

Figure 95. Free Aircraft and Pitch SAS Responses -- Cyclic Pitch Input (δ_{θ_m} = 1.84 Deg)

B

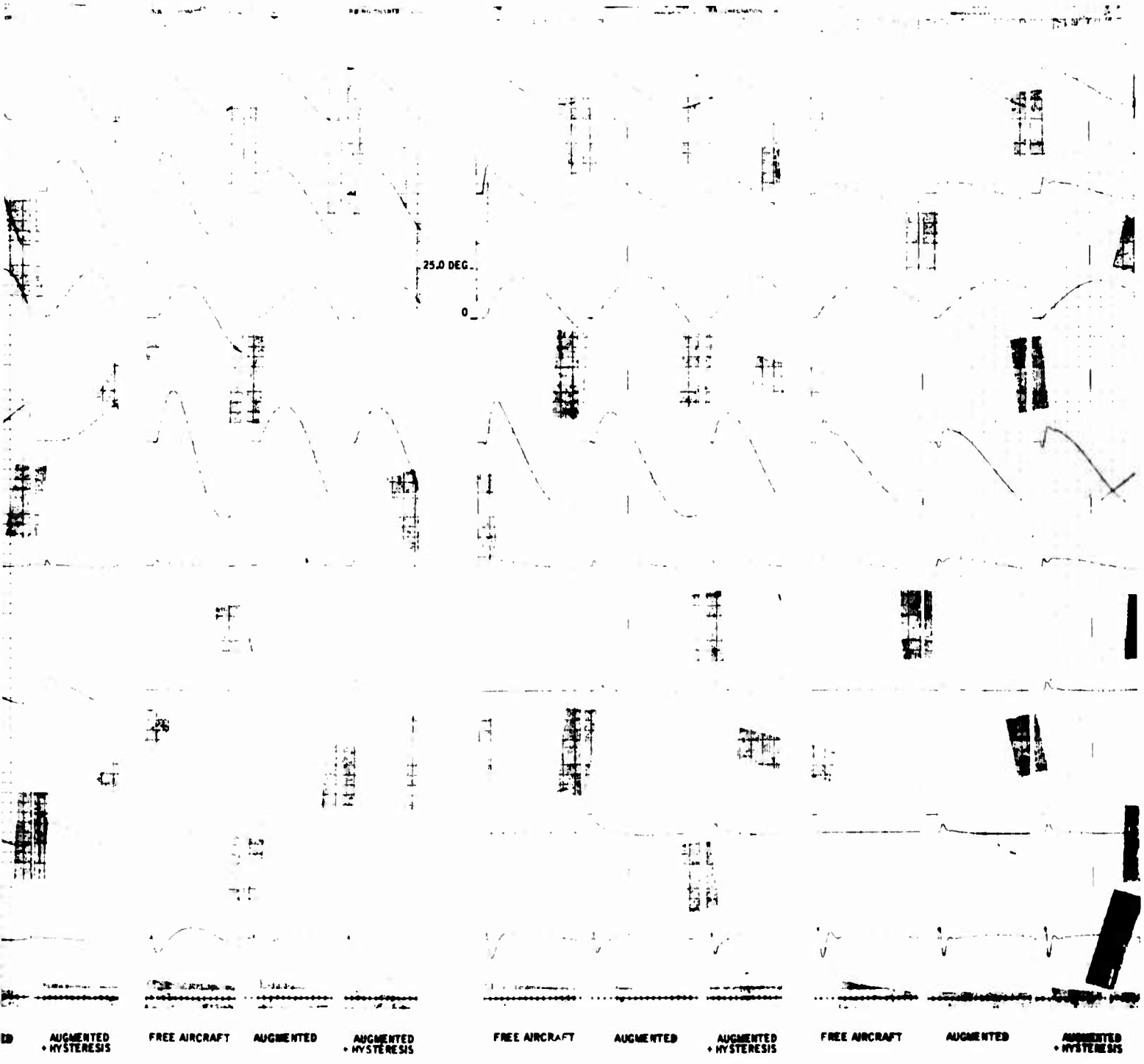

craft and Pitch SAS Responses -- Cyclic Pitch
= 1.84 Deg)
m

A review of these responses shows that the pitch SAS was designed with the intent to complement the free-aircraft characteristics rather than change them significantly. This was done by defining a system that produces a rate response proportional to stick input rather than the free aircraft's peak rate response proportional to stick input. A response of this type will provide the pilot with a vehicle that is easier to control when performing the tracking task.

During the previously mentioned pilot interview, it was learned that in the opinion of the UH-1E pilots interviewed, the pitch cyclic stick deflection/aircraft response characteristics were nearly what they wanted. They commented that it would be desirable if the vehicle response could be made more constant for a given stick displacement and if pitch-axis damping could be increased. These characteristics were kept in mind during the final pitch SAS development.

It may be noted that each of the rate responses of the augmented vehicle, as shown in Figure 95, has a characteristic dip occurring during the short term. This dip is due to an increase in system lags and is explained as follows. When a simple rate feedback is added to the vehicle, the inherent lags of the total system are accentuated. The next logical step is to add a lead network which compensates for the lags in the system. However, phase lead networks not only produce phase lead, but cause system gain to be increased by the product of the ratios of the shaping network's time constants. If this fact is not kept in view during the SAS development, high-frequency noise and body-bending problems could be created.

During the above discussion it was assumed that no phase lag was introduced by the rate sensor. However, the rate sensor defined for the FSAS program has a pure transport delay, which adds negative phase shift to the system frequency response. The transport delay is defined mathematically as $e^{-\tau S}$, where τ is the magnitude of the transport delay.

It can be shown mathematically that as τ increases, the phase lag of the system increases when excited with input signals having identical frequency spectrums. Therefore, when defining a rate sensor for flight control applications, the transport delay should be as small as possible. A rate gyro transport delay of 20 ms was defined for the FSAS.

During the development of the pitch SAS configuration, the transport delay, loop gains, and time constants were optimized to minimize the above-mentioned phase lag characteristics to provide the responses shown in Figure 95. The remaining dips on the time histories of Figure 95 are considered to be small. Their effects will not be felt by the pilots, nor do they present a stability problem as long as their magnitudes remain small.

Presented in Figure 96 are time histories showing pitch SAS performance when the aircraft is subjected to a vertical gust input. These time histories were recorded for the free and augmented aircraft with and without linkage backlash hysteresis.

These time histories show that high-speed damping ratio was increased from approximately 0.32 to 0.5.

The above discussion shows that the final pitch SAS configuration fulfills the requirements of the design goals. These design goals are briefly summarized as follows:

1. At hover, the pitch-angle excursion, 1 sec after the application of a step cyclic command of 1 in., shall be greater than 2.43 deg.

2. At the high-speed flight conditions, the pitch-axis damping ratio shall be increased to about 0.5 or greater.

Pitch SAS Parameter Variation Study

A parameter variation study was conducted on each parameter of the pitch SAS to determine their sensitivity to off-design tolerance variations and to establish the degree of stability margins present in the pitch control configuration. The parameters were varied over a sufficiently large range to show their effect on transient response and system stability.

Pitch SAS Gain Variation (K_θ)

Time histories for the pitch SAS gain variation are presented in Figures 97, 98, 99, and 100 for cyclic pitch input commands, and in Figures 101, 102, and 103 for vertical gust initial conditions.

As shown, when the rate gain is allowed to increase by 40 percent, the phase lag of the system increases to such an extent that the rate response begins to deteriorate. That is, a dip develops in the short-term rate response, and the pitch servoactuator time history shows that high-frequency components are beginning to develop. As the gain is allowed to decrease, the system damping decreases. For a 40-percent decrease in gain, system damping is 0.4; the design goal damping ratio was 0.5. Nominal system performance may be achieved for a ±20-percent tolerance on the pitch SAS rate gain.

Pitch SAS High-Pass Time Constant Variation (T_{HP})

Pitch SAS high-pass time constant parameter variations are shown in Figures 104, 105, 106, and 107 for cyclic pitch input commands, and in Figures 107, 108, and 109 for vertical gust initial conditions.

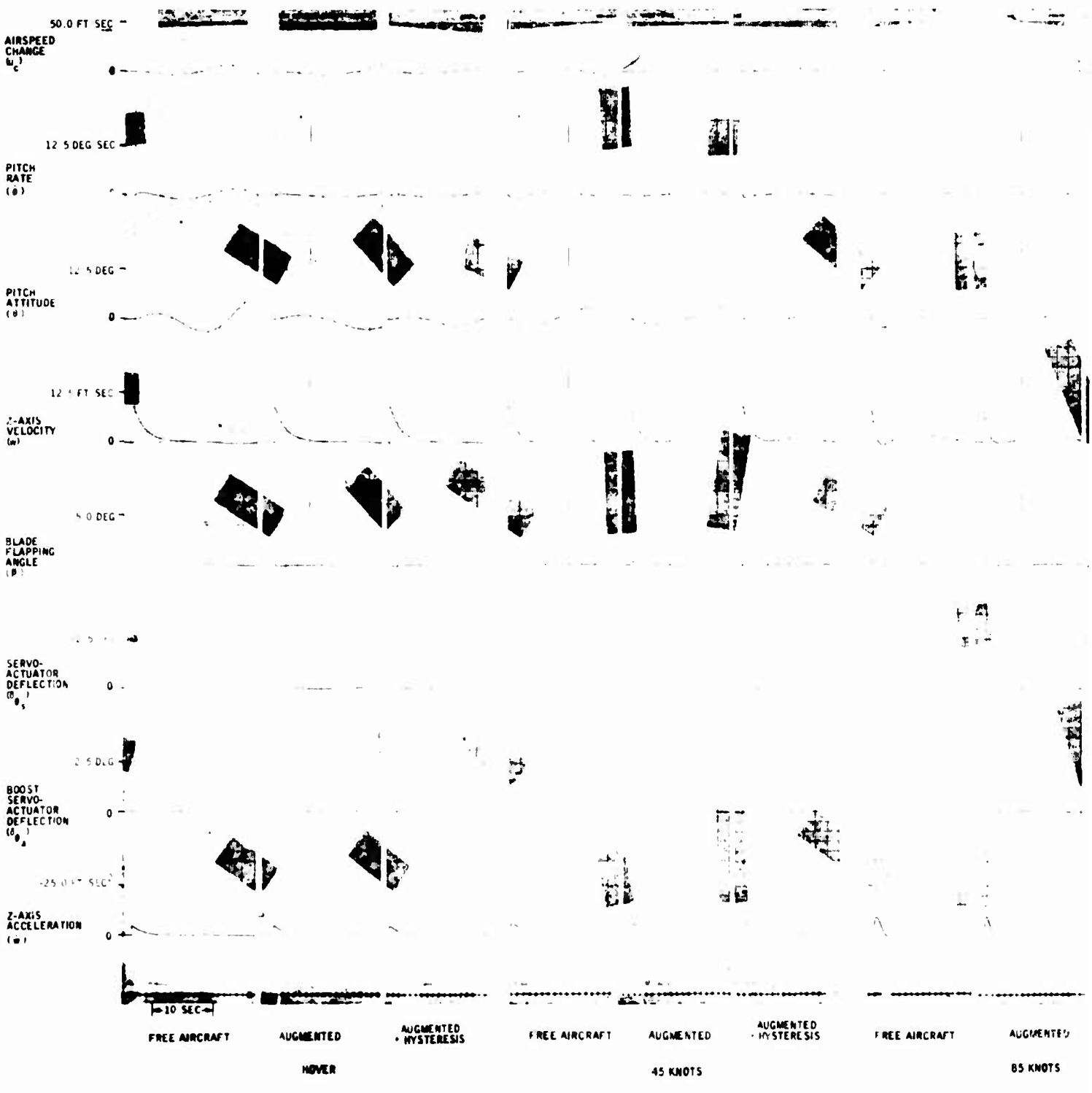

Figure 96. Free Aircraft and Pitch SAS Responses -- Vertical Gust (w_g = 10 Ft/Sec).

B

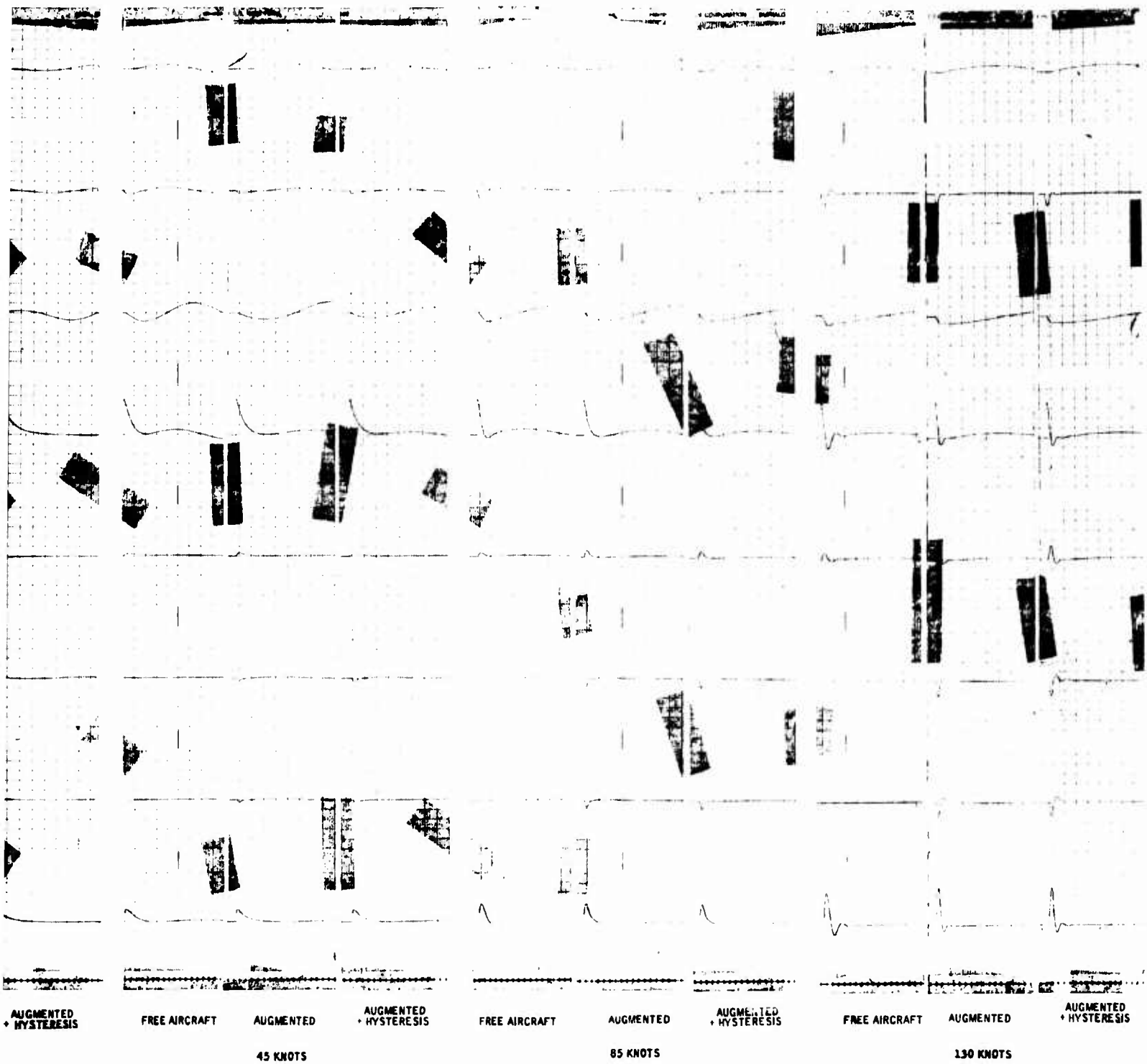

aft and Pitch SAS Responses --
st (w_g = 10 Ft/Sec).

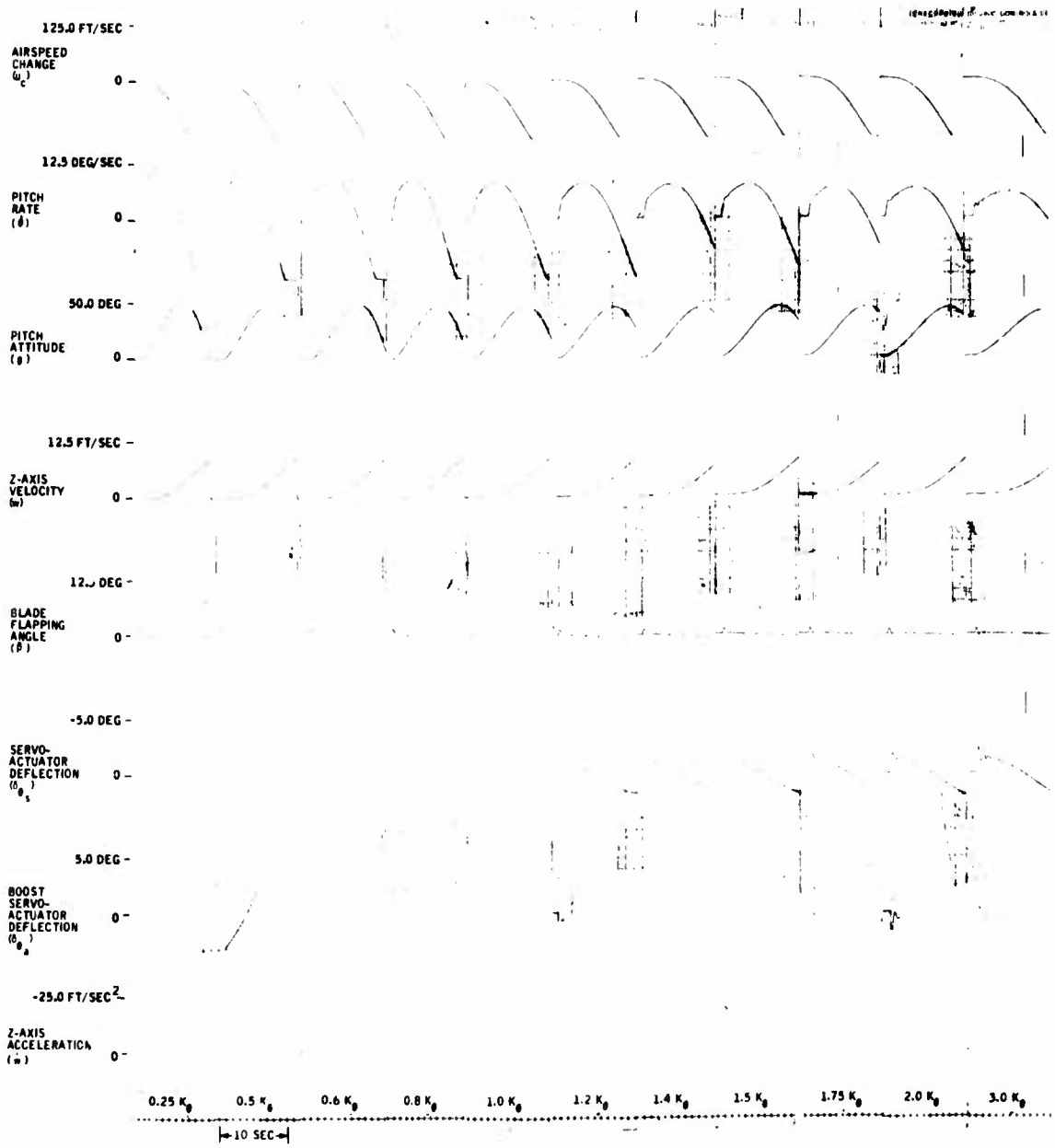

Figure 97. Pitch SAS Rate Gain Variation -- Cyclic Pitch Input (δ_{θ_m} = 1.84 Deg) at Hover.

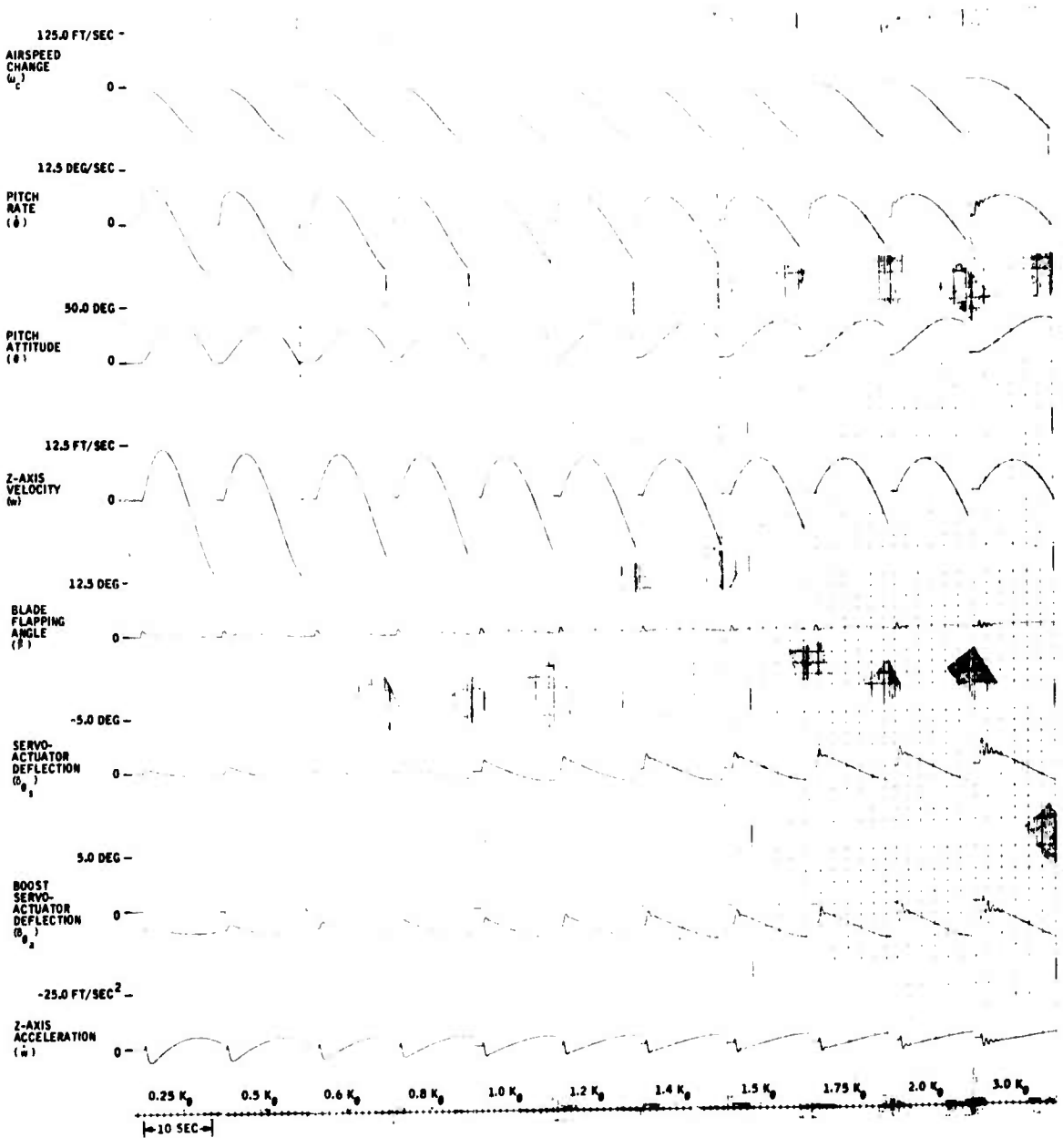

Figure 98. Pitch SAS Rate Gain Variation -- Cyclic Pitch Input (δ_{θ_m} = 1.84 Deg) at 45 Knots.

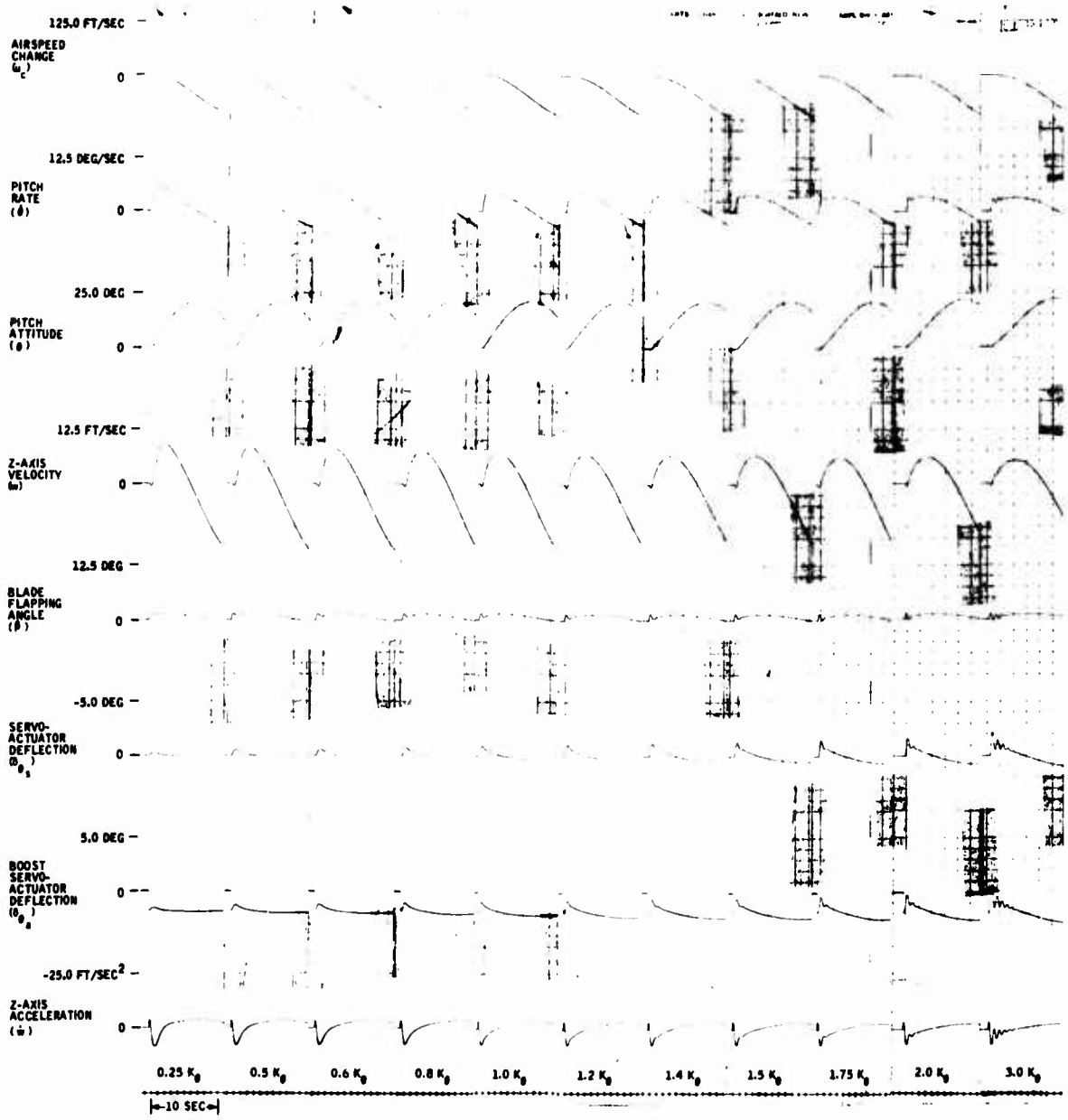

Figure 99. Pitch SAS Rate Gain Variation -- Cyclic Pitch Input (δ_{θ_m} = 1.84 Deg) at 85 Knots.

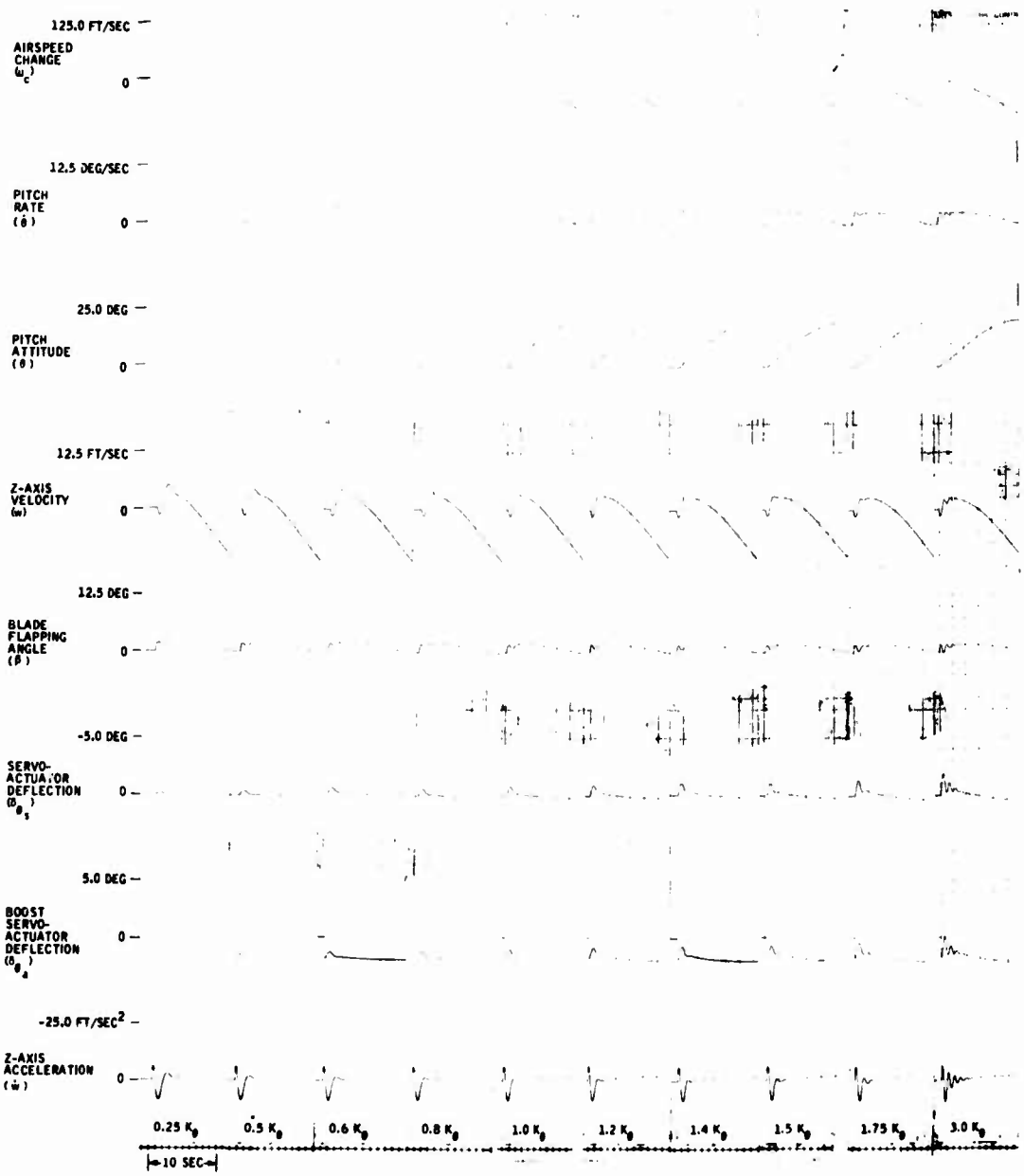

Figure 100. Pitch SAS Rate Gain Variation -- Cyclic Pitch Input (δ_{θ_m} = 1.84 Deg) at 130 Knots.

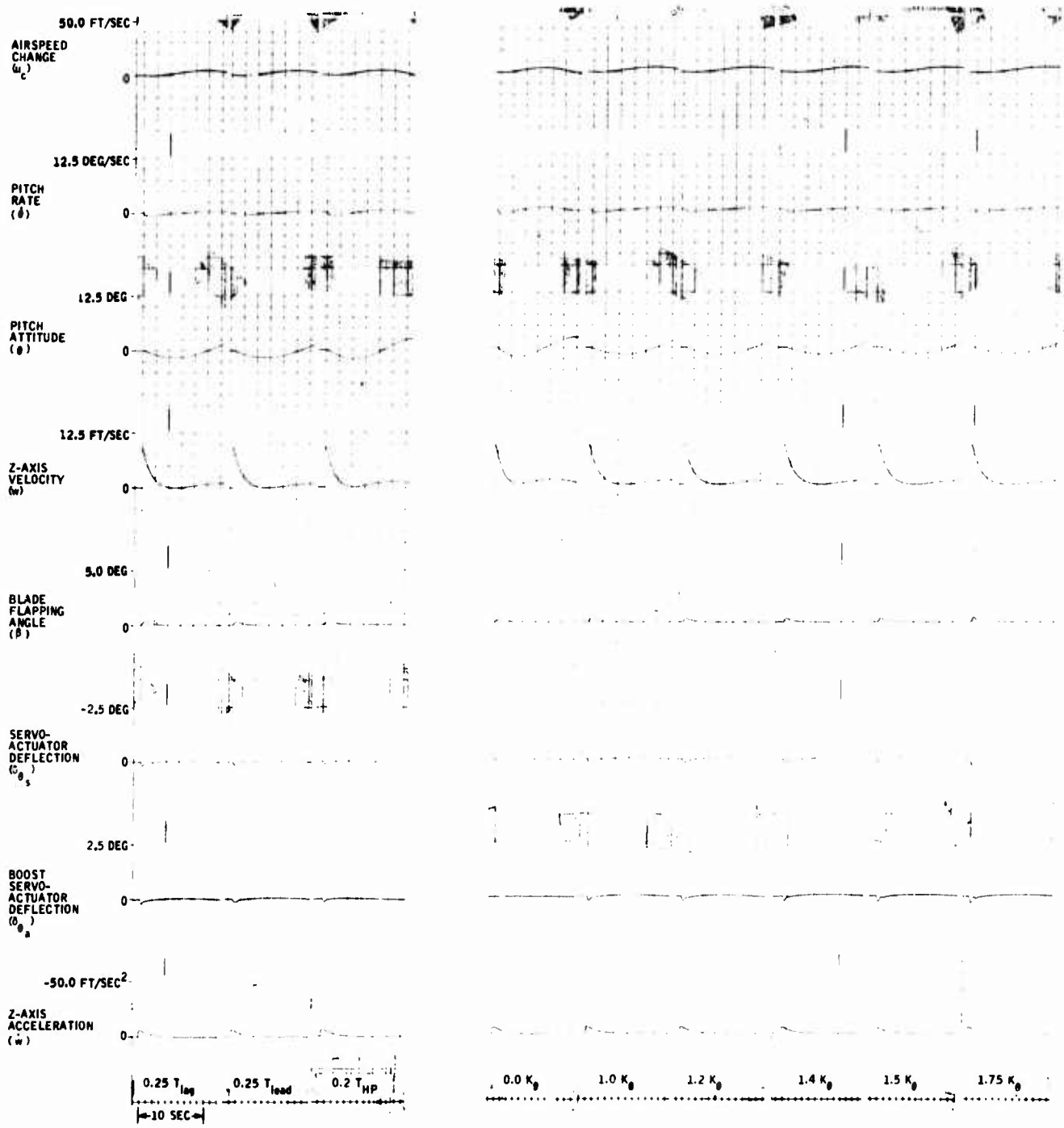

Figure 101. Pitch SAS Parameter Variation -- Vertical Gust Input (w_g = 10 Ft/Sec) at 45 Knots.

B

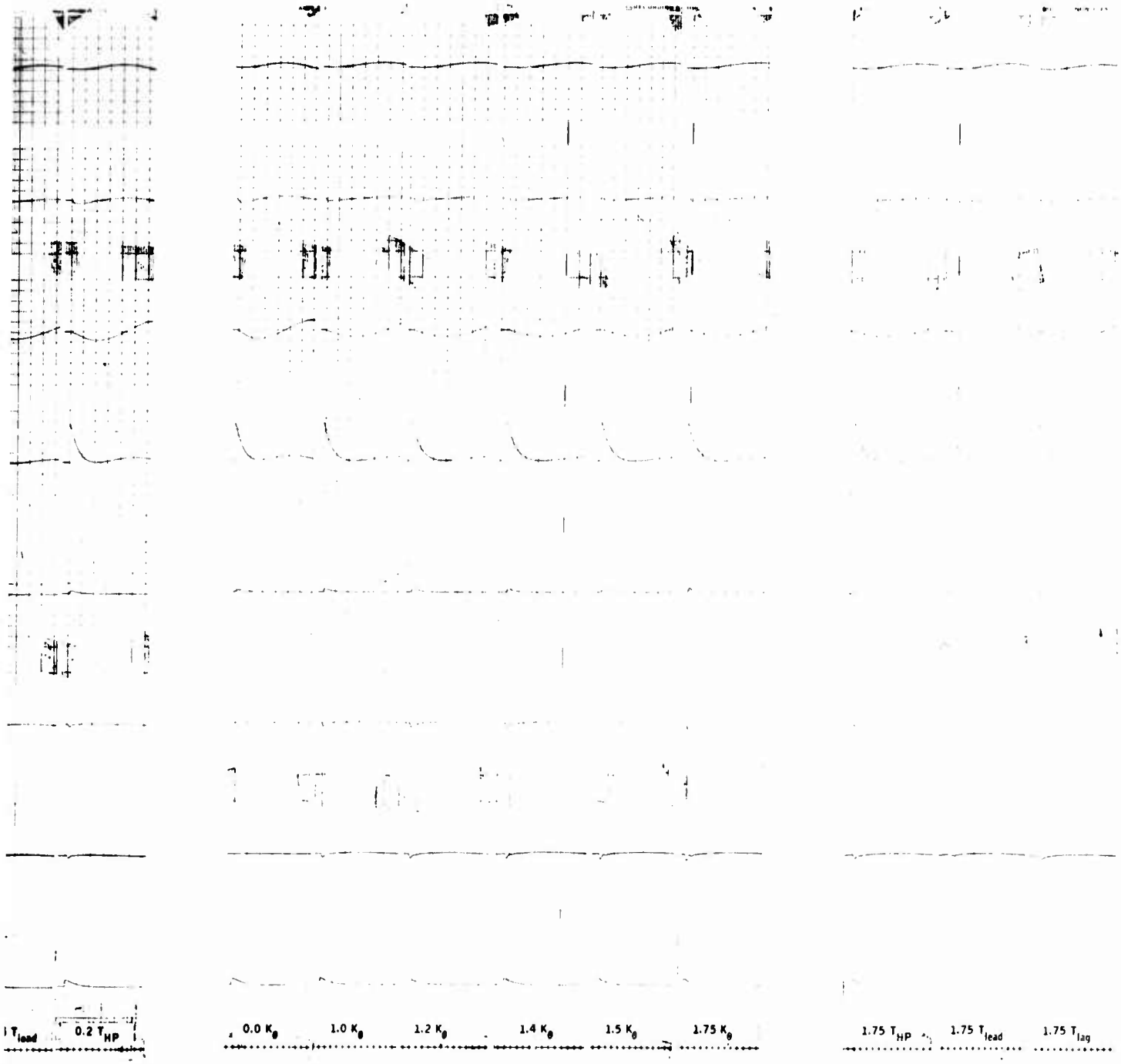

tch SAS Parameter Variation -- Vertical Gust
ut (w_g = 10 Ft/Sec) at 45 Knots.

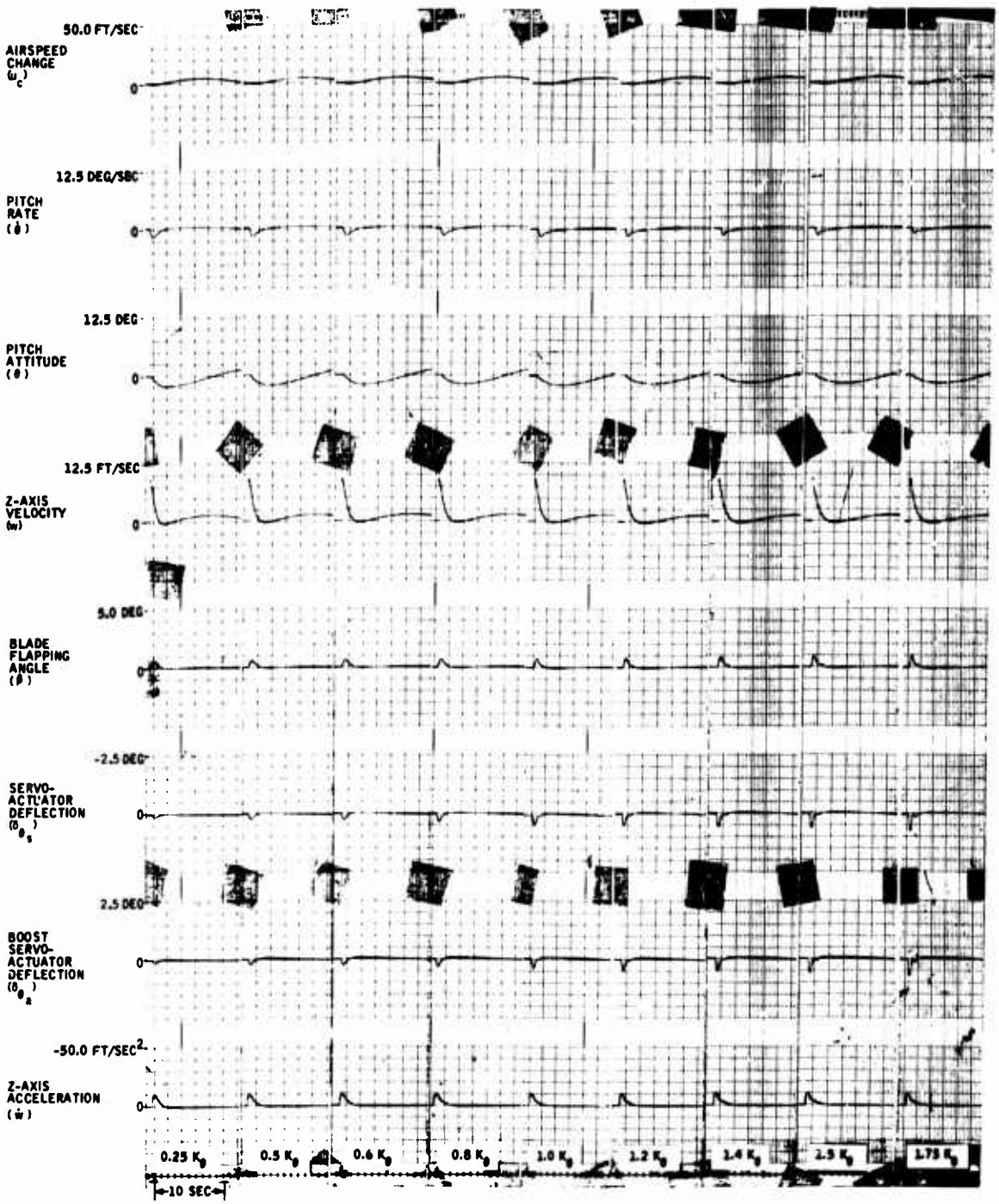

Figure 102. Pitch SAS Rate Gain Variation -- Vertical Gust Input (w_g = 10 Ft/Sec) at 85 Knots.

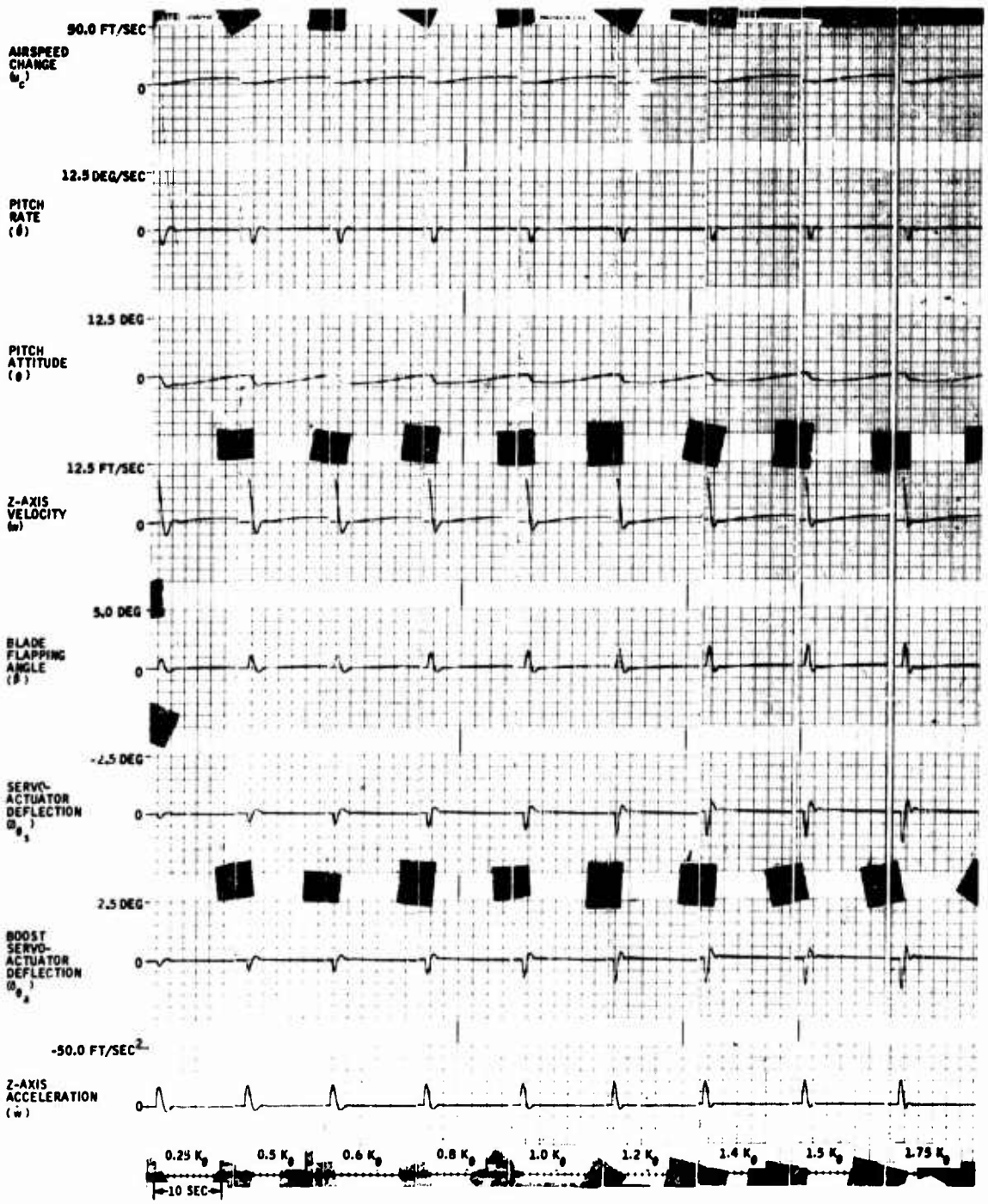

Figure 103. Pitch SAS Rate Gain Variation -- Vertical Gust Input (w_g = 10 Ft/Sec) at 130 Knots.

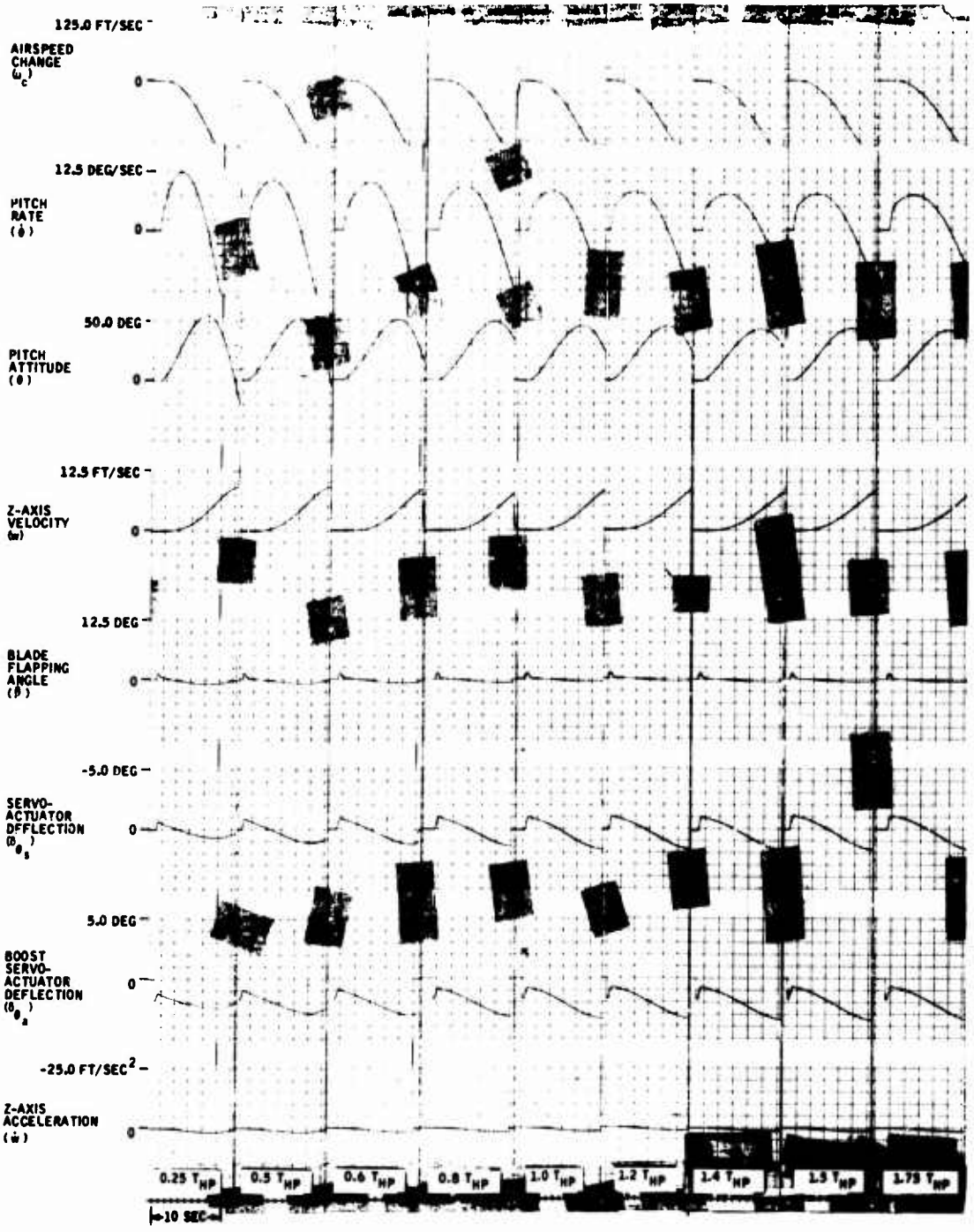

Figure 104. Pitch SAS High-Pass Time Constant Variation -- Cyclic Pitch Input (δ_{θ_m} = 1.84 Deg) at Hover.

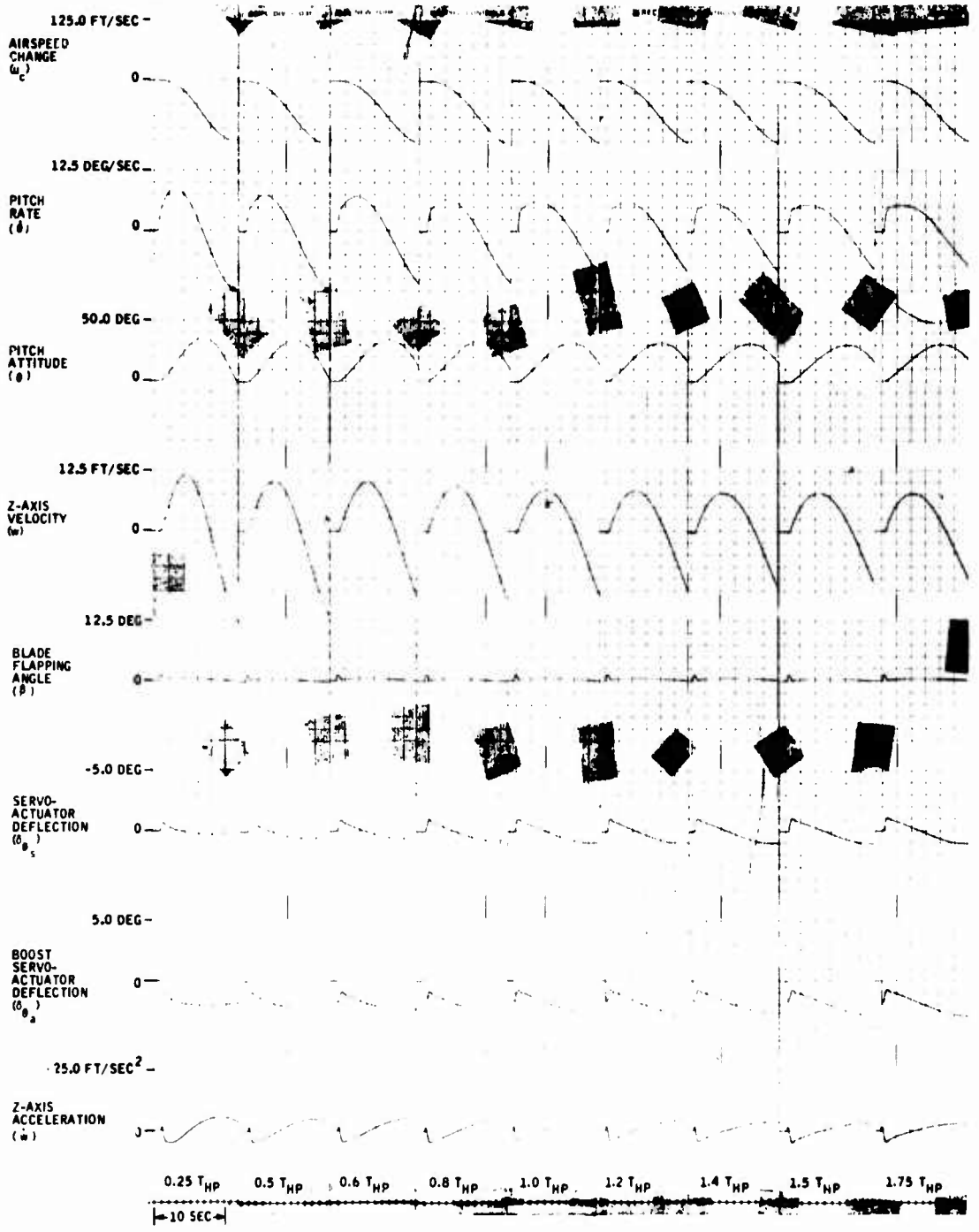

Figure 105. Pitch SAS High-Pass Time Constant Variation -- Cyclic Pitch Input (δ_{θ_m} = 1.84 Deg) at 45 Knots.

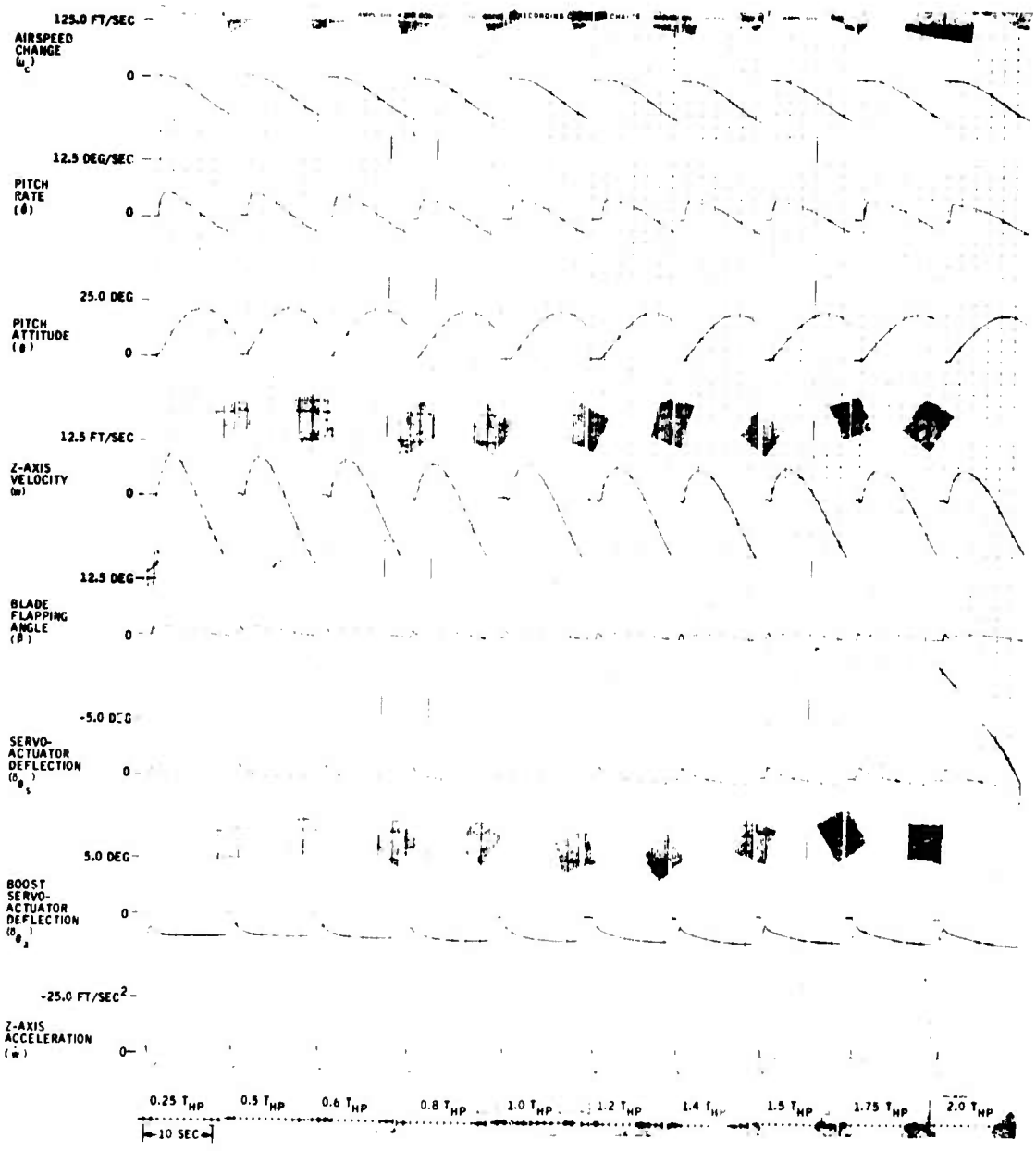

Figure 106. Pitch SAS High-Pass Time Constant Variation -- Cyclic Pitch Input (δ_{θ_m} = 1.84 Deg) at 85 Knots.

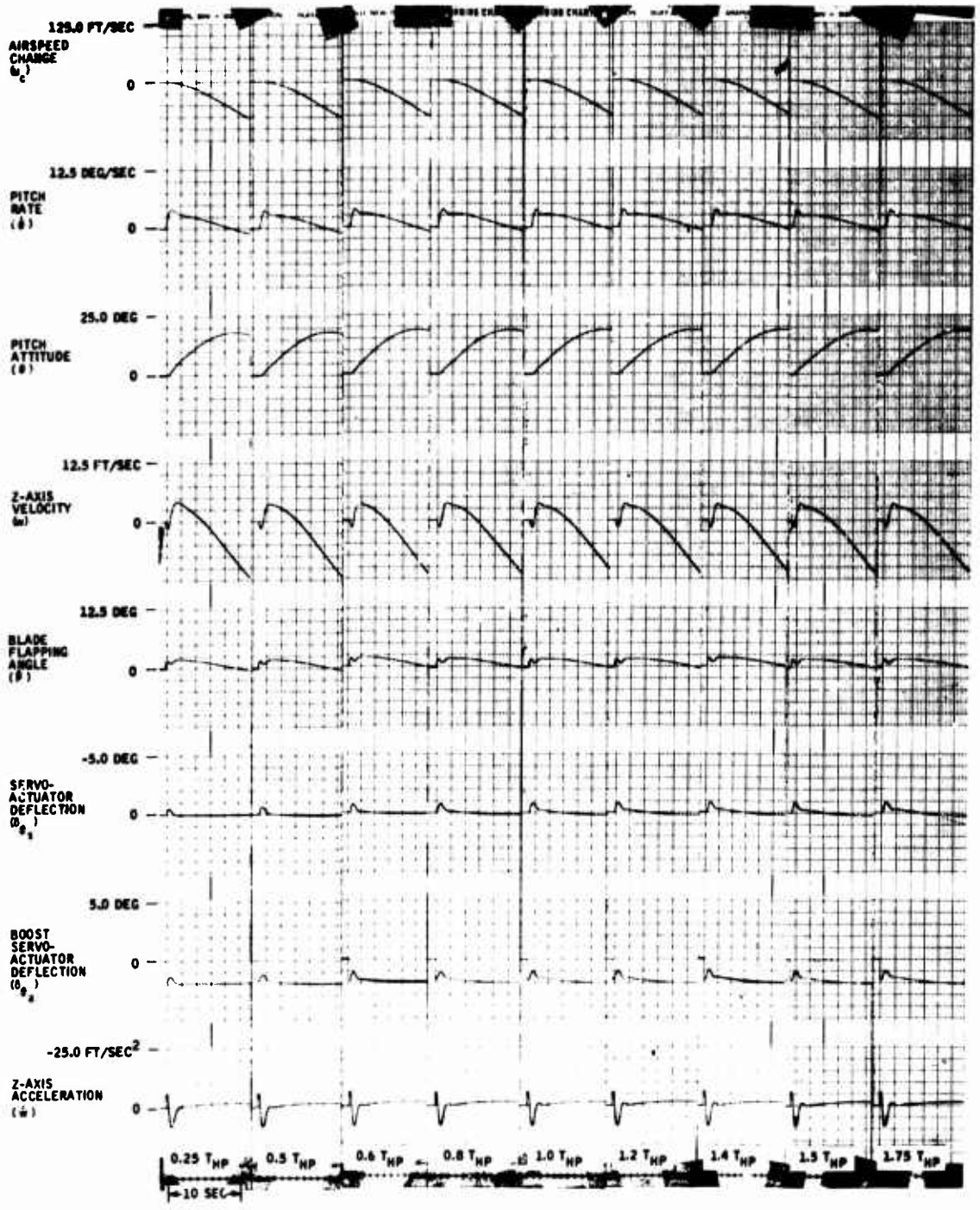

Figure 107. Pitch SAS High-Pass Time Constant Variation -- Cyclic Pitch Input (δ_{θ_m} = 1.84 Deg) at 130 Knots.

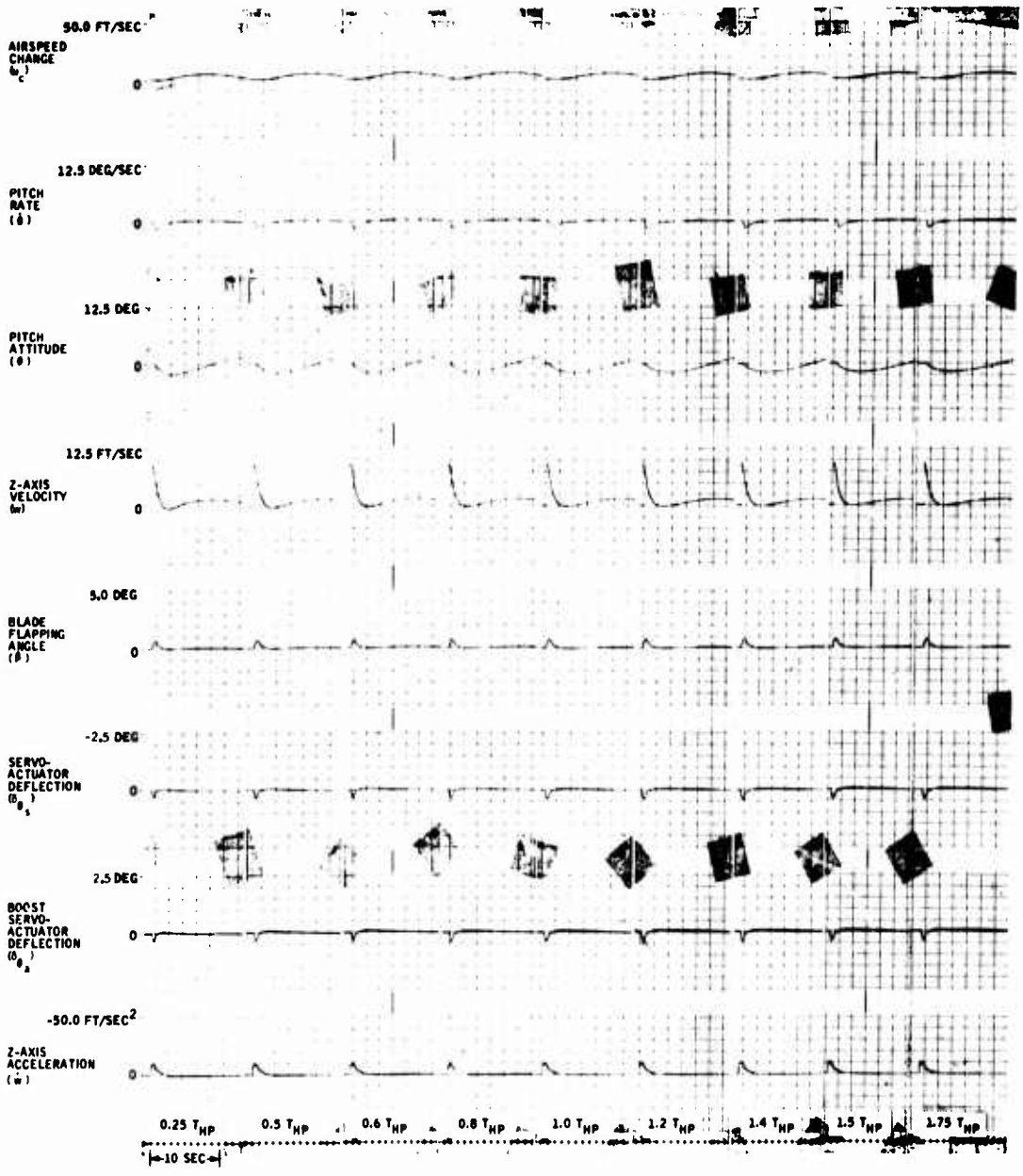

Figure 108. Pitch SAS High-Pass Time Constant Variation -- Vertical Gust Input (w_g = 10 Ft/Sec) at 85 Knots.

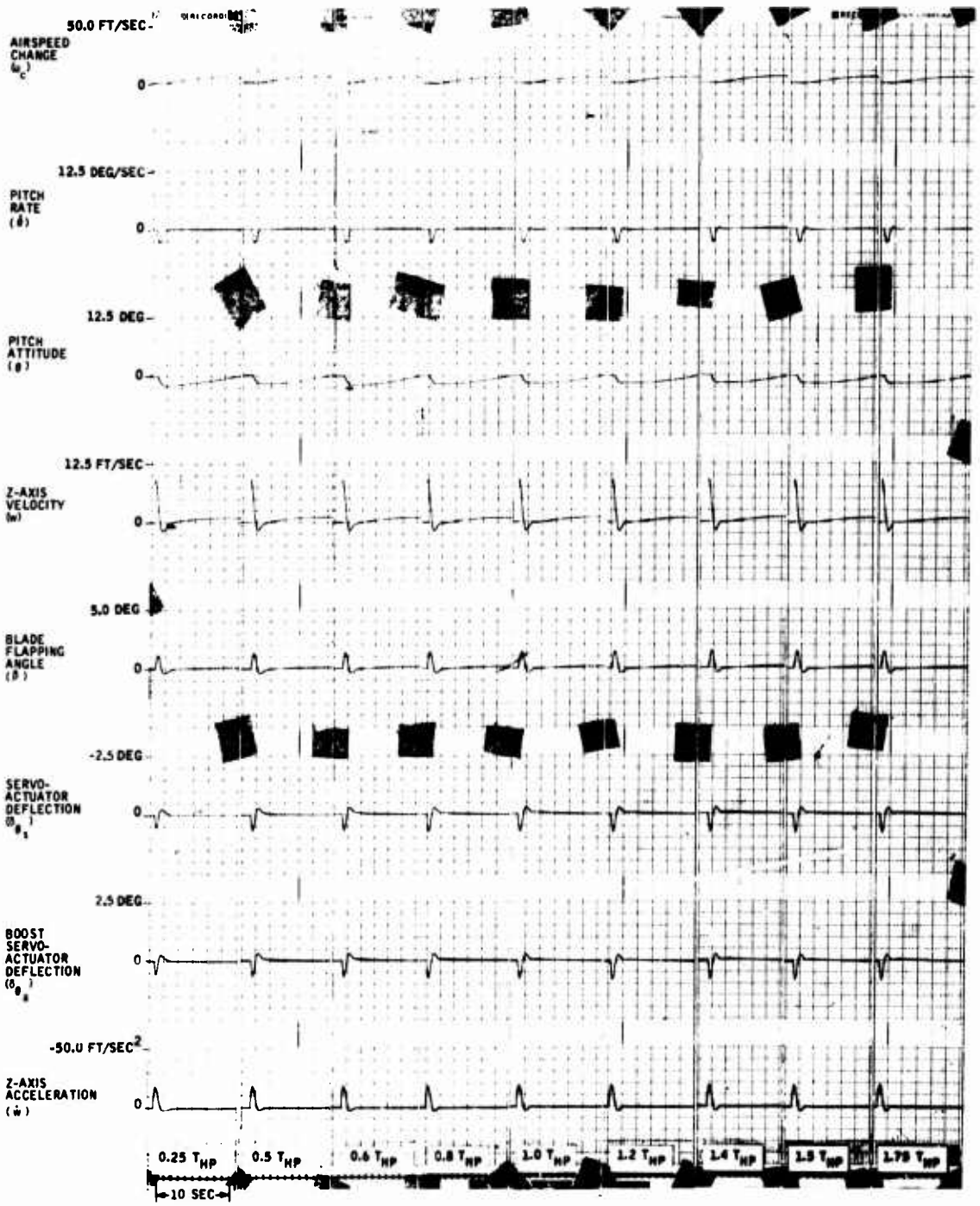

Figure 109. Pitch SAS High-Pass Time Constant Variation -- Vertical Gust Input (w_g = 10 Ft/Sec) at 130 Knots.

These responses show that relatively large variations in the high-pass time constant produce small changes in performance of the pitch SAS at the high-speed flight conditions. A ±40-percent tolerance variation may be permitted and still achieve near-nominal damping performance.

Pitch SAS Lead Time Constant Variation (T_{lead})

Pitch SAS lead time constant parameter variations are shown in Figure 110, 111, 112, and 113 for cyclic pitch input commands, and in Figures 101, 114, and 115 for vertical gust initial conditions.

Figures 110, 111, 112, and 113 show that as the lead time constant parameter approaches ±40 percent, its effect in compensating the unwanted system phase lag decreases. For a minus 40-percent tolerance, a noticeable dip develops in the pitch rate trace at low speed. At high speeds, a plus 40-percent tolerance in the lead time constant causes the system to show signs of becoming underdamped. This is apparent in the pitch servoactuator time histories. As the lead time constant is allowed to increase, high-frequency components begin to develop. This means that the system's phase margin has become too low.

Time histories for the 45-kn flight condition, Figure 101, show that variations in the lead time constant have little effect on pitch SAS damping performance, because the vehicle is sufficiently well-damped at low speeds.

The gust responses of Figures 114 and 115 show that, in general, the pitch SAS exhibits relatively good damping for large lead time constant tolerances (±40 percent). However, the stability consideration mentioned above for the cyclic commands must be kept in mind when establishing system tolerances.

Nominal system performance may be achieved for a ±20-percent lead time constant tolerance.

Pitch SAS Lag Time Constant Variation (T_{lag})

Pitch SAS lag time constant parameter variations are shown in Figures 116, 117, 118, and 119 for cyclic pitch input commands, and in Figures 101, 120, and 121 for vertical gust initial conditions.

Figures 116, 117, 118, and 119 show that decreasing the lag time constant actually causes pitch SAS performance to improve. This is due to the fact that pure phase lead with a unity gain amplitude response is the desired characteristic to compensate for the undesired phase lag generated in the free vehicle and rate sensor.

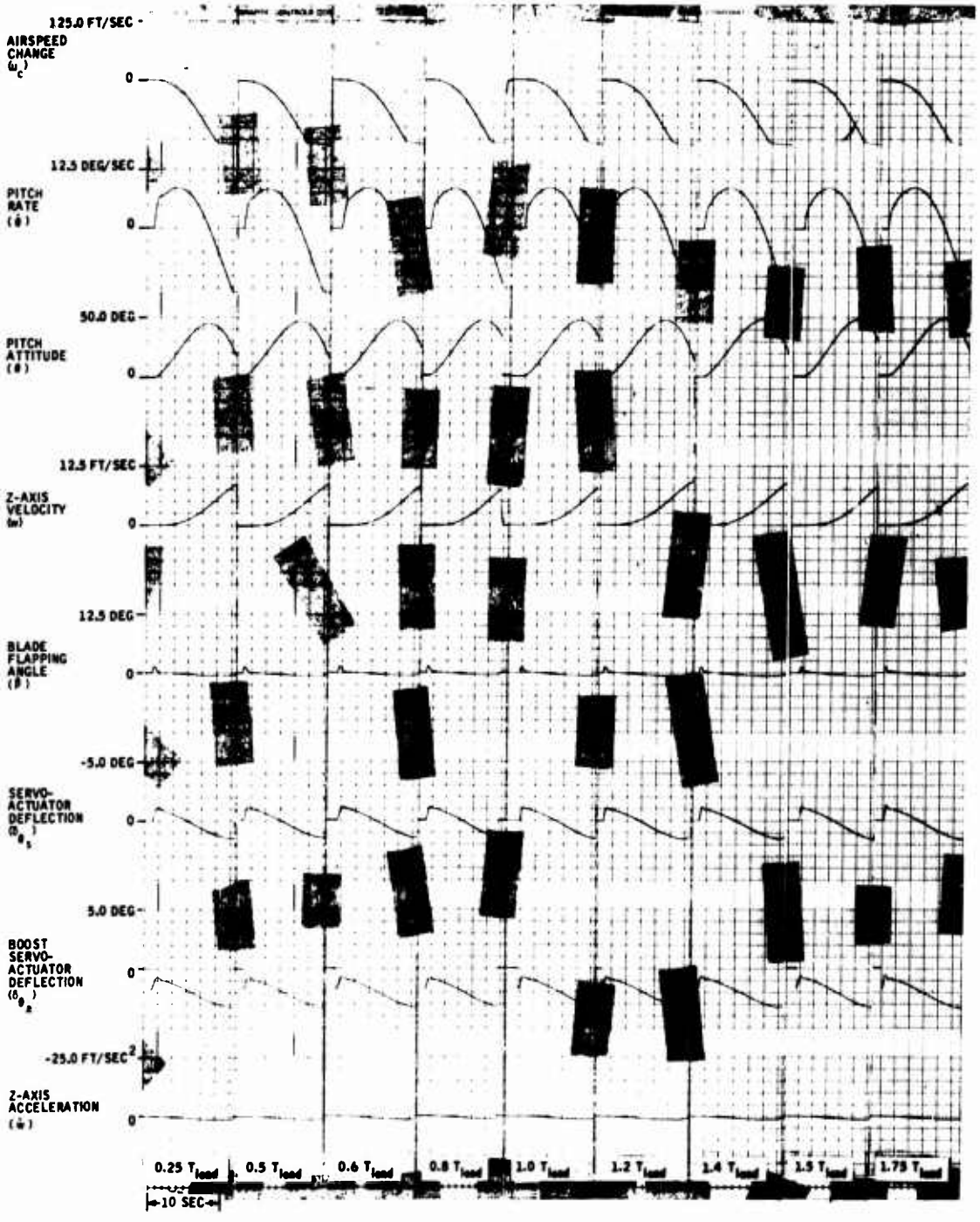

Figure 110. Pitch SAS Lead Time Constant Variation -- Cyclic Pitch Input (δ_{θ_m} = 1.84 Deg) at Hover.

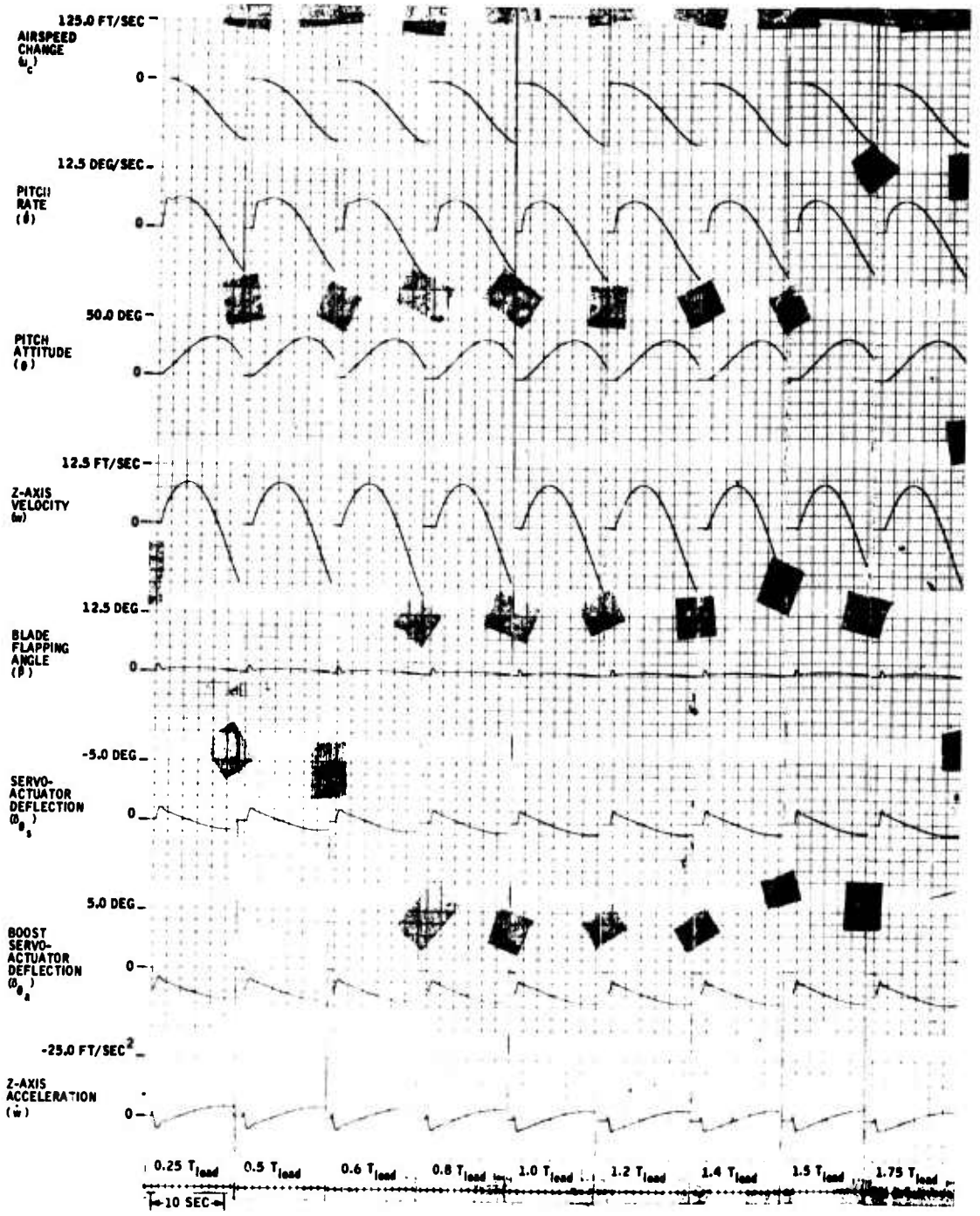

Figure 111. Pitch SAS Lead Time Constant Variation -- Cyclic Pitch Input ($\hat{o}_{\theta_m}$ = 1.84 Deg) at 45 Knots.

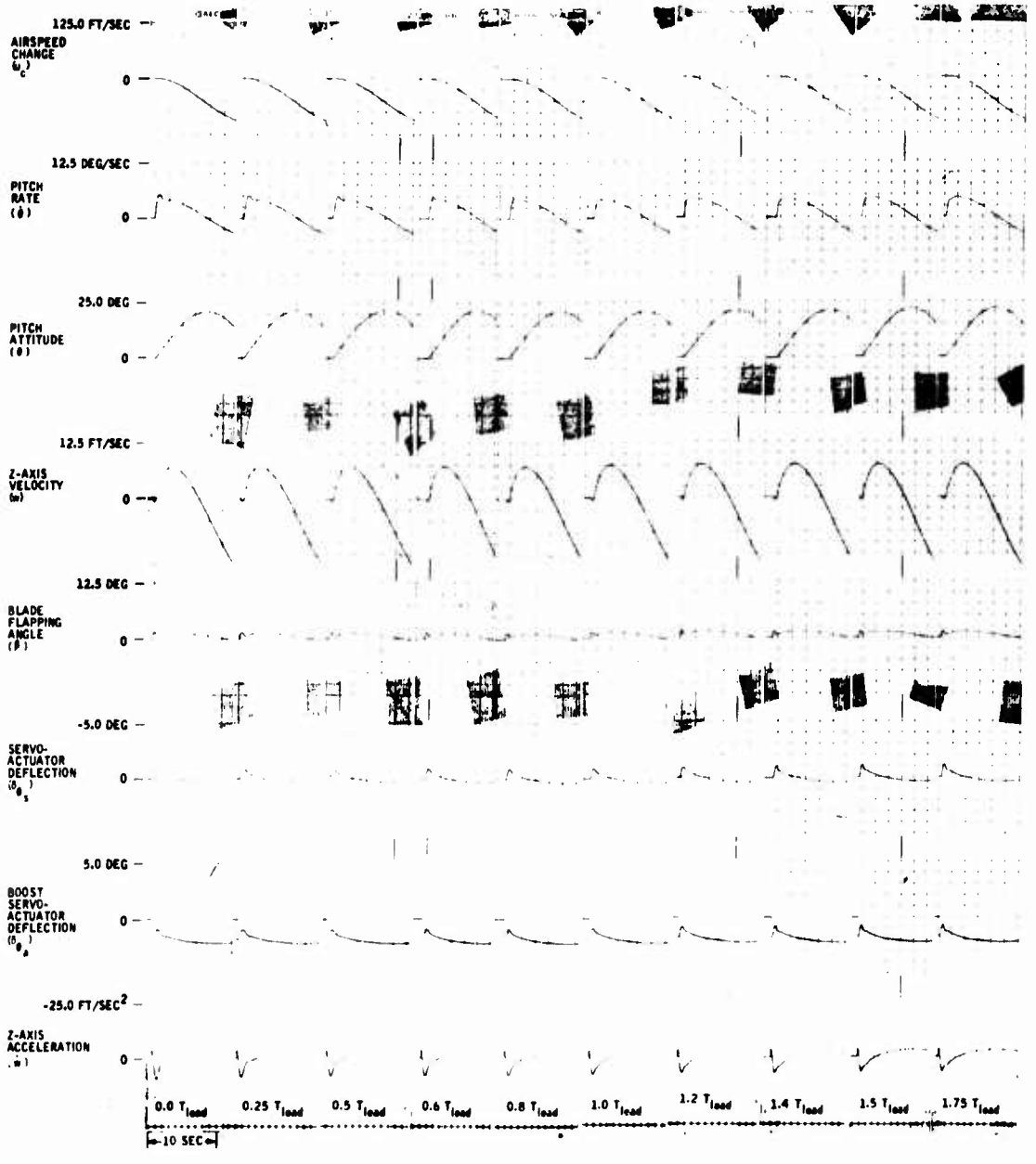

Figure 112. Pitch SAS Lead Time Constant Variation -- Cyclic Pitch Input (δ_{θ_m} = 1.84 Deg) at 85 Knots.

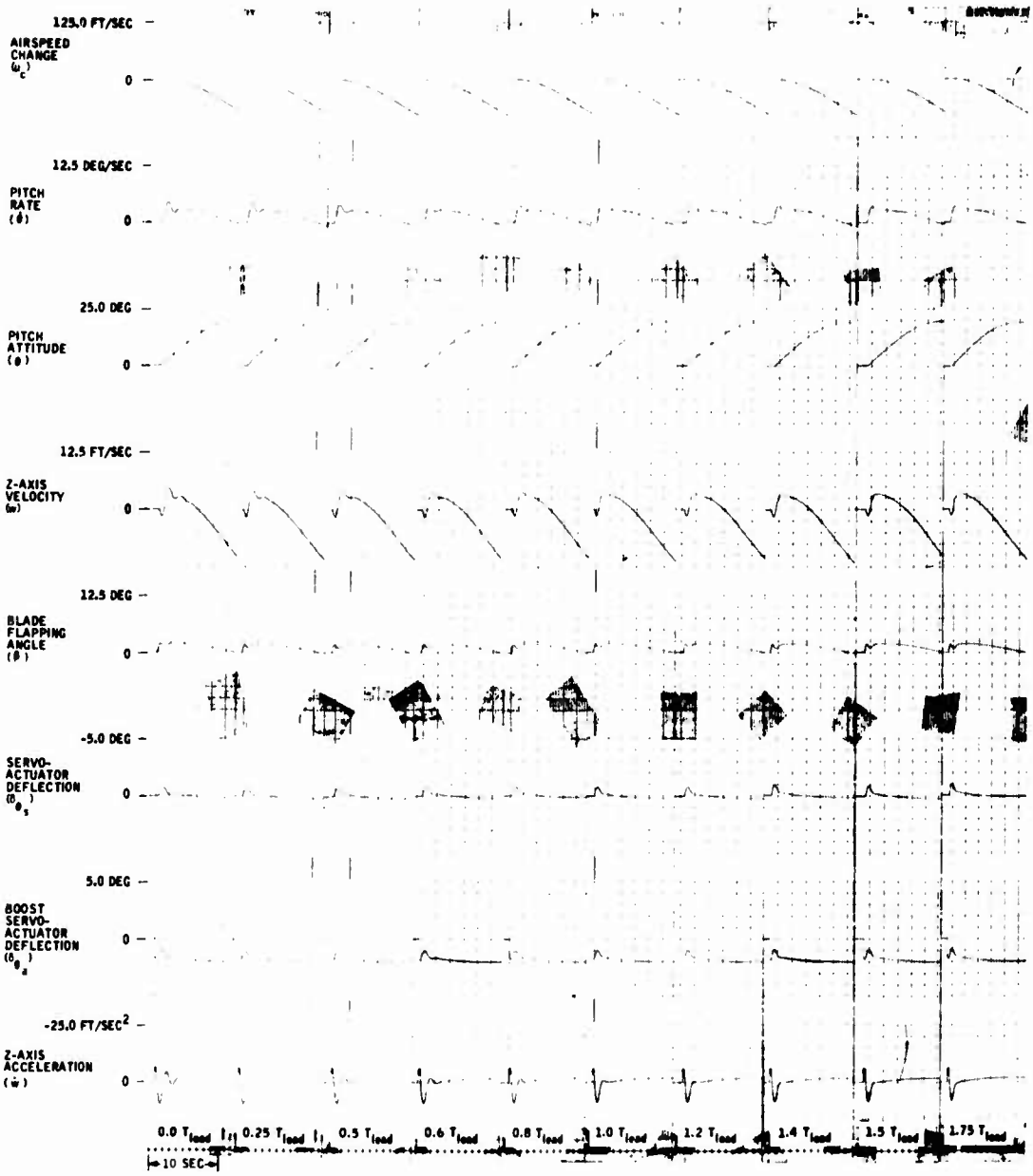

Figure 113. Pitch SAS Lead Time Constant Variation -- Cyclic Pitch Input (δ_{θ_m} = 1.84 Deg) at 130 Knots.

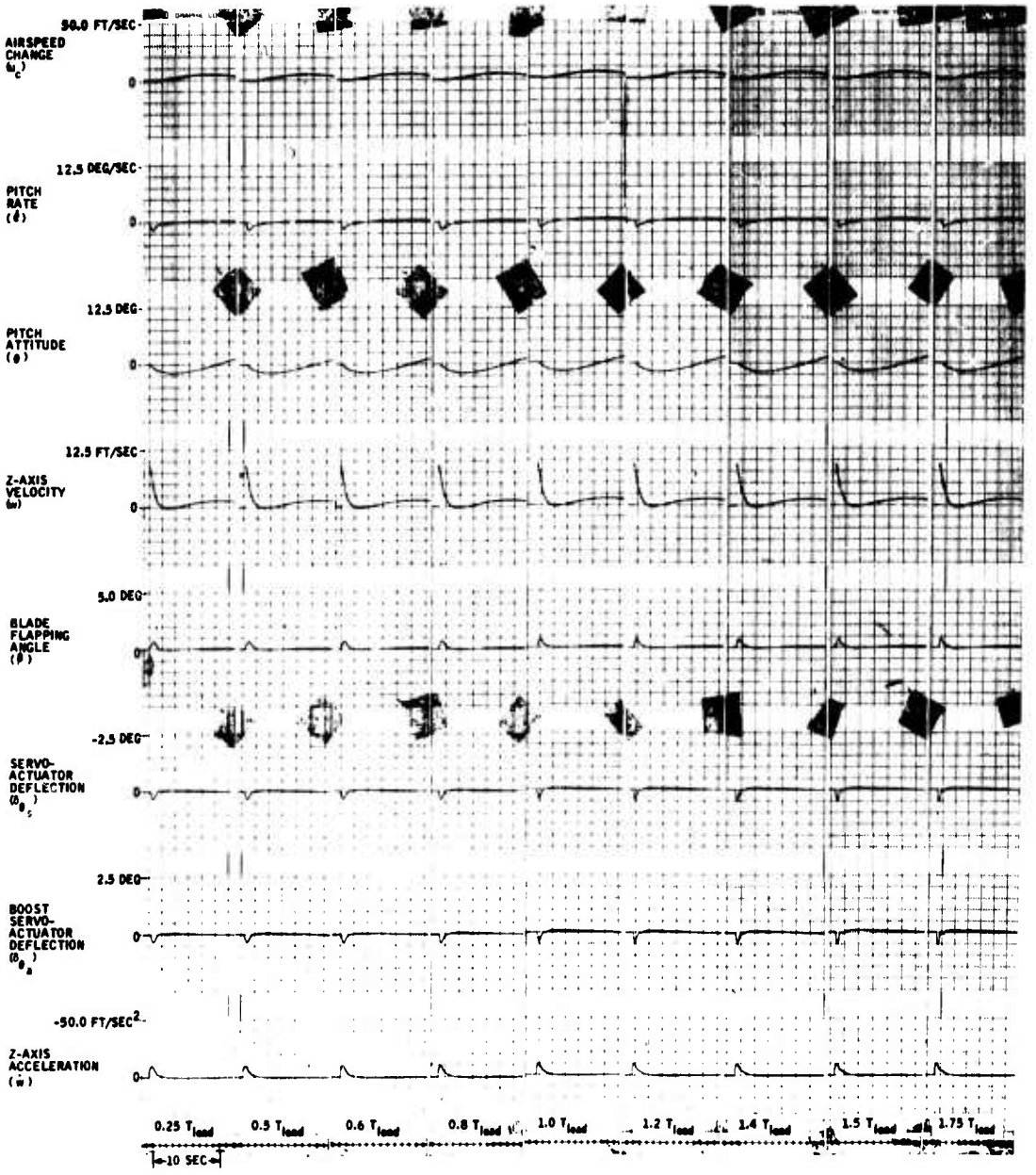

Figure 114. Pitch SAS Lead Time Constant Variation -- Vertical Gust Input (w_g = 10 Ft/Sec) at 85 Knots.

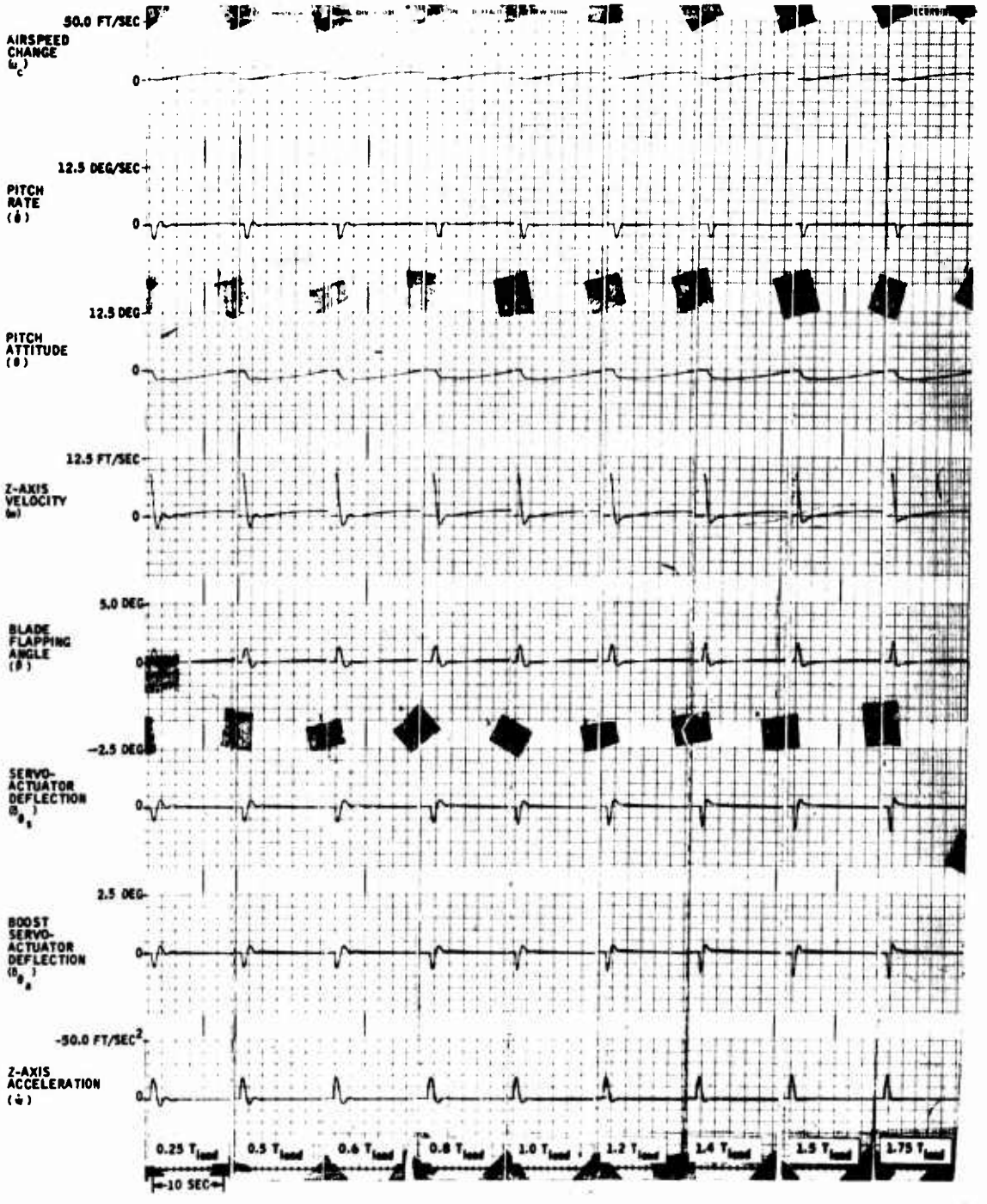

Figure 115. Pitch SAS Lead Time Constant Variation -- Vertical Gust Input (w_g = 10 Ft/Sec) at 130 Knots.

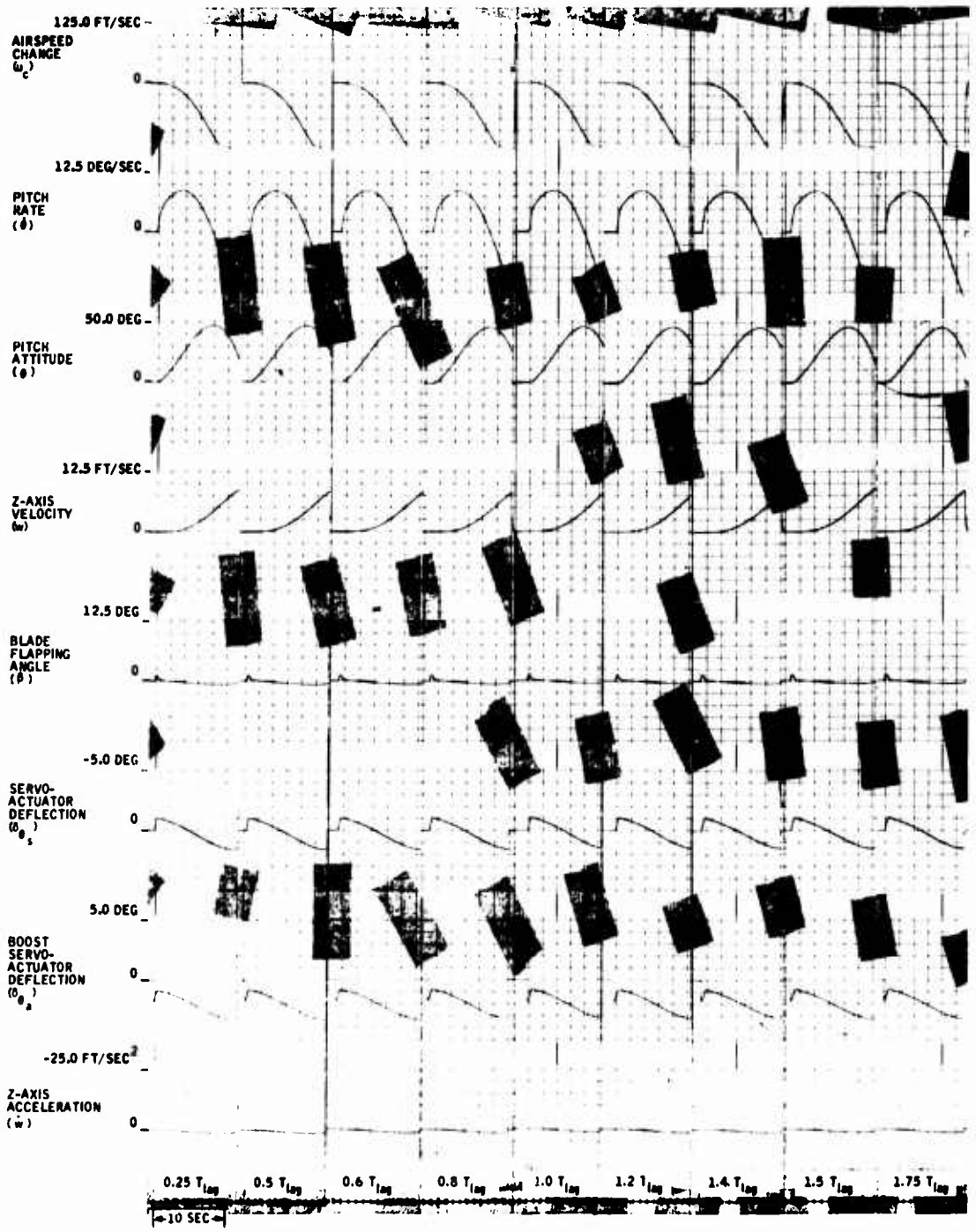

Figure 116. Pitch SAS Lag Time Constant Variation -- Cyclic Pitch Input (δ_{θ_m} = 1.84 Deg) at Hover.

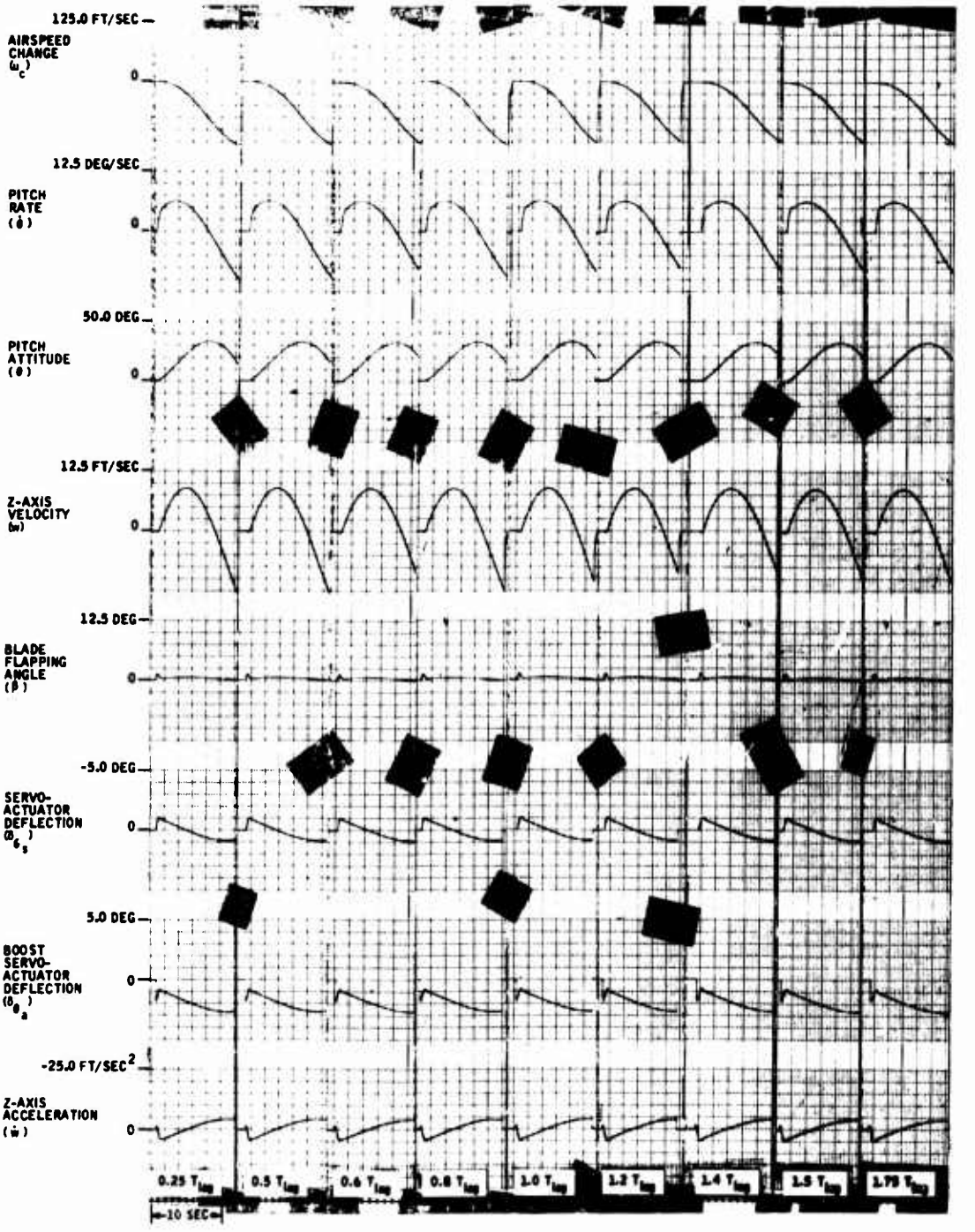

Figure 117. Pitch SAS Lag Time Constant Variation -- Cyclic Pitch Input (δ_{θ_m} = 1.84 Deg) at 45 Knots.

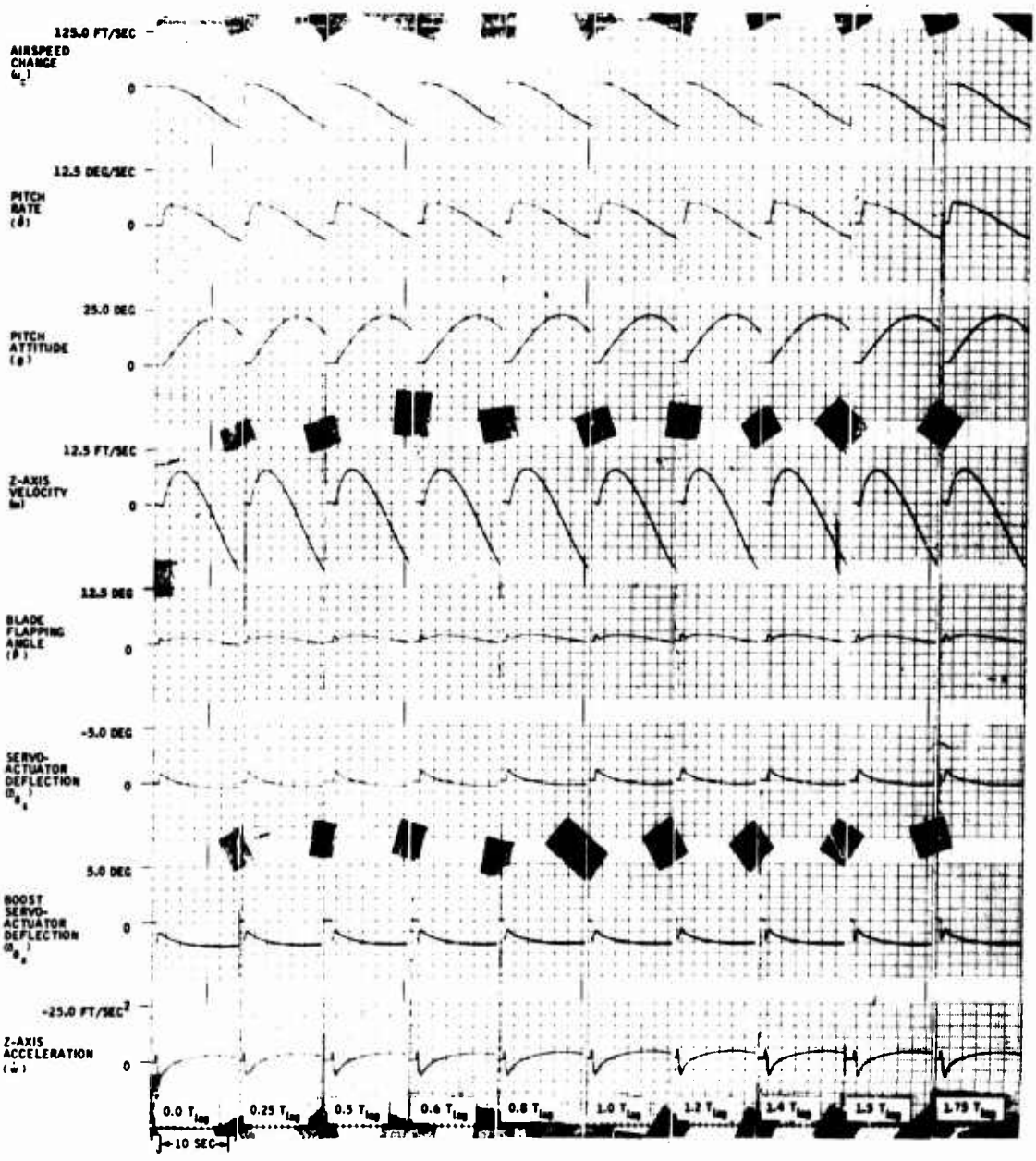

Figure 118. Pitch SAS Lag Time Constant Variation -- Cyclic Pitch Input (δ_{θ_m} = 1.84 Deg) at 85 Knots.

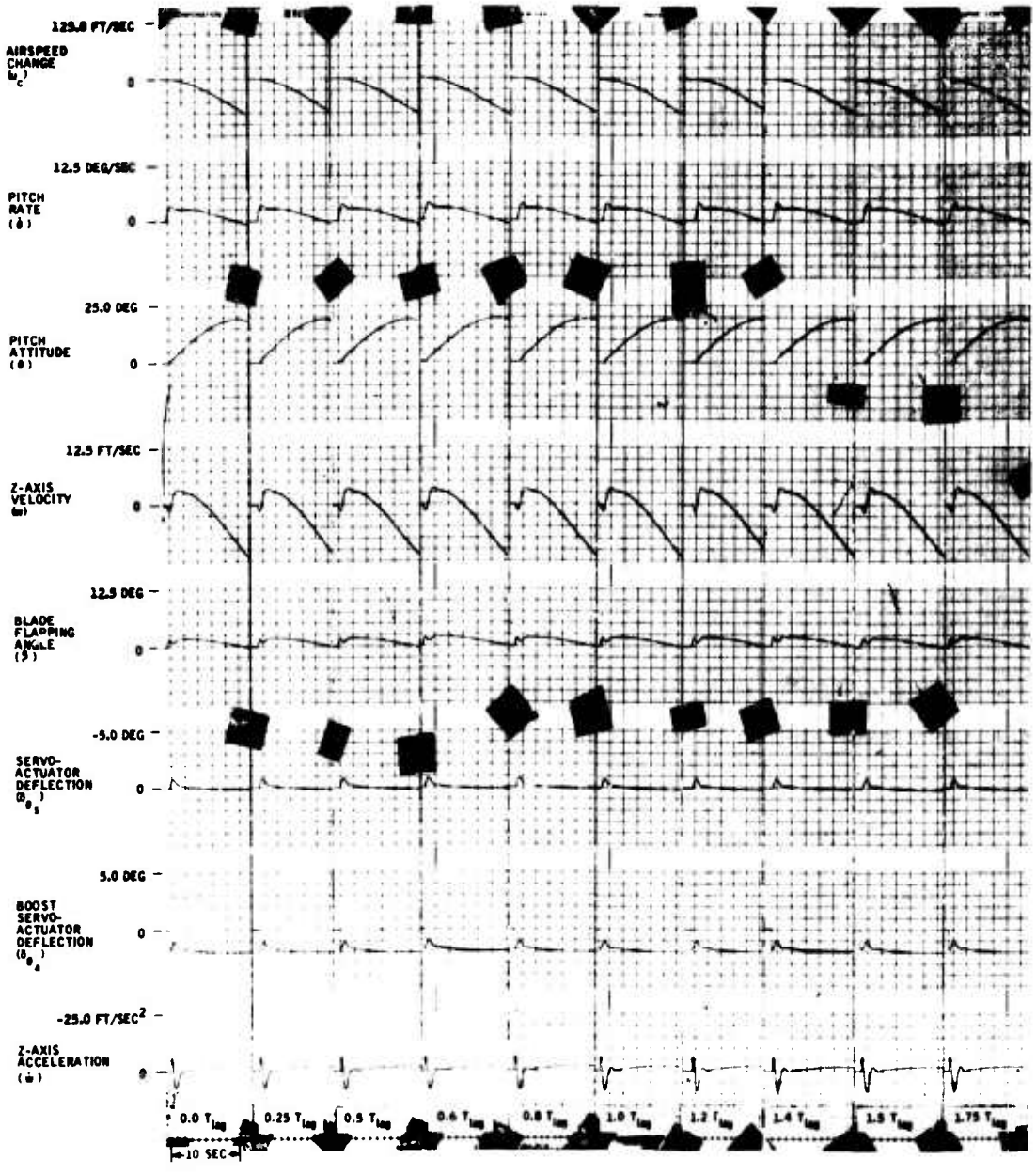

Figure 119. Pitch SAS Lag Time Constant Variation -- Cyclic Pitch Input (δ_{θ_m} = 1.84 Deg) at 130 Knots.

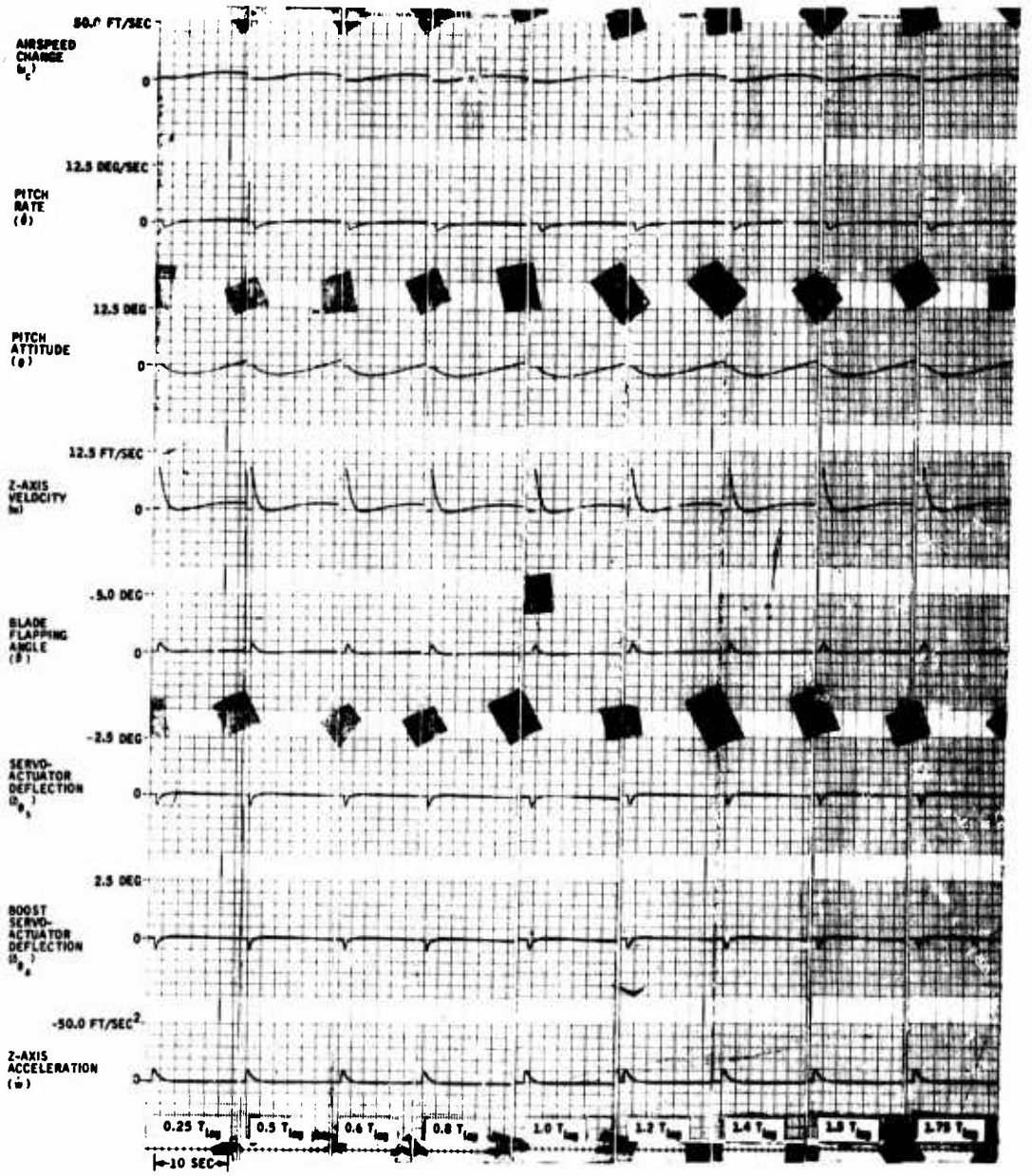

Figure 120. Pitch SAS Lag Time Constant Variation -- Vertical Gust Input (w_g = 10 Ft/Sec) at 85 Knots.

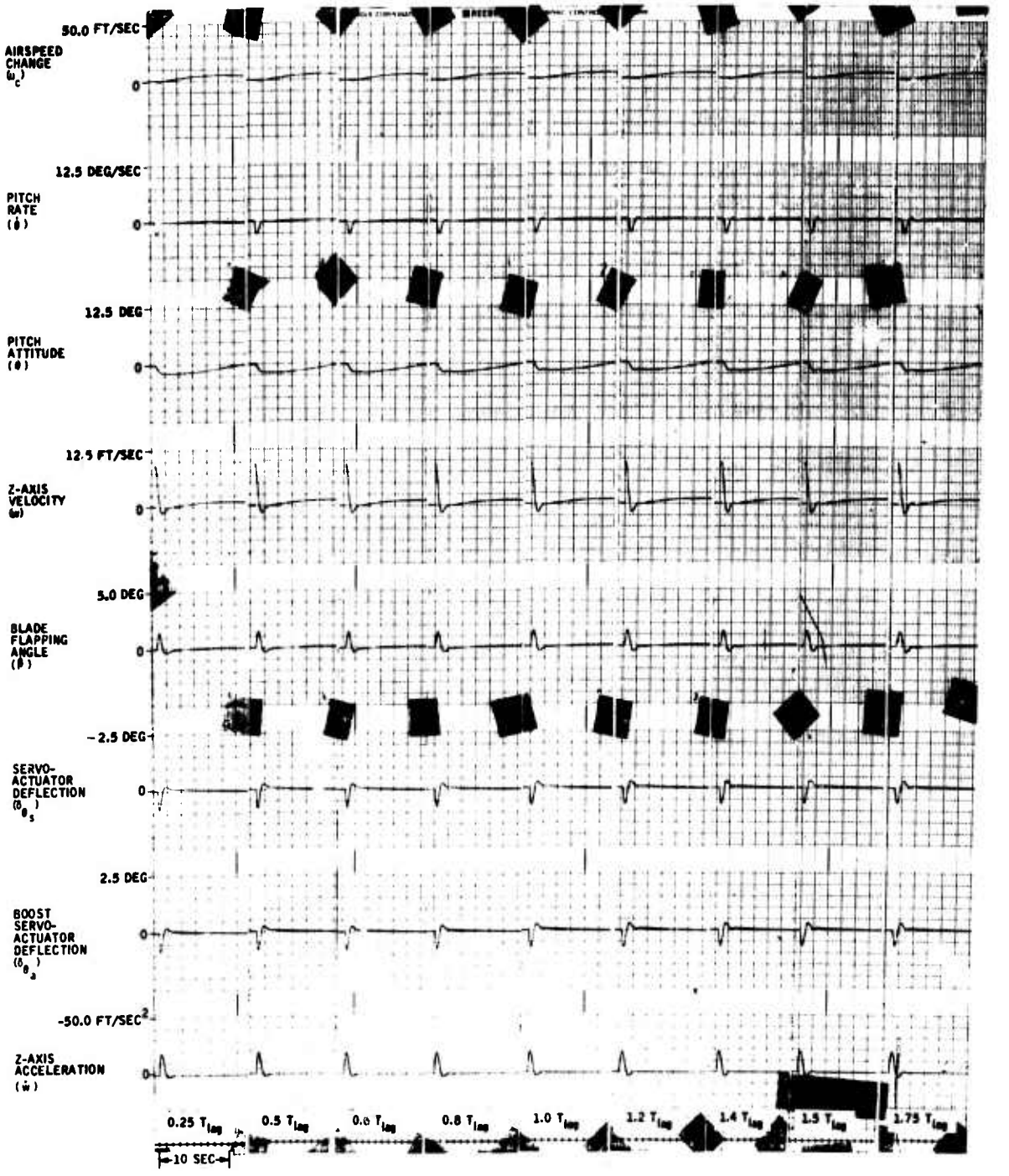

Figure 121. Pitch SAS Lag Time Constant Variation -- Vertical Gust Input (w_g = 10 Ft/Sec) at 130 Knots.

However, pure phase lead is impossible to generate. Small quantities of phase lead may be obtained from a lead-lag shaping network, but at the same time the high-frequency system gain increases by the product of the time constant ratios.

High-frequency gain must be considered so that the control system does not excite the body-bending and vibration modes of the aircraft. Therefore, the lead-lag shaping network time constants must be defined by setting the lead time constant to give phase lead at the frequency of interest and then setting the lag time constant while considering the resulting high-frequency dynamic gain.

This process was followed in defining the time constants for the pitch SAS lead-lag compensation network. A 40-percent decrease in the lag time-constant parameter results in a 63-percent increase in dynamic gain. The effects of this increase in gain can be seen by considering that only the rate gain, K_θ, increased by 63 percent, and all other parameters remained constant. A review of Figures 97, 98, 99, and 100 shows that a 63-percent increase in the rate gain causes the system to become underdamped, and stability problems may result.

The above argument also applies in judging system performance in light of lead network parametric variations. Allowing the lag to increase in value reduces the effectiveness of the lead-lag network in compensating for the undesired phase lag of the control system. Therefore, to achieve nominal system performance and avoid possible stability problems, the lead time constant of the lead-lag shaping network should be within 20 percent of its nominal value and the lead-lag time-constant ratio should be held within 20 percent of its nominal value.

Figures 120 and 121 show that the vehicle damping characteristics are quite tolerant of the lag-time parameter variations. Relatively large parameter variations may be made without significant effects on system damping. However, the stability considerations mentioned above for the cyclic pitch step inputs should be considered in evaluating system performance, in light of parameter variations.

CONCLUSIONS

1. The computer simulation analysis presented in this report shows that it is feasible to develop a fluidic (hydrofluidic) stability augmentation system (FSAS) to augment the damping and control response performance of the UH-1B helicopter.

2. This FSAS augments the damping and control response characteristics of the UH-1B in a manner that satisfies the requirements of the design goals. These design goals were generated in light of Military Specification MIL-H-8501A requirements and good engineering judgment.

3. This FSAS will maintain performance characteristics considered to be nominal when mechanized to typical off-design tolerances.

SECTION III
MATHEMATICAL MODEL - UH-1 ANALOG REPRESENTATION

The equations of motion and pertinent aerodynamic data were taken from abstracted reports received from the UH-1 helicopter manufacturer. The equations were simplified to "perturbation equations" and written in body-axis coordinates, with the vehicle's center of gravity as the reference. The simplified equations are linear and uncoupled, as they show vehicle response only to perturbations from trimmed flight conditions. The aerodynamic data are limited to specific flight conditions within the UH-1 speed regime: 0 kn, 43 kn, 100 kn, and 130 kn.

Longitudinal and lateral-directional derivatives are presented in Tables XV and XVI, respectively, at the end of this section. Also presented, in Figures 122 through 125, are analog computer mechanization block diagrams for the UH-1B lateral-directional plane, yaw SAS simulation, roll and pitch SAS simulation, and longitudinal-vertical plane, respectively.

NOMENCLATURE

The following nomenclature is used in the equations of motion and data:

Symbol	Meaning	Units
u	X-body-axis perturbation velocity	ft/sec
v	Y-body-axis perturbation velocity	ft/sec
w	Z-body-axis perturbation velocity	ft/sec
θ	Pitch angle	rad
ϕ	Roll angle	rad
ψ	Yaw angle	rad
X	X-body-axis force	lb
Y	Y-body-axis force	lb
Z	Z-body-axis force	lb
L	Rolling moment	ft-lb
M	Pitching moment	ft-lb
N	Yawing moment	ft-lb
β	Longitudinal blade flapping (pitch inclination of rotor)	rad

Symbol	Meaning	Units
K	Pitch inclination of stabilizer bar	rad
λ	Roll inclination of stabilizer bar	rad
γ	Lateral blade flapping (roll inclination of rotor)	rad
m	Vehicle mass	slugs
I_{xx}, I_{yy}, I_{zz}	Moments of inertia	slug-ft^2
X_u, X_w, etc.	Dimensionless aerodynamics	$\partial X/\partial u$, $\partial u/\partial w$, etc.
δ_θ	Cyclic pitch control	rad
δ_ϕ	Cyclic roll control	rad
δ_L	Collective control	rad
δ_ψ	Tail rotor control	rad

UH-1 EQUATIONS OF MOTION

Longitudinal - Vertical

- X-Axis

$$\dot{u} - \frac{X_u}{m} u - \frac{X_w}{m} w - \frac{X_{\dot{\theta}}}{m} \dot{\theta} + g\,\theta - \frac{X_{\dot{\beta}}}{m} \dot{\beta} - \frac{X_\beta}{m} \beta - \frac{X_K}{m} K = \frac{X_{\delta_\theta}}{m} \delta_\theta + \frac{X_{\delta_L}}{m} \delta_L$$

- Z-Axis

$$\dot{w} - \frac{Z_w}{m} w - \frac{Z_u}{m} u - \left(U_o + \frac{Z_{\dot{\theta}}}{m}\right) \dot{\theta} - \frac{Z_{\dot{\beta}}}{m} \dot{\beta} - \frac{Z_\beta}{m} \beta - \frac{Z_K}{m} K = \frac{Z_{\delta_\theta}}{m} \delta_\theta + \frac{Z_{\delta_L}}{m} \delta_L$$

- Pitch

$$\ddot{\theta} - \frac{M_{\dot{\theta}}}{I_{yy}} \dot{\theta} - \frac{M_u}{I_{yy}} u - \frac{M_{\dot{w}}}{I_{yy}} \dot{w} - \frac{M_w}{I_{yy}} w - \frac{M_{\dot{\beta}}}{I_{yy}} \dot{\beta} - \frac{M_\beta}{I_{yy}} \beta - \frac{M_K}{I_{yy}} K =$$

$$\frac{M_{\delta_\theta}}{I_{yy}} \delta_\theta + \frac{M_{\delta_L}}{I_{yy}} \delta_L$$

- Blade Flapping

$$\dot{\beta} - \frac{1}{\beta_{\dot{\beta}}}\beta - \frac{\beta_u}{\beta_{\dot{\beta}}}u - \frac{\beta_w}{\beta_{\dot{\beta}}}w - \frac{\beta_{\dot{\theta}}}{\beta_{\dot{\beta}}}\dot{\theta} - \frac{\beta_K}{\beta_{\dot{\beta}}}K = \frac{\beta_{\delta_\theta}}{\beta_{\dot{\beta}}}\delta_\theta + \frac{\beta_{\delta_L}}{\beta_{\dot{\beta}}}\delta_L$$

- Stabilizer Bar

$$\dot{K} + \dot{\theta} + 0.3K = 0$$

Lateral - Directional

- Y-Axis

$$\dot{v} - \frac{Y_v}{m}v - \left(W_o + \frac{Y_{\dot{\phi}}}{m}\right)\dot{\phi} - \left(g\cos\theta_o\right)\phi + \left(U_o - \frac{Y_{\dot{\psi}}}{m}\right)\dot{\psi} - \frac{Y_\lambda}{m}\lambda - \frac{Y_\gamma}{m}\gamma =$$

$$\frac{Y_{\dot{\lambda}}}{m}\dot{\lambda} + \frac{Y_{\delta_\phi}}{m}\delta_\phi + \frac{Y_{\delta_\psi}}{m}\delta_\psi$$

- Roll

$$\ddot{\phi} - \frac{L_{\dot{\phi}}}{I_{xx}}\dot{\phi} - \frac{L_v}{I_{xx}}v - \frac{L_{xz}}{I_{xx}}\ddot{\psi} - \frac{L_\gamma}{I_{xx}}\gamma - \frac{L_\lambda}{I_{xx}}\lambda = \frac{L_{\delta_\phi}}{I_{xx}}\delta_\phi + \frac{L_{\delta_\psi}}{I_{xx}}\delta_\psi$$

$$\frac{L_{\dot{\psi}}}{I_{xx}}\dot{\psi} + \frac{L_{\dot{v}}}{I_{xx}}\dot{v}$$

- Yaw

$$\ddot{\psi} - \frac{N_{\dot{\psi}}}{I_{zz}}\dot{\psi} - \frac{N_v}{I_{zz}}v - \frac{I_{xz}}{I_{zz}}\ddot{\phi} - \frac{N_{\dot{\phi}}}{I_{zz}}\dot{\phi} - \frac{N_\gamma}{I_{zz}}\gamma - \frac{N_\lambda}{I_{zz}}\lambda = \frac{N_{\delta_\phi}}{I_{zz}}\delta_\phi + \frac{N_{\delta_\psi}}{I_{zz}}\delta_\psi$$

- Blade Flapping (not included in simulation)

$$\dot{\gamma} - \frac{1}{\gamma_{\dot{\gamma}}}\gamma - \frac{\gamma_{\dot{\phi}}}{\gamma_{\dot{\gamma}}}\dot{\phi} - \frac{\gamma_{\dot{\psi}}}{\gamma_{\dot{\gamma}}}\dot{\psi} - \frac{\gamma_v}{\gamma_{\dot{\gamma}}}v - \frac{\gamma_\lambda}{\gamma_{\dot{\gamma}}}\lambda = \frac{\gamma_{\delta_\phi}}{\gamma_{\dot{\gamma}}}\delta_\phi$$

- Stabilizer Bar

$$\dot{\lambda} + \dot{\phi} + 0.3\lambda = 0$$

CONTROL STICK CHARACTERISTICS

To prepare the equations for use on the analog, they must first be scaled. The following sensitivities and authorities assigned to the controls are those characteristics on the UH-1 vehicle:

Control	Sensitivity	Authority
Cyclic pitch (δ_θ)	1.84 deg/in.	± 6.5 in.
Cyclic roll (δ_ϕ)	1.54 deg/in.	± 6.5 in.
Collective (δ_L)	1.33 deg/in.	+ 2 in. -- 7 in. (0 = 86 kn)
Tail rotor (δ_ψ)	2.0 deg/in.	± 3 in.
Pitch trim	0.46 deg/sec	

FORCES AND DISPLACEMENTS

Control	Bell UH-1B
Collective stick force	14 lb
Collective stick vertical travel	7 in.
Cyclic stick travel pitch	6.3 in.
Cyclic stick travel roll	6.2 in.
Cyclic stick B/O pitch	2 lb
Cyclic stick B/O roll	1 lb
Cyclic stick force gradient pitch	1.25 lb/in.
Cyclic stick force gradient roll	0.79 lb/in.
Tail rotor pedal travel	3.25 in.
Tail rotor pedal B/O	1 lb
Tail rotor pedal force gradient	7.3 lb/in.

SCALING

$\dot{u}$ u $\dot{v}$, v, $\dot{w}$, w	1 ft/sec = 1 volt
$\ddot{\phi}$, $\dot{\phi}$, ϕ, θ, $\dot{\theta}$, θ $\ddot{\psi}$, $\dot{\psi}$, ψ, $\dot{\lambda}$, λ δ_θ, δ_ϕ, δ_ψ, δ_L	1 rad = 100 volts

TABLE XV. UH-1 LONGITUDINAL DERIVATIVES

Derivative	Flight Condition			
	Hover (μ=0)	43 kn (μ=0.1)	85.5 kn (μ=0.2)	129 kn (μ=0.3)
X_u/m	-0.0060	-0.0158	-0.0280	-0.0416
X_w/m	-0.0480	-0.0255	0.0015	0.0445
$X_{\dot{\theta}}/m$	0.0188	4.0900	9.1600	15.2400
$X_{\dot{\beta}}/m$	0.0000	0.0000	0.0000	0.0000
X_β/m	-54.0000	-64.0000	-59.0000	-40.0000
X_K/m	-1.6800	-1.2800	-0.895	-0.5760
X_{δ_θ}/m	-10.5000	-8.0000	-5.6000	-3.6000
X_{δ_L}/m	-14.4000	-9.2000	-3.0000	7.0000
Z_u/m	-0.0315	-0.0165	-0.0005	0.0190
Z_w/m	-0.5520	-0.6340	-0.6580	-0.6150
(U_o+Z_q/m)	0.0015	73.1100	144.8000	215.7000
$Z_{\dot{\beta}}/m$	0.0000	0.0000	0.0000	0.0000
Z_β/m	0.0000	-48.0000	-95.0000	-145.0000
Z_K/m	0.0000	-7.6800	-15.2000	-23.2000
Z_{δ_θ}/m	0.0000	-48.0000	-95.0000	-145.0000
Z_{δ_L}/m	-253.0000	-284.0000	-316.0000	-353.0000
M_u/I_{yy}	0.00057	0.001427	0.002730	0.003750
M_w/I_{yy}	0.002255	-0.00725	-0.01672	-0.0277
$M_{\dot{w}}/I_{yy}$	0.0000	0.0000	0.0000	0.0000
$M_{\dot{\theta}}/I_{yy}$	-0.0025	-0.2400	-0.4950	-0.4400
$M_{\dot{\beta}}/I_{yy}$	0.0000	0.0000	0.0000	0.0000
M_β/I_{yy}	7.2300	8.2100	7.2200	4.2600
M_K/I_{yy}	0.2260	0.1130	0.0046	-0.0960
M_{δ_θ}/I_{yy}	1.4100	0.7080	0.0290	-0.6040
M_{δ_L}/I_{yy}	0.0000	-0.9230	-2.0050	-3.6300
$\beta_u/\beta_{\dot{\beta}}$	0.00442	0.00393	0.00368	0.00367
$\beta_w/\beta_{\dot{\beta}}$	0.0000	0.0023	0.0048	0.0075
$\beta_q/\beta_{\dot{\beta}}$	-1.0250	-1.0220	-1.0200	-1.0190
$1/\beta_{\dot{\beta}}$	-8.9000	-8.6800	-8.2500	-7.3500
$\beta_K/\beta_{\dot{\beta}}$	1.4220	1.4620	1.5200	1.6320
$\beta_{\delta_\theta}/\beta_{\dot{\beta}}$	8.9000	9.1500	9.5000	10.2000
$\beta_{\delta_L}/\beta_{\dot{\beta}}$	0.0000	2.0000	4.2500	7.2000

TABLE XVI. UH-1 LATERAL-DIRECTIONAL DERIVATIVES

Derivative	Flight Condition			
	Hover	52 kn	90 kn	121 kn
$L_{\dot{\phi}}/I_{xx}$	-0.987	-1.395	-1.228	-0.984
$L_{\dot{\psi}}/I_{xx}$	0.471	0.000	0.000	0.000
$L_{\dot{v}}/I_{xx}$	0.000	-0.0082	-0.0063	-0.0052
L_{v}/I_{xx}	-0.0223	-0.0317	-0.0376	-0.0384
$L_{\dot{\lambda}}/I_{xx}$	-0.158	-0.0219	-0.0191	-0.0148
L_{λ}/I_{xx}	3.160	0.320	0.320	0.323
$L_{\delta_{\psi}}/I_{xx}$	9.400	12.220	13.580	14.800
$L_{\delta_{\phi}}/I_{xx}$	66.500	37.000	34.000	58.000
$N_{\dot{\psi}}/I_{zz}$	-0.679	0.000	0.000	0.000
$N_{\dot{v}}/I_{zz}$	0.000	0.01232	0.00982	0.0081
N_{v}/I_{zz}	0.0209	0.0305	0.0386	0.0381
$N_{\delta_{\psi}}/I_{zz}$	-12.660	-16.500	-18.280	-19.850
$N_{\delta_{\phi}}/I_{zz}$	-0.896	-0.490	-0.480	-0.830
Y_{v}/m	-0.0376	-0.1097	-0.1467	-0.1722
$(U_{o} - Y_{\dot{\psi}}/m)$	-0.771	100.400	150.400	200.000
Y_{ϕ}/m	-1.610	-2.210	-1.9230	-1.660
$Y_{\dot{\lambda}}/m$	0.258	-0.353	-0.308	-0.266
Y_{λ}/m	5.150	5.150	5.150	5.650
$Y_{\delta_{\psi}}/m$	16.100	20.700	23.000	27.200
$Y_{\delta_{\phi}}/m$	10.300	5.600	5.400	9.300

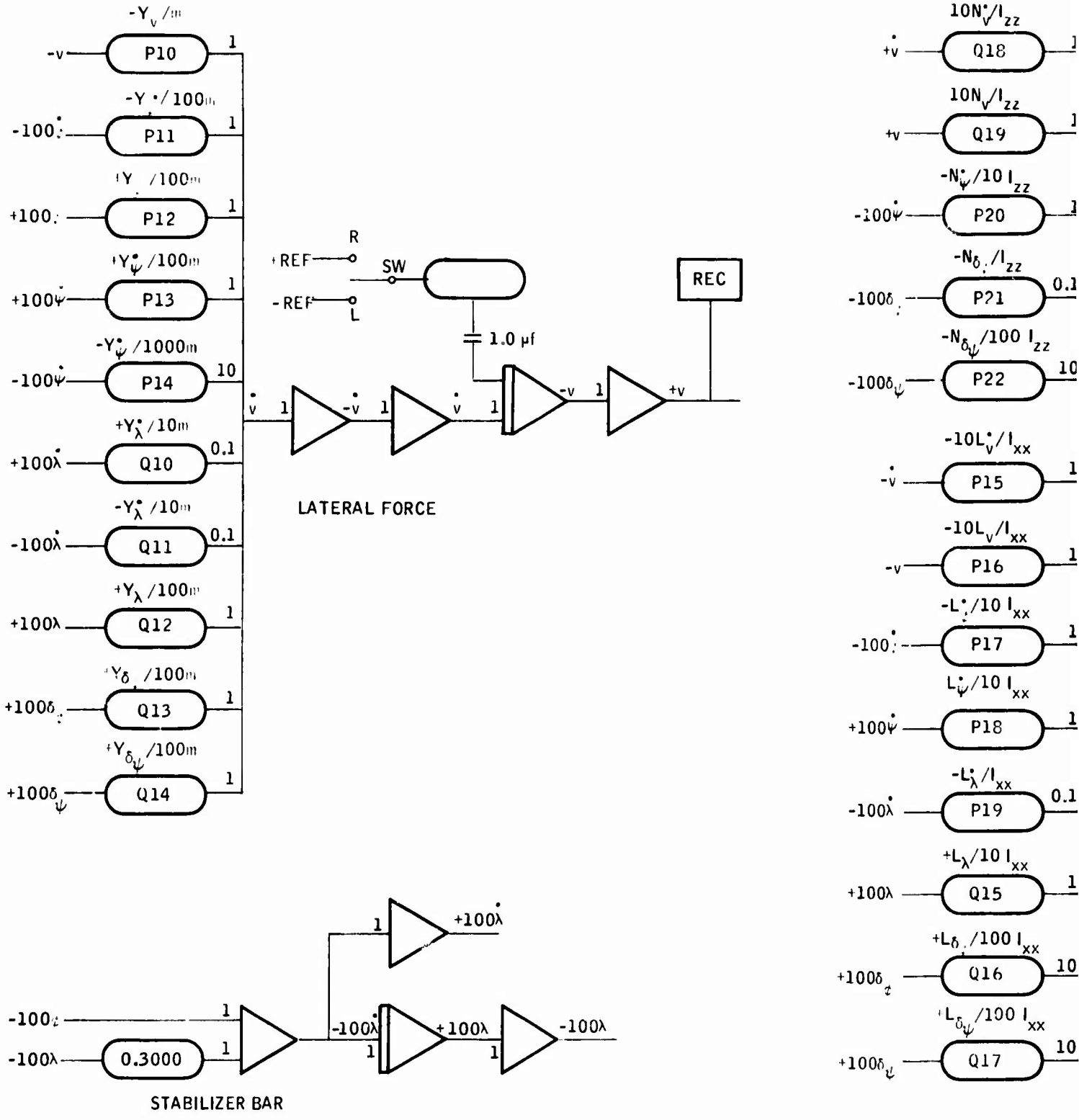

Figure 122. UH-1B Lateral-Directional Plane Simulation Diagram.

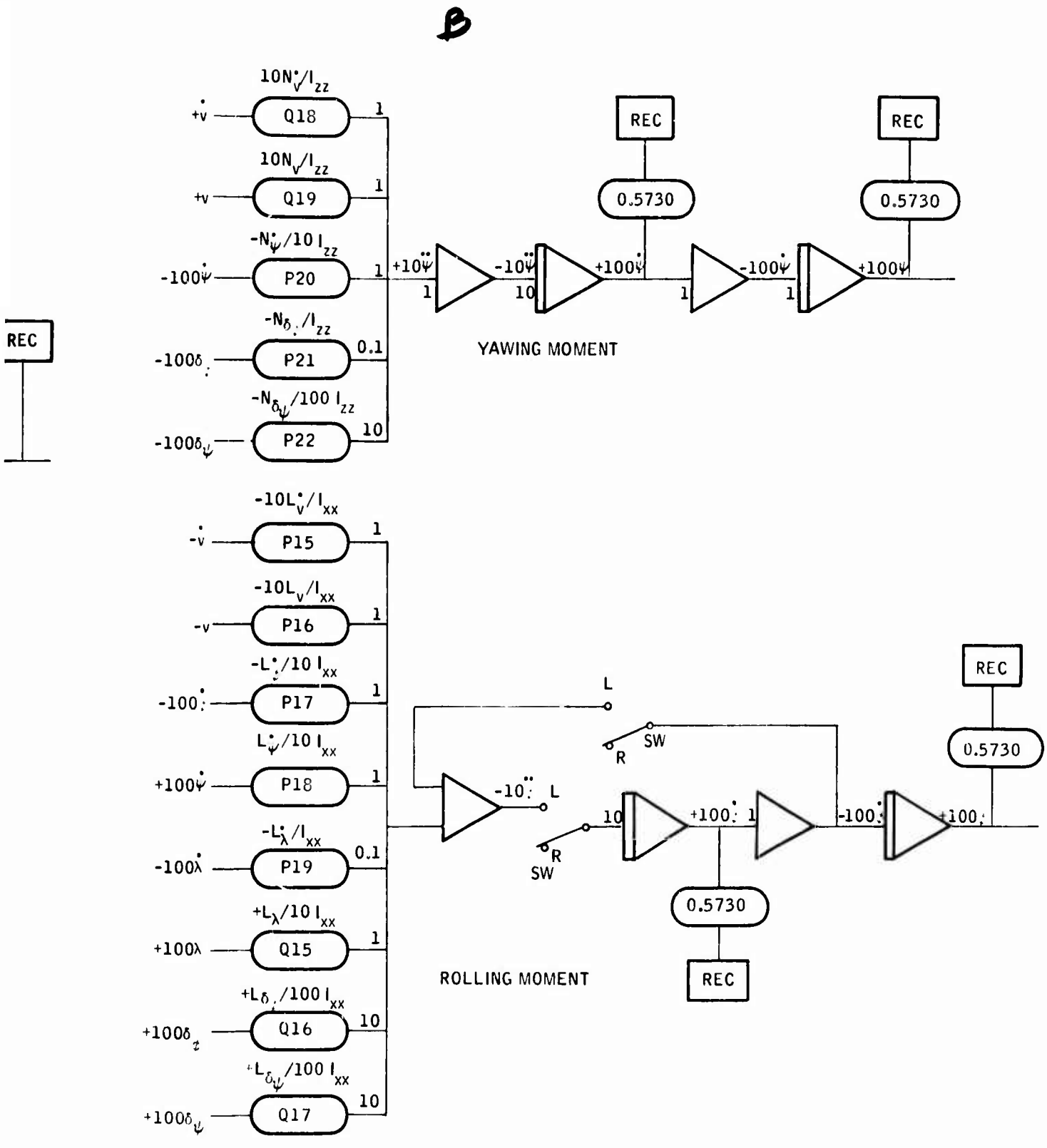
B
$10N_{\dot{v}}/I_{zz}$
+v̇
Q18
1
$10N_{v}/I_{zz}$
+v
Q19
1
$-N_{\dot{\psi}}/10\,I_{zz}$
$-100\dot{\psi}$
P20
1
$-N_{\dot{\delta}_{:}}/I_{zz}$
$-100\dot{\delta}_{:}$
P21
0.1
$-N_{\delta_{\psi}}/100\,I_{zz}$
$-100\delta_{\psi}$
P22
10
REC
$+10\ddot{\psi}$
1
$-10\ddot{\psi}$
10
$+100\dot{\psi}$
REC
0.5730
1
$-100\dot{\psi}$
REC
0.5730
1
$+100\psi$
YAWING MOMENT
$-10L_{\dot{v}}/I_{xx}$
-v̇
P15
1
$-10L_{v}/I_{xx}$
-v
P16
1
$-L_{\dot{:}}/10\,I_{xx}$
$-100\dot{:}$
P17
1
$L_{\dot{\psi}}/10\,I_{xx}$
$+100\dot{\psi}$
P18
1
$-L_{\dot{\lambda}}/I_{xx}$
$-100\dot{\lambda}$
P19
0.1
$+L_{\lambda}/10\,I_{xx}$
$+100\lambda$
Q15
1
$+L_{\dot{\delta}_{:}}/100\,I_{xx}$
$+100\delta_{:}$
Q16
10
$+L_{\delta_{\psi}}/100\,I_{xx}$
$+100\delta_{\psi}$
Q17
10
L
SW
R
$-10\ddot{:}$
L
R
SW
10
$+100\dot{:}$
1
$-100\dot{:}$
$+100:$
REC
0.5730
0.5730
REC
ROLLING MOMENT

Diagram.

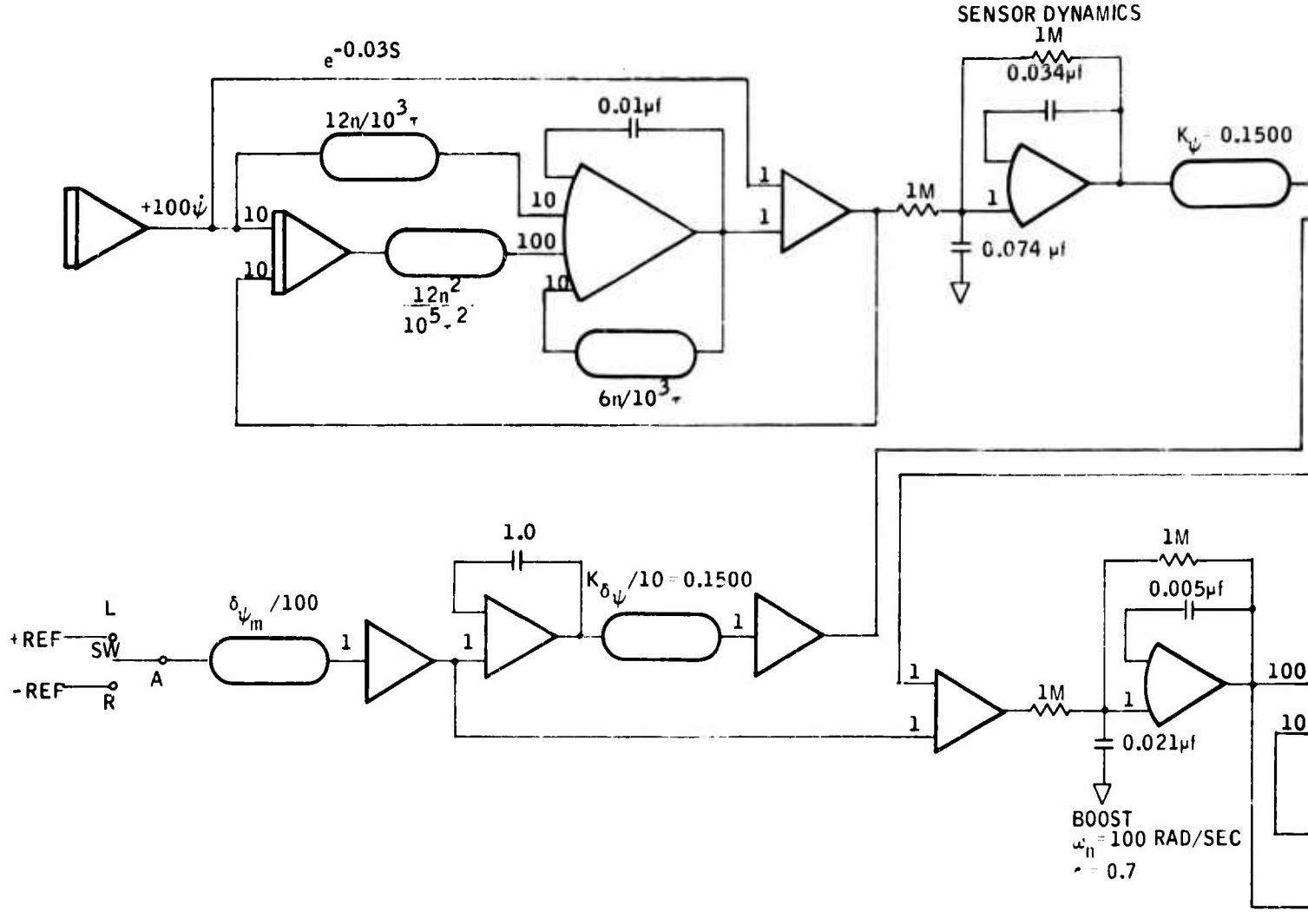

Figure 123. UH-1B Yaw SAS Simulation Diagram.

B

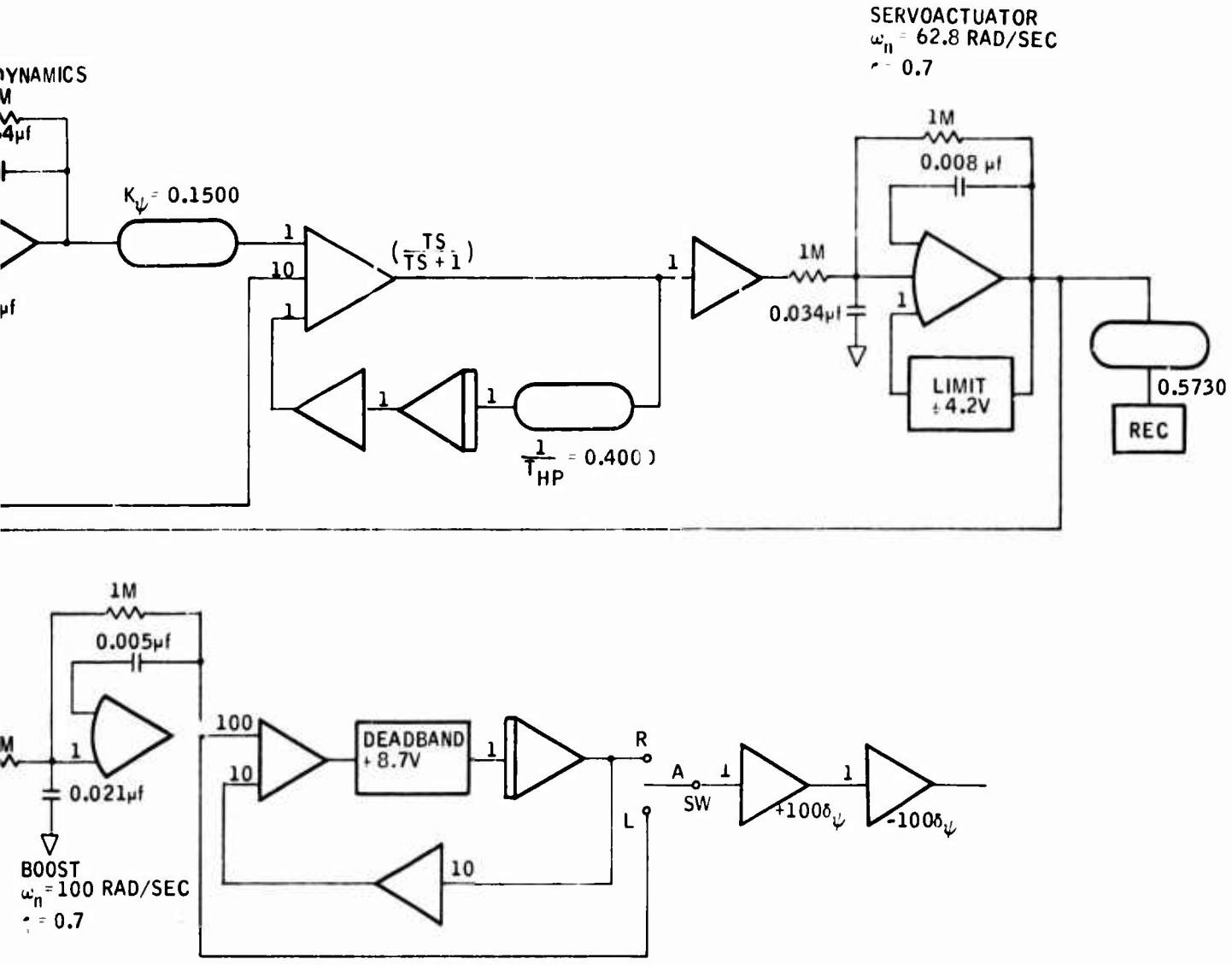
SERVOACTUATOR
ω_n = 62.8 RAD/SEC
ζ = 0.7
DYNAMICS
K_ψ = 0.1500
1
10
1
$\left(\frac{TS}{TS+1}\right)$
1
1M
0.008 µf
1M
0.034µf
1
LIMIT
±4.2V
0.5730
REC
1
1
$\frac{1}{T_{HP}}$ = 0.400)

1M
0.005µf
1
0.021µf
BOOST
ω_n = 100 RAD/SEC
ζ = 0.7
100
10
DEADBAND
±8.7V
1
R
L
A
SW
1
1
+100δ_ψ
-100δ_ψ
10

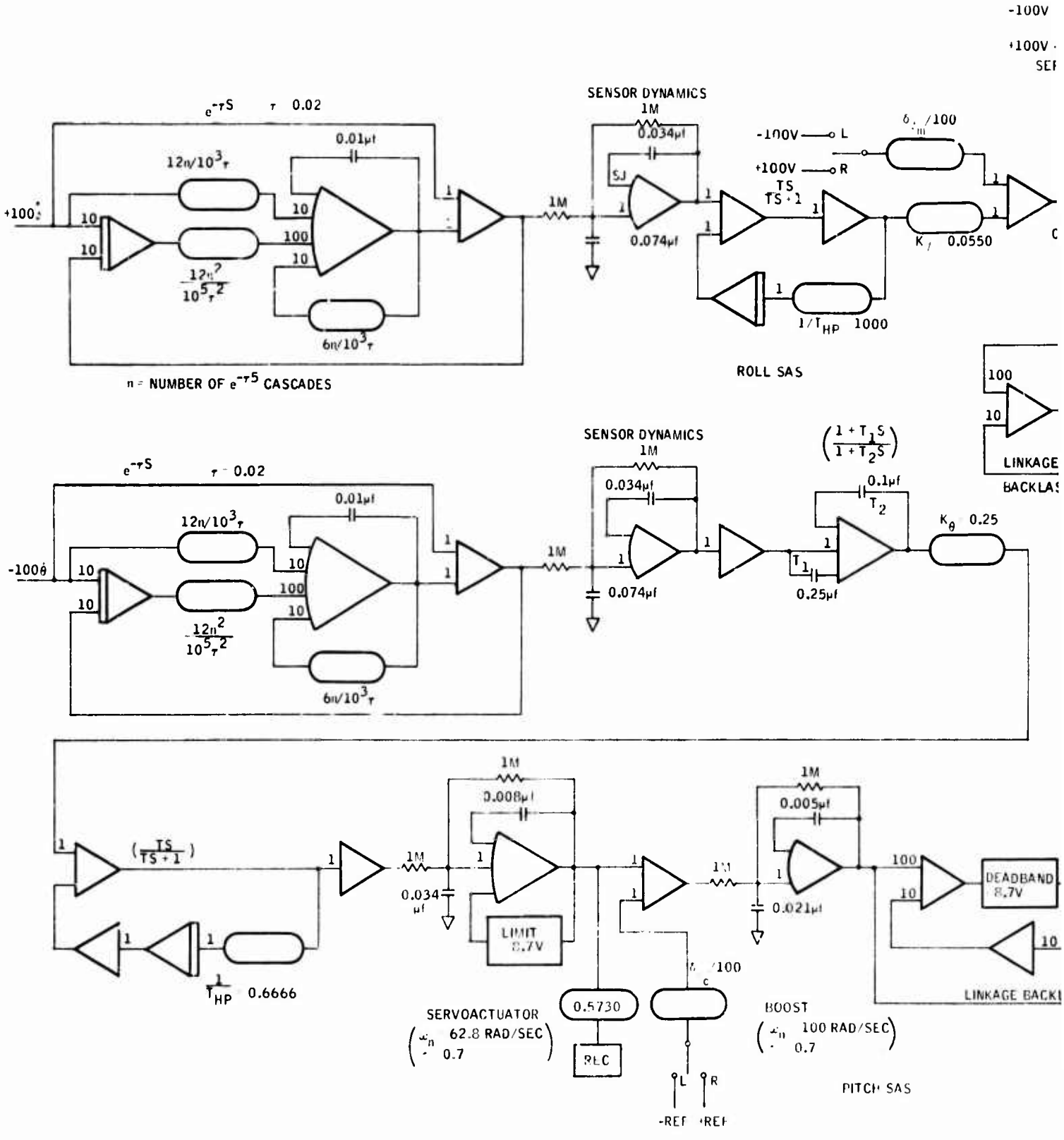

Figure 124. UH-1B Roll and Pitch SAS Simulation Diagram.

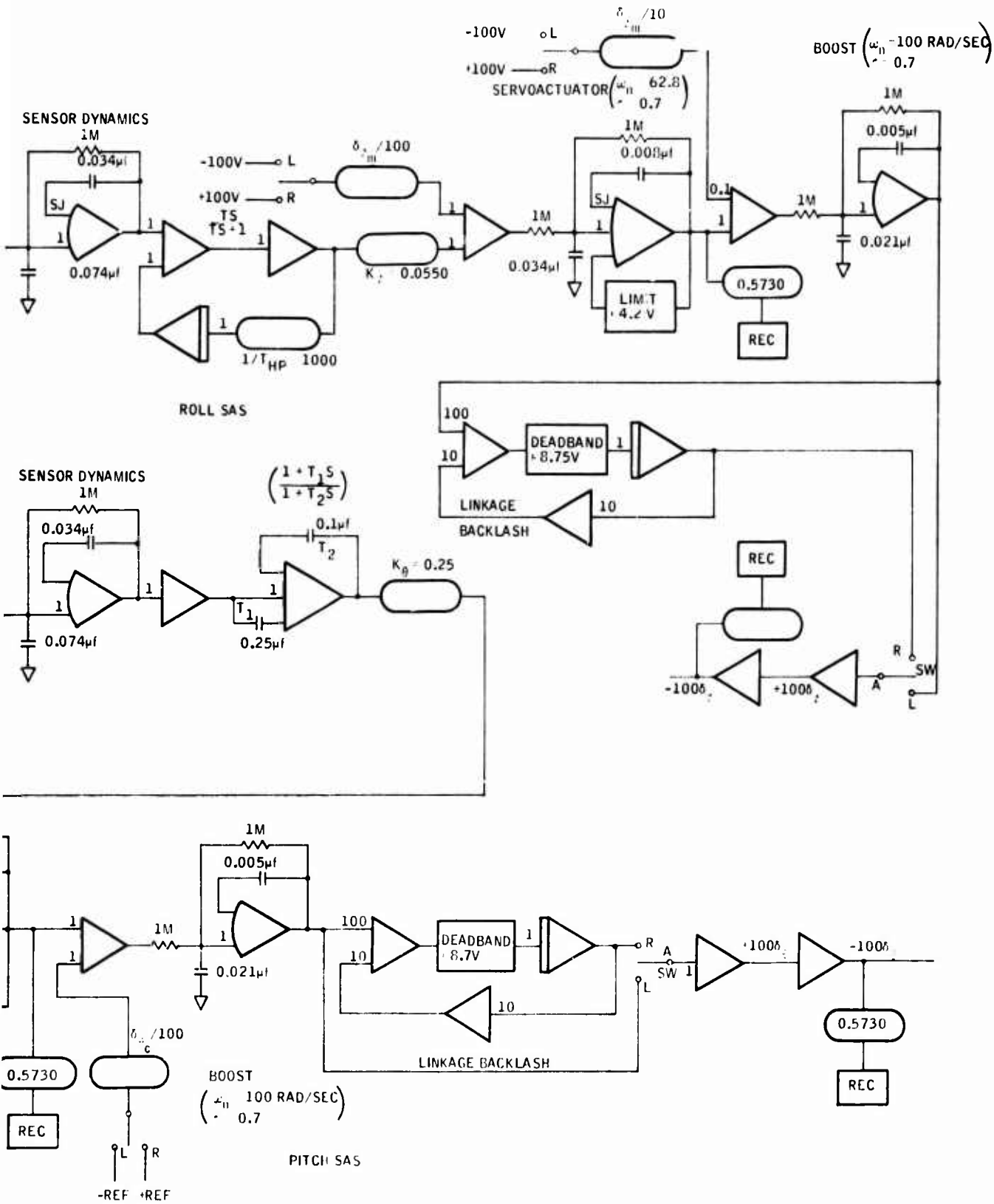

ıulation Diagram.

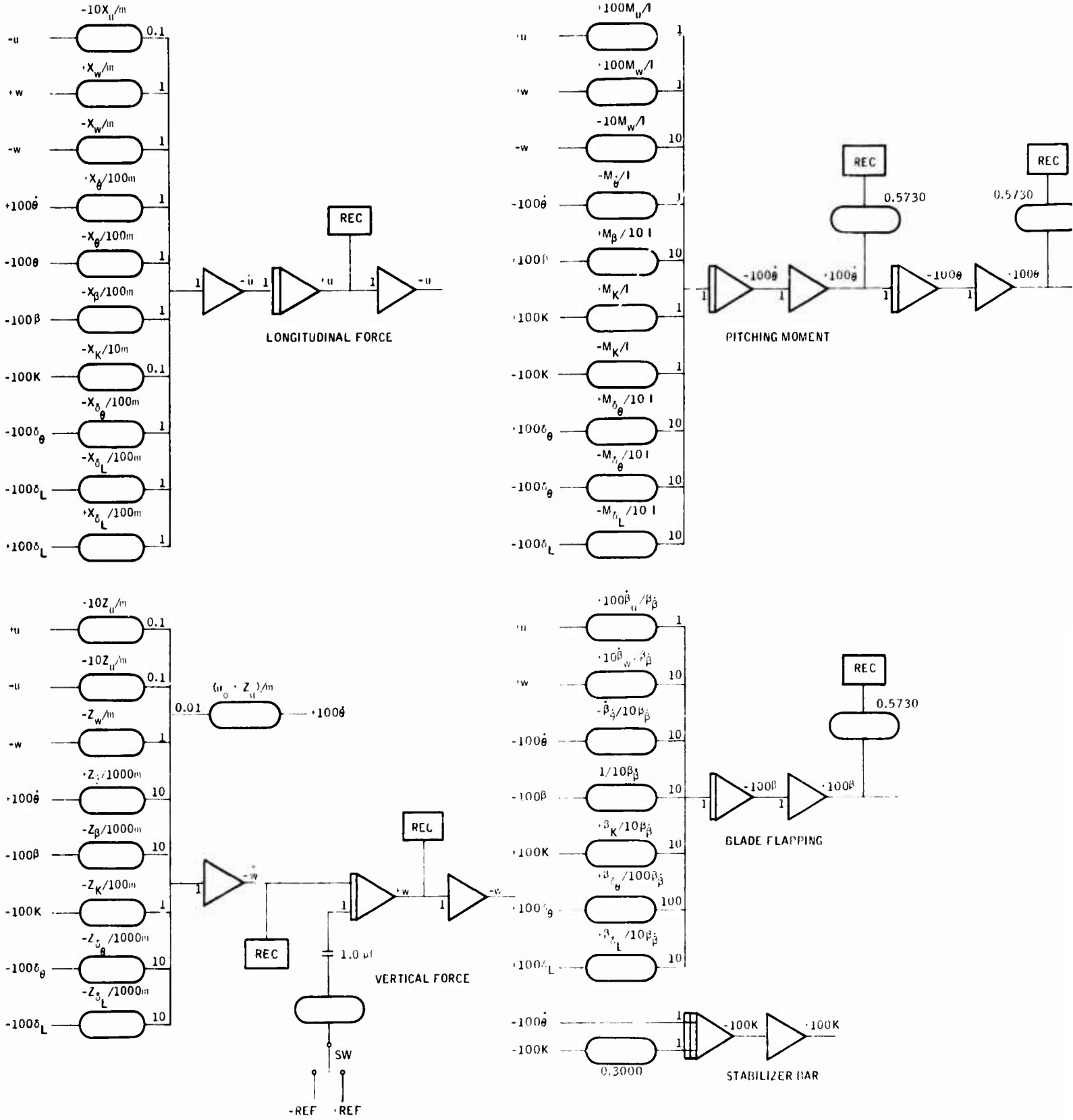

Figure 125. UH-1B Longitudinal-Vertical Plane Simulation Diagram.

SECTION IV
DETAIL SPECIFICATION NO. DS 21565-01 DATED 4 DECEMBER 1968, "PERFORMANCE/DESIGN AND QUALIFICATION REQUIREMENTS FOR THE HYDROFLUIDIC THREE-AXIS STABILITY AUGMENTATION SYSTEM"

1.0 SCOPE

This specification defines the preliminary design requirements for the YG1053A01 Three-Axis Hydrofluidic Stability Augmentation System (FSAS), hereafter referred to as the "system." The objective of this system is to augment the damping and improve the handling qualities of the UH-1C helicopter in three axes.

This specification defines both system requirements and a design approach to be used in meeting the requirements. Requirements in this specification are design goals which should be revised when development indicates more optimum techniques of obtaining the program objective.

2.0 APPLICABLE DOCUMENTS

The following documents and the applicable specifications referenced therein shall apply to the extent specified herein:

a. MIL-H-8501A, Helicopter Flying and Ground Handling Qualities, General Requirements for.

b. MIL-H-5606, Hydraulic Fluid, Petroleum Base, Aircraft, Missile and Ordnance.

c. MIL-STD-810A, Military Standard Environmental Test Methods for Aerospace and Ground Equipment.

3.0 REQUIREMENTS

3.1 General

The system shall consist of the following functional units:

a. Rate Sensor - Each axis shall have a vortex rate sensor which provides a differential pressure signal that is proportional to the aircraft angular rate in the specific axis.

b. Amplifiers - Accept and amplify differential pressure signals.

c. Shaping Networks - Usually a combination of resistors and capacitors (bellows) designed to provide the following functions:

1. Lag - With a characteristic of $\frac{1}{TS + 1}$

2. High-pass - With a characteristic of $\frac{TS}{1 + TS}$

3. Lead-lag - With a characteristic of $\frac{aTS + 1}{TS + 1}$

Note: T is a time constant and a is greater than 1.0.

d. Rudder Input Device - Provides an output which is a function of the rudder pedal displacement. This will reduce the tendency of the control system to "fight" the pilot in the yaw axis.

e. Servoactuator - The servoactuator, mounted in series with the aircraft power boost servoactuators, accepts differential pressure signals and converts them to displacements of the power boost servoactuator pilot valve. Weight, bulk, and power consumption shall be optimized to the extent possible without compromising reliable and demonstrable functioning. Interunit connections shall be accomplished in a manner that will permit replacement of individual functional components.

f. Flow Control Valve - Maintains a constant flow to the system when provided a differential pressure of over 500 psid.

g. Priority Valve - This optional device will reduce servoactuator-induced back-pressure surges.

h. Engage Valve - Solenoid-operated hydraulic valves will be remotely controlled from the cockpit to engage all or part of the system.

i. Cockpit Control Panel - Contains switches and indicators to selectively operate each axis of the system for exploratory investigation during flight test.

3.2 Environment

3.2.1 Vibration

A vibration scan with the three-axis FSAS energized and operating shall be conducted at the amplitudes and frequencies of Figure 514-2, Curve A, of MIL-STD-810A. A sinusoidal vibration cycling, per the test envelope, shall be conducted at a rate sufficiently slow to allow adequate identification and evaluation of the resonant frequency(s) or functional phenomena that may occur. Sinusoidal vibration cycle times shall be not less than 15 min for each of the three axes. Three-axis FSAS vibration testing shall be conducted with the hydraulic supply and connections simulating the actual aircraft installation as nearly as practicable. System performance shall be within specification limits when the vibration level is 0.2 g or less.

3.2.2 Temperature

The system shall operate within specification limits over the ambient temperature range from -25°F to +100°F when the operating fluid is in the range of +60°F to +185°F.

3.3 Power Supplies

Input power to the system shall be hydraulic fluid per MIL-H-5606 at a pressure of 1500 psig (nominal), which is obtained from the aircraft directional hydraulic power boost system. The system (except augmentation servoactuators) shall not require more than 2.5 gpm.

Electrical power for relays and solenoids will be 28 vdc.

3.4 System Performance

All performance requirements in this section pertain to normal operating conditions. Normal operating conditions are defined as: ambient temperature 70° ± 2°F; hydraulic fluid temperature 120° ± 10°F; hydraulic fluid pressure 1000 to 1500 psig ahead of flow regulator, with a maximum of 20 psig return pressure.

3.4.1 Pitch Axis

Pitch-axis requirements are summarized in Figures 126 and 127. The hardware schematic is shown in Figure 128 (Drawing No. C13511AA01).

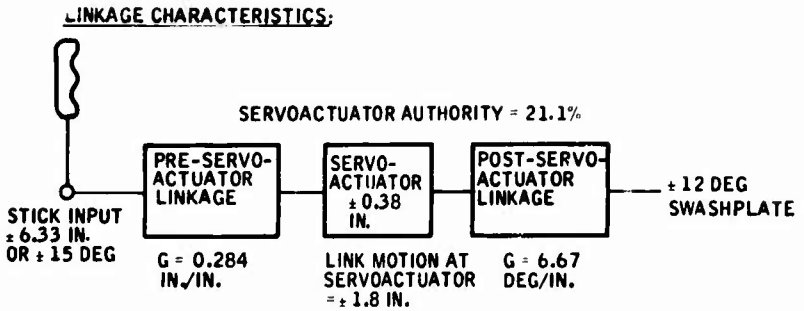

TRANSFER FUNCTION:

$$G\left[\frac{(1.5S)\ (0.25S+1)}{(1.5S+1)(0.1S+1)}\right]\left[\frac{e^{-0.02S}}{(0.05S+1)^2}\right]\left[\frac{(62.8)^2}{S^2+88S+(62.8)^2}\right]$$

HIGH-PASS; LEAD-LAG; RATE SENSOR; SERVOACTUATOR

G = 0.25 DEG SWASHPLATE/DEG/SEC PITCH RATE
= 0.0375 IN. SERVOACTUATOR/DEG/SEC
= 0.375 PSI/DEG/SEC

NOTE: DUE TO LEAD-LAG, GAINS AT HIGH FREQUENCY WILL BE:
0.625 DEG SWASHPLATE/DEG/SEC
0.0937 IN. SERVOACTUATOR/DEG/SEC
0.937 PSI/DEG/SEC

Figure 126. Pitch-Axis Requirements.

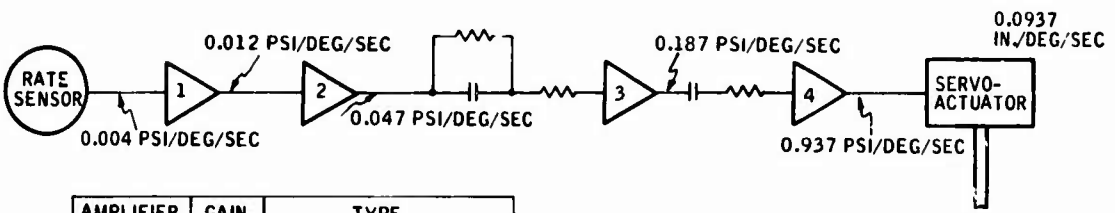

AMPLIFIER	GAIN	TYPE
1	3	HIGH OUTPUT IMPEDANCE
2	4	HIGH OUTPUT IMPEDANCE
3	4	HIGH OUTPUT IMPEDANCE
4	5	LOW OUTPUT IMPEDANCE

RATE SENSOR:

RANGE ± 40 DEG/SEC

$$\text{TRANSFER FUNCTION} = 0.004\left[\frac{e^{-0.02S}}{(0.05S+1)^2}\right] \text{ PSI/DEG/SEC}$$

SERVOACTUATOR:

(SAME AS YAW AXIS: 0.1 IN./PSI)

Figure 127. Pitch-Axis Component Gains.

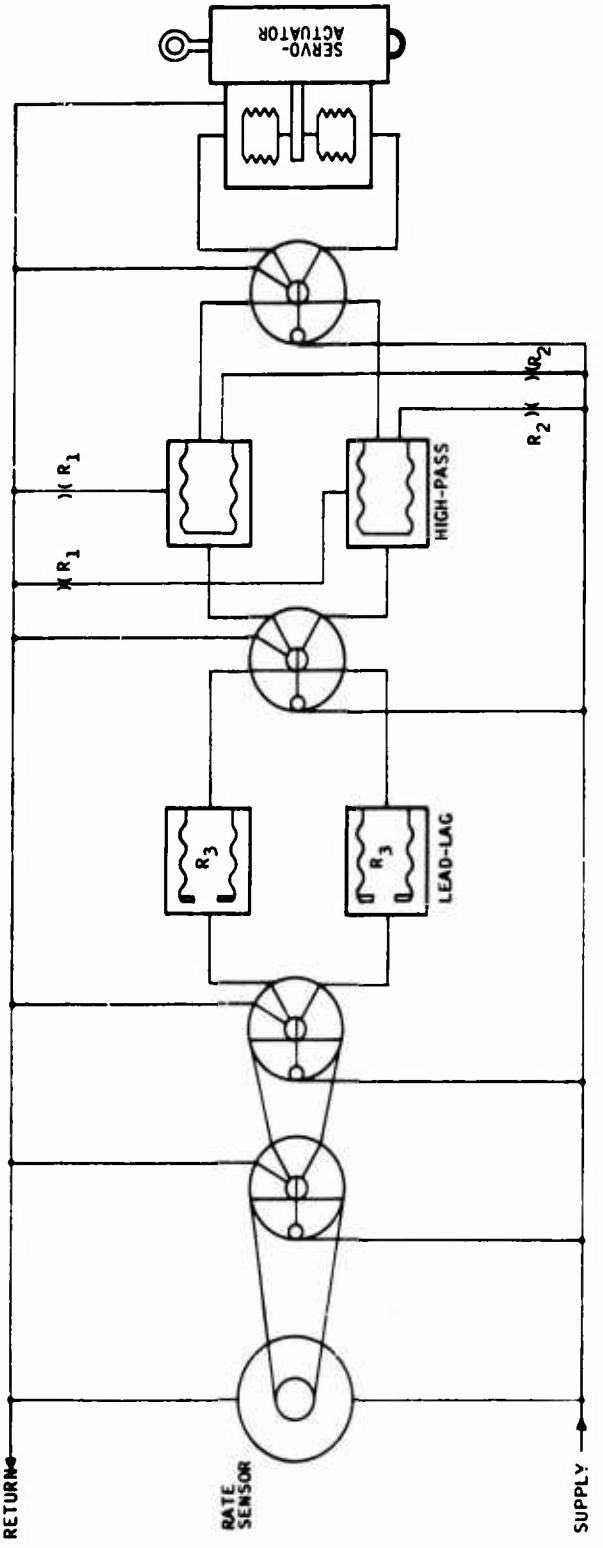

Figure 128. Pitch-Axis Hardware Schematic (Dwg. No. C13511AA01).

3.4.2 Roll Axis

Roll-axis requirements are summarized in Figures 129 and 130. The hardware schematic is shown in Figure 131 (Drawing No. C13513AA01).

3.4.3 Yaw Axis

Yaw-axis requirements are summarized in Figures 132, 133, and 134. The hardware schematic is shown in Figure 135 (Drawing No. C13512AA01).

3.4.4 Interconnection

Interconnection of the three subsystems is defined in Figure 136 (Drawing No. 10027822).

3.4.5 Range

The system shall have a range of at least ±40 deg/sec ahead of the high-pass and ± 100 percent actuator stroke downstream of the high-pass.

3.4.6 Linearity

The system shall meet the requirements of 3.4.1, 3.4.2, and 3.4.3 at input amplitudes of ± 1 deg/sec and ± 5 deg/sec.

3.4.7 Noise

Peak-to-peak noise at the actuator shall not exceed an equivalent of ± 0.5 deg/sec at maximum system dynamic gain.

3.4.8 Accuracy

The system shall maintain gain and time constants within ± 20 percent of the nominal requirements.

3.5 Component Performance

Performance shall be determined at room temperature ambient, with fluid at 120° ± 10°F, unless otherwise specified.

3.5.1 Vortex Rate Sensors

The vortex rate sensors shall meet the following performance requirements when the system is supplied with 2.2 gpm:

a. Scale Factor: 0.004 psid/deg/sec, when loaded into an amplifier (90 ohms typ)

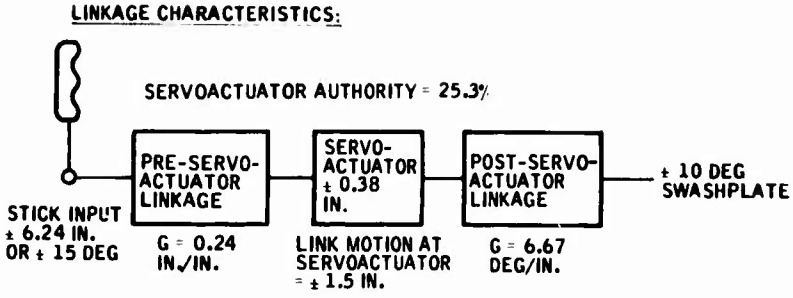

Figure 129. Roll-Axis Requirements.

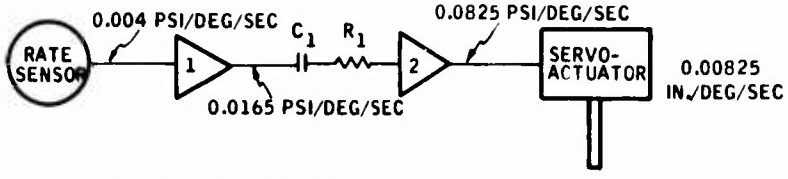

AMPLIFIER	GAIN	TYPE
1	4.1	HIGH OUTPUT IMPEDANCE
2	5.0	LOW OUTPUT IMPEDANCE

RATE SENSOR:

RANGE = ± 60 DEG/SEC

TRANSFER FUNCTION = $0.004\left[\frac{e^{-0.02S}}{(0.05S+1)^2}\right]$ PSI/DEG/SEC

SERVOACTUATOR:

(SAME AS YAW: 0.1 IN./PSI)

NOTE:

$R_1 \approx 150$ OHMS

$C_1 \approx 0.067$ IN.^{3}/PSI

Figure 130. Roll-Axis Component Gains.

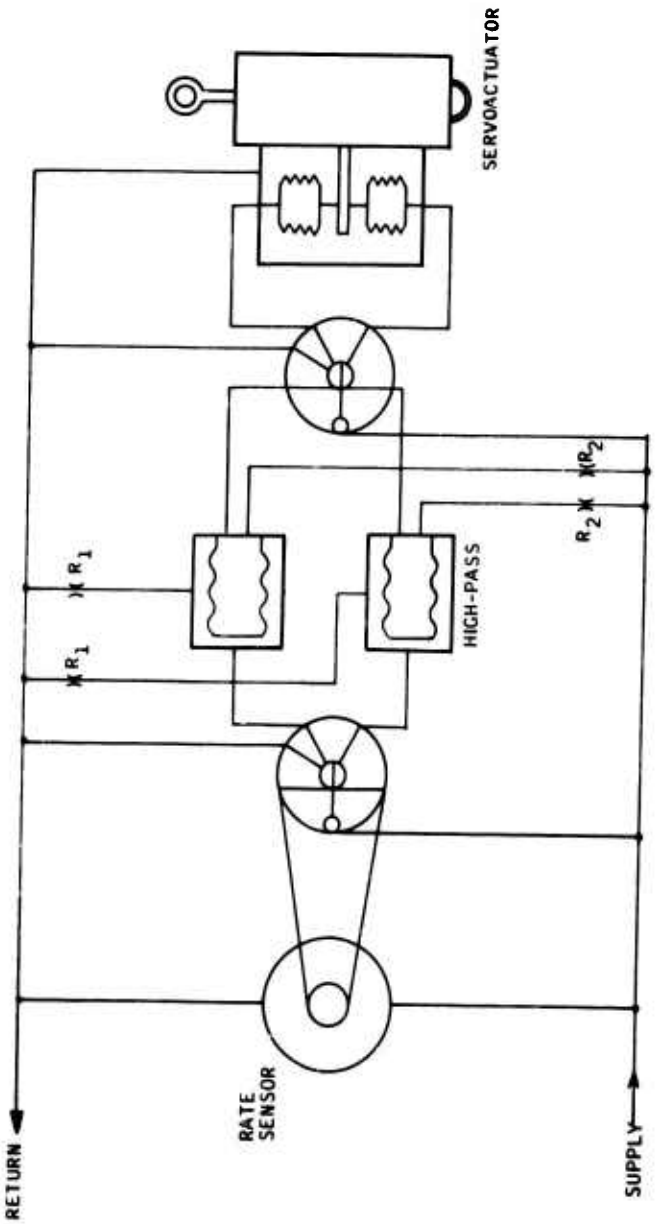

Figure 131. Roll-Axis Hardware Schematic (Dwg. No. C13513AA01).

LINKAGE CHARACTERISTICS:

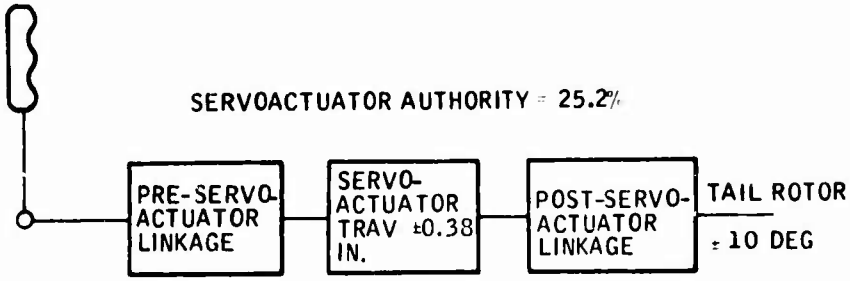

RUDDER PEDAL ± 3.25 IN. G = 0.46 IN./IN. LINKAGE MOTION AT SERVOACTUATOR ± 1.51 IN. G = 6.62 DEG/IN.

TRANSFER FUNCTIONS (RATE AND RUDDER PEDAL):

$$G\left(\frac{2.5S}{2.5S+1}\right)\frac{(e^{-0.03S}}{(0.05S+1)^2}\left[\frac{(62.8)^2}{S^2+2(0.7)\,62.8S+(62.8)^2}\right]$$

HIGH-PASS — RATE SENSOR — SERVOACTUATOR

G = 0.15 DEG TAIL ROTOR/DEG/SEC (OF YAW RATE)

= 0.0227 IN. SERVOACTUATOR/DEG/SEC

= 0.227 PSI/DEG/SEC

$$R\left[\frac{20S}{(20S+1)(S+1)}\right]\left[\frac{2.5S}{2.5S+1}\right]\left[\frac{(62.8)^2}{S^2+2(0.7)62.8S+(62.8)^2}\right]$$

RUDDER TDR — HIGH-PASS — SERVOACTUATOR

R = 1.5 IN. SERVOACTUATOR/IN. INPUT TO SERVOACTUATOR

= 0.69 IN. SERVOACTUATOR/IN. RUDDER PED DISPL

= 15 PSI (AT SERVOACTUATOR)/IN. INPUT TO SERVOACTUATOR

= 6.9 PSI / IN. RUDDER PED DISPL

Figure 132. Yaw-Axis Requirements.

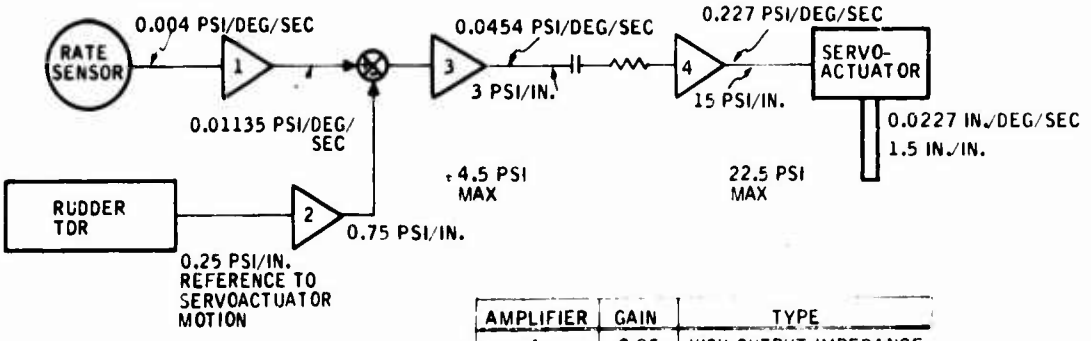

AMPLIFIER	GAIN	TYPE
1	2.85	HIGH OUTPUT IMPEDANCE
2	3.0	HIGH OUTPUT IMPEDANCE
3	4.0	HIGH OUTPUT IMPEDANCE
4	5.0	LOW OUTPUT IMPEDANCE

RUDDER TDR:

RANGE = ± 1.5 IN. (EQUIV SERVOACTUATOR INPUT)
= ± 0.375 PSID OUTPUT

TRANSFER FUNCTION = $0.25\left[\frac{20S}{(20S+1)(S+1)}\right]$ PSI/IN.

FOR CHARACTERISTICS AT SMALL INPUTS SEE FIG. 134

RATE SENSOR:

RANGE = ± 40 DEG/SEC OF YAW RATE

TRANSFER FUNCTION = $0.004\left[\frac{e^{-0.03S}}{(0.05S+1)^2}\right]$ PSI/DEG/SEC

SERVOACTUATOR:

RANGE = ± 0.38 IN.

TRANSFER FUNCTION = $0.1\left[\frac{(62.8)^2}{S^2 + 2(0.7)\,62.8S + (62.8)^2}\right]$ IN./PSID

Figure 133. Yaw-Axis Component Gains.

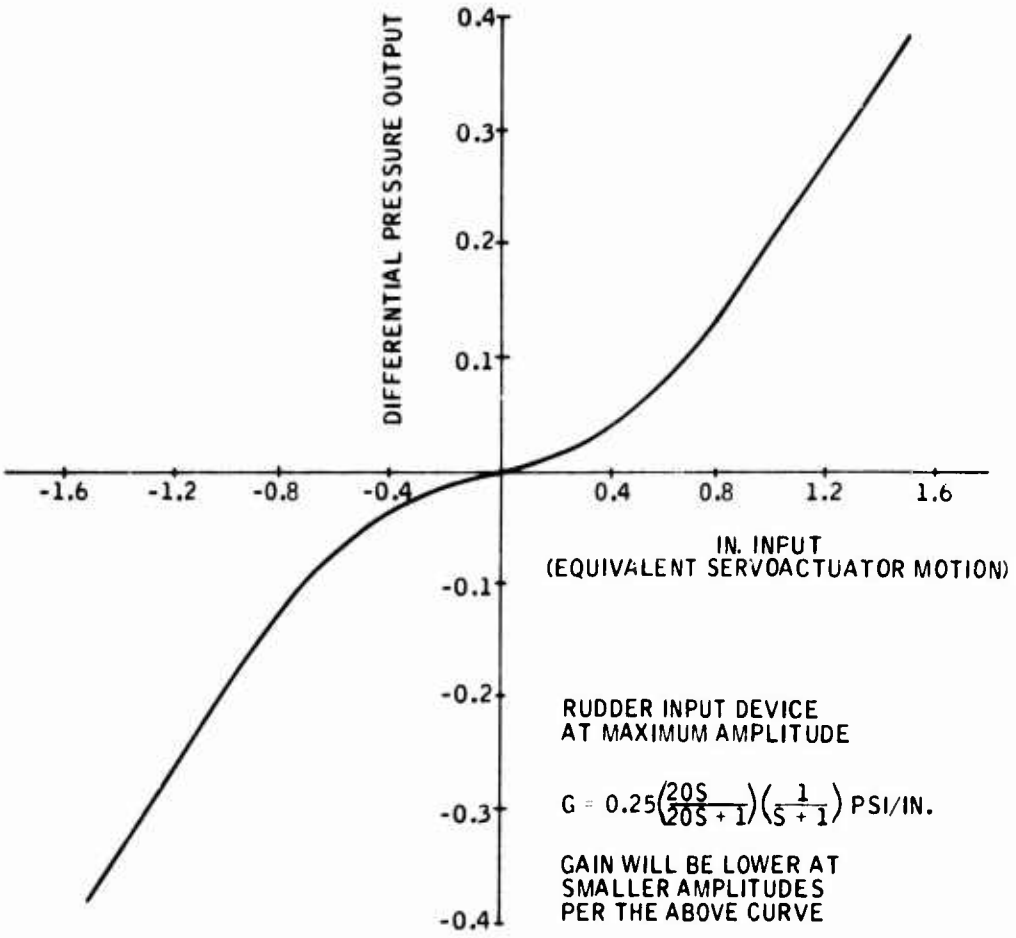

Figure 134. Yaw-Axis -- Differential Pressure Output Versus Inches Input (Equivalent Servoactuator Motion).

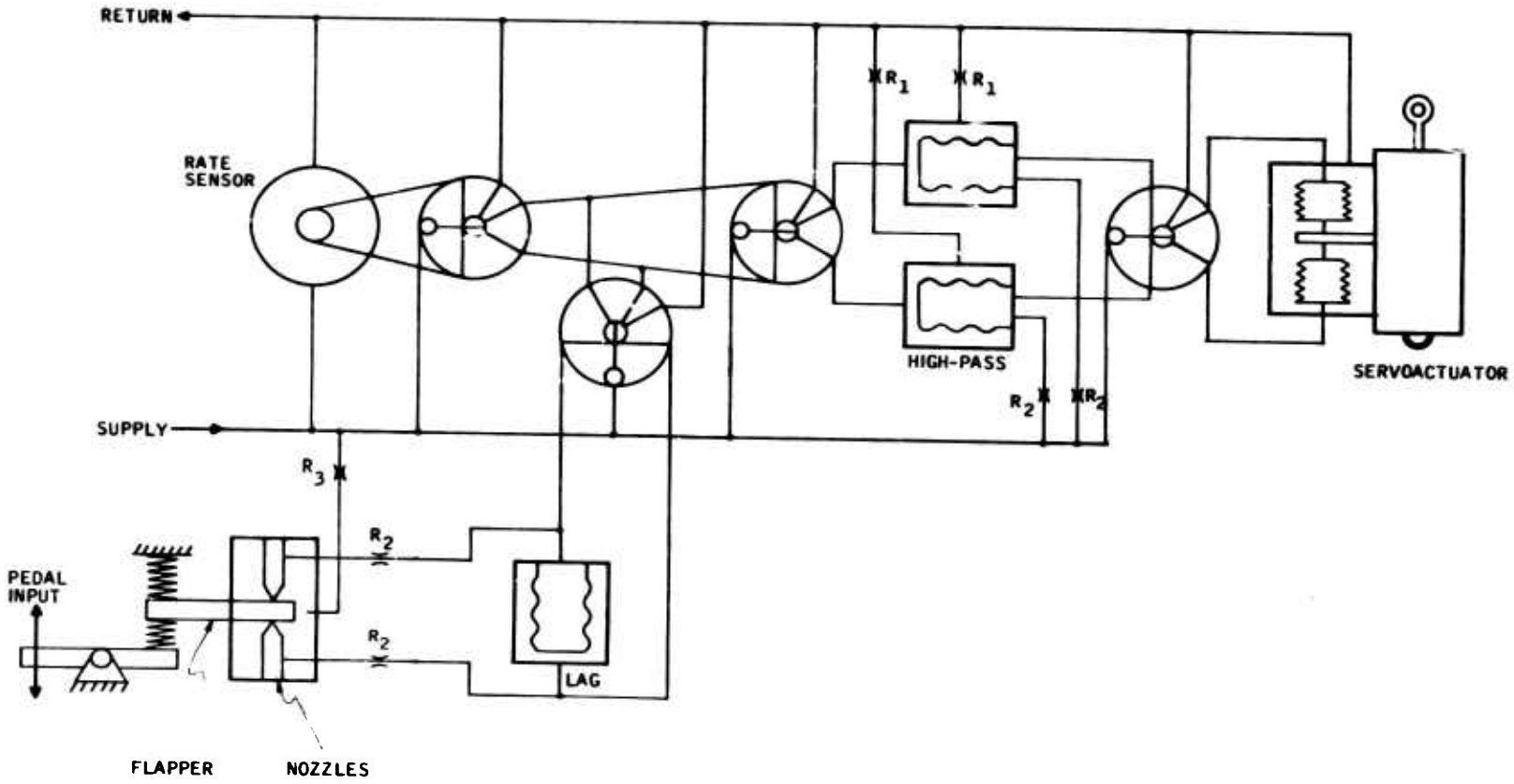

Figure 135. Yaw-Axis Hardware Schematic (Dwg. No. 13512AA01).

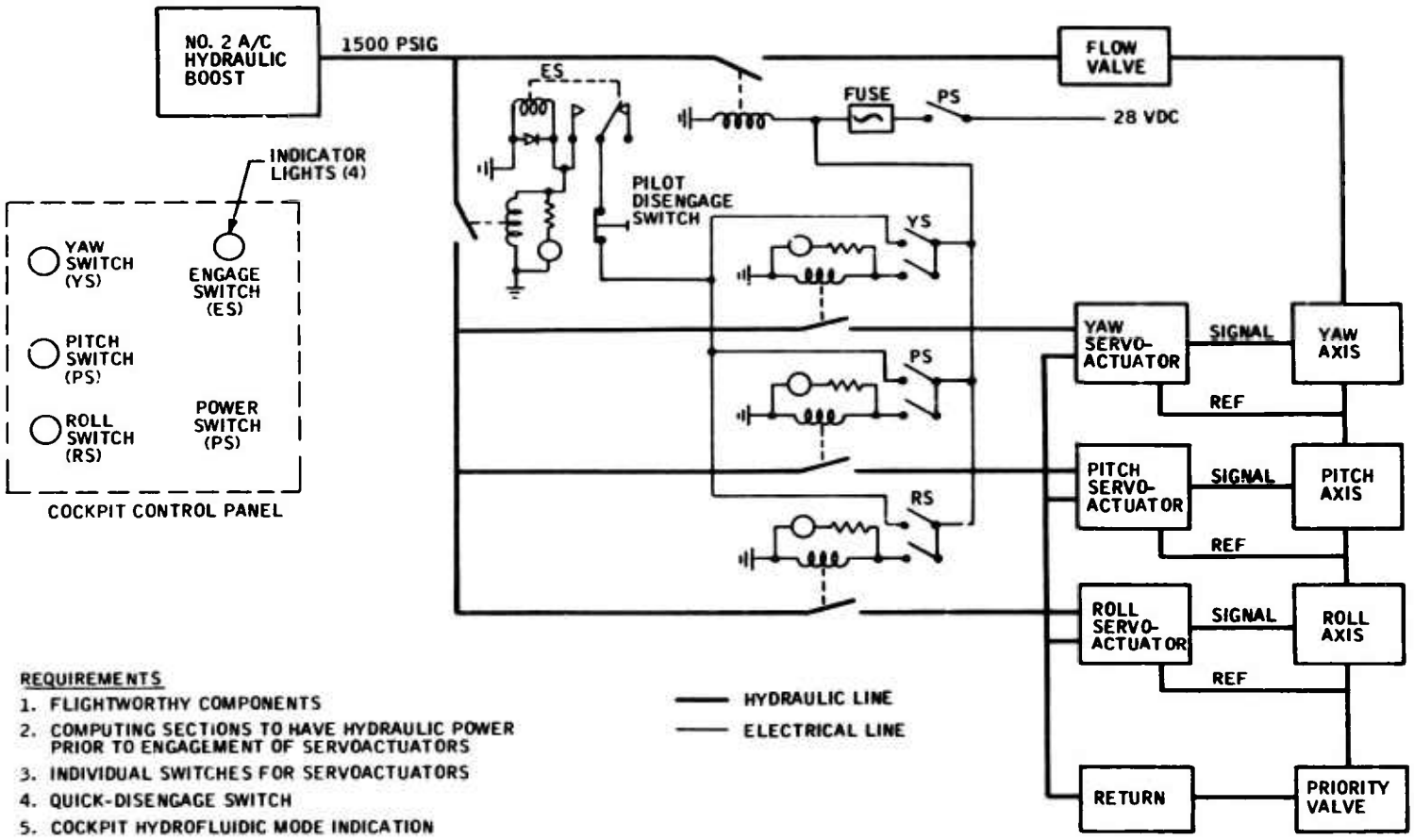

Figure 136. Hydraulic and Electrical Schematic for Installation of Hydraulic SAS (Dwg. No. 10027822).

b. Range: 40 deg/sec, minimum

c. Linearity: 5 percent of full scale

d. Time Delay: 0.020 sec or less for pitch and roll, 0.030 sec in yaw

e. Noise: 0.5 deg/sec, with up to ± 0.2 g vibration

f. Flow Bypass: Each sensor shall be capable of bypassing up to 0.5 gpm when an appropriate restrictor is installed. This will allow each axis to operate with its optimum flow when all three axes are connected in series.

g. Calibrate Button: A sensor calibrate button shall be used with the capability of inserting a signal equivalent to a step rate of about 5 deg/sec

3.5.2 Amplifiers

Amplifiers shall meet the following performance requirements when supplied with a flow of 0.075 gpm:

a. Input impedance: 80 ohms

b. Output impedance: 80 ohms

c. Gain and load: Requirements for each application are described in Figures 127, 130, and 133.

3.5.3 Servoactuator

The servoactuator shall meet the following performance requirements:

a. Transfer Stage

• P_c quiescent level (above R_c)	4 psig
• ΔP_c (full control signal range)	± 4 psid
• P_c max (above R_c)	10 psig
• R_c max	150 psi

b. Actuator Stage

• System pressure	1500 psi
• Stroke	± 0.38 in.
• Piston area	0.38 in.^{2}

• Output force	570 lb (max)
• Centering force	50 lb
• Threshold	0.4% max
• Rated velocity	15 in./sec, no load
• Dynamic response	90-deg phase lag at 10 Hz (minimum) at 25% rated input
• Hysteresis	2% of full stroke
• Supply proof pressure	4500 psi
• Burst pressure	7500 psi
• Neutral leakage	0.12 gpm
• Effective capacitance	0.0005 in.^{5}/lb

3.6 Performance Under Environmental Test Conditions

The system shall be compensated to minimize changes in performance with variations in temperature or fluid viscosity. Changes of more than ±20 percent in gain or time constant are expected to result in a detectable change in vehicle handling characteristics. It is also expected that the ±20-percent limitation will be exceeded when the fluid temperature is varied from 60°F to 185°F.

3.6.1 Closed-Loop UH-1B, FSAS, and Hardware Interface Simulation

When gain or time constant changes exceed ±20 percent, this effect on system performance can be observed by operating the hardware closed-loop. The computer simulation for this closure is shown in Tables XVII through XX and Figures 137, 138, and 139.

The simulation diagrams show the UH-1B equations of motion in six degrees of freedom and the FSAS and hardware interface. The tables list the potentiometer settings for the aerodynamic coefficients, simulated SAS, hardware interface, and function switch positions.

The function switch positions are divided in two groups:

a. Commands

b. Simulation and hardware switching

For the switches listed under the Command heading, a left engagement of any switch causes the vehicle to be commanded in a positive sense and a right engagement causes the vehicle to be commanded in the negative sense. The nature of the command is specified next to each switch.

TABLE XVII. FUNCTION SWITCH POSITION

Commands	Switch No.	L	C	R
Vertical Gust	00	+	0	-
Lateral Gust	01	+	0	-
Tail Rotor Command	02	+	0	-
Roll Cyclic Command	03	+	0	-
Pitch Cyclic Command	10	+	0	-
Roll Axis Fixed	11	Fixed	Free	Free
Simulation & Hardware				
	12	$\dot{\phi}$ Sim	-	$\dot{\psi}$ Sim
	13	$\dot{\phi}$ Axis	-	$\dot{\psi}$ Axis
	20	$\dot{\phi}$ Sim	-	$\dot{\phi}$ Hardware
	21	$\dot{\psi}$ Hardware	-	$\dot{\psi}$ Sim

TABLE XVIII. POTENTIOMETER ASSIGNMENT SHEET FOR THE UH-1B FSAS

Parameter Description	Setting
$\dot{\phi}$ Scale	
ϕ Servoactuator	
$\dot{\psi}$ Scale	
$\dot{\psi}$ Servoactuator	
θ Scale	
$\dot{\theta}$ Servoactuator	
$w_g/100$	0.1000
$v_g/100$	0.1000
$\delta_{\psi_m}/10$	0.3500
$\delta_{\phi_m}/10$	0.1350
$\delta_{\theta_m}/10$	0.3220
$12n/10^3T$	0.6000
$12n^2/10^5T^2$	0.3000
$6n/10^3T$	0.3000
100 $\dot{\theta}$ Scale	0.5730
100 θ Scale	0.5730
100 B_F Scale	0.5730
100 ψ Scale	0.5730
100 $\dot{\psi}$ Scale	0.5730
100 $\dot{\phi}$ Scale	0.5730
100 ϕ Scale	0.5730
	Roll SAS Simulation
$K_{\dot{\phi}}$	0.0550
$1/T_{HP}$	0.1000
	Yaw SAS Simulation
$K_{\dot{\psi}}$	0.1500
$1/T_{HP}$	0.4000

TABLE XIX. UH-1 LONGITUDINAL-VERTICAL POTENTIOMETER SETTINGS

Parameter Description	Potentiometer Settings			
	Hover (μ=0)	43 kn (μ=0.1)	85.5 kn (μ=0.2)	129 kn (μ=0.3)
$-10\ X_u/m$	0.0600	0.1580	0.2800	0.4160
$+\ X_w/m$	0	0	0.0015	0.0445
$-\ X_w/m$	0.0480	0.0255	0	0
$+\ X_{\dot{\theta}}/100\ m$	0.0002	0.0409	0.0916	0.1524
$-\ X_\theta/100\ m$	0.3222	0.3222	0.3222	0.3222
$-\ X_\beta/100\ m$	0.5400	0.6400	0.5900	0.4000
$-\ X_{\delta_{\theta m}}/100\ m$	0.1050	0.0800	0.0560	0.0360
$+\ 10\ Z_u/m$	0	0	0	0.1900
$-\ 10\ Z_u/m$	0.3150	0.1650	0.0050	0
$-\ Z_w/m$	0.5520	0.6340	0.6580	0.6150
$+\ (U_o+Z_\theta)/m$	0.0015	0	0	0
$+\ Z_{\dot{\theta}}/1000\ m$	0	0.0731	0.1448	0.2157
$-\ Z_\beta/1000\ m$	0	0.0480	0.0950	0.1450
$-\ Z_{\delta_{\theta m}}/1000\ m$	0	0.0480	0.0950	0.1450
$+\ 100\ M_u/I$	0.0570	0.1427	0.2730	0.3750
$+\ 100\ M_w/I$	0.2255	0	0	0
$-\ 10\ M_w/I$	0	0.0725	0.1672	0.2770
$-\ M_{\dot{\theta}}/I$	0.0025	0.2400	0.4950	0.4400
$+\ M_\beta/10\ I$	0.7230	0.8210	0.7220	0.4260
$+\ M_{\delta_{\theta m}}/10\ I$	0.1410	0.0708	0.0029	0
$-\ M_{\delta_{\theta m}}/10\ I$	0	0	0	0.0604
$+\ 100\ \beta_u$	0.4420	0.3930	0.3680	0.3670
$+\ 10\ \dot{\beta}_w$	0	0.0230	0.0480	0.0750
$-\ \beta_\theta/10$	1.025	1.022	1.020	1.019
$-\ \beta_{\dot{\beta}}/10$	0.8900	0.8680	0.8250	0.7350
$+\ \beta_{\delta_{\theta m}}/100$	0.0890	0.0915	0.0950	0.1020

TABLE XX. UH-1 LATERAL-DIRECTIONAL POTENTIOMETER SETTINGS

Parameter Description	Potentiometer Settings			
	Hover (μ=0)	42 kn (μ=0.1)	90 kn (μ=0.2)	121 kn (μ=0.3)
$-Y_v/m$	0.038	0.1100	0.1470	0.1720
$-Y_{\dot{\phi}}/100$ m	0.0161	0.0221	0.0192	0.0166
$+Y_{\phi}/100$ m	0.3220	0.3220	0.3220	0.3220
$+Y_{\dot{\psi}}/100$ m	0.0077	0	0	0
$-Y_{\dot{\psi}}/100$ m	0	0.1004	0.1504	0.2000
$+Y_{\delta_{\phi m}}/100$ in	0.1030	0.0560	0.0540	0.0930
$+Y_{\delta_{\psi}}/100$ m	0.1610	0.2070	0.2300	0.2720
$-10\,L_{\dot{v}}/I_{xx}$	0	0.0820	0.0634	0.0520
$-10\,L_v/I_{xx}$	0.2230	0.3170	0.3760	0.3840
$-L_{\dot{\phi}}/10\,I_{xx}$	0.0987	0.1395	0.1228	0.0984
$+L_{\dot{\psi}}/10\,I_{xx}$	0.0471	0	0	0
$+L_{\delta_{\phi m}}/100\,I_{xx}$	0.6650	0.370	0.3400	0.5800
$+L_{\delta_{\psi}}/100\,I_{xx}$	0.0940	0 1222	0.1358	0.1480
$+10\,N_{\dot{v}}/I_{zz}$	0	0.1232	0.0982	0.0815
$+10\,N_v/I_{zz}$	0.2090	0.3050	0.3860	0.3810
$-N_{\dot{\psi}}/10\,I_{zz}$	0.0679	0	0	0
$-N_{\delta_{\phi m}}/I_{zz}$	0.8960	0.4900	0.4800	0.8300
$-N_{\delta_{\psi}}/100\,I_{zz}$	0.1266	0.1650	0.1828	0.1985

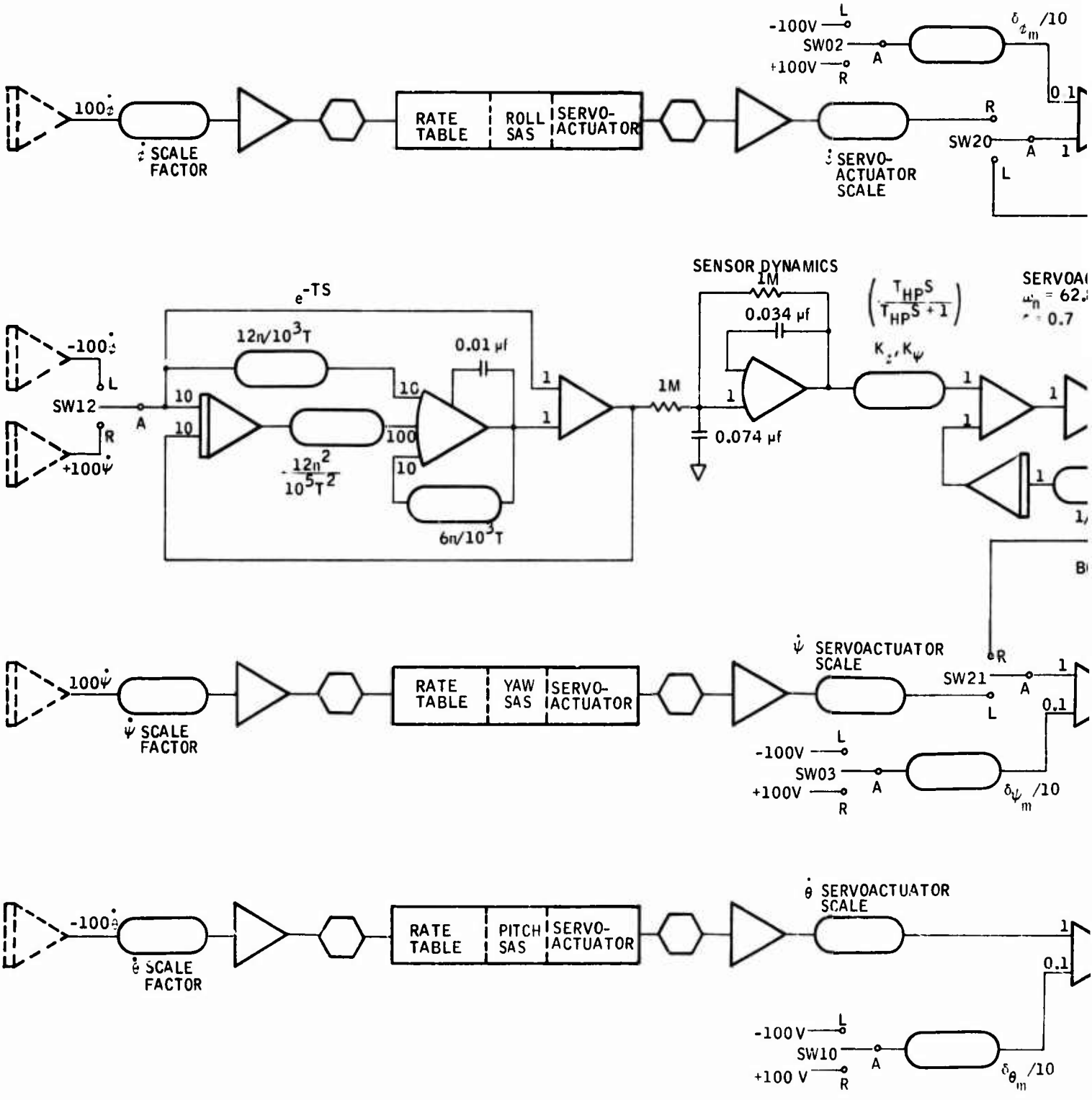

Figure 137. FSAS and Hardware Interface Simulation Diagram (Closed-Loop).

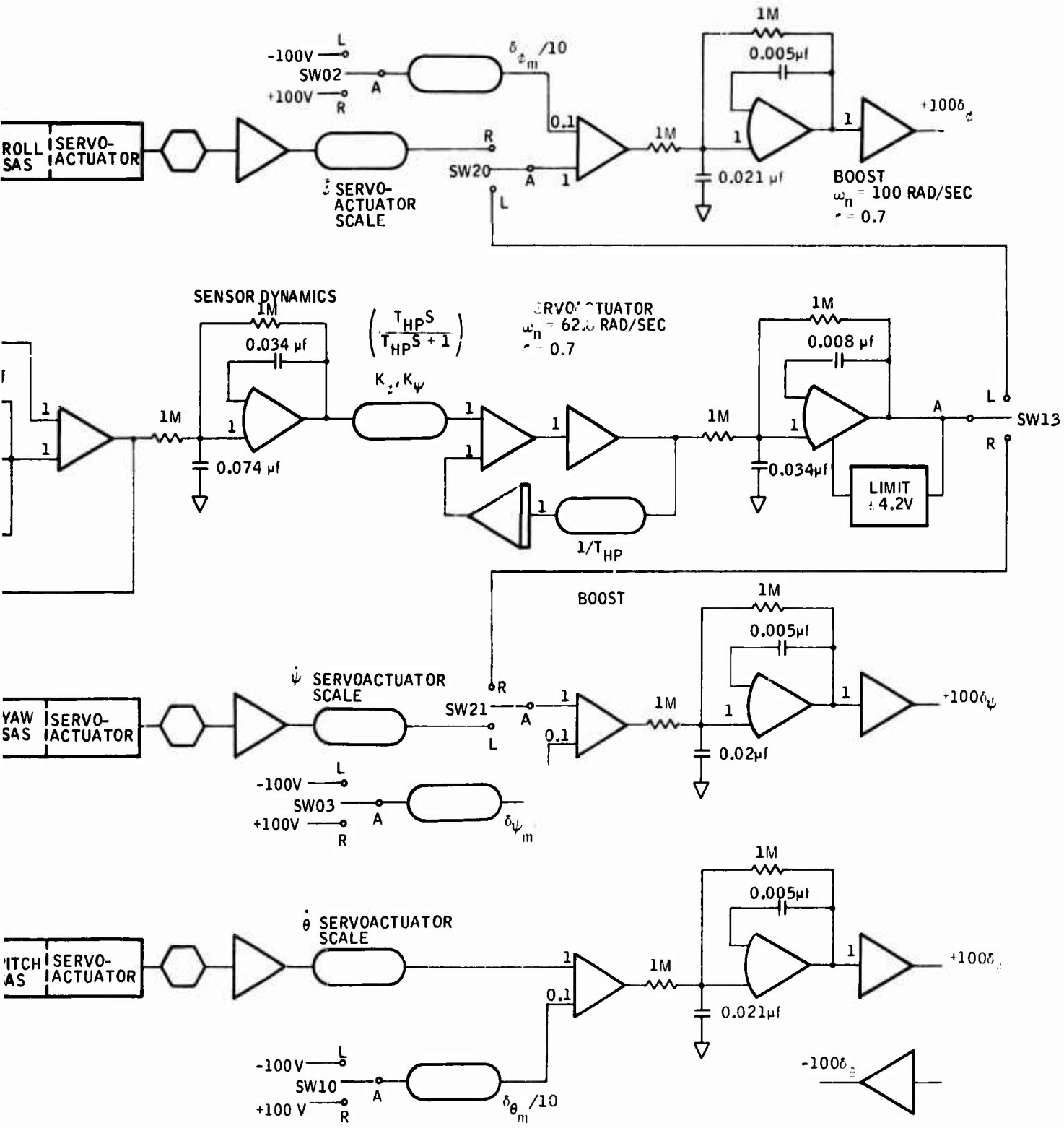

ce Simulation Diagram

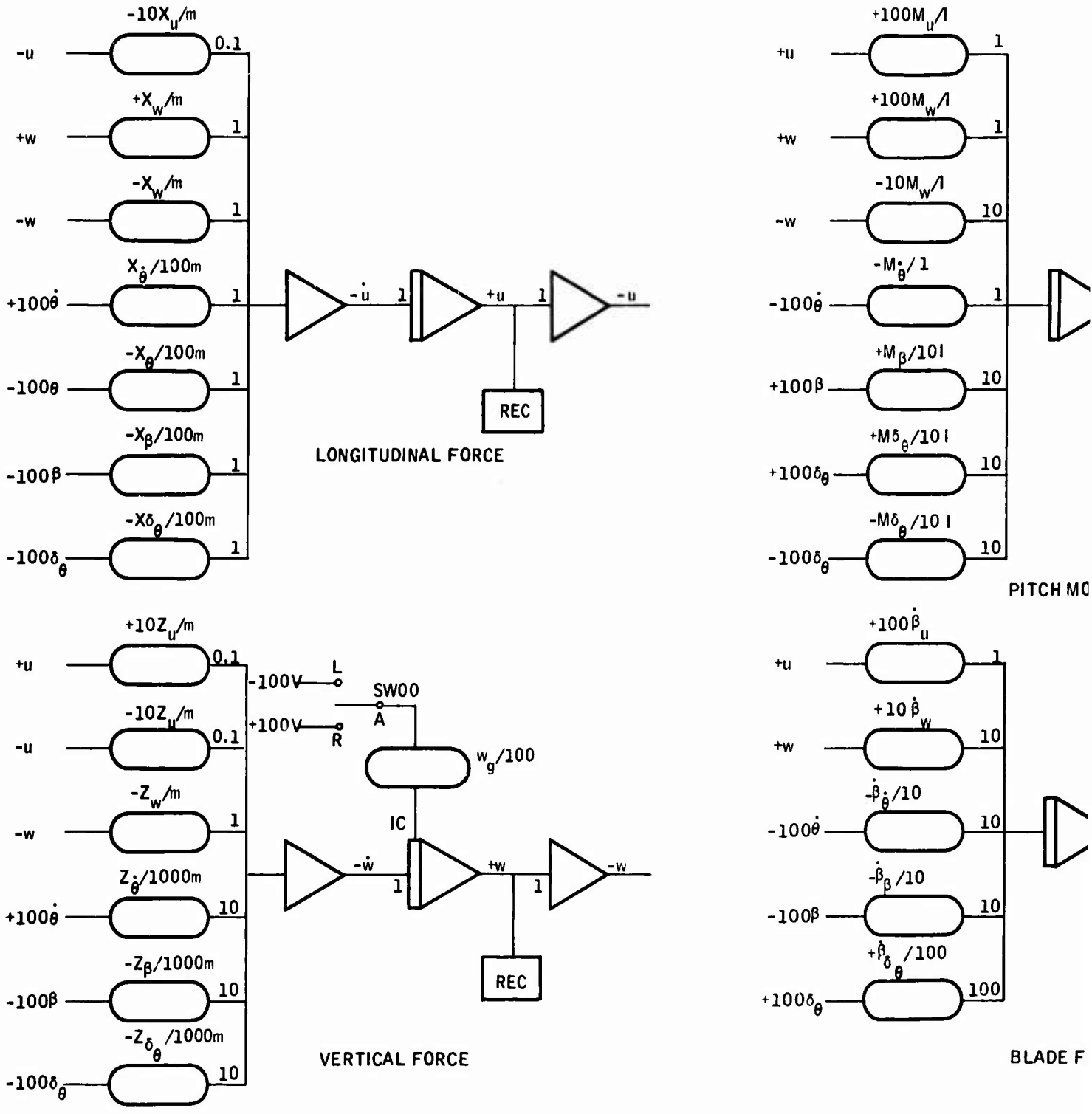

Figure 138. UH-1B Longitudinal-Vertical Plane Simulation Diagram (Closed-Loop).

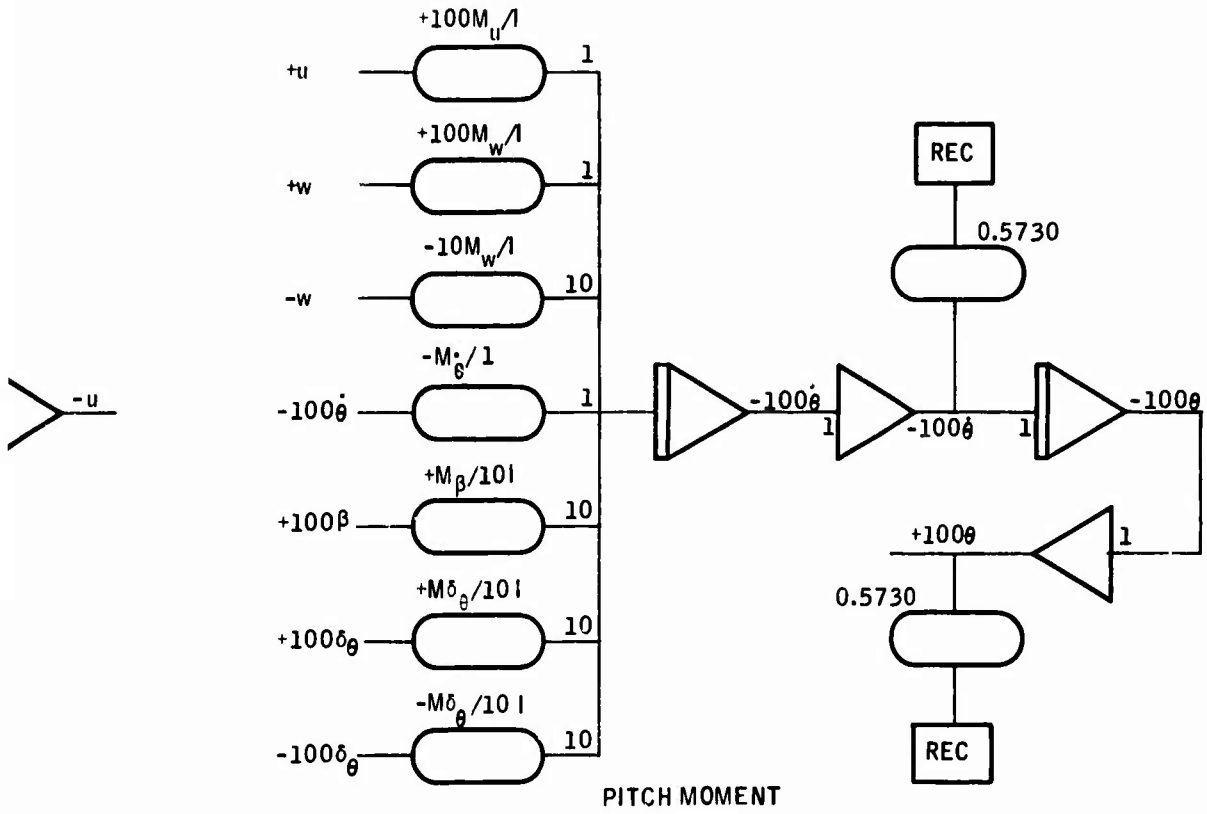

PITCH MOMENT

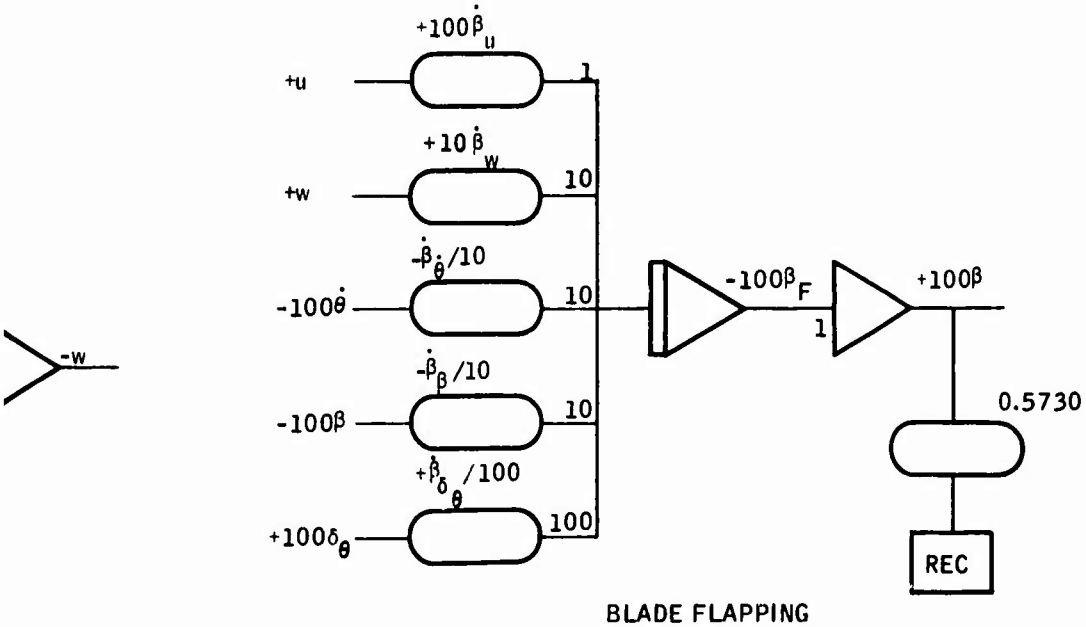

BLADE FLAPPING

ane Simulation Diagram

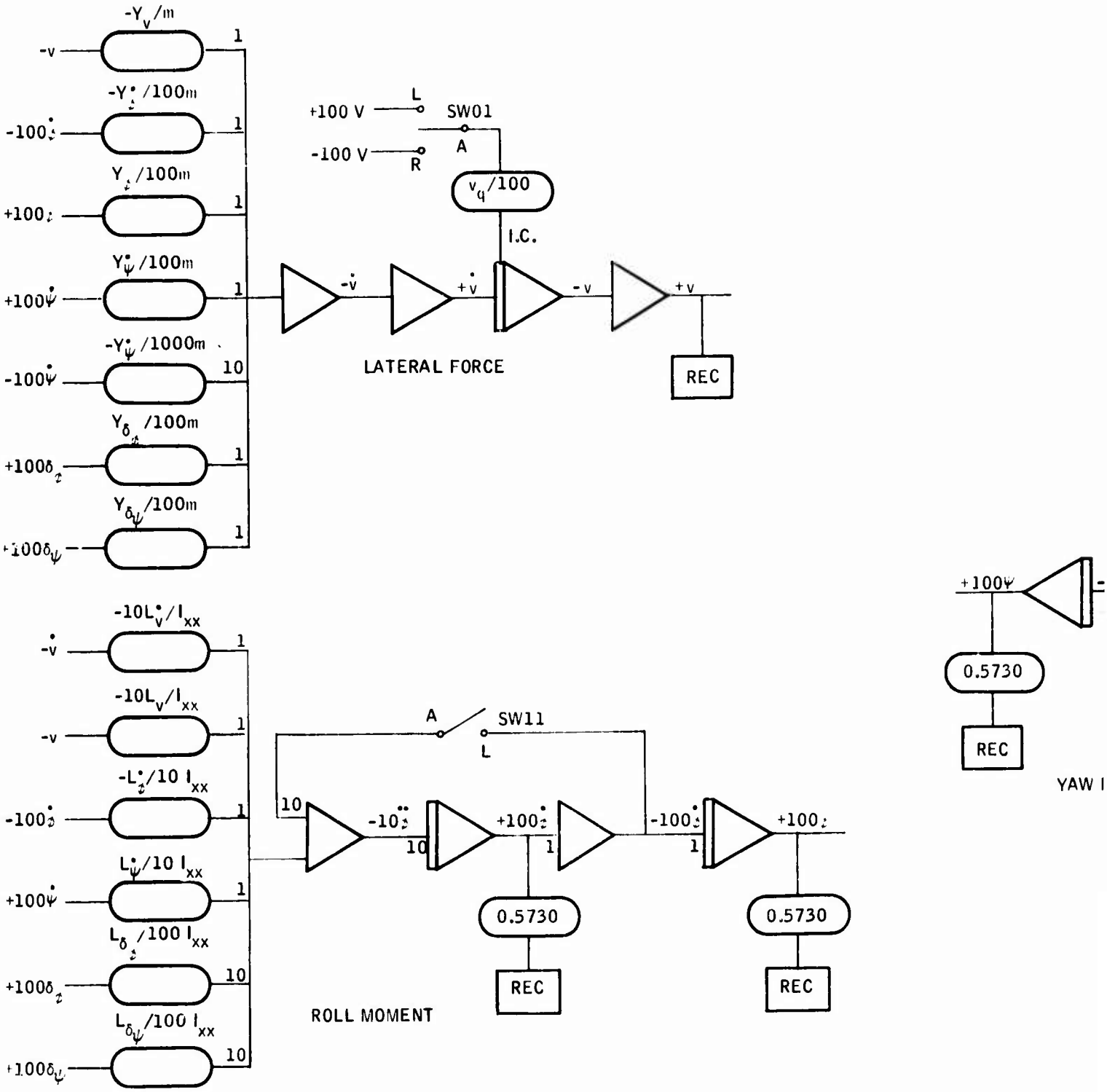

Figure 139. UH-1B Lateral-Directional Plane Simulation Diagram (Closed-Loop).

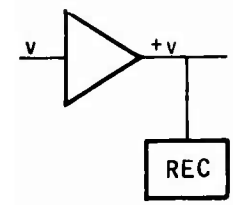

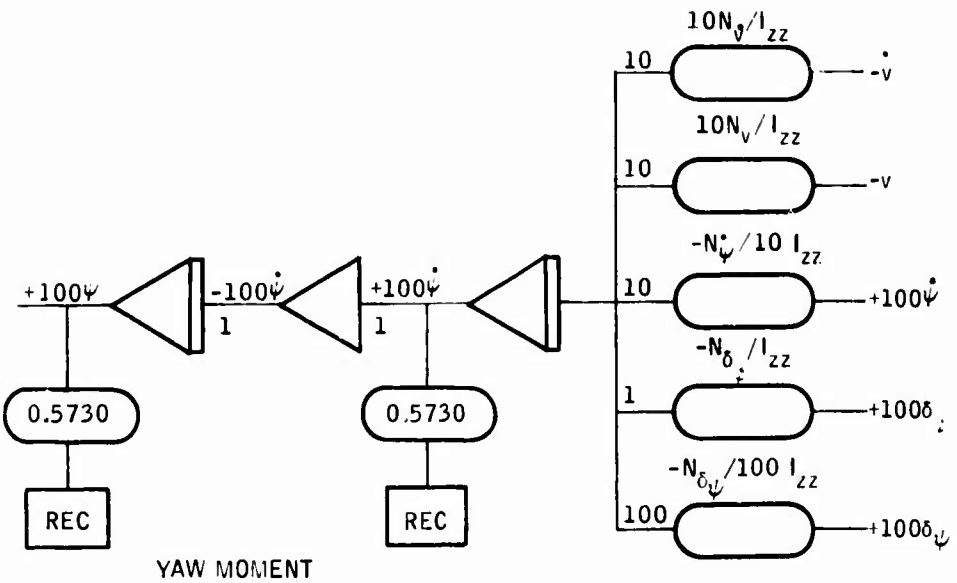

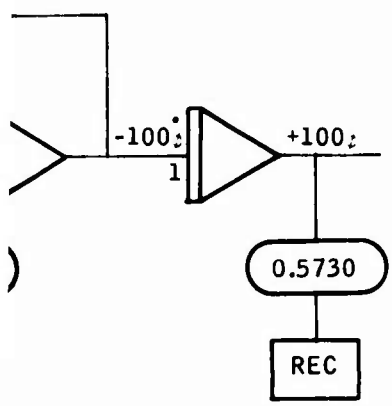

ane Simulation Diagram

The switches listed under the Simulation and Hardware heading cause the simulated roll-axis and yaw-axis hardware to be engaged for a left throw of the switches. A right throw of the switches causes the yaw-axis simulation and roll-axis hardware to be engaged.

3.6.2 Closed-Loop Performance Guidelines

The following guidelines shall be used in evaluating FSAS performance when tested in accordance with the closed-loop system tests specified in Paragraph 4.3:

a. Response Characteristics - The aircraft's response to gust inputs shall be smooth and well-controlled. These characteristics shall be obtained by increasing the damping of the unaugmented vehicle in the pitch and yaw axes. The damping ratio and 90 percent response time of the augmented vehicle for a 10-ft/sec gust input for the flight conditions of interest are as follows:

Axis	Airspeed (kn CAS)	Damping	$T_{90\%}$ (sec)
Pitch	85 to 130	0.5 or greater	1.0 to 1.5
	45	0.5 or greater	2.0 to 2.5
	Hover	0.5 or greater	*
Yaw	90 to 120	0.6 or greater	1.0 to 1.5
	60	0.5 or greater	2.0 to 2.5
	Hover	0.5 or greater	*

*At the hover flight condition, the time to damp the gust may be significantly longer to account for the free-vehicle damping characteristics.

b. Control Effectiveness - The augmented vehicle control effectiveness (steady-state rate response/control stick input during the short term) consistent with good system performance should be approximately as follows.

Axis	Airspeed (kn CAS)	Control Effectiveness
Roll	Hover	24.0 deg/sec/in. δ_ϕ
	60	17.0 deg/sec/in. δ_ϕ
	90	17.0 deg/sec/in. δ_ϕ
	120	20.0 deg/sec/in. δ_ϕ
Yaw	Hover	Should be approximately 22 deg/sec/in. δ_ψ at end of 2 sec
Pitch	Hover	7.5 deg/sec at the end of 2 sec
	45	5.0 deg/sec/in. δ_θ
	85	4.5 deg/sec/in. δ_θ
	130	3.0 deg/sec/in. δ_θ

The time to achieve 90 percent of the steady-state rate for the above control effectiveness shall be between 0.3 to 0.8 sec.

c. Control Power - Control power shall be such that when the helicopter is hovering, a rapid 1-inch step displacement from trim of the controls shall produce an angular displacement at the end of 1 sec as follows:

Axis	Angular Displacement (deg)
Yaw, pedal input	$\psi = 5.9$
Roll, cyclic input	$\phi = 1.45$
Pitch, cyclic input	$\theta = 2.43$

3.7 Product Configuration

Figure 136 (Dwg. No. 10027822) defines the overall installation of the system. Servoactuator size limitations are defined in Figure 140 (Dwg No. 10027825). The yaw-axis servoactuator will be the same size as the roll-axis servoactuator. No problem in fitting it into the available space in the aircraft is foreseen. The pitch- and roll-axis servoactuators are the limiting units.

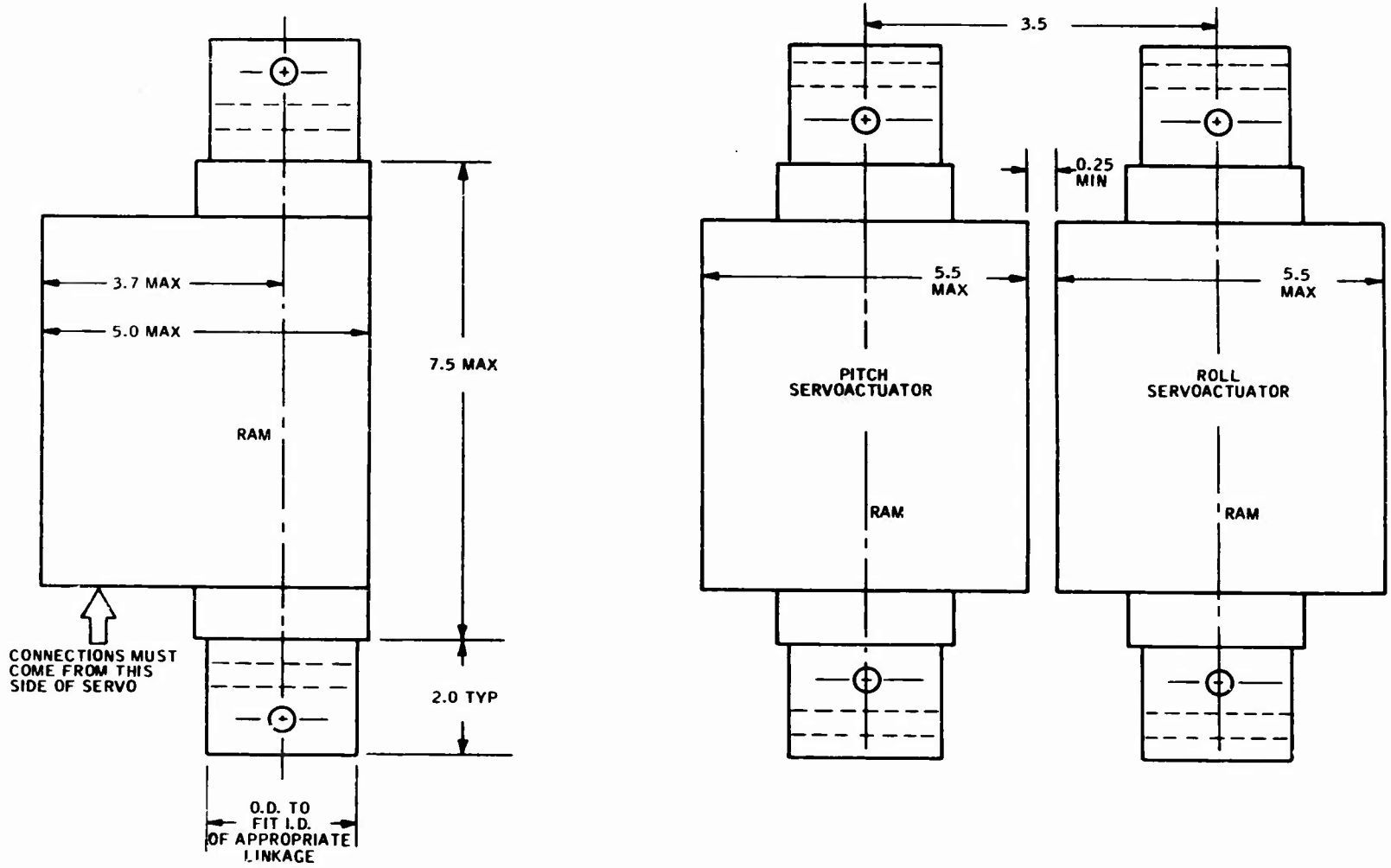

Figure 140. Allowable Envelope of Servoactuators for Hydraulic SAS (Dwg. No. 10027825).

4.0 QUALITY ASSURANCE

Conformance of the hardware to program objective shall be evaluated with the following tests. Vibration tests must be completed before performance tests are conducted.

4.1 Vibration

A vibration scan with the three-axis FSAS energized and operating shall be conducted at the amplitudes and frequencies of Figure 514-2, Curve A, of MIL-STD-810A. A sinusoidal vibration cycling, per the test envelope, shall be conducted at a rate sufficiently slow to allow adequate identification and evaluation of the resonant frequency(s) or functional phenomena that may occur. Sinusoidal vibration cycle times shall be not less than 15 minutes per each of the three axes. Three-axis FSAS vibration testing shall be conducted with the hydraulic supply and connections simulating the actual aircraft installation as nearly as practicable.

Performance under 0.2-g vibration shall conform to noise limitations of Paragraph 3.4.7.

4.2 Open-Loop Tests

Conformance to dynamic range requirements of Paragraph 3.4.5 shall be determined by imposing rates of ± 40 deg/sec and measuring output of the appropriate stage amplifier of each axis, as follows:

1. Pitch-axis gain and response requirements shall be determined by measuring system output at 0.02, 0.4, 4.0 and 10 Hz. Amplitudes of ± 1 deg/sec and + 5 deg/sec shall be used. Response shall be measured with fluid temperatures of 60°F, 120°F, and 185°F. Results are to be compared with the temperature requirements of 3.2.2, the response requirements of 3.4.1 (as plotted on Figure 141), and the linearity requirements of 3.4.6.

2. Repeat above with roll axis. Results are to be compared with the requirements of 3.2.2, 3.4.2 (as plotted on Figure 142), and 3.4.6.

3. Repeat above with yaw axis. Results are to be compared to 3.2.2, 3.4.3 (as plotted on Figure 143), and 3.4.6.

4. With a test adapter plate installed on the yaw-axis package, determine that rudder input device meets the requirements of 3.2.2, 3.4.3 (as plotted on Figure 144), and 3.4.6.

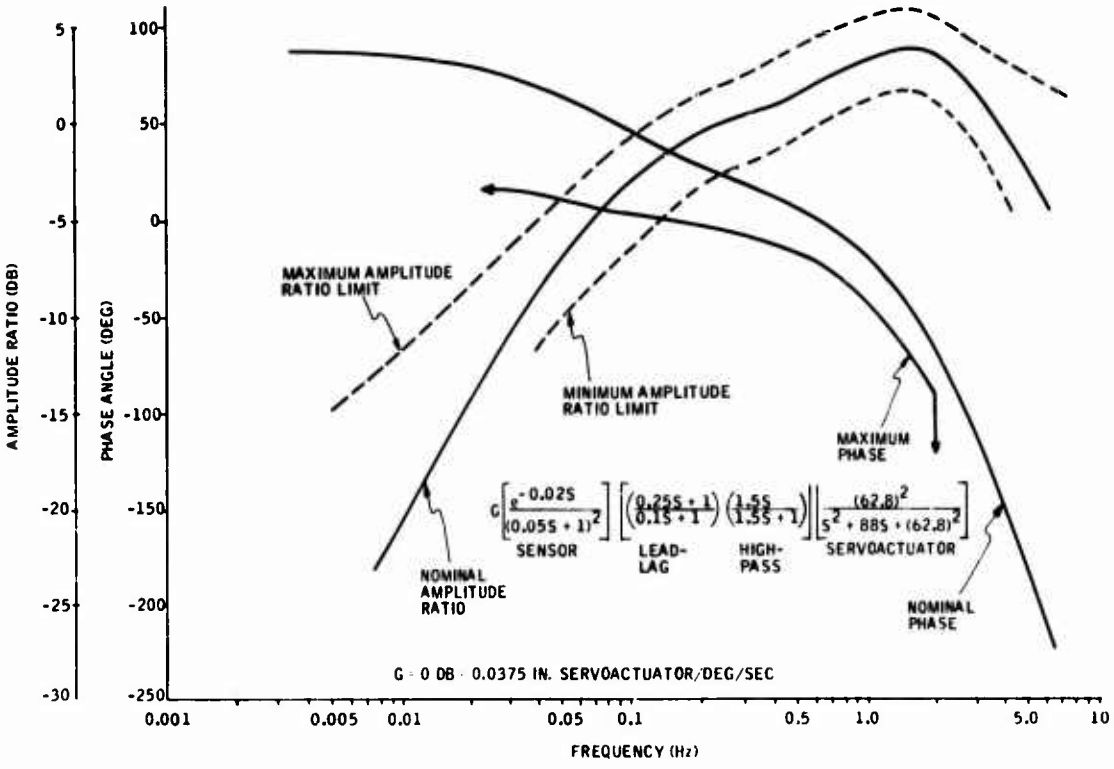

Figure 141. Pitch-Axis Response Requirements.

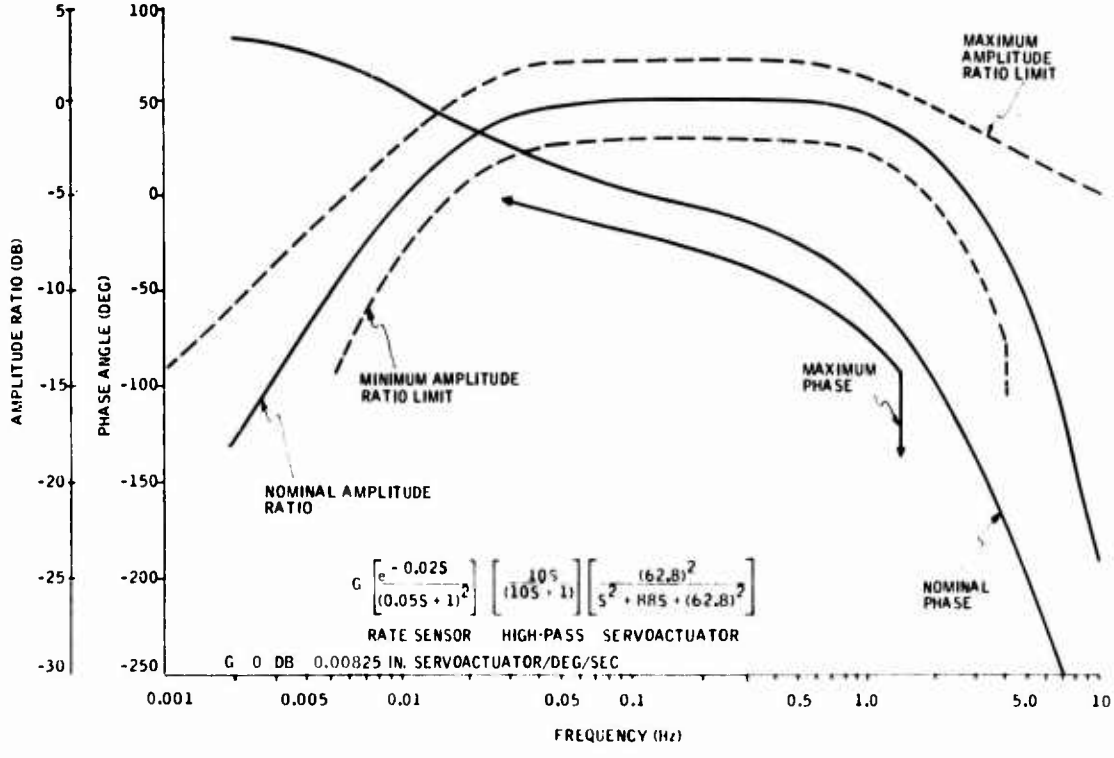

Figure 142. Roll-Axis Response Requirements.

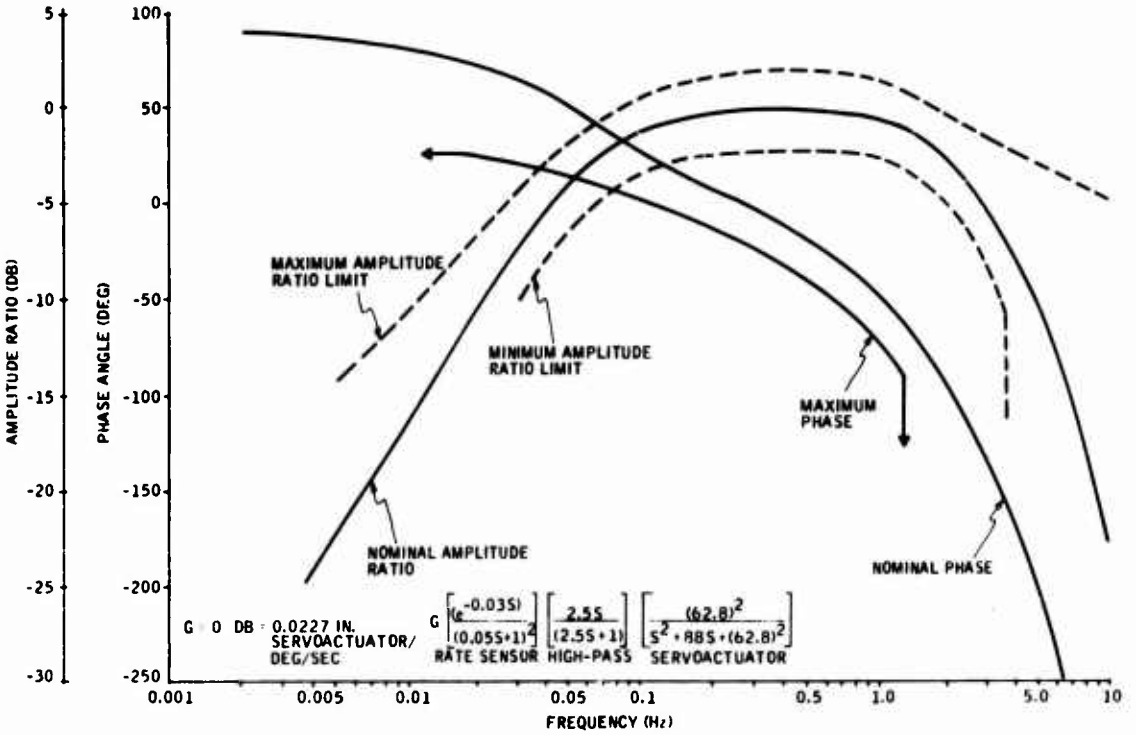

Figure 143. Yaw-Axis Response Requirements.

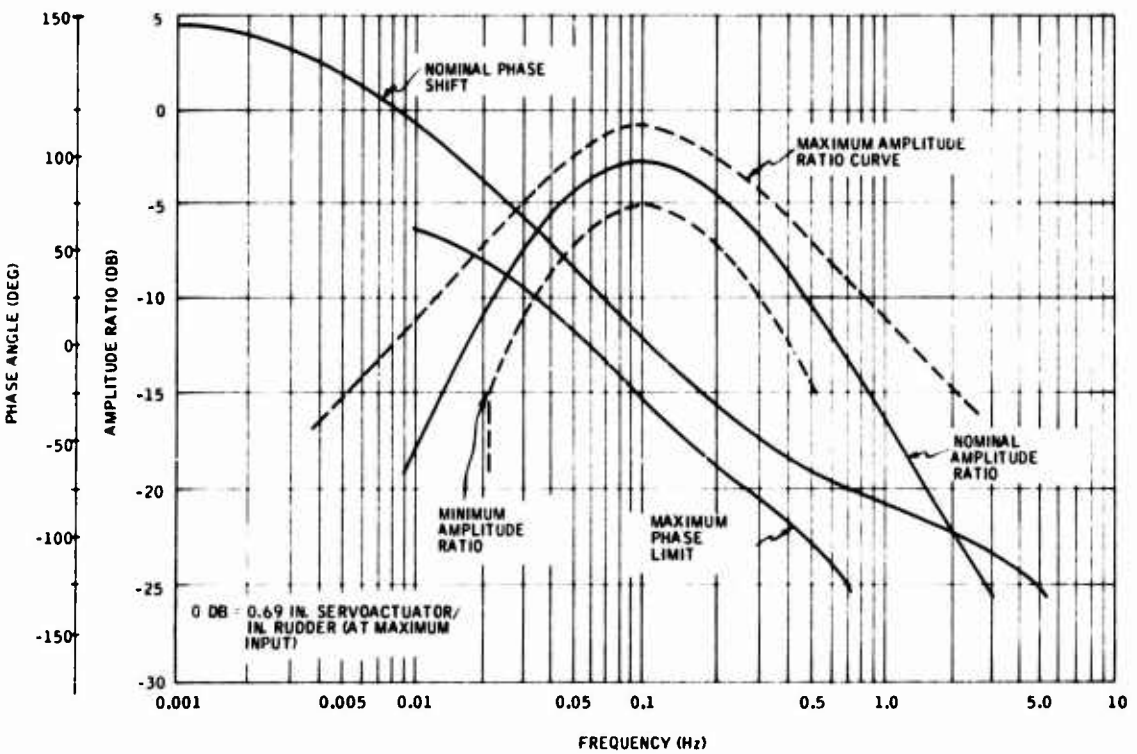

Figure 144. Rudder Input Response Requirements.

4.3 Closed-Loop Tests

The system, mounted on a computer-controlled rate table and operating with flight test regulators, shall be operated closed-loop, with an analog computer simulating the aircraft, as follows:

1. Determine conformance to Paragraph 3.6, with a fluid temperature of 60°F and a room temperature of ambient.

2. Repeat with fluid at 120°F.

3. Repeat with fluid at 185°F.

4. With the rate table "off" on the above three conditions, the noise shall meet the requirements of Paragraph 3.4.7.

4.4 Verification

1. Inspect systems for quality of workmanship and conformance to installation drawings.

2. Determine that system contains all features described in Paragraph 3.7.

3. Establish that power required does not exceed amount specified in Paragraph 3.3.

APPENDIX II
FLIGHTWORTHINESS REPORT* FOR THE THREE-AXIS HYDROFLUIDIC STABILITY AUGMENTATION SYSTEM FOR THE UH-1B HELICOPTER

1.0 ABSTRACT

1.1 Object

To determine flightworthiness of the three-axis hydrofluidic stability augmentation system for the UH-1B helicopter. Test per Detailed Test Plan No. 21192-034.

1.2 Conclusions

The unit was tested in accordance with the referenced test plan and is considered to be flightworthy for the following reasons: (1) the controllers were pressure-tested to 2250 psi without failure; (2) the entire system was vibrated at working pressure without failure or excessive leakage.

Closed-loop tests are considered to be the only critical performance parameters (see paragraph 3.4.1 of the Detailed Test Plan). [The closed-loop performance is summarized in Section V, "Closed-Loop Acceptance Testing," of the main text.]

2.0 UNIT TESTED

One YG1053A01 Three-Axis Hydrofluidic Stability Augmentation System, consisting of three fluidic rate controllers and three servo-actuators, P/N 85112010.

3.0 REFERENCE DOCUMENTS

Detailed Test Plan No. 21192-034
Detailed Specification No. 21565-01
Memo, P.J. Ekstrom to R.A. Evans, dated 27 July 1970

4.0 PROCEDURES AND RESULTS

The three controllers were received from the Honeywell Aero Model Shop and tested with 2250 psi static pressure. It was necessary to

*Honeywell Aero Engineering Test Report No. AEX-53737, dated August 1970.

increase the thickness of the cover plates on the rate sensor and high-pass sections. All three controllers (yaw, pitch, and roll) passed the pressure test.

The entire system was assembled using the spool valve servoactuators. See Figure 145 for the schematic of the system and Figure 146 for an overall view of the system. The complete package is mounted on a 24-in. -diameter mount that was attached to a rate table. Hydraulic flow was supplied through a temperature control unit. The flow controller and pressure relief valves were set for the correct supply flow and pressure. It was necessary to bleed the air from the servoactuators to obtain correct system operation.

A function generator was used to drive the rate table that furnished the input to the system. Sine wave inputs of 2 deg/sec peak-to-peak were applied to the system after the system temperature had stabilized at 120°F. The output motion of all three servoactuators was recorded while the system was driven at various frequencies. The input was increased to 5 deg/sec as per paragraphs 7. 1. 1 to 7. 1. 5 of the Detailed Test Plan. The results are presented in Tables XXI through XXIV.

System temperature was increased to 180°F, and the entire test sequence was repeated. Results are presented in Tables XXV through XXVIII. System temperature was then decreased to 60°F, and the test sequence was repeated. Results are presented in Tables XXIX through XXXII.

The entire system, including the mounting base, was moved to the vibration test area. The unit was vibrated per paragraph 7. 2 of the Detailed Test Plan. During vibration, the system did not develop any leaks. It was necessary to tie some of the signal lines to the base and to each other to prevent them from resonating. The lines will be tied down in the aircraft installation. Some null shifts occurred during vibration, but disappeared when the vibration level was reduced per paragraph 7. 2. 2 of the Detailed Test Plan.

The system was remounted on the rate table and post-vibration frequency response was performed per paragraph 8. 1 of the Detailed Test Plan. Results are presented in Tables XXXIII through XXXV. The response at ±1 deg/sec was not repeated.

Closed-loop tests were conducted per paragraph 9. 0 of the Detailed Test Plan. A Pace analog computer was used to simulate the helicopter dynamics during the closed-loop tests. [Results of the closed-loop tests and flightworthiness conclusions are covered in Section V, "Closed-Loop Acceptance Testing," of the main text.]

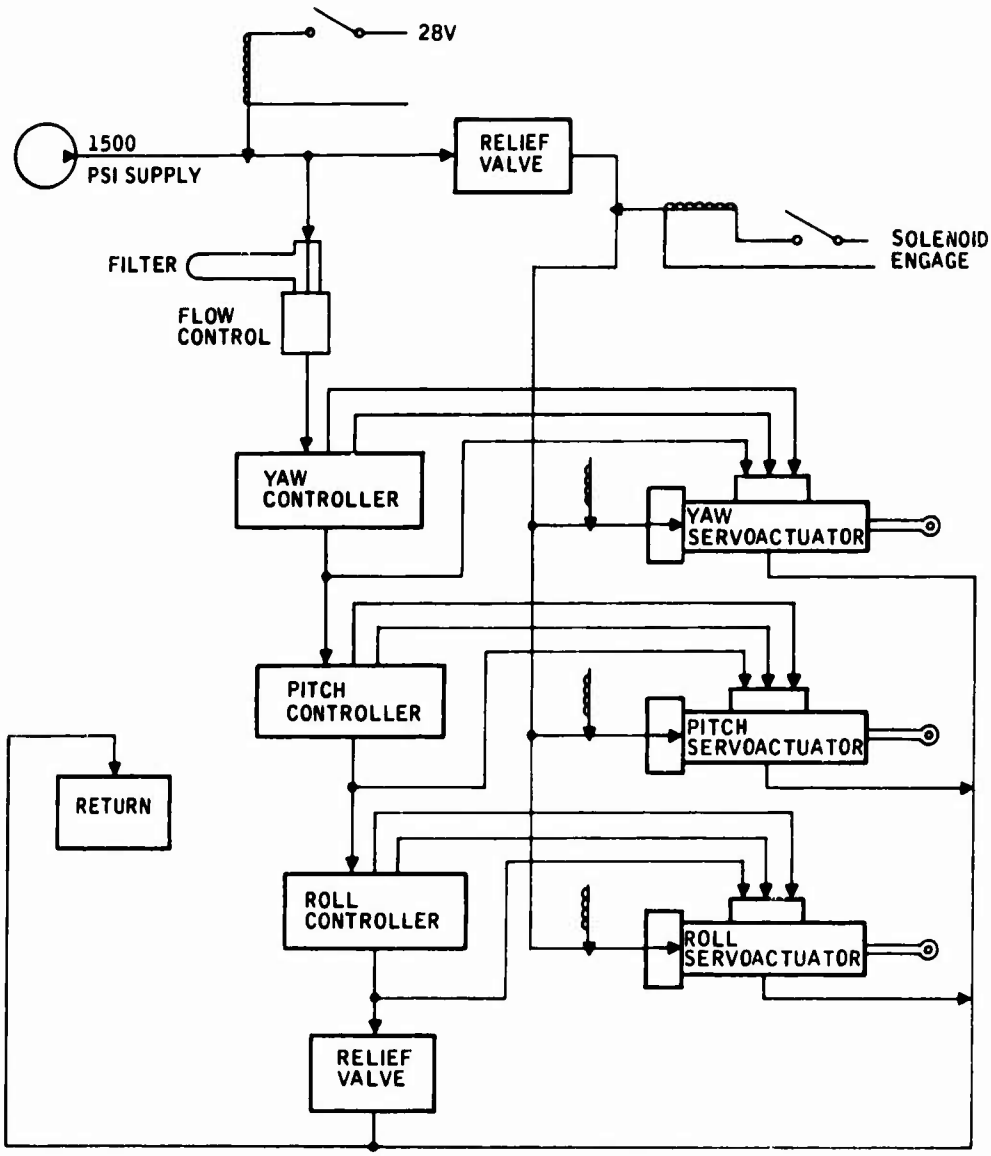

Figure 145. System Schematic.

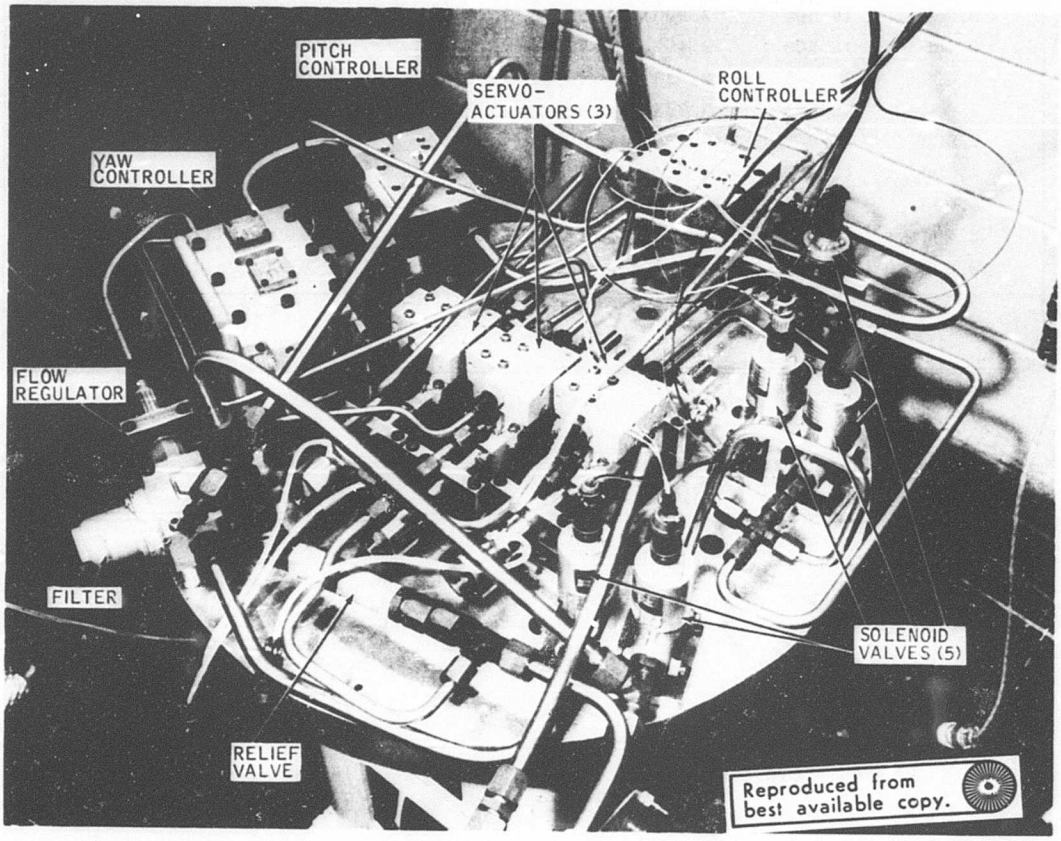

Figure 146. Three-Axis Hydrofluidic SAS.

TABLE XXI. PITCH AXIS -- TEMPERATURE = 120°F

±1-Deg/Sec Input				±2.5-Deg/Sec Input			
Frequency (Hz)	Amplitude* (mm)	Ratio	Decibels	Frequency (Hz)	Amplitude** (mm)	Ratio	Decibels
0.020	2.500	0.333	-9.542	0.020	5.000	0.267	-11.481
0.040	5.000	0.667	-3.522	0.040	12.500	0.667	-3.522
0.060	8.000	1.067	0.561	0.060	19.000	1.013	0.115
0.100	11.000	1.467	3.327	0.100	26.500	1.413	3.005
0.250	16.500	2.200	6.848	0.250	39.500	2.107	6.472
0.400	18.500	2.467	7.842	0.400	45.000	2.400	7.604
0.600	20.500	2.733	8.734	0.600	50.000	2.667	8.519
1.000	28.000	3.733	11.442	1.000	61.000	3.253	10.247
2.000	33.000	4.400	12.869	2.000	78.000	4.160	12.382
4.000	42.000	5.600	14.964	4.000	80.000	4.267	12.602
6.000	27.000	3.600	11.126	6.000	66.000	3.520	10.931
8.000	13.000	1.733	4.778	8.000	38.000	2.027	6.136
10.000	8.000	1.067	0.561	10.000	18.000	0.960	-0.355

*Ref. 7.500 mm
**Ref. 18.750 mm

TABLE XXII. ROLL AXIS -- TEMPERATURE = 120°F

±1-Deg/Sec Input				±2.5-Deg/Sec Input			
Frequency (Hz)	Amplitude* (mm)	Ratio	Decibels	Frequency (Hz)	Amplitude** (mm)	Ratio	Decibels
0.020	3.500	0.848	-1.427	0.020	8.000	0.776	-2.203
0.040	4.000	0.970	-0.267	0.040	10.000	0.970	-0.265
0.060	4.500	1.091	0.756	0.060	10.000	0.970	-0.265
0.100	4.500	1.091	0.756	0.100	10.500	1.018	0.159
0.250	5.000	1.212	1.671	0.250	10.500	1.018	0.159
0.400	5.000	1.212	1.671	0.400	11.000	1.067	0.563
0.600	5.000	1.212	1.671	0.600	11.000	1.067	0.563
1.000	5.000	1.212	1.671	1.000	11.500	1.115	0.949
2.000	5.000	1.212	1.671	2.000	13.000	1.261	2.014
4.000	7.000	1.697	4.593	4.000	16.000	1.552	3.817
6.000	9.000	2.182	6.776	6.000	16.000	1.552	3.817
8.000	4.500	1.091	0.756	8.000	9.500	0.921	-0.711
				10.000	4.000	0.388	-8.224

*Ref. 4.125 mm
**Ref. 10.310 mm

TABLE XXIII. YAW AXIS -- TEMPERATURE = 120°F

±1-Deg/Sec Input				±2.5-Deg/Sec Input			
Frequency (Hz)	Amplitude* (mm)	Ratio	Decibels	Frequency (Hz)	Amplitude** (mm)	Ratio	Decibels
0.020	3.000	0.264	-11.557	0.020	5.000	0.176	-15.079
0.040	6.500	0.573	-4.842	0.040	11.000	0.388	-8.231
0.060	7.000	0.617	-4.198	0.060	15.000	0.529	-5.537
0.100	9.000	0.793	-2.01	0.100	20.000	0.705	-3.038
0.250	12.000	1.057	0.484	0.250	24.000	0.846	-1.454
0.400	13.000	1.145	1.179	0.400	25.000	0.881	-1.100
0.600	13.000	1.145	1.179	0.600	26.500	0.934	-0.594
1.000	15.000	1.322	2.422	1.000	29.000	1.022	0.189
2.000	18.000	1.586	4.006	2.000	31.000	1.093	0.769
4.000	22.000	1.938	5.749	4.000	45.000	1.586	4.006
6.000	21.000	1.850	5.344	6.000	35.000	1.233	1.823
8.000	10.000	0.881	-1.100	8.000	17.000	0.599	-4.450
				10.000	7.500	0.264	-11.557

*Ref. 11.350 mm
**Ref. 28.375 mm

TABLE XXIV. RUDDER INPUT DEVICE-- ±0.004-IN. INPUT AT 120°F

Frequency (Hz)	Amplitude (mm)	Ratio	Decibels
0.010	5.500	0.149	-16.557
0.027	13.500	0.365	-8.757
0.064	23.000	0.622	-4.129
0.080	25.000	0.676	-3.405
0.139	28.000	0.757	-2.421
0.357	26.000	0.703	-3.065
0.769	18.000	0.486	-6.259
1.064	13.000	0.351	-9.085
2.857	7.000	0.189	-14.462
3.571	6.000	0.162	-15.801
6.124	5.400	0.146	-16.716

*Ref. 37.000 mm

TABLE XXV. PITCH AXIS -- TEMPERATURE = 180°F

±1-Deg/Sec Input				±2.5-Deg/Sec Input			
Frequency (Hz)	Amplitude* (mm)	Ratio	Decibels	Frequency (Hz)	Amplitude** (mm)	Ratio	Decibels
0.250	20.000	2.667	8.519	0.020	5.000	0.267	-11.481
0.400	23.000	3.067	9.733	0.040	6.000	0.320	-9.897
0.600	25.000	3.333	10.458	0.060	9.000	0.480	-6.375
1.000	28.000	3.733	11.442	0.100	10.000	0.533	-5.460
2.000	45.000	6.000	15.563	0.250	11.500	0.613	-4.246
4.000	35.000	4.667	13.380	0.400	19.500	1.040	0.341
6.000	27.000	3.600	11.126	0.600	20.000	1.067	0.561
8.000	10.000	1.333	2.499	1.000	28.000	1.493	3.483
10.000	5.000	0.667	-3.522	2.000	33.000	1.760	4.910
				4.000	35.000	1.867	5.421
				6.000	27.000	1.440	3.167
				8.000	15.000	0.800	-1.938
				10.000	10.000	0.533	-5.460

*Ref. 7.500 mm

**Ref. 18.750 mm

TABLE XXVI. ROLL AXIS -- TEMPERATURE = 180°F

±1-Deg/Sec Input				±2.5-Deg/Sec Input			
Frequency (Hz)	Amplitude* (mm)	Ratio	Decibels	Frequency (Hz)	Amplitude* (mm)	Ratio	Decibels
0.020	3.000	0.727	-2.766	0.020	3.000	0.727	-2.766
0.040	4.000	0.970	-0.267	0.040	3.000	0.727	-2.766
0.060	5.000	1.212	1.671	0.060	3.500	0.848	-1.427
0.100	5.000	1.212	1.671	0.100	3.500	0.848	-1.427
0.250	5.000	1.212	1.671	0.250	3.500	0.848	-1.427
0.400	4.500	1.091	0.756	0.400	4.000	0.970	-0.267
0.600	5.000	1.212	1.671	0.600	4.000	0.970	-0.267
1.000	5.000	1.212	1.671	1.000	4.000	0.970	-0.267
2.000	5.000	1.212	1.671	2.000	3.500	0.848	-1.427
4.000	5.000	1.212	1.671	4.000	4.000	0.970	-0.267
6.000	7.000	1.697	4.593	6.000	5.000	1.212	1.671
				8.000	3.000	0.727	-2.766
				10.000	1.500	0.364	-8.787

*Ref. 4.125 mm

TABLE XXVII. YAW AXIS -- TEMPERATURE = 180°F

±1-Deg/Sec Input				±2.5-Deg/Sec Input			
Frequency (Hz)	Amplitude* (mm)	Ratio	Decibels	Frequency (Hz)	Amplitude* (mm)	Ratio	Decibels
0.020	5.000	0.441	-7.121	0.020	2.000	0.176	-15.079
0.040	6.000	0.529	-5.537	0.040	3.500	0.308	-10.219
0.060	7.500	0.661	-3.599	0.060	5.000	0.441	-7.121
0.100	8.000	0.705	-3.038	0.100	6.500	0.573	-4.842
0.250	11.000	0.969	-0.272	0.250	8.000	0.705	-3.038
0.400	10.000	0.881	-1.100	0.400	9.000	0.793	-2.015
0.600	14.000	1.233	1.823	0.600	9.000	0.793	-2.015
1.000	13.000	1.145	1.179	1.000	10.000	0.881	-1.100
2.000	15.000	1.322	2.422	2.000	10.000	0.881	-1.100
4.000	21.000	1.850	5.344	4.000	13.500	1.189	1.507
6.000	21.000	1.850	5.344	6.000	11.000	0.969	-0.272
8.000	6.000	0.529	-5.537	8.000	6.000	0.529	-5.537
				10.000	2.000	0.176	-15.079

*Ref. 11.350 mm

TABLE XXVIII. RUDDER INPUT DEVICE--±0.04-IN. INPUT AT 180°F

Frequency (Hz)	Amplitude* (mm)	Ratio	Decibels
0.011	7.500	0.203	-13.863
0.058	16.500	0.446	-7.014
0.202	21.000	0.568	-4.920
0.367	21.000	0.568	-4.920
0.735	15.000	0.405	-7.842
1.760	7.500	0.203	-13.863
3.520	5.000	0.135	-17.385
6.250	5.000	0.135	-17.385

* Ref. 37.000 mm

TABLE XXIX. PITCH AXIS -- TEMPERATURE = 60°F

±1-Deg/Sec Input				±2.5-Deg/Sec Input			
Frequency (Hz)	Amplitude* (mm)	Ratio	Decibels	Frequency (Hz)	Amplitude* (mm)	Ratio	Decibels
0.020	1.000	0.053	-25.460	0.020	1.000	0.053	-25.460
0.040	2.500	0.133	-17.501	0.040	2.000	0.107	-19.439
0.060	4.000	0.213	-13.419	0.060	3.500	0.187	-14.579
0.100	5.000	0.267	-11.481	0.100	5.000	0.267	-11.481
0.250	7.000	0.373	-8.558	0.250	7.000	0.373	-8.558
0.400	9.000	0.480	-6.375	0.400	8.000	0.427	-7.398
0.600	10.000	0.533	-5.460	0.600	9.000	0.480	-6.375
0.800	12.000	0.640	-3.876	1.000	12.000	0.640	-3.876
1.000	13.000	0.693	-3.181	2.000	18.000	0.960	-0.355
2.000	19.000	1.013	0.115	4.000	23.000	1.227	1.775
4.000	28.000	1.493	3.483	8.000	7.000	0.373	-8.558
6.000	15.000	0.800	-1.938	10.000	3.000	0.160	-15.918
8.000	7.000	0.373	-8.558				

*Ref. 18.750 mm

TABLE XXX. ROLL AXIS -- TEMPERATURE = 60°F

±1-Deg/Sec Input				±2.5-Deg/Sec Input			
Frequency (Hz)	Amplitude* (mm)	Ratio	Decibels	Frequency (Hz)	Amplitude** (mm)	Ratio	Decibels
0.020	3.500	0.424	-7.448	0.020	4.000	0.389	-8.205
0.040	4.500	0.545	-5.265	0.040	5.000	0.486	-6.266
0.060	5.000	0.606	-4.350	0.060	6.000	0.583	-4.683
0.100	5.000	0.606	-4.350	0.100	6.000	0.583	-4.683
0.250	5.500	0.667	-3.522	0.250	6.000	0.583	-4.683
0.400	5.000	0.606	-4.350	0.400	7.000	0.680	-3.344
0.600	6.000	0.727	-2.766	0.600	7.000	0.680	-3.344
0.800	6.000	0.727	-2.766	1.000	7.000	0.680	-3.344
1.000	6.000	0.727	-2.766	2.000	8.000	0.778	-2.184
2.000	7.000	0.848	-1.427	4.000	10.000	0.972	-0.246
4.000	9.000	1.019	0.756	6.000	11.000	1.069	0.582
6.000	7.000	0.848	-1.427	8.000	5.000	0.486	-6.266
				10.000	0.500	0.049	-26.266

*Ref. 8.250 mm

**Ref. 10.287 mm

TABLE XXXI. YAW AXIS -- TEMPERATURE = 60°F

±1-Deg/Sec Input				±2.5-Deg/Sec Input			
Frequency (Hz)	Amplitude* (mm)	Ratio	Decibels	Frequency (Hz)	Amplitude** (mm)	Ratio	Decibels
0.020	0.500	0.044	-27.121	0.020	2.500	0.038	-21.100
0.040	2.000	0.176	-15.079	0.040	5.500	0.194	-14.251
0.060	3.000	0.264	-11.557	0.060	7.000	0.247	-12.157
0.100	4.000	0.352	-9.059	0.100	9.000	0.317	-9.974
0.250	5.000	0.441	-7.121	0.250	11.000	0.388	-8.231
0.400	5.000	0.441	-7.121	0.400	12.000	0.423	-7.475
0.600	5.500	0.485	-6.293	0.600	12.000	0.423	-7.475
0.800	6.000	0.529	-5.537	1.000	12.000	0.423	-7.475
1.000	6.500	0.573	-4.842	2.000	16.000	0.564	-4.976
2.000	6.500	0.573	-4.842	4.000	22.000	0.775	-2.210
4.000	10.000	0.881	-1.[illegible]0	6.000	24.000	0.846	-1.454
6.000	10.000	0.881	[illegible]	8.000	7.500	0.264	-11.557
				10.000	1.500	0.053	-25.537

*Ref. 11.350 mm

**Ref. 28.375 mm

TABLE XXXII. RUDDER INPUT DEVICE -- ±0.04-IN. INPUT AT 60°F

Frequency (Hz)	Amplitude* (mm)	Ratio	Decibels
0.014	4.000	0.043	-27.272
0.074	11.500	0.124	-18.099
0.139	12.500	0.135	-17.375
0.400	10.500	0.114	-18.890
0.769	8.000	0.087	-21.252
1.087	7.500	0.081	-21.812
2.083	4.500	0.049	-26.249
3.330	4.500	0.049	-26.249
3.571	4.500	0.049	-26.249

*Ref. 92.400 mm

TABLE XXXIII. PITCH AXIS -- ±2.5-DEG/SEC INPUT

A. 180°F				B. 120°F				C. 60°F			
Frequency (Hz)	Amplitude* (mm)	Ratio	Decibels	Frequency (Hz)	Amplitude** (mm)	Ratio	Decibels	Frequency (Hz)	Amplitude** (mm)	Ratio	Decibels
0.010	1.000	0.107	-19.439	0.010	3.000	0.160	-15.918	0.010	0.500	0.027	-31.481
0.020	2.000	0.213	-13.419	0.020	6.000	0.320	-9.897	0.020	1.000	0.053	-25.460
0.040	4.000	0.427	-7.398	0.040	11.500	0.613	-4.246	0.040	2.200	0.117	-18.612
0.060	6.500	0.693	-3.181	0.060	21.000	1.120	0.984	0.060	3.200	0.171	-15.357
0.100	8.000	0.853	-1.378	0.100	23.000	1.227	1.775	0.100	5.000	0.267	-11.481
0.250	13.000	1.387	2.839	0.250	33.500	1.787	5.041	0.250	7.000	0.373	-8.558
0.400	16.000	1.707	4.643	0.400	37.000	1.973	5.904	0.400	8.000	0.427	-7.398
0.600	18.000	1.920	5.666	0.600	42.000	2.240	7.005	0.600	9.000	0.480	-6.375
0.800	17.000	1.813	5.170	1.000	52.000	2.773	8.860	1.000	11.500	0.613	-4.246
1.000	18.000	1.920	5.666	2.000	66.000	3.520	10.931	2.000	17.000	0.907	-0.851
2.000	23.000	2.453	7.795	4.000	70.000	3.733	11.442	4.000	23.500	1.253	1.961
4.000	28.000	2.987	9.504	6.000	66.000	3.520	10.931	6.000	17.000	0.907	-0.851
6.000	23.000	2.453	7.795	8.000	34.000	1.813	5.170	8.000	8.000	0.427	-7.398
8.000	13.000	1.387	2.839	10.000	20.000	1.067	0.561	10.000	4.000	0.213	-13.419
10.000	8.000	0.853	-1.378								

*Ref. = 9.375 mm
**Ref. = 18.750 mm

TABLE XXXIV. ROLL AXIS -- ±2.5-DEG/SEC INPUT

A. 180°F				B. 120°F				C. 60°F			
Frequency (Hz)	Amplitude* (mm)	Ratio	Decibels	Frequency (Hz)	Amplitude ** (mm)	Ratio	Decibels	Frequency (Hz)	Amplitude** (mm)	Ratio	Decibels
0.010	2.000	0.194	-14.257	0.010	3.500	0.337	-9.438	0.010	2.000	0.193	-14.299
0.020	4.500	0.436	-7.214	0.020	5.500	0.530	-5.513	0.020	3.000	0.289	-10.777
0.040	5.500	0.533	-5.471	0.040	7.000	0.675	-3.418	0.040	4.000	0.386	-8.279
0.060	6.500	0.630	-4.020	0.060	7.000	0.675	-3.418	0.060	4.000	0.386	-8.279
0.100	6.500	0.630	-4.020	0.100	7.500	0.723	-2.819	0.100	4.000	0.386	-8.279
0.250	7.000	0.678	-3.376	0.250	8.000	0.771	-2.258	0.250	4.000	0.386	-8.279
0.400	7.000	0.678	-3.374	0.400	8.000	0.771	-2.258	0.400	4.500	0.434	-7.256
0.600	7.000	0.678	-3.376	0.600	8.000	0.771	-2.258	0.600	4.500	0.434	-7.256
0.800	7.000	0.678	-3.376	1.000	8.500	0.819	-1.731	1.000	4.500	0.434	-7.256
1.000	7.000	0.678	-3.376	2.000	8.500	0.819	-1.731	2.000	5.000	0.482	-6.340
2.000	8.000	0.775	-2.216	4.000	10.000	0.964	-0.320	4.000	6.500	0.627	-4.061
4.000	8.000	0.775	-2.216	6.000	13.000	1.253	1.959	6.000	9.000	0.867	-1.235
6.000	10.000	0.969	-0.278	8.000	18.000	1.753	4.786	8.000	15.500	1.494	3.487
8.000	16.000	1.550	3.805	10.000	13.000	1.253	1.959	10.000	8.500	0.819	-1.731
10.000	10.000	0.969	-0.278								

*Ref. = 10.325 mm
**Ref. = 10.375 mm

TABLE XXXV. YAW AXIS -- ±2.5-DEG/SEC INPUT

A. 180°F				B. 120°F				C. 60°F			
Frequency (Hz)	Amplitude* (mm)	Ratio	Decibels	Frequency (Hz)	Amplitude* (mm)	Ratio	Decibels	Frequency (Hz)	Amplitude* (mm)	Ratio	Decibels
0.010	2.000	0.070	-23.046	0.010	2.500	0.088	-21.108	0.010	1.000	0.035	-29.066
0.020	2.500	0.088	-21.108	0.020	5.000	0.176	-15.087	0.020	2.500	0.088	-21.108
0.040	5.000	0.176	-15.087	0.040	9.000	0.317	-9.982	0.040	5.000	0.176	-15.087
0.060	7.000	0.246	-12.164	0.060	11.500	0.405	-7.852	0.060	7.000	0.246	-12.164
0.100	11.000	0.387	-8.239	0.100	15.000	0.528	-5.545	0.100	9.000	0.317	-9.982
0.250	13.000	0.458	-6.788	0.250	17.000	0.599	-4.457	0.250	11.000	0.387	-8.239
0.400	14.000	0.493	-6.144	0.400	19.000	0.669	-3.491	0.400	11.500	0.405	-7.852
0.600	14.000	0.493	-6.144	0.600	20.000	0.704	-3.046	0.600	11.500	0.405	-7.852
0.800	15.000	0.528	-5.545	1.000	21.000	0.739	-2.622	1.000	12.000	0.423	-7.483
1.000	14.000	0.493	-6.144	2.000	23.000	0.810	-1.832	2.000	14.000	0.493	-6.144
2.000	17.000	0.599	-4.457	4.000	27.000	0.951	-0.439	4.000	16.000	0.563	-4.984
4.000	20.000	0.704	-3.046	6.000	34.000	1.197	1.563	6.000	23.500	0.827	-1.645
6.000	27.000	0.951	-0.439	8.000	17.000	0.599	-4.457	8.000	10.500	0.370	-8.643
8.000	17.000	0.599	-4.457	10.000	8.500	0.299	-10.478	10.000	3.000	0.106	-19.524
10.000	8.000	0.282	-11.005								

*Ref. = 28.400 mm

5.0 RECOMMENDATIONS

The system should be operated at a fluid temperature of 120°F, which is the nominal design condition, and the temperature of best performance. All signal lines should be tied to the aircraft to prevent null shift during flight.

APPENDIX III
FLIGHTWORTHINESS REPORT* FOR THE SPOOL VALVE SERVOACTUATORS

1.0 ABSTRACT

1.1 Object

To determine operating parameters, performance characteristics, vibration levels, and overall flightworthiness of three spool valve servoactuators to be used in the three-axis hydrofluidic stability augmentation system.

1.2 Conclusions

An operating parameter of 1000 psig provided the best overall operating performance and should be used. The devices were subjected to a 2000-psig proof-pressure test. No adverse effects were observed.

The devices were subjected to vibration in each of the mutually perpendicular axes. All resonant points were above 100 Hz, and the amplitude of the offsets was insignificant at 0.7 g.

On the basis of these tests (see Figure 147 for test setup schematic and Tables XXXVI through XLII for test results) and the performance characteristics summarized in Table XLIII, each device is considered flightworthy.

Frequency response (amplitude) ratio and phase shift) for each device is plotted in Figures 148 through 154. A maximum peaking of 4 db was observed using a small input pressure differential.

2.0 UNITS TESTED

Three Hydraulic Research and Manufacturing Company hydrofluidic servoactuators, P/N 85112010, S/Ns 2, 5, and 6.

3.0 PROCEDURES AND RESULTS

Each device was tested in the test setup shown in Figure 147. The amplifier (FG1001AA010, S/N 2) was used to simulate actual operating conditions for the servoactuator.

Servoactuator S/N 5 was selected to be used for baseline information prior to vibration tests. Oil temperature was maintained at 120°F

*Honeywell Aero Engineering Test Report No. AEX-53982, dated August 1970.

during all testing. The device was operated at a supply pressure of 1500 psig, and a frequency response test was conducted. Results are shown in Figure 148. Peaking was 7.82 db and was considered unsuitable. The supply pressure was lowered to 1000 psig. Peaking was then only 3.1 db at an input of ±1.14 psid (Figure 149) to 4.05 db at an input of ±0.33 psid (Figure 150). This was considered satisfactory, and all further testing was conducted at this pressure.

The units were subjected to vibration in each of the three mutually perpendicular axes at frequencies from 5 to 500 to 5 Hz at an amplitude of 2 g . Servoactuator S/N 5 was instrumented as shown in Figure 147 to simulate actual operating conditions. All resonant points were found to be above 100 Hz, and the amplitudes of the offsets were insignificant when the vibration input was lowered to 0.7 g. Vibration of 2 g was supplied for 30 sec at each discernible resonant point.

After vibration, servoactuator S/N 5 was again tested for frequency response at high input amplitude (Figure 151) and low input amplitude (Figure 152). A decrease of less than 1 db was noted after vibration.

Operational characteristics consisting of servoactuator gain, oscillating threshold, null offset, center lock null, and frequency response were taken for all three servoactuators. Results are presented in Table XXXVI.

All frequency response data are based on "system" response (servoactuator output motion versus input to the amplifier). "System" response and actual servoactuator response of servoactuator S/N 6 are compared in Figure 153. This was typical for all three servoactuators and is shown here as an example.

The instruments used during testing are shown in the block diagram of the test setup in Figure 147. All readings are estimated to be accurate to ±3 percent or better, except for phase angles, which are based on an average of four readings and also operator technique. The values obtained indicate, because of the lack of scatter, relatively accurate results.

4.0 RECOMMENDATIONS

None. Data submittal only.

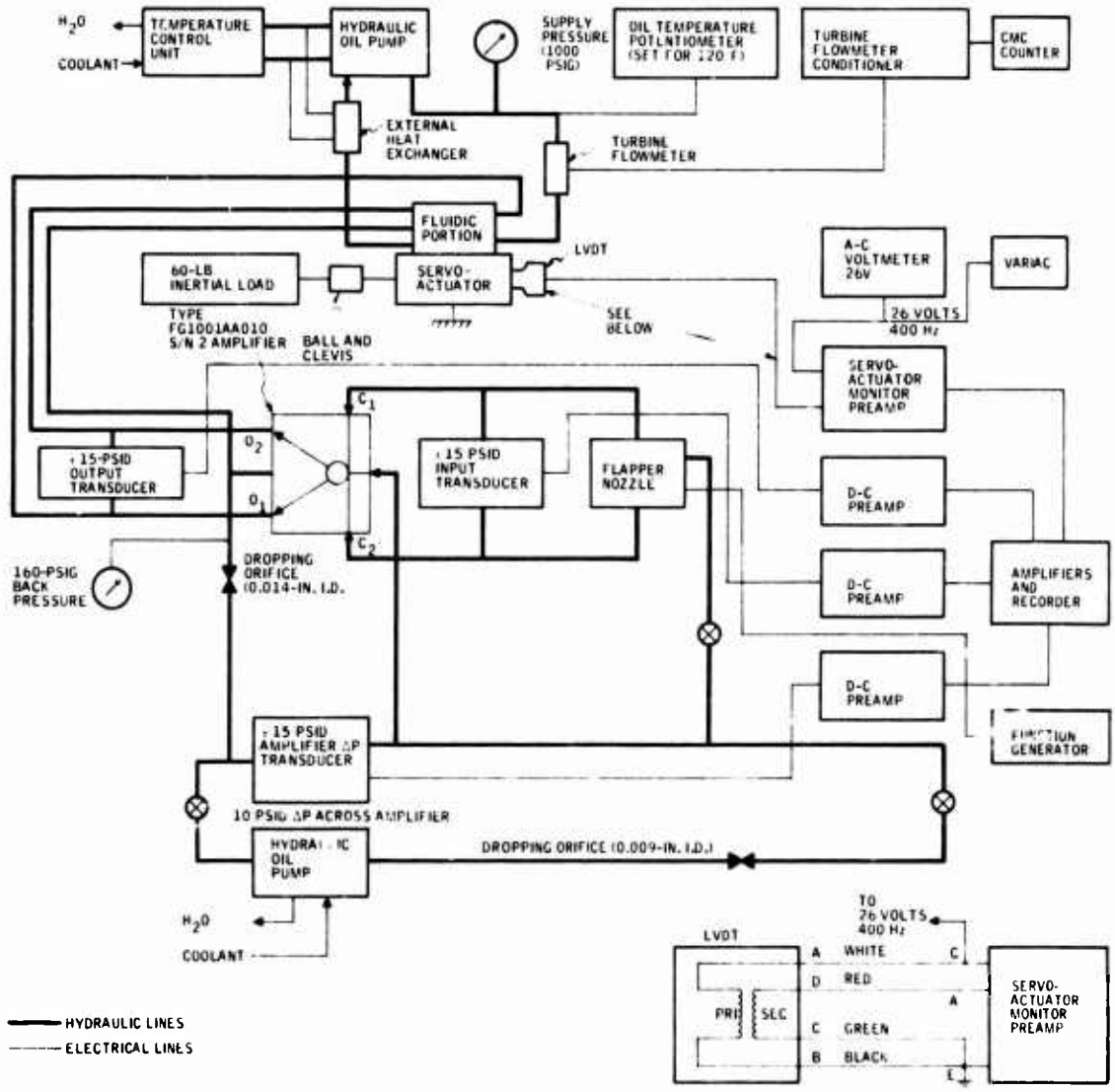

Figure 147. Spool Valve Servoactuator Test Setup.

TABLE XXXVI. FREQUENCY RESPONSE DATA FOR SPOOL VALVE SERVOACTUATOR S/N 5 (SUPPLY PRESSURE = 1500 PSIG; INPUT SIGNAL = ± 1.24 PSID)

Frequency (Hz)	System Motion (in.)	System Phase Shift (deg)	System Attenuation (db)
0.2	0.220	-	-1.0220
0.4	0.220	-	-1.1900
0.7	0.220	-	-1.1900
1.0	0.212	5.3	-1.1500
2.0	0.218	10.3	-0.7060
3.0	0.230	20.2	-0.2380
4.0	0.280	32.4	1.4670
5.0	0.368	44.8	3.4462
5.5	0.424	-	5.0716
6.0	0.530	88.4	6.6300
7.0	0.486	139.5	5.8628
8.0	0.360	-	3.6482
10.0	0.160	-	-3.3880

TABLE XXXVII. FREQUENCY RESPONSE DATA FOR SPOOL VALVE SERVOACTUATOR S/N 5 (SUPPLY PRESSURE = 1000 PSIG; INPUT SIGNAL = ±1.14 PSID)

Frequency (Hz)	System Motion (in.)	System Phase Angle (deg)	System Attenuation (db)
0.2	0.200	-	-1.1300
0.4	0.200	-	-1.0620
0.7	0.205	-	-0.8760
1.0	0.206	10.1	-0.8100
1.5	0.210	-	-0.6680
2.0	0.214	23.2	-0.4740
3.0	0.240	42.1	0.4980
4.0	0.276	64.4	1.6628
5.0	0.288	96.9	2.0280
5.5	0.273	-	1.5692
6.0	0.245	129.2	0.6280
7.0	0.182	168.0	-1.9600
8.0	0.130	-	-4.8820
9.0	0.090	-	-8.0680
10.0	0.070	-	-10.2580
15.0	0.020	-	-20.3460

TABLE XXXVIII. FREQUENCY RESPONSE DATA FOR SPOOL VALVE SERVOACTUATOR S/N 5 (SUPPLY PRESSURE = 1000 PSIG; INPUT SIGNAL = ±0.33 PSID)

Frequency (Hz)	System Motion (in.)	System Phase Angle (deg)	System Attenuation (db)
0.2	0.0600	-	-0.828
0.4	0.0600	-	-0.518
0.7	0.0620	-	-0.546
1.0	0.0630	8.78	-0.924
1.5	0.0636	-	-0.714
2.0	0.0632	20.40	-0.772
2.5	0.0660	-	0.000
3.0	0.0711	37.08	0.820
4.0	0.0845	50.50	2.137
5.0	0.0964	81.50	3.215
5.5	0.0950	-	3.221
6.0	0.0892	121.50	2.619
6.5	0.0772	-	1.496
7.0	0.0660	158.80	-0.640
8.0	0.0446	-	-3.402
10.0	0.0196	-	-10.544

TABLE XXXIX. FREQUENCY RESPONSE DATA FOR SPOOL VALVE SERVOACTUATOR S/N 5 (SUPPLY PRESSURE = 1000 PSIG; INPUT SIGNAL = ±1.10 PSID)

Frequency (Hz)	System Motion (in.)	System Phase Shift (deg)	System Attenuation (db)
0.2	0.200	-	-0.8280
0.4	0.200	-	-0.8280
0.7	0.200	-	-0.6500
1.0	0.200	12.1	-0.6500
1.5	0.203	-	-0.5180
2.0	0.210	23.8	-0.2280
3.0	0.230	39.3	0.4814
4.0	0.250	66.0	1.2892
4.5	0.252	-	1.1762
5.0	0.253	97.6	1.3934
5.5	0.245	-	1.1076
6.0	0.229	131.8	0.5224
7.0	0.184	153.0	-1.3700
8.0	0.133	-	-3.5040
9.0	0.098	-	-7.0320
10.0	0.072	-	-9.1680

TABLE XL. FREQUENCY RESPONSE DATA FOR SPOOL VALVE SERVOACTUATOR S/N 5 (SUPPLY PRESSURE = 1000 PSIG; INPUT SIGNAL = ±0.35 PSID)

Frequency (Hz)	System Motion (in.)	System Phase Shift (deg)	System Attenuation (db)
0.2	0.0660	-	-0.6120
0.4	.0660	-	-0.6120
0.7	0.0650	-	-0.7440
1.0	0.0660	11.9	-0.6120
1.5	0.0680	-	-0.3540
2.0	0.0680	24.4	-0.3540
3.0	0.0752	37.2	1.0538
4.0	0.0860	54.4	1.6916
4.5	0.0920	-	2.2722
5.0	0.0954	87.4	2.5874
5.5	0.0946	-	2.5162
6.0	0.0906	123.2	2.1442
7.0	0.0670	154.4	0.0520
8.0	0.0540	-	-2.2500
10.0	0.0270	-	-7.8300

TABLE XLI. FREQUENCY RESPONSE DATA FOR SPOOL VALVE SERVOACTUATOR S/N 6 (SUPPLY PRESSURE = 1000 PSIG; INPUT SIGNAL = ±1.25 PSID)

Frequency (Hz)	System Motion (in.)	Servoactuator Motion/Input (in./psid)	Servoactuator Phase Shift (deg)	System Phase Shift (deg)	Servoactuator Attenuation (db)	System Attenuation (db)
0.2	0.206	0.0824	-	-	-1.682	-1.6820
0.4	0.204	0.08192	-	-	-1.734	-1.7020
0.7	0.208	0.08188	-	-	-1.734	1.5240
1.0	0.208	0.08188	7.9	10.6	-1.734	-1.4220
1.5	0.209	0.08195	-	-	-1.916	-1.3820
2.0	0.216	0.08339	21.5	22.6	-1.576	-1.1000
3.0	0.234	0.08447	34.3	40.2	-1.462	-0.4000
4.0	0.256	0.08420	49.4	64.8	-1.494	0.3824
5.0	0.276	0.08000	63.0	90.0	-1.938	1.0308
6.0	0.268	0.08121	84.5	124.0	-1.808	0.7804
7.0	0.220	0.07534	90.0	152.0	-2.464	-0.9340
8.0	0.168	0.08440	-	-	-1.474	-3.0000
10.0	0.088	0.07857	-	-	-2.092	-8.6120

TABLE XLII. FREQUENCY RESPONSE DATA FOR SPOOL VALVE SERVOACTUATOR S/N 2 (SUPPLY PRESSURE = 1000 PSIG; INPUT SIGNAL = ±1.18 PSID)

Frequency (Hz)	System Motion (in.)	System Phase Shift (deg)	System Attenuation (db)
0.2	0.205	-	-1.260
0.4	0.206	-	-1.220
0.7	0.208	-	-1.062
1.0	0.208	8.7	-1.062
1.5	0.210	-	-0.974
2.0	0.214	22.7	-0.810
3.0	0.232	42.5	-0.114
4.0	0.245	60.5	0.628
5.0	0.256	91.4	0.740
6.0	0.245	117.9	0.265
7.0	0.210	151.2	-0.974
8.0	0.160	-	-2.074
9.0	0.126	-	-5.416
10.0	0.095	-	-7.872

TABLE XLIII. SUMMARY OF PERFORMANCE CHARACTERISTICS

S/N	Gain (in. displ. / psid)	Oscillating Threshold		Operating Null (in. displ.)	Center Lock Null (in. displ.)
		PSID P/P	Equiv. In. Displ.		
5	0.0875*	0.0300	0.002625	0.0195 ±0.0085 Ext.	0.0058 ±0.0062 Ext.
5	0.0905**	0.0180	0.001629	0.0160 ±0.0070 Ext.	0.0057 ±0.0097 Ext.
6	0.0820**	0.0210	0.001722	0.0048 ±0.0080 Ext.	0.0020 ±0.0300 Ext.
2	0.0860**	0.0255	0.002253	0.0008 ±0.0068 Ret.	0.0040 ±0.0104 Ext.

* Before vibration.

** After vibration.

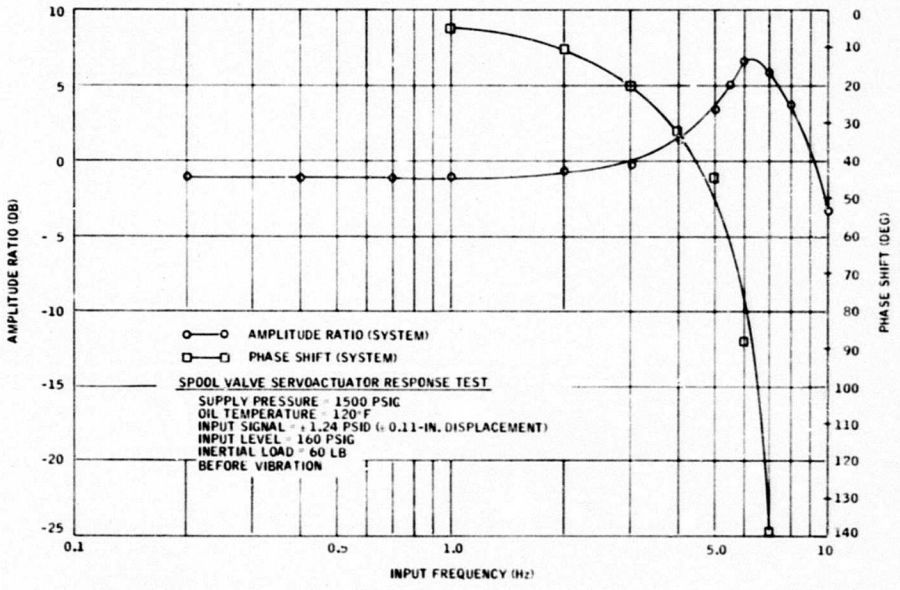

Figure 148. Frequency Response for Spool Valve Servoactuator S/N 5 (Supply Pressure = 1500 PSIG; Input Signal = ±1.24 PSID).

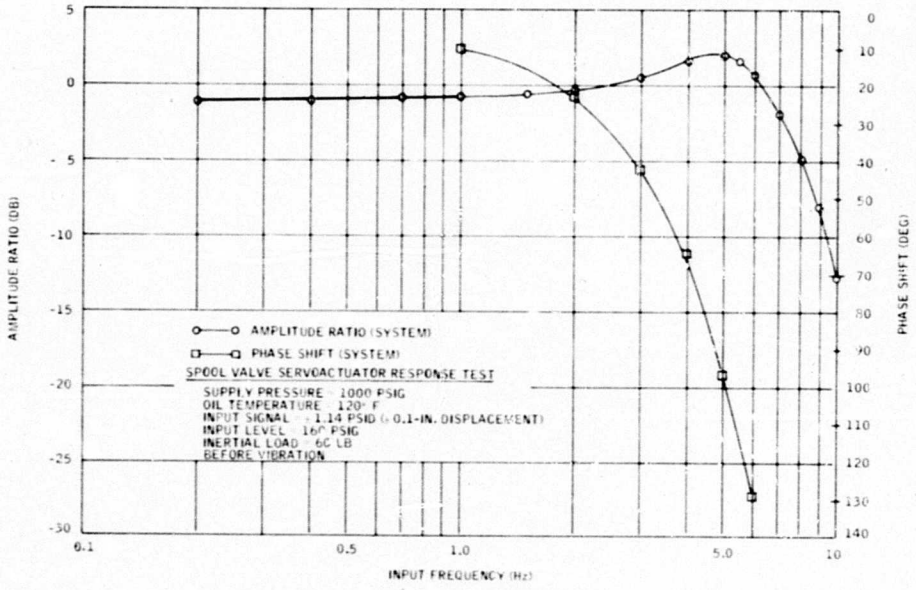

Figure 149. Frequency Response for Spool Valve Servoactuator S/N 5 (Supply Pressure = 1000 PSIG; Input Signal = ±1.14 PSID).

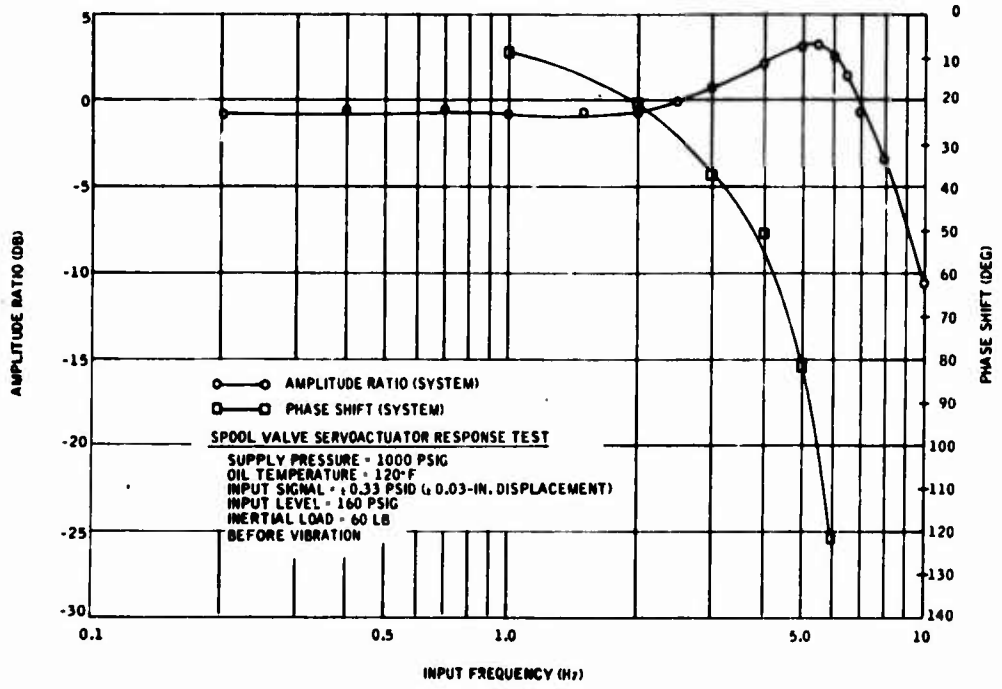

Figure 150. Frequency Response for Spool Valve Servoactuator S/N 5 (Supply Pressure = 1000 PSIG; Input Signal = ±0.33 PSID).

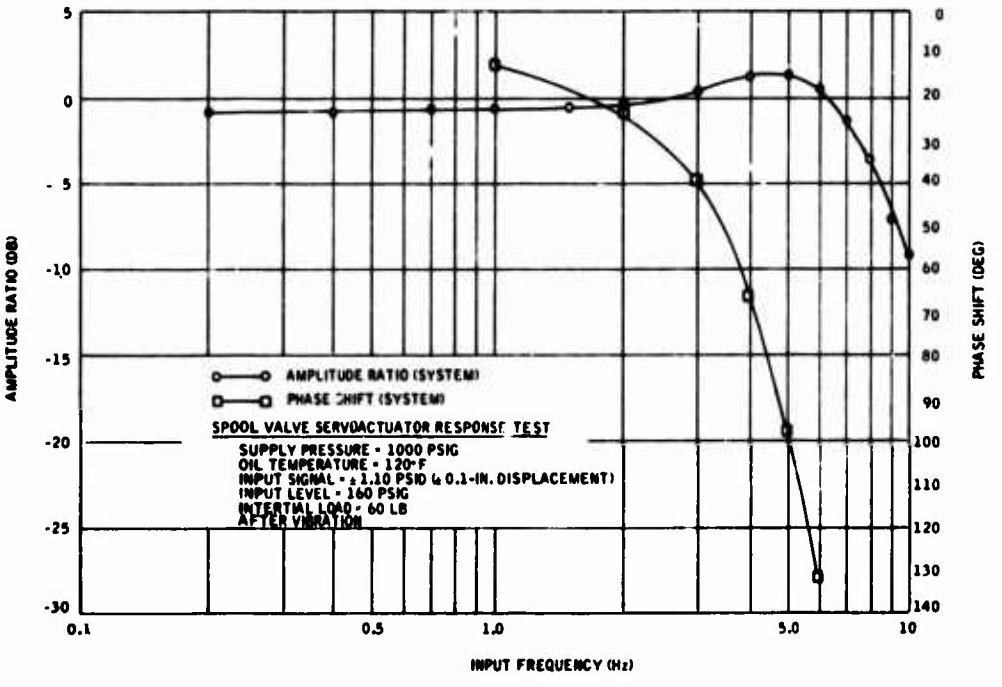

Figure 151. Frequency Response for Spool Valve Servoactuator S/N 5 (Supply Pressure = 1000 PSIG; Input Signal = ±1.10 PSID).

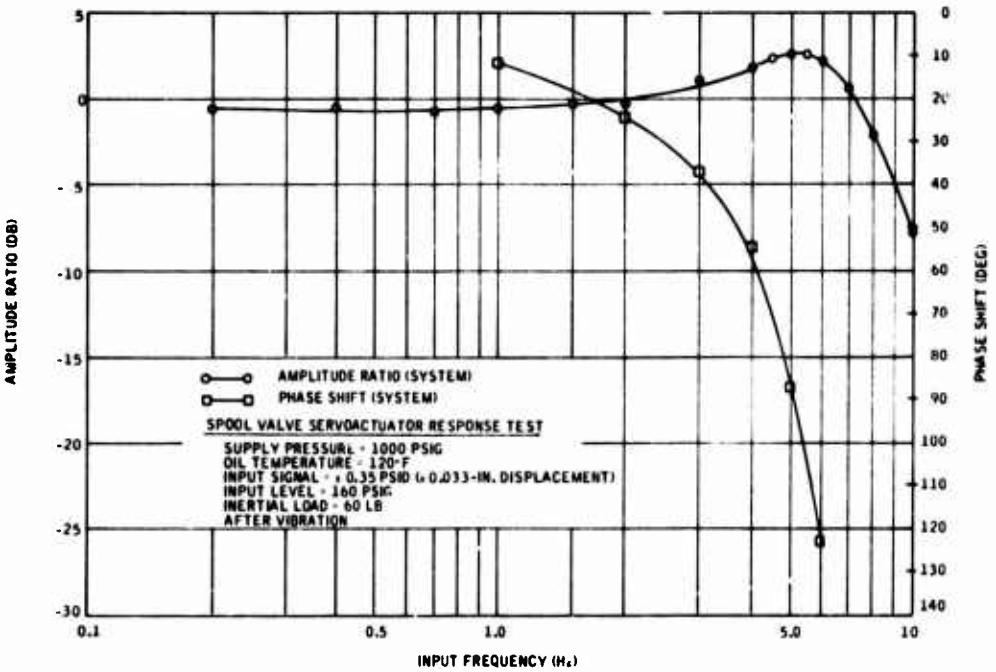

Figure 152. Frequency Response for Spool Valve Servoactuator S/N 5 (Supply Pressure = 1000 PSIG; Input Signal = ±0.35 PSID).

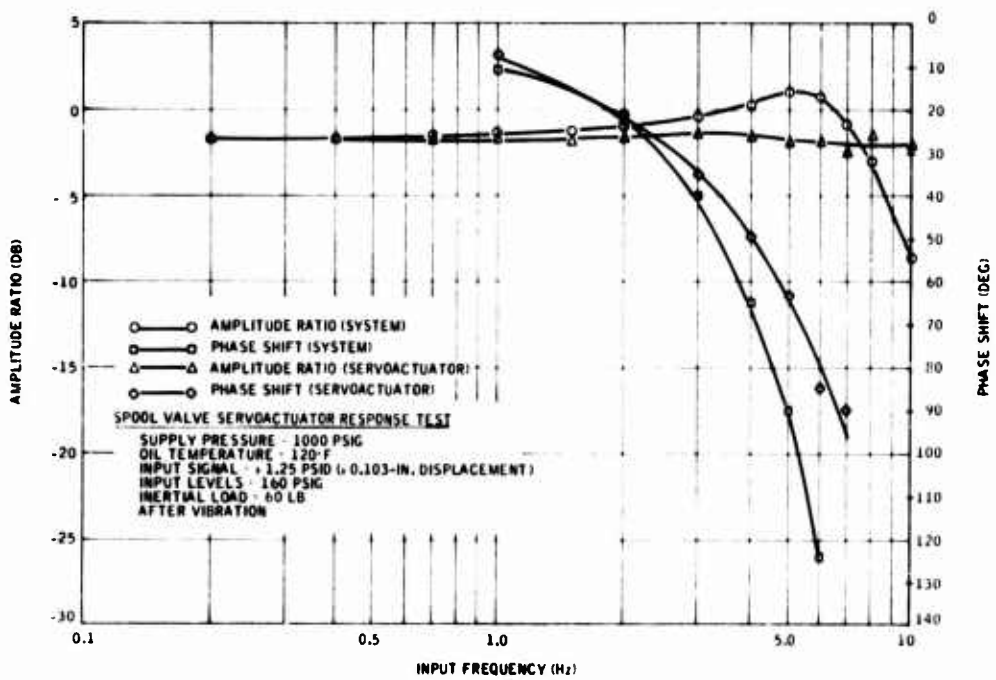

Figure 153. Frequency Response for Spool Valve Servoactuator S/N6 (Supply Pressure = 1000 PSIG; Input Signal = ±1.25 PSID).

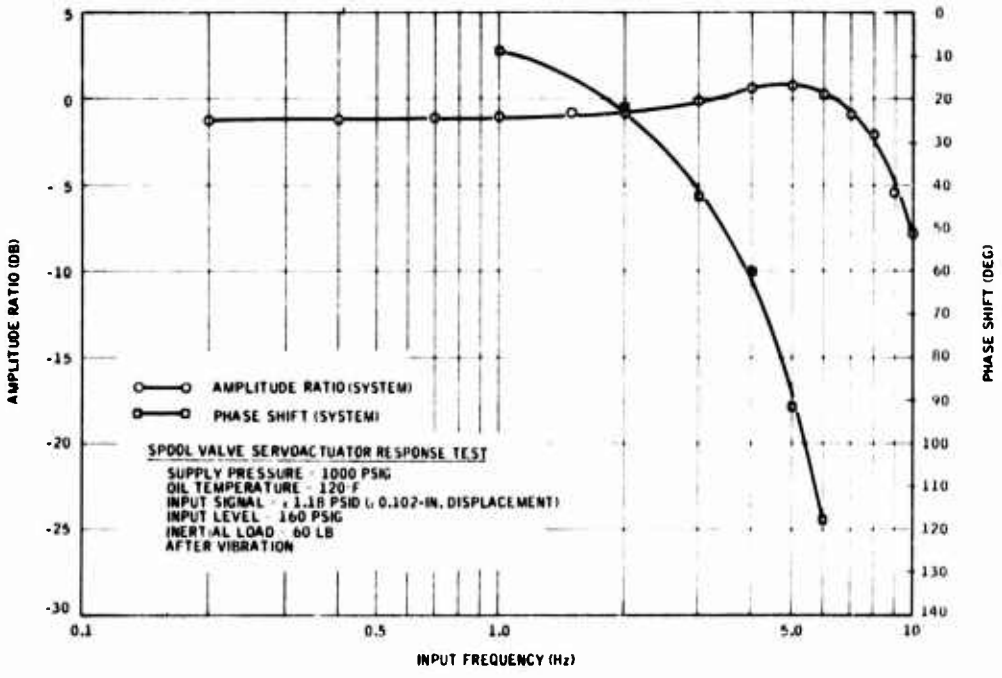

Figure 154. Frequency Response for Spool Valve Servoactuator S/N 2 (Supply Pressure = 1000 PSIG; Input Signal = ±1.18 PSID).

APPENDIX IV
FLIGHTWORTHINESS REPORT* FOR THE VORTEX VALVE SERVOACTUATORS

1.0 ABSTRACT

1.1 Object

To determine the flightworthiness of three hydrofluidic vortex valve servoactuators.

1.2 Conclusion

None of the three servoactuators exhibited leakage or permanent damage during the testing, and all are considered flightworthy. Frequency response data before and after vibration are comparable, and tests at 60°F and 185°F working fluid temperature revealed no significant deterioration in performance.

2.0 UNITS TESTED

Three General Electric Company hydrofluidic vortex valve servoactuators, Part No. 24SA31AA, S/Ns 1, 2, and 3.

3.0 PROCEDURES AND RESULTS

The servoactuators were unpacked and inspected for damage. The mounting brackets which hold each end of the servoactuator barrels were fabricated, and all servoactuators were mounted parallel to each other. The supply lines for all three servoactuators were paralleled, and all drain lines were paralleled. Signals were supplied to the servoactuator signal inputs from a fluid amplifier mounted on the same test plate. The supply pressure to the servoactuator was increased to 1500 psig, and the servoactuators were cycled from stop to stop with no indication of damage or leakage.

An electrical input valve was connected to the signal input of the fluid amplifier. A function generator was used to drive this valve and furnish signal inputs to the servoactuators. A 1000-psi pressure was applied to all servoactuators, and the working fluid temperature was stabilized at 120°F. The input from the signal generator was adjusted to drive the servoactuators ±0.2 in. at input frequencies of 0.1 to 12 Hz. Input signals,

*Honeywell Aero Engineering Test Report No. AEX-54103, dated October 1970.

input ΔP to amplifier, output ΔP from the amplifier, and servoactuator ram position were recorded. Phase shift from the input to the amplifier to the servoactuator ram position was also recorded. The same test procedures were followed for all three servoactuators.

The test plate assembly used in the frequency response tests was mounted in the vibration driver. The units were energized with hydraulic pressure (1000 psi) and stabilized at 120°F fluid temperature. Servoactuator S/N 2 was connected to the output of the fluid amplifier. Signals were not applied to the servoactuators during testing. Ram position for the three servoactuators and input ΔP into S/N 2 were recorded.

The units were subjected to vibration in each of the mutually perpendicular axes at frequencies from 5 to 500 Hz at 2 g in a 30-min.scan. There was no leakage during or after vibration. Servoactuators S/N 1 and 3, which were not connected to a signal source, did not exhibit any null shifts. Servoactuator S/N 2 had null shifts of up to 0.04 in. maximum in the vicinity of 250 to 300 Hz. This null shift was reduced when the signal lines from the amplifier to the servoactuator were tied down.

After vibration, frequency tests were repeated at 120°F fluid temperature. Tables XLIV, XLV, and XLVI show the before and after performance of the three servoactuators. Note that the average servoactuator gain is really the average servoactuator gain for the first four frequency points and, as such, is not a d-c servoactuator gain.

Each servoactuator was also tested with the working fluid temperature at 60°F and 185°F. Frequency response tests at these temperatures were conducted in the same manner as the tests at fluid temperature of 120°F. Tables XLVII, XLVIII, and XLIX list the results of the extreme-temperature tests. Performance characteristics are summarized in Table L. Results of the frequency response tests are plotted in Figures 155 through 160.

The servoactuators had no significant change in performance and are considered to be flightworthy. Vibration testing indicated that care should be exercised in securing the servoactuator signal lines.

4.0 RECOMMENDATIONS

None. Data submittal only.

TABLE XLIV. SERVOACTUATOR S/N 1 -- PRE- AND POST-VIBRATION AT 120°F

Pre-Vibration*				Post-Vibration**			
Frequency*** (Hz)	Motion (in.)	Phase (deg)	Attenuation (db)	Frequency*** (Hz)	Motion (in.)	Phase (deg)	Attenuation (db)
0.20	0.408	-5	-0.14	0.10	0.456	2	-0.77
0.40	0.408	-8	-0.14	0.20	0.456	-5	-0.77
1.00	0.408	-11	0.00	0.40	0.456	-9	-0.83
2.00	0.490	-56	1.72	1.00	0.490	-14	0.00
3.00	0.340	-98	-1.30	1.50	0.524	-23	0.58
4.00	0.245	-120	-4.44	2.00	0.530	-55	0.70
5.00	0.190	-132	-6.76	2.50	0.422	-83	-1.00
6.00	0.156	-138	-8.86	3.00	0.347	-99	-3.00
7.00	0.122	-142	-10.99	4.00	0.313	-115	-4.04
8.00	0.095	-146	-12.91	5.00	0.190	-130	-8.35
9.00	0.075	-149	-15.27	6.00	0.143	-138	-10.99
10.00	0.061	-149	-16.75	8.00	0.088	-144	-15.01
11.00	0.048	-149	-18.80	9.00	0.068	-147	-16.85
12.00	0.042	-149	-19.58	10.00	0.054	-150	-18.94
				11.00	0.048	-160	-19.79
				12.00	0.034	-148	-22.24

*Average servoactuator gain 0.1 to 5 Hz = 0.085 in./psi. Average amplifier gain 0.1 to 5 Hz = 8.4425 psi/psi.

**Average servoactuator gain 0.1 to 5 Hz = 0.089 in./psi. Average amplifier gain 0.1 to 5 Hz = 9.6377 psi/psi.

***Ref. = 1.0 Hz.

TABLE XLV. SERVOACTUATOR S/N 2 -- PRE- AND POST-VIBRATION AT 120°F

Pre-Vibration*				Post-Vibration**			
Frequency*** (Hz)	Motion (in.)	Phase (deg)	Attenuation (db)	Frequency*** (Hz)	Motion (in.)	Phase (deg)	Attenuation (db)
0.20	0.394	-4	-0.31	0.10	0.401	2	-0.56
0.40	0.401	-5	-0.16	0.20	0.401	-5	-0.56
1.00	0.415	-12	0.00	0.40	0.401	-8	-0.56
2.00	0.503	-34	1.80	1.00	0.435	-14	0.00
3.00	0.340	-77	-1.48	1.50	0.462	-26	0.67
4.00	0.252	-109	-3.96	2.00	0.483	-31	1.20
5.00	0.197	-124	-5.95	2.50	0.435	-71	0.15
6.00	0.136	-134	-9.04	3.00	0.354	-97	-1.66
7.00	0.129	-138	-10.38	4.00	0.258	-109	-4.23
8.00	0.102	-143	-12.31	5.00	0.197	-124	-6.88
9.00	0.075	-146	-15.00	6.00	0.150	-133	-9.42
10.00	0.061	-145	-16.37	7.00	0.122	-137	-11.30
11.00	0.052	-146	-17.71	8.00	0.095	-141	-13.20
12.00	0.037	-142	-20.28	9.00	0.082	-143	-14.25
				10.00	0.061	-144	-16.89
				11.00	0.048	-143	-18.62
				12.00	0.041	-139	-19.96

*Average servoactuator gain 0.1 to 5 Hz = 0.078 in./psi. Average amplifier gain 0.1 to 5 Hz = 8.4369 psi/psi.

**Average servoactuator gain 0.1 to 5 Hz = 0.079 in./psi. Average amplifier gain 0.1 to 5 Hz = 9.6610 psi/psi.

***Ref. = 1.0 Hz.

TABLE XLVI. SERVOACTUATOR S/N 3 -- PRE- AND POST-VIBRATION AT 120°F

Pre-Vibration*				Post-Vibration**			
Frequency*** (Hz)	Motion (in.)	Phase (deg)	Attenuation (db)	Frequency*** (Hz)	Motion (in.)	Phase (deg)	Attenuation (db)
0.20	0.204	-3	-0.15	0.10	0.442	2	-0.79
0.40	0.204	-6	0.10	0.20	0.442	-5	-0.79
1.00	0.204	-12	0.00	0.40	0.442	-8	-0.79
2.00	0.248	-53	1.27	1.00	0.476	-16	0.00
3.00	0.286	-94	2.77	1.50	0.510	-22	0.31
4.00	0.211	-116	-0.37	2.00	0.54	-48	1.01
5.00	0.150	-128	-3.58	2.50	0.442	-75	-0.64
6.00	0.102	-135	-6.67	3.00	0.360	-94	-2.42
7.00	0.082	-141	-8.85	4.00	0.258	-115	-5.45
8.00	0.057	-145	-11.71	5.00	0.197	-127	7.51
9.00	0.045	-149	-13.56	6.00	0.156	-135	-9.81
10.00	0.033	-148	-16.32	7.00	0.122	-139	-12.09
11.00	0.026	-148	-18.10	8.00	0.102	-141	-13.23
12.00	0.023	-143	-18.81	9.00	0.075	-144	-15.77
				10.00	0.061	-145	-17.36
				11.00	0.048	-146	-19.39
				12.00	0.041	-144	-20.57

*Average servoactuator gain 0.1 to 5 Hz = 0.083 in./psi. Average amplifier gain 0.1 to 5 Hz = 8.2931 psi/psi.

**Average servoactuator gain 0.1 to 5 Hz = 0.086 in./psi. Average amplifier gain 0.1 to 5 Hz = 9.6667 psi/psi.

***Ref. = 1.0 Hz.

TABLE XLVII. SERVOACTUATOR S/N 1 AT 60°F AND 185°F

60°F*				185°F**			
Frequency*** (Hz)	Motion (in.)	Phase (deg)	Attenuation (db)	Frequency*** (Hz)	Motion (in.)	Phase (deg)	Attenuation (db)
0.10	0.428	-11	-0.17	0.10	0.354	1	0.00
0.20	0.428	-9	-0.17	0.20	0.340	-3	0.08
0.40	0.428	-11	0.18	0.40	0.367	-8	0.08
1.00	0.428	-20	0.00	1.00	0.354	-12	0.00
1.50	0.462	-30	0.66	1.50	0.272	-20	-0.59
2.00	0.510	-43	1.87	2.00	0.306	-22	0.75
2.50	0.510	-64	1.87	2.50	0.313	-31	0.31
3.00	0.428	-89	0.35	3.00	0.340	-32	1.66
4.00	0.265	-114	-3.99	4.00	0.340	-69	1.66
5.00	0.252	-128	-8.26	5.00	0.286	-90	0.15
6.00	0.170	-134	-11.32	6.00	0.211	-117	-2.49
7.00	0.122	-136	-14.05	7.00	0.184	-130	5.43
8.00	0.082	-149	-17.33	8.00	0.129	-139	-9.24
9.00	0.054	-137	-20.47	9.00	0.109	-146	-10.24
10.00	0.034	-137	-24.29	10.00	0.088	-144	-12.04
11.0	0.014	-142	-31.83	11.00	0.068	-150	-15.51
12.00	0.007	-144	-37.57	12.00	0.048	-145	-18.61

*Average servoactuator gain 0.1 to 5 Hz = 0.161 in./psi. Average amplifier gain 0.1 to 5 Hz = 5.9644 psi/psi.

**Average servoactuator gain 0.1 to 5 Hz = 0.135 in./psi. Average amplifier gain 0.1 to 5 Hz = 8.6729 psi/psi.

***Ref. = 1.0 Hz.

TABLE XLVIII. SERVOACTUATOR S/N 2 AT 60°F and 185°F

60°F*				185°F**			
Frequency*** (Hz)	Motion (in.)	Phase (deg)	Attenuation (db)	Frequency*** (Hz)	Motion (in.)	Phase (deg)	Attenuation (db)
0.10	0.449	-12	-0.65	0.10	0.354	2	-0.17
0.20	0.456	-10	-0.52	0.20	0.367	-5	-0.05
0.40	0.469	-12	-0.12	0.40	0.367	-7	-0.05
1.00	0.476	-19	0.00	1.00	0.360	-7	0.00
1.50	0.422	-30	0.70	1.50	0.347	-12	-0.12
2.00	0.435	-43	1.16	2.00	0.354	-24	-0.17
2.50	0.442	-61	1.29	2.50	0.306	-22	1.01
3.00	0.394	-83	0.49	3.00	0.326	-28	1.29
4.00	0.326	-114	-3.56	4.00	0.360	-70	2.15
5.00	0.204	-119	-7.50	5.00	0.320	-102	-1.04
6.00	0.129	-129	-11.33	6.00	0.231	-116	-3.86
7.00	0.068	-124	-16.61	7.00	0.197	-126	-5.24
8.00	0.016	-128	-28.70	8.00	0.163	-133	-7.09
9.00	0.041	-109	-24.86	9.00	0.122	---	-9.38
10.00	0.034	-103	-26.54	10.00	0.102	-142	-10.75
				11.00	0.082	-143	-12.69
				12.00	0.068	-140	-13.83

*Average servoactuator gain 0.1 to 5 Hz = 0.145 in./psi. Average amplifier gain 0.1 to 5 Hz = 5.8525 psi/psi.

**Average servoactuator gain 0.1 to 5 Hz = 0.115 in./psi. Average amplifier gain 0.1 to 5 Hz = 8.5192 psi/psi.

***Ref. = 1.0 Hz.

TABLE XLIX. SERVOACTUATOR S/N 3 AT 60°F AND 185°F

60°F*				185°F**			
Frequency*** (Hz)	Motion (in.)	Phase (deg)	Attenuation (db)	Frequency*** (Hz)	Motion (in.)	Phase (deg)	Attenuation (db)
0.10	0.360	-10	-0.09	0.10	0.292	2	-0.85
0.20	0.333	-13	0.00	0.20	0.299	-1	-0.90
0.40	0.333	-16	0.00	0.40	0.292	-3	-1.10
1.00	0.333	-24	0.00	1.00	0.313	-4	0.00
1.50	0.381	-37	1.36	1.50	0.286	-12	-0.79
2.00	0.354	-53	1.59	2.00	0.299	-20	-0.39
2.50	0.340	-73	1.48	2.50	0.313	-20	0.27
3.00	0.279	-93	-0.24	3.00	0.354	-31	1.33
4.00	0.156	-121	-5.26	4.00	0.340	-73	0.72
5.00	0.224	-127	-0.38	5.00	0.286	-95	-1.05
6.00	0.150	-133	-11.55	6.00	0.197	-114	-4.01
7.00	0.102	-137	-14.64	7.00	0.170	-124	-6.05
8.00	0.075	-146	-17.08	8.00	0.136	-135	-8.46
9.00	0.034	-130	-23.55	9.00	0.109	-142	-10.40
10.00	0.054	-145	-22.06	10.00	0.095	-145	-11.33
11.00	0.030	-141	-26.75	11.00	0.068	-146	-13.51
12.00	0.019	-136	-30.57				

*Average servoactuator gain 0.1 to 5 Hz = 0.154 in./psi. Average amplifier gain 0.1 to 5 Hz = 5.6457 psi/psi.

**Average servoactuator gain 0.1 to 5 Hz = 0.110 in./psi. Average amplifier gain 0.1 to 5 Hz = 8.7227 psi/psi.

***Ref. = 1.0 Hz.

TABLE L. SUMMARY OF PERFORMANCE CHARACTERISTICS

S/N	Gain* (in./psi)	Threshold (equiv. in. displ.)	Null Offset (in. displ.)	Center Lock Null (in. displ.)
1	0.114	0.0067	0.002 Ret.	0.007 Ret.
2	0.112	0.0066	0.001 Ret.	0.003 Ext.
3	0.112	0.0075	0.069 Ret.	0.005 Ret.

*Steady-state.

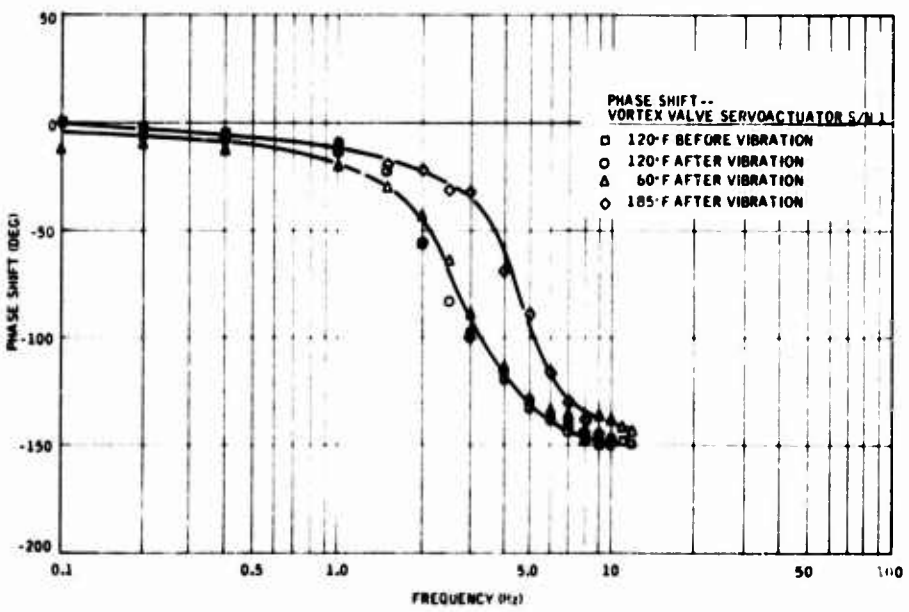

Figure 155. Frequency Response (Phase Shift) for Vortex Valve Servoactuator S/N 1.

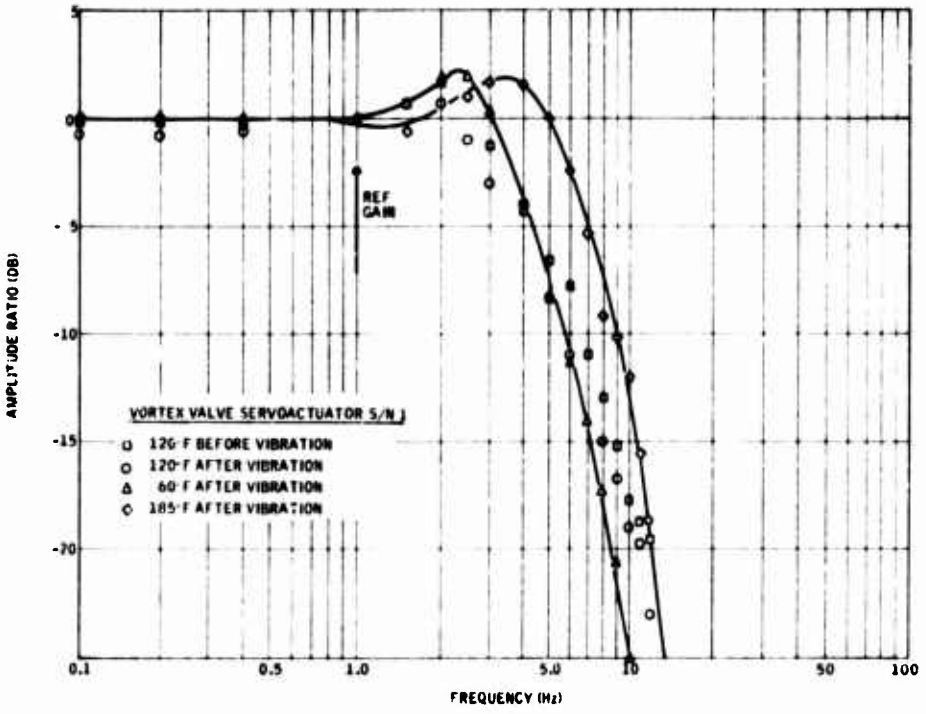

Figure 156. Frequency Response for Vortex Valve Servoactuator S/N 1.

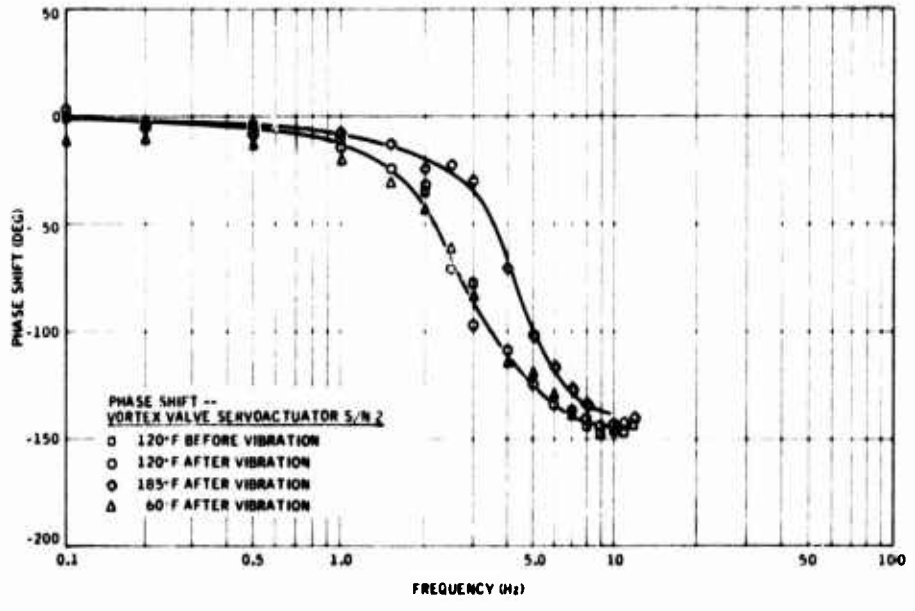

Figure 157. Frequency Response (Phase Shift) for Vortex Valve Servoactuator S/N 2.

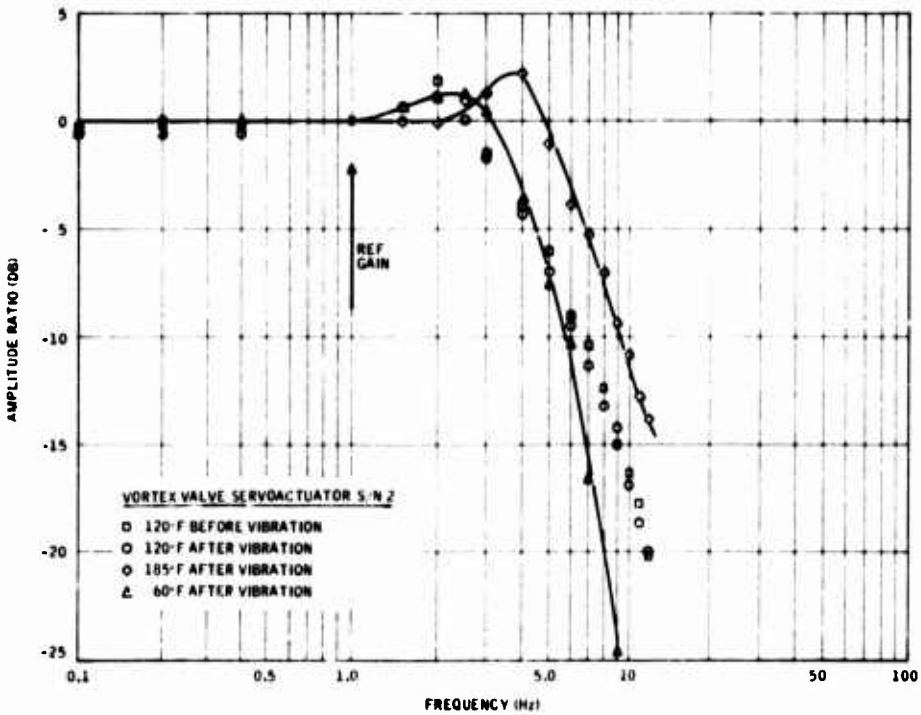

Figure 158. Frequency Response for Vortex Valve Servoactuator S/N 2.

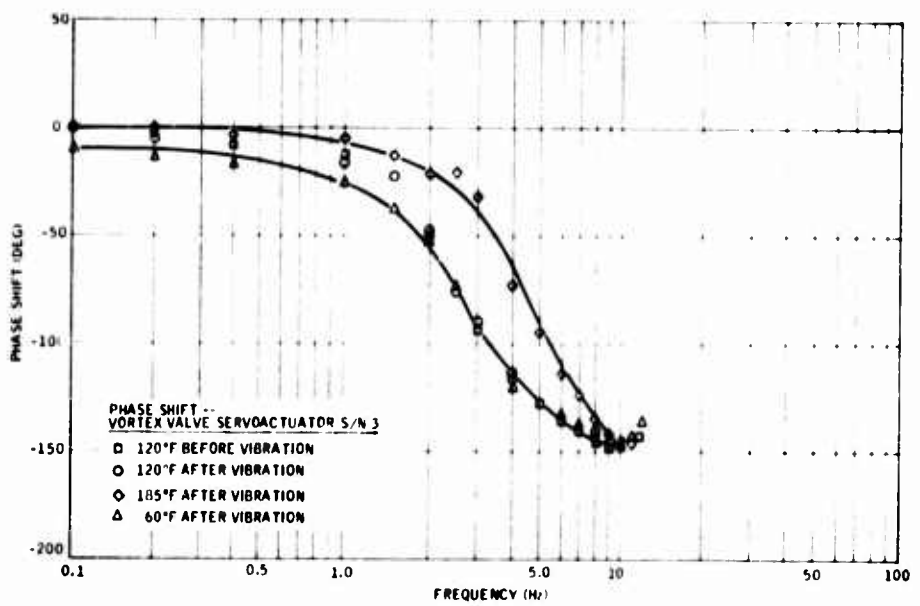

Figure 159. Frequency Response (Phase Shift) for Vortex Valve Servoactuator S/N 2.

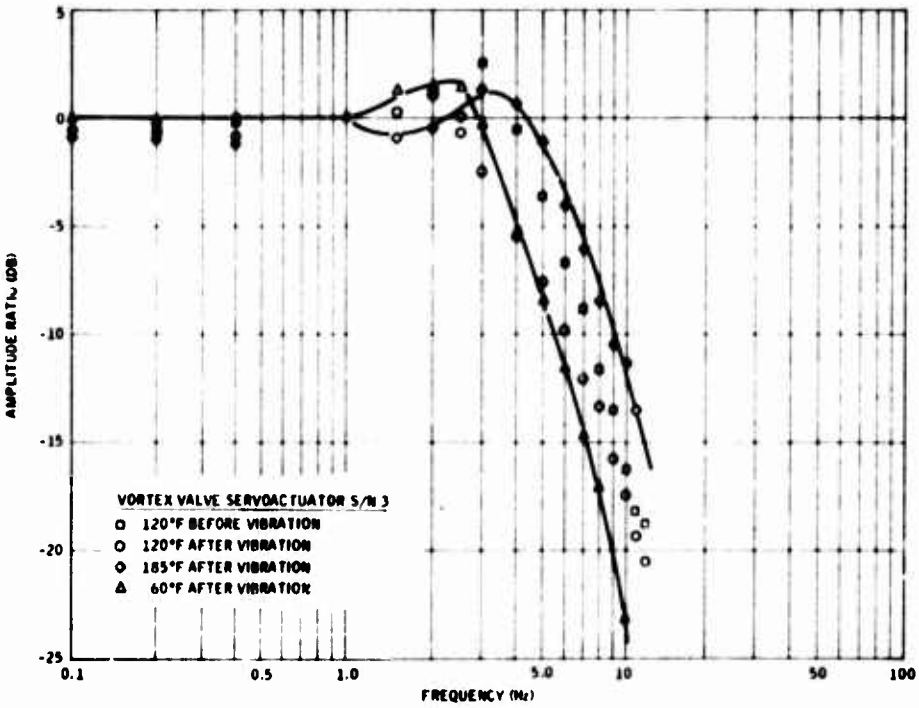

Figure 160. Frequency Response for Vortex Valve Servoactuator S/N 3.